T.C.
DOKUZ EYLÜL UNIVERSITY
IZMIR INTERNATIONAL
BIOMEDICINE AND GENOME
INSTITUTE

CHARACTERIZATION OF ALTERATIONS IN EPIGENOME CAUSED BY IDH1 MUTATIONS AT THE EARLIEST STAGES OF GLIOMAGENESIS

BURCU EKİNCİ GÖRGÜN

MOLECULAR BIOLOGY AND GENETICS

Ph.D. THESIS

İZMİR-2023

THESIS CODE: DEU.IBG.PhD-2017850061

T.C.
DOKUZ EYLÜL UNIVERSITY
IZMIR INTERNATIONAL
BIOMEDICINE AND GENOME
INSTITUTE

CHARACTERIZATION OF ALTERATIONS IN EPIGENOME CAUSED BY IDH1 MUTATIONS AT THE EARLIEST STAGES OF GLIOMAGENESIS

MOLECULAR BIOLOGY AND GENETICS

Ph.D. THESIS

BURCU EKİNCİ GÖRGÜN

Advisor: Asst. Prof. Dr. Yavuz OKTAY

(This thesis was supported by TÜBİTAK-117Z981)

THESIS CODE: DEU.IBG.PhD-2017850061

Dokuz Eylül University Izmir International Biomedicine and Genome Institute
Department of Genomics and Molecular Biotechnology,
Molecular Biology and Genetics PhD program student Burcu Ekinci Görgün has successfully completed the PhD thesis entitled
"Characterization of alterations in epigenome caused by IDH1 mutations at the earliest stages of gliomagenesis" on date of 13/11/2023.

HEAD OF THE COMMITTEE
Asst. Prof. Yavuz OKTAY

MEMBER
Prof. Dr. Şermin GENÇ

MEMBER
Prof. Dr. Ahmet Okay ÇAĞLAYAN

MEMBER
Asst. Prof. Cihangir YANDIM

MEMBER
Assoc. Prof. Kemal Uğur TÜFEKCİ

Dokuz Eylül Universitesi İzmir Uluslararası Biyotıp ve Genom Enstitüsü Genom Bilimleri ve Moleküler Biyoteknoloji Anabilim Dalı,
Moleküler Biyoloji ve Genetik Doktora programı öğrencisi Burcu Ekinci Görgün,
"Gliom oluşumunun erken aşamalarında IDH1 mutasyonlarının epigenomda yol açtığı değişimlerin karakterizasyonu" konulu Doktora tezini 13/11/2023 tarihinde başarı olarak tamamlamıştır.

BAŞKAN
Dr. Öğr. Üyesi Yavuz OKTAY

JÜRİ ÜYESİ
Prof. Dr. Şermin GENÇ

JÜRİ ÜYESİ
Prof. Dr. Ahmet Okay ÇAĞLAYAN

JÜRİ ÜYESİ
Dr. Öğr. Üyesi Cihangir YANDIM

JÜRİ ÜYESİ
Doç. Dr. Kemal Uğur TÜFEKCİ

INDEXES

INDEX OF FIGURES

INDEX OF TABLES

LIST OF ABBREVIATIONS

ADP:	Adenosine diphosphate
ATP:	Adenosine triphosphate
CNS:	Central Nervous System
ChIP:	Chromatin immunoprecipitation
Chr:	Chromosome
C-P4H:	Collagen prolyl 4-hydroxylases
CRISPR:	Clustered regularly interspaced short palindromic repeats
D2-HG:	D2-Hydroxyglutarate
EDTA:	Ethylenediaminetetraacetic acid
FISH:	Flurescence In Situ Hybridization
Gfap+:	Glial fibrillated acidic protein positive
G-CIMP:	Genome-wide CpG island methylator phenotype
GBM:	Glioblastoma
H3K4me3:	Tri-methylation at the 4th lysine residue of the histone H3
H3K9me3:	Tri-methylation at the 9th lysine residue of the histone H3
H3K27me3:	Tri-methylation of lysine 27 on histone H3 protein.
H3K27ac:	Acetylation of the lysine residue at N-terminal position of the histone H3
hESC:	Human embryonic stem cell
HIF-PHD:	Hypoxia inducible factor-prolyl hydroxylase domain protein
hiPSC:	Human induced pluripotent stem cell
HGG:	High Grade Glioma
IDH:	Isocitrate dehydrogenase
IgG:	Immunoglobulin G
IHA:	Immortalized human astrocyte
IF:	Immunoflurescence
JmjC:	Jumonji-C
JMJD2A:	Jumonji domain containing 2A
KDMs:	Histon lysine demethylases
LGG:	Low Grade Glioma
LDH:	Lactate dehydrogenase

MEF:	Mouse embryonic fibroblast
miRNA:	MicroRNA
ncRNA:	Non-coding RNA
NSC:	Neural stem cell
NPC:	Neural progenitor cell
OCT4:	Octamer-binding transcription factor-4
PAX6:	Paired box 6
PI:	Propodium Iodide
piRNA:	Piwi interacting RNA
ROS:	Reactive oxygen species
siRNA:	Small interfering RNA
Sox1:	SRY-Box Transcription Factor-1
Sox2:	SRY-Box Transcription Factor-2
SVZ:	Subventricular Zone
TCA:	Tricarboxylic cid
TCGA:	The Cancer Genome Atlas
TERT:	Telomerase reverse transcriptase
TET:	Ten-eleven translocation methylcytosine
WHO:	World Health Organization
WT:	Wild Type
5mC:	5-methylcytosine
5-hmC:	5-hydroxymethylcytosine
5fC:	5-formylcytosine
5-caC:	5-carboxylcytosine
α-KG:	α-ketoglutarate

ACKNOWLEDGEMENT

First and foremost, I would like to express my sincere gratitude to my advisor Asst. Prof. Yavuz Oktay for his mentorship and kindness throughout my doctoral study. I am grateful to him for giving me the freedom to pursue, rationalize, and test my scientific questions. I would also like to thank him very much for giving me the opportunity to become a member of Oktay Lab.

I would like to express my gratitude to all past and present members of the Oktay Laboratory, especially Tutku Yaraş, Aykut Kuruoğlu, Ece Sönmezler Adalı, Berfin Demirözer, Şimal Kayıkcı, and Delfin Alpsoy. I thank them wholeheartedly for always making me feel their presence by my side, for their support, and for their invaluable friendships. I am especially grateful to Tutku Yaraş for teaching me that one can be closer than a friend, even closer than a sister, adding value to my life, and making this journey more enjoyable.

I would like to extend my sincere thanks to my other committee members Prof. Dr. Şermin Genç, Prof. Dr. Ahmet Okay Çağlayan, Asst. Prof. Cihangir Yandım and Assoc. Prof. Kemal Uğur Tüfekci for dedicating their valuable time to attend my defense, accepting our invitation, and providing valuable comments.

I would also like to acknowledge the scholarships I received from The Council of Higher Education (CoHE) (YÖK 100/2000) and the Scientific and Technological Research Council of Turkey (TUBITAK)-BIDEB 2211-A National PhD Scholarship Program for providing financial support during my study. Furthermore, I would like to thank to TÜBİTAK (The Scientific and Technological Research Council of Turkey, project number: 117Z981) for covering experimental expenses of my PhD project.

I would especially like to thank Prof. Dr. Hatice Güneş Özhan, Assoc. Prof. Dr. Hani Alotaibi and Dr. Serap Erkek for sharing their knowledge and experiences. I would also like to thank Soheil Akbari and Kemal Uğur Tüfekci for their support, understanding and invaluable friendship during my time at IBG.

My deepest gratitude is to my family who has always been with me on this long journey. I would like to express my sincere gratitude to my mother Hüryaşar Ekinci, my father Memet Ekinci and also my brother Mehmet Fatih Ekinci for their unconditional love and endless understanding. I would also like to thank my husband, Serhan Görgün, for his love and his patience during my PhD life. I am also grateful for always being there for me and for their support.

CHARACTERIZATION OF ALTERATIONS IN EPIGENOME CAUSED BY IDH1 MUTATIONS AT THE EARLIEST STAGES OF GLIOMAGENESIS

Burcu Ekinci Görgün; Izmir International Biomedicine and Genome Institute, Dokuz Eylul University Health Campus, Balcova, 35340, Izmir/ Türkiye

ABSTRACT

Isocitrate dehydrogenase (IDH1/2) mutations, which have been shown to develop before other mutations known to play a role in glioma development, are believed to trigger gliomagenesis. Studies to date have mostly used heterogeneous tumor samples or cells with oncogenic mutations when investigating the early stages of glioma development. This limits our knowledge of how gliomagenesis is triggered by IDH1/2 mutations. Moreover, examination of epigenomic changes caused by IDH1/2 mutations has not gone beyond classical histone methylation analyzes based on methylation arrays, RNA-seq and expression microarrays, and ChIP-seq. The aim of this study was to understand the permanent changes caused by the IDH1-R132H mutation, which is the earliest seen in gliomagenesis, in the epigenome of neural progenitor cells (NPCs) cultured in a 3D environment. For this, firstly, conditioned medium with Immortalized Human Astrocytes (IHAs) expressing doxycycline-inducible IDH1 (Mutant and wild type) was obtained. These media samples were then delivered for specified periods of time to NPCs differentiated from human pluripotent stem cells (hiPSC) in an alginate-based 3D matrix. RT-qPCR and RNA-seq analyzes were performed by isolating RNA from cells taken at three time points (day 0, day 14, day 17) from NPCs exposed to different media. Key genes reported to be altered in IDH1 mutant gliomas were checked by RT-qPCR. Then, epigenetic marks in histones and DNA were analyzed by ChIP-qPCR and MeDIP-qPCR. In selecting the loci for these analyses, we particularly prioritized the aim of furthering the mechanistic information regarding the IDH1-MYC relationship in the risk of glioma located at 8q24, which we brought to the literature for the first time in our group's previous studies, and directly demonstrating it in an *in vitro* model. Our findings indicate that one of the direct targets of the oncogenic changes that occur in the IDH1-MYC axis, which we think are initiators of gliomagenesis, is the ID1 (inhibitor of differentiation) gene, and that as a result of the induction of this gene, the cells take on a less differentiated phenotype.

Keywords: Glioma, Isocitrate Dehydrogenase, IDH1, Immortalized Human Astrocytes, Neural Progenitor Cells, NPCs, ID1.

GLİOM OLUŞUMUNUN ERKEN AŞAMALARINDA IDH1 MUTASYONLARININ EPİGENOMDA YOL AÇTIĞI DEĞİŞİMLERİN KARAKTERİZASYONU

Burcu Ekinci Görgün, İzmir Biyotıp ve Genom Enstitüsü, Dokuz Eylül Üniversitesi Sağlık Yerleşkesi, 35340, İzmir/ Türkiye

ÖZET

Glioma gelişiminde rol oynadığı bilinen diğer mutasyonlardan önce geliştiği gösterilen izositrat dehidrogenaz (IDH1/2) mutasyonlarının gliomagenezi tetiklendiğine inanılmaktadır. Bugüne kadar yapılan çalışmalarda, glioma gelişiminin erken aşamaları araştırılırken çoğunlukla heterojen tümör örnekleri veya onkogenik mutasyonlara sahip hücreler kullanılmıştır. Bu durum, gliomagenezin IDH1/2 mutasyonlarıyla nasıl tetiklendiği hakkındaki bilgilerimizi kısıtlamaktadır. Ayrıca, IDH1/2 mutasyonlarının neden olduğu epigenomik değişimlerin incelenmesi metilasyon dizileri, RNA-seq ve ekspresyon mikrodiziler ile ChIP-seq temelli klasik histon metilasyon analizlerinin ötesine geçememiştir. Bu çalışmanın amacı, gliomagenezde en erken görülen IDH1-R132H mutasyonunun, 3 boyutlu ortamda kültürlenen nöral progenitör hücrelerin (NPH) epigenomunda yol açtığı kalıcı değişimlerin anlaşılmasıdır. Bunun için öncelikle, doksisiklinle indüklenebilir IDH1 (Mutant ve vahşi tip) ifade eden İmmortalize İnsan Astrositleri (IHA'lar) ile koşullandırılmış ortam elde edildi. Bu ortam örnekleri daha sonra, insan pluripotent kök hücrelerden (hiPSC) farklılaştırılmış NPH'lere aljinat bazlı bir 3D matris içinde belirli sürelerde verildi. Farklı besiyerlerine maruz bırakılan NPH'lerden üç zaman noktasında (gün 0, gün 14, gün 17) alınan hücrelerden RNA izole edilerek RT-qPCR ve RNA-seq analizleri gerçekleştirildi. RT-qPCR ile IDH1 mutant gliomalarda değiştiği bildirilen anahtar genler kontrol edildi. Daha sonra, ChIP-qPCR ve MeDIP-qPCR ile histon ve DNA'daki epigenetik işaretler analiz edildi. Bu analizler için lokus seçiminde özellikle, grubumuzun önceki çalışmalarında literatüre ilk kez kazandırdığımız 8q24 yerleşimli gliom riskinde IDH1-MYC ilişkisine dair mekanistik bilgiyi, daha ileriye taşımayı ve *in vitro* bir modelde doğrudan gösterme amacını ön planda tuttuk. Elde ettiğimiz bulgular, IDH1-MYC ekseninde oluşan ve gliomagenezi başlatıcı olduğunu düşündüğümüz onkogenik değişimlerin doğrudan hedeflerinden birinin ID1 (*farklılaşma inhibitörü*) geni olduğuna, bu genin indüklenmesi sonucunda ise hücrelerin daha az differensiye bir fenotipe büründüğüne işaret etmektedir.

Anahtar Kelimeler: Glioma, İzositrat Dehidrojenaz, IDH1, İmmortalize İnsan Astrositleri, Nöral Progenitör Hücreler, NPH'ler, ID1.

1. INTRODUCTION AND OBJECTIVES

1.1. Statement and Importance of the Problem

Gliomas, which have a poor prognosis and high morbidity and mortality, are the most common and devastating brain tumors that are often untreatable (González-Castro et al., 2019; Haddock et al., 2022; S. Xu et al., 2020). It is known that the development of the gliomas is triggered by isocitrate dehydrogenase (IDH1/2) mutations, as it has been shown to develop before genetic alterations such as 1p/19q codeletion, or TP53 mutations or the "genome-wide methylation change" phenotype (G-CIMP), that are known to play a role in glioma development (Suzuki et al., 2015). It has been shown that mutant IDH1/2 acquires a neomorphic enzymatic activity and converts alpha-ketoglutarate (α-KG) to 2-hydroxyglutarate (2-HG), and this oncometabolite inhibits α-KG-dependent dioxygenases competitively (Dang et al., 2009). Additionally, it has been shown that the G-CIMP phenotype occurs in different cell types as a result of mutant IDH1/2 expression or 2-HG exposure and also moves the cells to a less differentiated state (Turcan et al., 2012). However, information on the pathways by which the cascade initiated by IDH1/2 mutations triggers or facilitates gliomagenesis is limited. In comprehensive multi-omic studies conducted for years, either patient tumor samples or glioma models created by combining many oncogenic mutations were used. However, IDH1/2 mutations are genetic changes that occur at the earliest stage of gliomagenesis, when other oncogenic changes are not yet evident. On the other hand, recent studies have shown that the effects of mutant IDH1 inhibitors are time / stage-dependent, and some of the IDH mutations effects on the epigenome are permanent (Johannessen et al., 2016).

1.2. Aims of the Study

In this study, we aimed to develop a novel solution to this problem of modeling the earliest stages of gliomagenesis, by culturing iPSC-derived NPCs without oncogenic mutations in IHA-IDH1-WT or IHA-IDH1-R132H conditioned medium in an alginate hydrogel-based 3D environment that should better reflect *in vivo* conditions. Thus, the effects of mutant IDH in the earliest stages of glioma formation would be observed with minimal confounders. Additionally,

we aimed to examine whether the effects of mutant IDH on the epigenome were permanent after IHA conditioned media were replaced with neural progenitor media.

The specific goals of this study are as follows: 1) Differentiation of iPSCs into Neural progenitor cells (NPCs); 2) Maintenance of iPSCs-derived NPCs free of oncogenic mutations in alginate-based three-dimensional culture; 3) Determination of the time-dependent changes in the reversible and irreversible effects of IDH1 mutation on the transcriptome by RNA-seq analysis after the application of IHA conditioned media and neural progenitor media to alginate-based 3D NPC cultures for the specified periods of time; 4) Determination of changes in histone modifications (H3K4me3 and H3K27ac) associated with regulatory regions in specified time periods by ChIP-qPCR; 5) Detection of methylation changes of regulatory regions with MeDIP-qPCR in specified time periods; 6) Targeting candidate regions with CRISPR, either alone or multiplexed; 7) Identification of epigenomic changes that, when targeted, significantly reduce or eliminate the permanent effects of IDH mutation.

1.3. Hypothesis of the Study

The hypothesis of this study was that wild-type NPCs exposed to conditioned media obtained from IDH1-R132H expressing cells could recapitulate the earliest oncogenic changes induced by the IDH1 mutations during gliomagenesis.

2. GENERAL INFORMATION

2.1. Brain Tumors

The brain, the most complex part of the human body, has billions of active cells. The brain, the most important organ of the central nervous system (CNS), is responsible for the control and functioning of most body activities (Lah et al., 2020; Nayak et al., 2022; Seetha & Raja, 2018). Therefore, the spinal cord and the brain are evolutionarily the best protected from damage throughout a person's life. Because each part of the brain has a unique function, it can cause severe mental or physical disability when disturbed. Therefore, various damage may occur in other parts of the body during the treatment of tumors in the CNS (Lauko et al., 2022). Brain tumors consist of tissues that have no physiological function as a result of uncontrolled cell proliferation inside of the brain or around the brain. In addition to increasing the size and

pressure due to tumors in the brain, it also causes swelling, causing abnormal neurological symptoms (Abd-Ellah et al., 2019). The worldwide incidence rate of primary malignant brain and other CNS tumors was 3.5 per 100,000 population in 2020, according to data from the United States Central Brain Tumor Registry. Additionally, when looking at the data of 2020, according to gender, the incidence rates in men are 3.9 per 100,000 population and the number of newly diagnosed male cases is 168,346, while the incidence rates in women are 3.0 per 100,000 population and the number of newly diagnosed female cases is 139,756(Sung et al., 2021). There are around 150 different types of brain tumors, including currently known benign and malignant tumors. Unlike benign tumors, malignant tumors have a higher potential to spread outside the brain. That's why malignant brain tumors are generally called brain cancer. Accurate grading along with early diagnosis is staminal for the patient in brain tumors, as in other tumors. Manual techniques are difficult to approach due to brain tumor density. Therefore, automated computer-based methods are much more useful for tumor detection (Reddy et al., 2020). Today, the use of deep learning and machine learning is preferred to improve detection algorithms for brain tumors so that tumors can be located without surgical intervention (Nayak et al., 2022).

2.1.1. The WHO Classification of Tumors of the Central Nervous System

The international classification of human tumors began with the decision of the WHO Executive Board in 1956 and the World Health Assembly in 1957 and was published by the World Health Organization (WHO). The WHO tumor classification, known as the ‘WHO Blue Books’, is regularly updated. The globally accepted goals for grading and classification of human tumors have remained the same to date. Each classification was created with the consensus of the International Working Group (Louis et al., 2007). The classification of nervous system tumors, following the histological typing of nervous system tumors first performed by Zülch, was published as the first edition in 1979. (Louis et al., 2007).

The second edition, edited in 1993 by Kleihues et al., showed advances made by incorporating immunohistochemistry into diagnostic pathology (Louis et al., 2007).

In 2000, in the third edition edited by Kleihues and Cavenee, genetic profiles were introduced as additional aids to the identification of brain tumors. (Louis et al., 2007).

In 2007, the 4th edition of the WHO CNS classification was created by consensus of an international working team of 25 geneticists and pathologists and with the contribution of more than 70 international experts (Louis et al., 2007). As a result of increasing knowledge about the genetic basis of CNS neoplasms, the 2007 edition of the classification is focused on CNS neoplasms. In 2007, morphology has been still an important parameter for WHO CNS classification, a lot of genomic data were added in to 2007 WHO CNS classification (Rousseau et al., 2008).

2016 WHO CNS tumors classification was published as the fourth version as a revised version of the 2007 WHO CNS classification. For the first time in this classification, histology information and molecular parameters have been used to identify CNS tumors, and this 2016 CNS WHO classification shows a massive remodeling of tumors. With molecular studies for a clearer understanding of tumor formation, understanding the mechanism of gliomagenesis and classification with new biomarkers has become stronger and finding new therapeutic targets has become easier (Louis et al., 2016). Markers based on molecular classification that make the classification clearer, such as IDH mutation status (mutant or wild type), 1p/19q codeletion, TERT mutation, loss of expression in the *ATRX* gene, P53 mutation, and H3K27M mutations in 2016 WHO CNS tumor classification have correlated genotypic and phenotypic parameters (Reifenberger et al., 2017). Compared with the 2007 WHO CNS classification, the most significant improvement in the 2016 WHO glioma classification is that different glioma entities are separated according to status of isocitrate dehydrogenase 1 and 2 (IDH1/2) mutations. The observation that IDH mutations present in most grade II and III gliomas has been an important step in understanding the disease (Reifenberger et al., 2017). CNS tumor classifications were mostly based on histological findings. Later, it was understood that molecular biomarkers were important in adjunctive and diagnostic treatment and would contribute to more accurate classification (Louis et al., 2021).

In 2021, the new the WHO Classification of CNS Tumors (WHO CNS5) was published and is the sixth edition according to international standards when looking at the classification of spinal cord tumors and brain (Figure 1). WHO CNS5 is based on the updated WHO CNS classification published in 2016, many developments resulting from later studies, and many suggestions of the consortium to inform molecular and practical approaches CNS Tumor Taxonomy (cIMPACT-NOW). In 2021 classification, the role and importance of molecular diagnosis has been increased in addition to known approaches to tumor characterization,

especially immunohistochemistry and histology. In this classification, a more precise classification could be made by considering many molecular changes as well as clinicopathological features. To standardize this classification with other fifth edition Blue books, "entity" has been replaced with "type" and "variant" has been replaced with "subtype" (Louis et al., 2021). In previous classifications, there was no specific standard for tumor nomenclature. Some tumor naming included details such as specific location and specific mutation. In addition, there were tumor names that did not have location or genotype information in their naming, although they appeared in certain locations or had specific genotypes. The WHO CNS5 classification uses a simpler nomenclature whenever possible, and attempts are made to use only clinically useful location, age, or genetic modifiers. In addition, the Roman numerals used in naming have been replaced by Arabic numerals, and neoplasms have been classified within types, not between different tumor types. Histochemical staining, microscopy, immunohistochemistry, and molecular genetic techniques were used in classification. In recent years, methods such as Fluorescent in situ hybridization (FISH) technique, expression profiling and nucleic acid-based DNA-RNA sequencing have begun to be used. The information found by these methods is used for tumor classification and identification in the revised fourth version (WHO 2016) and WHO CNS5 (Louis et al., 2021). In addition, methylome profiling, which has become popular in the past decade, has come to be used in the classification of CNS tumors because it can identify the methylation pattern of DNA throughout the genome. It is more effective for accurate classification, especially when used together with standard methods used in previous classifications such as histology. This method is also very effective in classifying tumors that show unusual morphological features. However, this method can not be helpful for targeted gene therapy and treatments in which specific mutations are precursors. Therefore, a distinct methylation signature has been identified for nearly all tumor types in the 2021 classification (Louis et al., 2021).

Figure 1. World Health Organization Classification of Central Nervous System Tumors 2021 (Overview of WHO CNS5 Classification). In grey cells, new tumour types are shown (McNamara et al., 2022).

2.1.2. Gliomas

When we look at the overall CNS malignancies, gliomas, which are known to constitute 81% of this malignancy, are primary brain tumors (S. Xu et al., 2020) and are generally divided into two categories: Circumscribed gliomas are known as benign tumors that can be treated with surgery. Diffuse gliomas are malignant tumors that cannot be treated with surgery alone (Yang et al., 2022). In the WHO CNS 2016 classification, it has been shown that the progenitor of gliomas is glial and precursor cells, and that these cells evolve into oligodendroglioma, astrocytoma, oligoastrocytoma and ependymoma (Ostrom et al., 2018; N. Zhang et al., 2012). The WHO CNS classification published in 2021 has shown that grading within tumor type is a more accurate grading, thus dividing gliomas into 4 different families (Figure 2). In addition, gliomas are graded according to their aggressiveness. CNS WHO grade 1 and 2 are called low-grade gliomas (LGG) and possess a median survival of 11.6 years. The survival time is very short in CNS WHO grade 3 and 4, that is, high-grade gliomas (HGG) (Louis et al., 2021; Yang et al., 2022) (Figure 2). While the survival time for patients of grade 3 is approximately 3 years, the overall survival time (OS) for patients of grade 4 is approximately 15 months (Bleeker et al., 2012). LGGs account for 6% of CNS tumors in adults and have a better prognosis (Ostrom et al., 2019). CNS WHO grade 1 LGG is more common in children and shows a good prognosis (Campian & Gutmann, 2017). Grade 2 LGG has a higher potential to recur in children and progresses to HGG with a poor prognosis (Duffau & Taillandier, 2015). Glioblastoma (GBM), the common type of gliomas, constitutes the majority of WHO CNS Grade 4. Glioblastomas are among the malignant tumors that are fatal and prone to recurrence (Weller & Le Rhun, 2020) (Figure 2).

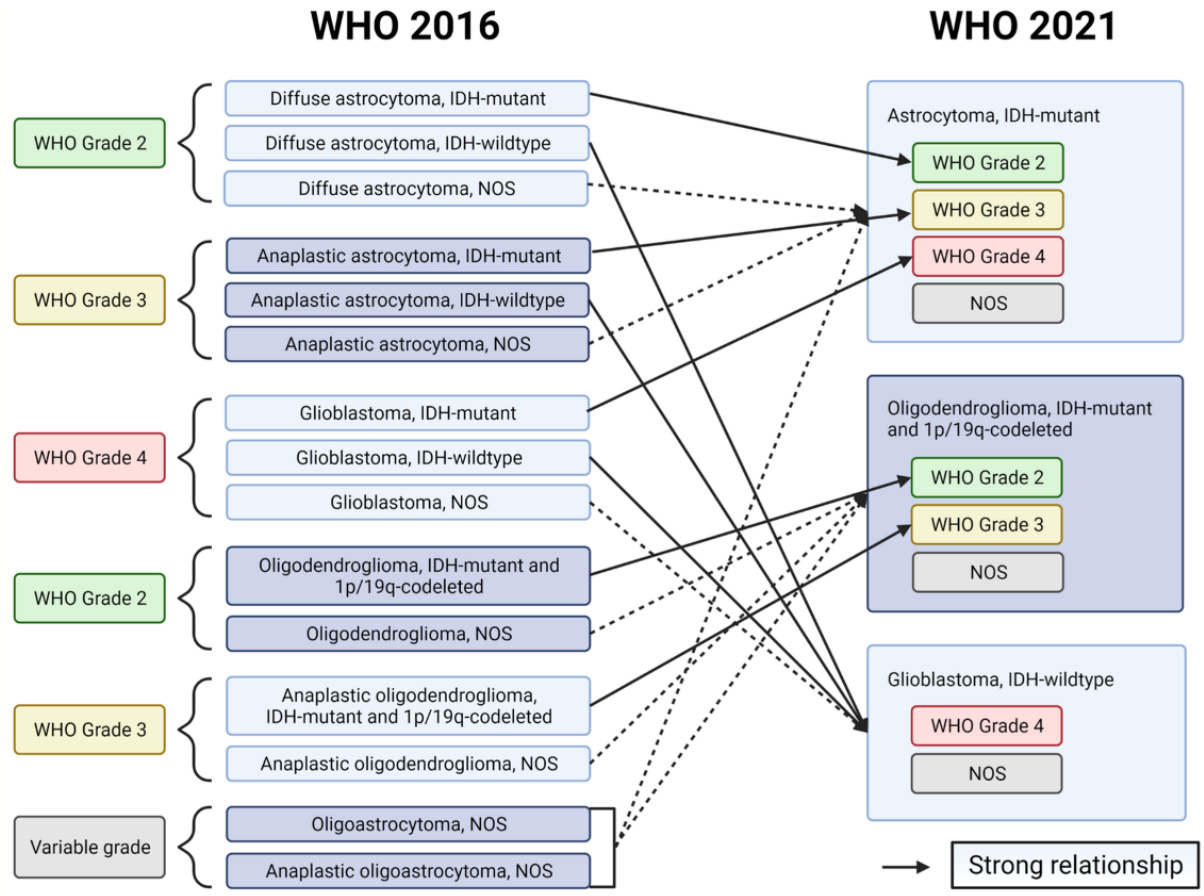

Figure 2. Schematic representation of the definition of disease entities changing from WHO 2016 to WHO 2021. Strong correlations between WHO 2016 and WHO 2021 classifications are expressed by solid lines. The dotted lines show how the disease entity defined in WHO 2016 will probably be classified in WHO 2021 (Whitfield & Huse, 2022).

2.1.2.1. Origin Of Gliomas

The cell of origin is the healthy cell that receives the first genetic hit to initiate cancer. Since identifying the cells that initiate tumorization in organs and tissues is of great importance for their treatments, a lot of work is being done in these areas (Visvader, 2011). To investigate the origin of gliomas, it is necessary to thoroughly investigate the cell lines in the CNS. It is known that glioblastomas can occur near the subventricular zone (SVZ) or in areas further away from the SVZ. Factors such as tumor location, subtypes, clinical outcomes and growth rate determine it. When looking at the cancer genome atlas data, proneural and neural subtypes of

GBM are proximal to the SVZ, while mesenchymal and classical TCGA subtypes are distal to the SVZ. The formation of GBMs in different regions is an indication that the cells of origin are different (Bohman et al., 2010; Lim et al., 2007; Steed et al., n.d.). LGGs with IDH mutations are localized in the frontal lobe, and these tumors have much higher rate of TERT promoter mutation than midline tumors with IDH wild type. Knowing the location and type of gliomas allows personalized treatment. But why some gliomas have preferential locations is a matter of curiosity (Brat et al., 2015; Lai et al., 2011; Z.-L. Sun et al., 2015).This is because different glioma subtypes have different cells of origin and different neurological niche signals. In the adult mammalian brain, neural stem cells (NSCs) are found in the SVZ lining the lateral ventricles and in the subgranular regions of the dentate gyrus of the hippocampus (Picard-Riera et al., 2004). NSCs, which have self-renewal properties, exhibit multipotency, and are quiescent glial fibrillated acidic protein positive (GFAP+), have the ability to differentiate into progenitor cells to produce neuronal and glial lineages. progenitor cells and NSCs express Nestin along with other markers (such as EGFR, Glast, Sox2, Tlx, Gli1) (Doetsch et al., 1999; Mich et al., 2014). Considering the development and differentiation potential of NSCs, they may be strong candidates as the cell of origin of glioma. Additionally, when looking at the characteristics of NSCs, they appear to be very similar to gliomas. For example; The characteristics of NSCs, such as the transcriptional circuit that governs the identity of NSCs, motility, expression of antigens on the cell surface, and activation of developmental signaling pathways, are similar to gliomas (Cahill & Turcan, 2018). In addition, the failure of mature astrocytes with combined activation of Ras and Akt and combined deletion of Pten, Tp53, Nf1 and Rb 1 to form gliomas in mice further strengthened the conclusion that NSCs are glioma origin cells (S. Alcantara Llaguno et al., 2009; Holland et al., 2000; Jacques et al., 2010). Again, various studies have shown that the probability of tumor formation in *in vivo* studies is very low unless PDGF retroviral transfection and loss of the Ink4a-Arf locus are performed in mature astrocytes (Bachoo et al., n.d.; Dai et al., 2001; Uhrbom et al., 2002) . Considering all these outcomes, the role of differentiated astrocytes in glioma formation is still debated. On the other hand, it has been observed that neural progenitor cells (NPCs) and oligodendrocyte precursor cells (OPCs) with inactivation of NF1, Pten and TP53 cause the formation of different subtypes of GBM (S. R. Alcantara Llaguno et al., 2015). Additionally, the incidence of gliomas increases with age. The underlying reasons for the increased risk of glioma with age are unknown. But age-related

changes in the brain microenvironment, such as accumulation of mutations and weakening of the immune system, are considered risk factors for glioma origin cells (Cahill & Turcan, 2018).

2.2. Isocitrate Dehydrogenase (IDH)

The IDH genes encode the enzyme isocitrate dehydrogenase, which is involved in the Krebs cycle to convert isocitrate to α-ketoglutarate (α-KG) and reduce NAD(P)+ to NAD(P)H (Reitman & Yan, 2010; X. Sun & Turcan, 2021). In human cells, there are three isozymes of IDH as IDH1, IDH2 and IDH3, which are encoded by five genes. Although all enzymes catalyze the same chemical reaction, each enzyme has unique biological properties. IDH1 localized in the cytosol and peroxisomes of cells and IDH2 localized in mitochondria act as homodimers, while IDH3 localized in mitochondria form a heterotetramer containing two α, one β and one γ subunits (Cohen et al., 2013; Kloosterhof et al., 2011; Reitman & Yan, 2010). Nicotinamide adenine dinucleotide phosphate (NADP+) is used by IDH1 and IDH2 as cofactor, while IDH3 uses Nicotinamide adenine dinucleotide (NAD+) as cofactor. While NADP+ dependent IDH1 and IDH2 have significant amino acid sequence similarity, they are unrelated to NAD+ dependent IDH3 (Ichimura, 2012). IDH1 takes part in glucose and lipid metabolisms and has an important role in protection against reactive oxygen species (ROS). IDH2 has a regulatory role on the tricarboxylic acid (TCA) cycle, as well as protecting cells against oxidative stress. IDH3 acts as the central enzyme in the tricarboxylic acid (TCA) cycle (Figure 3). IDH1 and IDH2, which catalyze reversible reactions, have no known allosteric modifiers. The reaction catalyzed by IDH3 is irreversible, and unlike IDH1 and IDH2, the chemical reaction catalyzed by IDH3 is regulated by various positive (calcium, ADP and citrate) and negative (ATP, NADH and NADPH) allosteric effectors (Gabriel et al., 1986; Reitman & Yan, 2010).

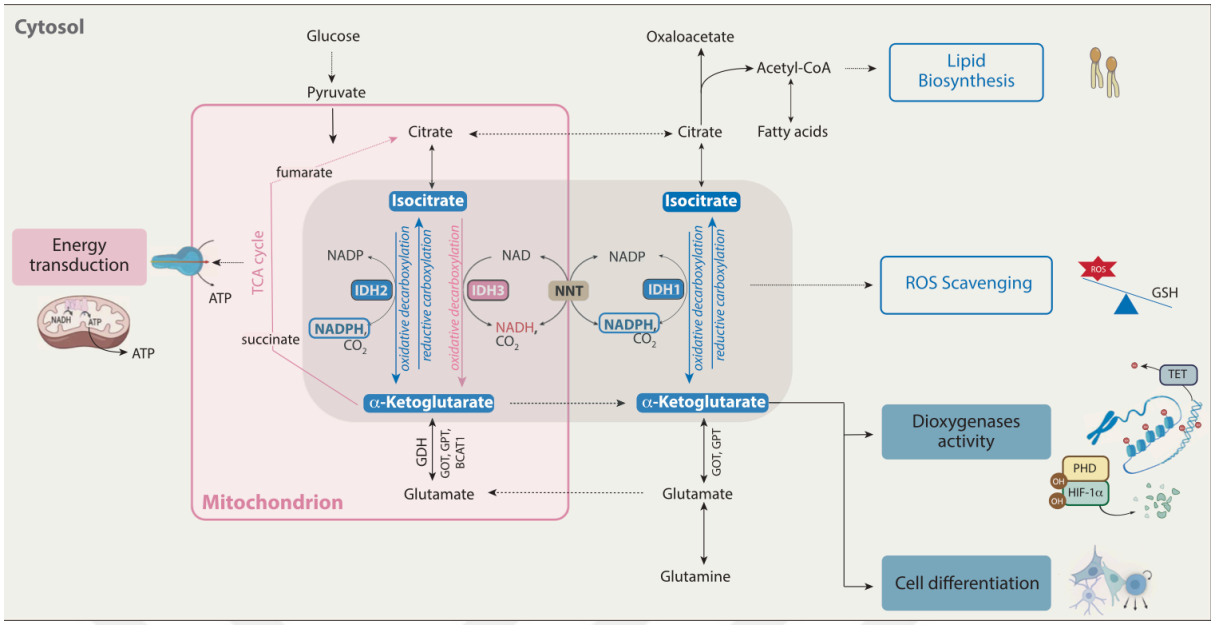

Figure 3. Metabolic functions of wild-type IDH1, IDH2 and IDH3 enzymes. All three isoforms of IDH catalyze the conversion of isocitrate to α-ketoglutarate and carbon dioxide with the production of reduced equivalent NAD(P)H. IDH1 is involved in the cytosol, while IDH2 and IDH3 are involved in the tricarboxylic acid (TCA) cycle in the mitochondria. Depending on their isoform, localization and cofactor in the cell, IDH enzymes take part in different cellular events such as energy production, lipogenesis, glutamine metabolism, epigenetic profile, responses to hypoxia and the redox state of the cell (Alzial et al., 2022).

2.2.1. IDH Mutation

In recent years, recurrent somatic mutations in IDH1 andaIDH2 have been described in many cancer types. Low-grade gliomas, primary glioblastomas, secondary glioblastomas, cartilage and bone tumors, intrahepatic cholangiocarcinoma, and acute myeloid leukemia also occur, as well as, albeit at a low rate, angioimmunoblastic T-cell lymphoma, myelodysplastic syndrome and other solid tumors. A tumor-associated mutation in the IDH3 gene has not been reported so far (Solomou et al., 2023). IDH changes are missense mutations. The aminoacid residues R132 and R100 in IDH1 and R172 and R140 in IDH2 are predominantly affected. These arginines are located at the substrate binding sites of enzymes. It enables enzymes to form hydrophilic interactions with the α/β carboxylate of Isocitrate (Solomou et al., 2023; Ward

et al., 2012). When looking at IDH1 mutations, the arginine residue with a high positivity is replaced by one of the low polarity amino acids cysteine, histidine, lysine or glycine. Therefore, the IDH1 mutation lowers the affinity for isocitrate and increases the enzyme's affinity for α-KG and NADPH (Solomou et al., 2023; Ward et al., 2010). IDH1 mutations are heterozygous because only one copy of the IDH gene is mutated. Therefore, in tumor cells, IDH1 enzyme, which is a homodimer, turns into a heterodimer structure due to a mutation. The wild-type monomer of the enzyme enables the conversion of isocitrate to α-KG; The mutant monomer exhibits neomorphic activity, converting α-KG to the D2-enantiomer of Hydroxyglutarate and using NADPH as a cofactor (Figure 4). There is also the L2-enantiomer of hydroxyglutarate, but a negligible amount is produced. As a result, in IDH mutant tumors, the amount of α-KG decreases while D2-HG accumulates. Besides being a biomarker in IDH mutant malignancies, D2-HG is an oncometabolite because it competitively inhibits the enzymatic activities of α-KG -dependent dioxygenases (W. Xu et al., 2011).

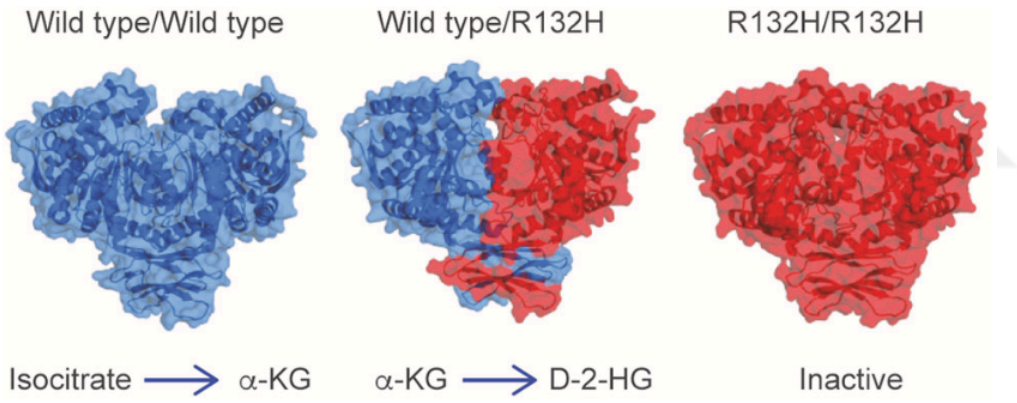

Figure 4. IDH1 Dimerisation. The homodimer formed with two wild-type IDH1 monomers converts isocitrate to α-KG. In IDH1 mutant cells, the heterodimer consisting of a wild-type monomer and an R132H mutant monomer converts α-KG to D-2-HG. According to studies, the homodimer formed with two IDH mutant monomers is not catalytically active (Han et al., 2020).

2.2.2. Cellular Functions of IDH Mutation and 2-HG

It is known that IDH, which gains neomorphic activity through mutation, has effects on cellular metabolism, epigenetic regulation and redox homeostasis (Han et al., 2020). The most common effect of IDH mutation in cells is that D-2HG competitively inhibits α-KG-dependent enzymes. They are structurally very similar to each other. The only difference between them is the presence of a hydroxyl group in D-2HG instead of the oxygen atom linked to C2 in α-KG. Because of this similarity, D-2HG, α-KG follow a competitive attitude (W. Xu et al., 2011). There are more than 60 α-KG-dependent enzymes known so far in mammalian cells, such as Hypoxia inducible factor-prolyl hydroxylase domain protein (HIF-PHD), histone lysine demethylases (KDMs), ten-eleven translocation methylcytosine (TET) family enzymes, collagen prolyl 4-hydroxylases (C-P4H). Their inhibition by 2HG causes angiogenesis, histone modifications, abnormal collagen maturation and DNA hypermethylations, and thus tumorigenesis (Krell et al., 2013) (Figure 5).

D2-HG accumulation leads to depletion of Krebs cycle substrates and withdrawal of carbohydrates from the Krebs cycle. It is known that the Krebs cycle can use different carbohydrate sources to produce ATP (Dang et al., 2009; Maus & Peters, 2017; Reitman et al., 2011). Most studies show that a-KG level is reduced in IDH mutant cells. To compensate for the loss of α-KG, Glutamate dehydrogenase 2, which catalyzes the conversion of glutamate to α-KG, has been shown to increase in IDH mutant cells (Waitkus et al., 2018) . At the same time, it has been shown that the cells in IDH mutant gliomas are sensitive to the inhibition of glutaminase, which provides the breakdown of glutamate, thus supporting the dependence of these cells on glutamate (Seltzer et al., 2010) . On the other hand, NADPH depletion in IDH mutant cells reduces *de novo* lipogenesis and increases dependence on exogenous lipid sources (Badur et al., 2018).

In other tumors, the response is by increasing the expression of lactate dehydrogenase (LDH) to resolve the need for an energy source (Doherty & Cleveland, 2013). LDH enables the conversion of pyruvate to L-lactate, which is used as the primary fuel for energy. But in IDH mutant gliomas, LDH is silenced by hypermethylation of the promoter region. This epigenetic silencing may be the reason why IDH mutant gliomas grow more slowly than IDH wild-type gliomas (Chaumeil et al., 2016; Chesnelong et al., 2014; Khurshed, 2017; Le et al., 2010). In

IDH1 mutant gliomas, energy production is mostly done by oxidative phosphorylation (Hvinden et al., 2021).

In the literature, it is still not fully understood how IDH mutation affects hypoxia levels and angiogenesis. Due to the decrease in the α -KG level and the increase in D2-HG expression, the (HIF-PHD) responsible for the degradation of hypoxia inducible factor (HIF) will be inhibited, HIF will become stable and expression of vascular endothelial growth factor (VEGF), the target gene of HIF, would increase. Studies on mouse embryos expressing IDH1-R132H have shown that HIF1-α is increased. (Chowdhury et al., 2011a; Sasaki et al., 2012; W. Xu et al., 2011c; S. Zhao, 2009) However, later studies showed that no relationship was found between HIF1-α expression and IDH mutation in the brains of both glioma patients and mutant mice (Bardella et al., 2016; Metellus et al., 2011; Williams et al., 2011) . Additionally, recent studies have shown that IDH mutations reduce HIF and VEGF levels and are associated with the inhibition of angiogenesis signaling pathways (Polívka et al., n.d.; Solomou et al., 2023). More studies are required to elucidate the relationship between D2-HG and hypoxia.

The main sources of NADPH in the cell are IDH1 and IDH2. Due to IDH mutations, the NADPH/NADP+ ratio is increased in the cell, thus ROS accumulate in the cell and damage DNA, RNA, lipid and protein in the cell, enzymatic reactions and gene expression are disrupted (Behrend et al., 2003; Itsumi et al., 2015; Liu et al., 2019). Thus, features such as genomic instability, increased cellular motility and invasiveness are observed in cells (Behrend et al., 2003).

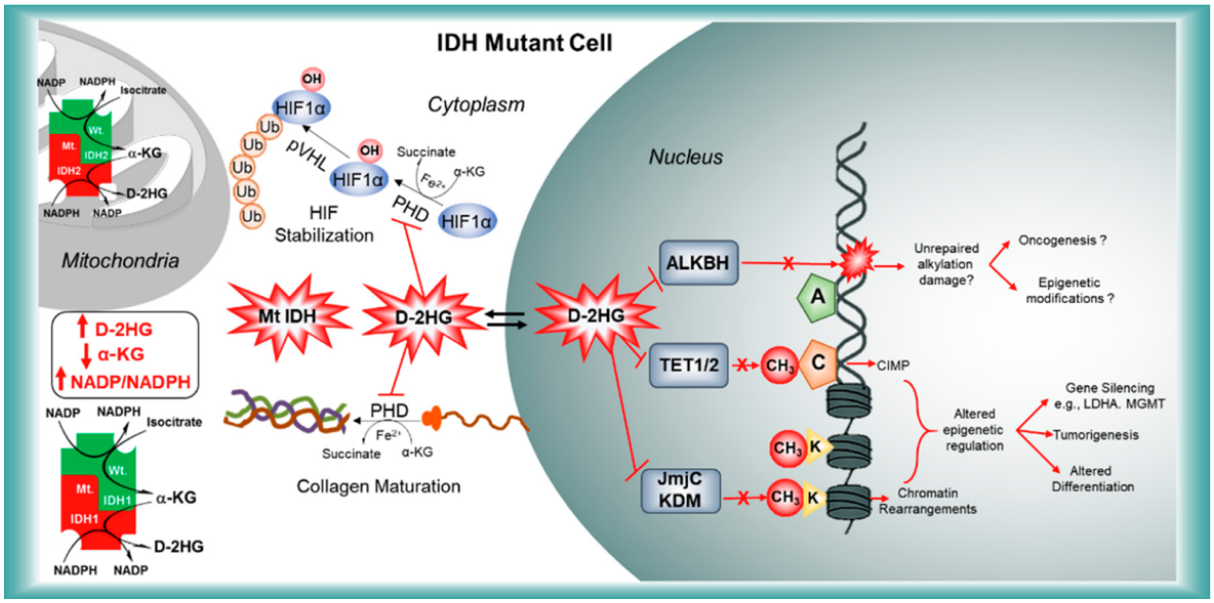

Figure 5. Downstream biological effects of IDH mutations (Madala et al., 2018)

How KDMs, which are histone demethylases, and TET family enzymes, which are DNA demethylases, are affected by IDH mutation, are explained in detail in the “epigenetic modification of IDH mutation and 2-HG” section.

2.2.3. Epigenetic Modification of IDH Mutation and 2-HG

In addition to causing metabolic changes, many clinical studies have shown that IDH mutations have a direct relationship with CpG island (GCI) hypermethylation. In particular, glioma-G-CIMP has been shown to be an important marker for solid tumors with IDH mutation (Christensen et al., 2011; Noushmehr et al., 2010). Mechanistic studies have shown that both global DNA hypermethylation and histone methylation occur in cells that gain neomorphic activity due to IDH1 mutation. It is interesting that DNA hypermethylations also differ among tumor types with IDH1 mutations (Unruh et al., 2019). Methyltransferases and demethylases are known to control DNA methylation. In the demethylation process, the iron- and α -KG-dependent TET enzyme mediates DNA demethylation by catalyzing the conversion of 5-methylcytosine (5mC) to 5-hydroxymethylcytosine (5-hmC), 5-formylcytosine (5fC) and 5-carboxylcytosine (5-caC). It is converted to 5-caC cytosine by DNA glycosylase and base excision DNA repair (Kohli & Zhang, 2013). TET enzymes, which work dependent on α -KG, are blocked in the presence of 2-HG due to 2-HG, which has a competitive attitude with α -KG (X. Sun & Turcan, 2021). It has been shown that IDH mutation alone is sufficient to trigger hypermethylation (Duncan et al., 2012; Turcan et al., 2012). In addition, although it is known that DNA methylation is a reversible process, it is thought that the methylation sites in the cells still exist even when the IDH mutant enzyme is turned off, which is irreversible after the IDH mutant cells decide on oncogenesis, and IDH mutations play a role in malignancy (Turcan et al., 2018).

Lysine methylation is one of the most important post-translational modifications of histone tails that regulate chromatin organization and gene transcription (Lu et al., 2012). Histone methylation is controlled in cells by histone methyltransferases as G9a, GLP, SET and EZH2, and histone demethyltransferases such as KDM, LSS and JARID (Chowdhury et al., 2011b). Histone lysine demethylases (KDMs) containing the Jumonji-C (JmjC) region, which is dependent on α-KG, just like TET enzymes, are inhibited by 2-HG (Miller et al., 2023). Thus, it is known that histone methylation increases. For example, it has been shown in many studies

that methylation markers of histone (such as H3K27me3, H3K9me3 and H3K4me3) accumulate in IDH mutant cancers (Ceccarelli et al., 2016; Lu et al., 2012).

2.2.4. IDH1 Mutation in Human Glioma

The relationship of IDH mutation with glioma was first revealed by gene expression analysis using sequencing technology in samples taken from 22 glioblastoma patients. Recurrent mutations in IDH1 were seen in 12% of these GBM patients (Parsons et al., 2008). Later, studies found that the IDH mutation was a typical mutation appearing in diffuse low-grade astrocytomas and oligodendrogliomas. IDH mutant gliomas have been shown to have a safer prognosis than IDH-wild-type gliomas (Yan et al., 2009)

In addition, IDH mutations have been found to occur together with prognostically important molecular changes such as ATRX and TP53 mutations, 1p19q codeletion and TERT mutations. (Brat et al., 2015; Eckel-Passow et al., 2015; Reuss et al., 2015). Since IDH mutation, 1p19q codeletion and TERT promoter mutation were common in oligodendrogliomas, IDH mutation, TP53 mutation and ATRX mutation were frequently seen in astrocytomas, and were used to define astrocytomas and oligodendrogliomas until the WHO-CNS5 classification (Reuss, 2023). It is accepted that IDH1/2 mutations trigger the development of gliomas, as they have been shown to develop before disorders such as TP53 mutations or 1p/19q codeletion or the “genome-wide CpG island methylator” phenotype (G-CIMP), which are known to play a role in glioma development (Suzuki et al., 2015).

2.3. Epigenetic Regulation

Spatiotemporal regulation of gene expression in eukaryotic cells, influenced by the structure and organization of DNA, regulates biological processes such as cell fate and status, embryonic development, cell fate and status, and response to disease (Albini et al., 2019). In addition to environmental signals, transcription factors and cofactors being effective in cell fate regulation, epigenetic modifications and non-coding RNAs (ncRNA, miRNA, siRNA and piRNA) are of great importance (He et al., 2020). Therefore, genome-wide analysis of DNA sequence and molecular components is important to understand genome activity and systems biology. Epigenetics is outlined as mitotic and meiotic heritable changes that occur in genome

activity due to environmental factors, without any change in nucleotide sequence (Retis-Resendiz et al., 2021). Epigenetic regulation plays a critical role in important cellular mechanisms such as cell differentiation and growth, gene expression and genome stability (Meissner, 2010; Putiri & Robertson, 2011). While cellular identity can remain stable for a long time by transferring epigenetic states from offspring to offspring, epigenetic signs can be reprogrammed using kind of strategies such as cell fusion, nuclear transfer, and ectopic expression of transcription factors. Recently, pluripotent cells have become an ideal tool in epigenetic research. Its use has become widespread in large projects, such as the ENCODE Project and the US National Research Institutes, and is even used as the basic cell type (Meissner, 2010). The reason why pluripotent cells are a good model is that their epigenetic marks are characteristic, provide information about the possible future potential of differentiated cells, and also allow to examine the relationship between epigenetic modifications and dynamics that occur during differentiation (Meissner, 2010).

3. MATERIALS AND METHODS

3.1. Type of Research

This is an *in vitro* experimental study.

3.2. Place and Time Frame of the Research

All experimental studies were performed at Izmir Biomedicine and Genome Center between 2018-2023.

3.3.Research Materials

3.3.1. Cell lines

The cell lines used to produce the conditioned media and to generate the neural progenitor cells are listed in the table.

Table 1. List of used cells to produce conditioned media and to generate NPCs

Cell Lines	Properties	Supplied From
IHA-IDH1-WT **IHA-IDH1-R132H**	Immortalized Human Astrocytes +Tet ON with IDH1-WT +Tet ON with IDH1-R132H	Gift from Prof. Timothy A. Chan and Sevin Turcan (Turcan et al., 2018)
iPSCs	Induced Pluripotent Stem Cells	Applied Stem Cell #ASE-9202

3.3.2. Chemicals

Chemicals	Vendor	Identifier
Ethanol	Isolab	#920.026.2500
Lipofectamine™ Stem Reagent	Invitrogen by Thermo Fisher Scientific	#STEM00003
Paraformaldehyde	Sigma-Aldrich	#158127-100G
Trpan Blue Solution	Sigma-Aldrich	
SafeView DNA Stain	Genemark	#C118-1
Ribonucleic acid, transfer from baker's yeast	Sigma-Aldrich	#R8508
VECTASHIELD PLUS Antifade Mounting Medium	Vector Laboratories	#H-1900
T4 DNA Ligase	New England BioLabs (NEB)	#M0202L
Quick CIP	New England BioLabs (NEB)	#M0525S
BsmBI-v2	New England BioLabs (NEB)	#R0739S
Q5 High-Fidelity DNA Polymerase	New England BioLabs (NEB)	#M0491L
T4 Polynucleotide Kinase	New England BioLabs (NEB)	#M0201S
100 bp DNA Ladder	New England BioLabs (NEB)	#N3231S
1 kb DNA Ladder	New England BioLabs (NEB)	#N3232S
FuGENE HDTransfection Reagent	Promega	#E2311
Mitomycin-C	Biovision	#2713
Formaldeyhde Solution about 37%	Sigma-Aldrich	#1.04003.2500
2-Mercaptoethanol	Sigma-Aldrich	#M3148
TRI Reagent	Sigma Life Science	#93289-100ml
Dynabeads™ M-280 Sheep Anti-Rabbit IgG	Invitrogen by Thermo Fisher Scientific	#11203D
Alginic acid sodium salt from Brown algea	Sigma-Aldrich	#A1112-100G
BSA	Cell Signaling Technology	#9998S
Deoxynucleotide(dNTP) mix	New England BioLabs (NEB)	#N0447S
Doxycycline Hyclate	Sigma Aldrich	#D9891-5G

3.3.3. Kits

Kits	Vendor	Identifier
ProtoScript^{R} First Strand cDNA Synthesis Kit	New England BioLabs (NEB)	#E6300S
Go Taq^{R} qPCR Master Mix	Promega	#A6001
RNeasy Mini Kit	Qiagen	#74104
Direct-Zol^{TM} RNA MiniPrep Plus	Zymo Research	#R2072
Monarch DNA Gel Extraction Kit	New England BioLabs (NEB)	#T1020S
ChIP DNA Clean & Concentrator	Zymo Research	#D5205
DNA Clean & Concentrator	Zymo Research	#D4033
Nucleospin Plasmid	Macherey-Nagel	#740588.50
QIAMP DNA Mini Kit	Qiagen	#51304
Amaxa P3 Primary Cell 4D-Nucleofector X Kit L	Lonza	#V4XP-3024
NucleoSnap Plasmid Midi	Macherey-Nagel	#740494.50

3.3.4. Solutions

Solutions	Vendor	Identifier
DMEM, High Glucose Medium	Thermo Fisher Scientific, Gibco	#41965-039
Heat Inactivated Fetal Bovine Serum (FBS)	Thermo Fisher Scientific, Gibco	#10500-064
L-Glutamine	Thermo Fisher Scientific, Gibco	#25030024
Mitomycin-C	Biovision	#2713-5
Trypsin-EDTA (0.25%)	Thermo Fisher Scientific, Gibco	#25200056
Penicillin Streptomycin	Thermo Fisher Scientific, Gibco	#151401-122
Knock-Out Serum	Thermo Fisher Scientific, Gibco	#10828-028
DMEM/F-12 Medium	Thermo Fisher Scientific, Gibco	#31331028
Glutamax 100x	Thermo Fisher Scientific, Gibco	#35050
MEM-NEAA	Thermo Fisher Scientific, Gibco	#11140-035
10X PBS	Thermo Fisher Scientific, Gibco	#70011036
D-PBS (Without Ca++ and Mg++)	STEMCELL Technologies	#37350
Matrigel, hESC-Qualified matrix, LDEV-Free	Corning	#354277
0.5M EDTA, pH 8	Invitrogen	#15575-038
Opti-MEM™ Reduced Serum Medium	Gibco	#31985062
Sodium Pyruvate	Gibco	
mTESR Basal Medium	STEMCELL Technologies	#85851
mTESR 5X Supplement	STEMCELL Technologies	#85852
STEMdiff™ SMADi Neural Induction Kit	STEMCELL Technologies	#08581
STEMdiff™ Neural Progenitor Medium	STEMCELL Technologies	#05833
STEMdiff™ Neural Progenitor Freezing Medium	STEMCELL Technologies	#05838
Gentle Cell dissociation Reagent	STEMCELL Technologies	#07174
Dispase in DMEM/F-12	STEMCELL Technologies	#07923
Human FGF-Basic	PeproTech	#100-18B-50
Human EGF	PeproTech	# AF-100-15
y-27632 (ROCK Inhibitor)	Sigma-Aldrich	#Y0503
D-PBS (Without Ca++ and Mg++)	STEMCELL Technologies	#37350
Accutase	STEMCELL Technologies	#07920

3.3.5. Antibodies

Antibodies	Vendor	Identifier
Nestin (10C2) Mouse mAb, IF	Cell Signaling	#33475
SOX1 Antibody pAb, IF	Cell Signaling	#4194
Sox2 (D6D9) XP Rabbit mAb, IF	Cell Signaling	#3579
Oct4 (D7057) Mouse mAb, IF	Cell Signaling	#75463
Pax6 (D3A9V) Rabbit mAb, IF	Cell Signaling	#60433
Goat Anti-Mouse IgG H&L (Alexa Fluor 488), IF	Abcam	#Ab150113
Goat Anti-Rabbit IgG H&L (Alexa Fluor 555), IF	Abcam	#Ab150078
Hoechst, IF		
Anti-trimethyl-Histone H3(Lys4) Antibody, ChIP	Sigma-Aldrich	#ab8895
Histone H3K27ac Antibody (pAb), ChIP	Active Motif	#39133
Normal Rabbit IgG	Cell Signaling	#2729
5-Hydroxymethylcytosine antibody	Active Motif	#39791
AbFlex 5-methylcytosine antibody	Active Motif	# 91187
Cell Health Assay Kit	Cell Signaling	#13837

3.3.6. Equipments

Equipments	Vendor
Refrigerator (+4^{0}C)	Bosch, Stuttgart, Germany
Refrigerator (-20^{0}C)	Bosch, Stuttgart, Germany
-80^{0}C freezer	Eppendorf, Hamburg, Germany
Centrifuge 5810R	Eppendorf, Hamburg, Germany
mySPIN^{TM} mini centrifuge	Thermo Fisher Scientific, Waltham, MA,USA
Vortex	Thermo Fisher Scientific, Waltham, MA,USA
NanoDrop 2000	Thermo Fisher Scientific, Waltham, MA,USA
SimplyApp Thermal Cycler	Applied Biosystems, Foster City, CA, USA
Light Cycler 480 II	Roche Applied Science, Mannheim, Germany
Power Supply Unit for Electrophoresis	Bio-Rad, Hercules, CA, USA
Incubator	Thermo Fisher Scientific, Waltham, MA, USA
Water Bath	Nüve, Ankara, Turkey
Fluorescence Microscopy	Olympus Life Science, Waltham, MA, USA
Confocal Microscopy, LSM 880	Zeiss, Germany
Light Microscopy	Olympus Life Science, Waltham, MA, USA
Horizontal Laminar Airflow Cabinet	Thermo Fisher Scientific, Waltham, MA, USA
Gel Doc^{TM} XR+ with Image Lab^{TM} Software	Bio-Rad, Hercules, CA, USA
Bioruptor Sonicator	Diagenode, Liege, Belgium
BD LSRFortessa^{TM} Flow Cytometer	BD Biosciences, San Jose, CA
Qubit 3 florometer	Thermo Fisher, Waltham, MA, USA, #Q33216
2100 Bioanalyser	Agilent, ABD, #G2939BA

3.4. Variables of the Study

Dependent variables in this study;

Expression levels of MEOX2, JMJD2A, L1-CAM, TERT and ID1 in NPCs cultured in 3D environment with IHA conditioned medium

Cell growth of NPCs cultured in 3D environment with IHA conditioned medium

H3K4me3 and H3K27ac binding site in NPCs cultured in 3D environment with IHA conditioned medium

ID1 and MYC expression levels in NPCs nucleofected with pLVahU6-sgRNAxhUbC-dCas9-KRAB-T2a-GFP plasmids

Independent variables in this study;

The presence of IDH1 expression in iPSC-derived NPCs and IHA cells.

3.5. Tool for Data Collection

3.5.1. Maintenance of IPSCs

Table 2. Media contents used in Feeder-Dependent Culture of hiPSCs and media contents used for the maintenance of hiPSCs

Name of used media for cell culture	Preparing Media
Human Embryonic Stem Cell (hESC) Media (200 ml)	156 ml DMEM/F-12 Medium
	40 ml Knockout-Serum
	3 ml HEPES (15mM Last Concentration)
	364 µl 2-Mercaptoethanol (55µM stock)
	2 ml MEM-NEAA (100X)
MEF Media (50 ml)	43 ml High-Glucose DMEM
	5ml FBS
	0.5 ml Penicillin/Streptomycin
	0.5 ml Glutamax
	0.5 ml Sodium Pyruvate (100X)
	0.5 ml MEM-NEAA (Non-essential amino acids, 100X)
mTeSR Media (50ml)	40 ml mTeSR Basal Media
	10 ml 5X mTeSR Supplement

Mouse Embryonic Fibroblast (MEF) cell line was used as feeder cell for better growth after IPSCs cells were removed from liquid nitrogen. A 10 cm plate was coated with 0.1% gelatin and put in incubator for at least 30 minutes. MEF media were prepared for MEF cells (Table 2). MEF cells were removed from liquid nitrogen and quickly thawed in a 37 ºC water bath. It was transferred into 15 ml conical tube containing 10ml MEF medium with the help of a pipette. It was gently pipetted and centrifuged for 2 minutes at 2400 rpm. The supernatant was withdrawn with the help of vacuum, MEF medium was added onto the cells, pipetted and transferred to a gelatin-coated 10 cm plate. After checking whether it was distributed homogeneously or not, with the help of a microscope, it was placed in an incubator at 37 ºC with 5% CO_2. When the cell density reached 85-90% in the cell culture dish, it was treated with Mitomycin-C to a last concentration of 10 µg/ml for 3 hours at 37 ºC and 5% CO_2. The 6-well plate was coated with 0.1% gelatin and incubated at 37 ºC 5% CO_2 for at least 30 minutes. After Mitomycin-C treatment, the medium on the cells was removed. Then, 2 ml trypsin was added and incubated for 2-3 minutes at 37 ºC, 5% CO_2. After it was seen through the microscope that the cells were detached, 4 ml MEF medium was added and transferred to a 15 ml conical tube and centrifuged for 2 minutes at 2400 rpm. The supernatant was removed and MEF medium was added onto the cells and gently pipetted until a homogeneous distribution. Enough cells (approximately $3x10^6$ cells) to cover 80-90% of the wells of the 6-well plate were added to each well and incubation of the cells was carried out at 37 °C in an incubator with 5% CO_2. This is because the IPSCs should not be in contact with the plastic cell culture dish. Colonies of IPSCs must form on MEF cells. The next day, firstly, the density of MEF cells and whether they were spread homogeneously into the wells were checked. After checking the cells, HESC medium was prepared (Table 2). IPS cells were removed from liquid nitrogen and quickly thawed at room temperature. It was poured into a conical tube containing 10 ml of HESC medium and centrifuged for 2 minutes at 100 g. Meanwhile, HESC medium was added into the 15 ml conical tube according to the number of wells in which IPS cells would be seeded, and Y-compound was added to a final concentration of 10 µg/ml (Y-compound added only on the day when IPS cells opened). After centrifugation, the supernatant on the IPS cells was carefully removed by decanting. HESC medium containing Y-compound was added onto the IPS cells and slowly pipetted several times using a serological pipette without disturbing the colony structure. The medium on the MEFs was removed and IPS cells were transferred onto the MEFs with a serological pipette. Then, the cells were checked under the microscope and incubated at 37 ºC

and 5 % CO_2. HESC medium was changed and incubated until the cell colonies reached a sufficient size (Figure 6). After the colonies reached a sufficient size, IPS cells were removed from MEF cells and seeded on matrigel. To transfer the IPS cell colonies to matrigel-coated plates, the medium on the IPS cell colonies and MEFs was withdrawn. The well was washed three times with DMEM/F12 medium and 1 ml of dispase in DMEM/F12 was added to the well and incubated for 5 minutes at 37 °C and 5% CO_2. Dispase was withdrawn with the help of a pipette and the well was washed 3 times with DMEM/F12. 1 ml mTesR complete medium was added to each well (Table 2). Since the IPS cell colonies were visible to the naked eye, the areas where the colonies were located were excavated with the help of a 2 ml serological pipette (care was taken to ensure that as few MEF cells as possible were detected). Then, the cells were removed from the wells into a 15 ml conical tube and centrifuged for 2 minutes at 100 g. The supernatant was discarded and 6 ml DMEM/F12 medium was added onto the cells and centrifuged again under the same conditions. Meanwhile, mTesR complete medium (1.5 ml for each well) suitable for the number of wells to be planted was transferred to a 15 ml conical tube and Y-compound was added to a final concentration of 10 µg/ml (Y-compound was used only when passing it over the MEF to the matrigel-coated plate. It was not used in subsequent passages). After centrifugation, the supernatant was discarded and mTesR complete medium with Y-compound with a last concentration of 10 µg/ml was added onto the cells, and the cells were gently pipetted using a serological pipette to prevent the colonies from dispersing. Medium was drawn from the 6-well plate covered with matrigel, and IPS cells were evenly distributed into the wells of this 6-well plate covered with matrigel.

The mTseR complete medium was changed every day until the cell colonies reached a sufficient size and incubation was provided at 37 °C in an incubator with 5% CO_2 (Figure 6).

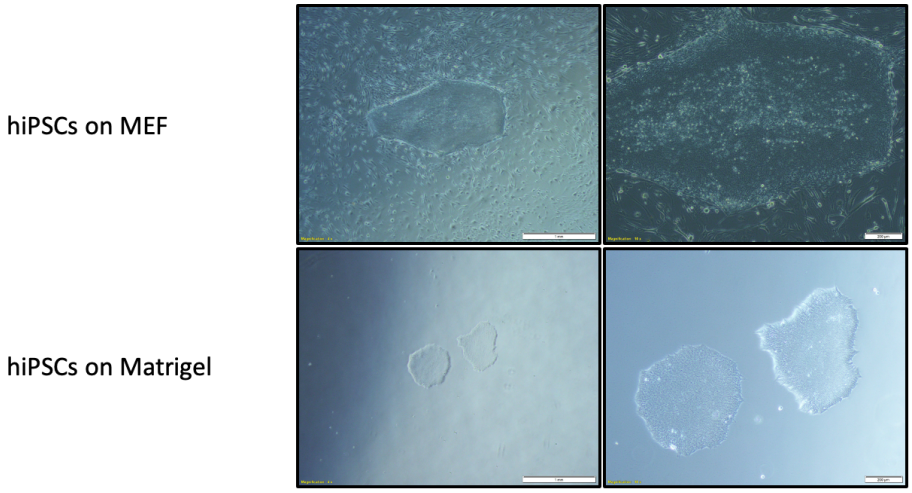

Figure 6. Figure shows iPSC colony on MEF-coated plate and iPSC colony on matrigel-coated plate.

3.5.2. Differentiation of hiPSCs into Neural Progenitor Cells (NPCs)

Table 3. Contents of media used for the differentiation and maintenance of hiPSCs into NPCs

Name of used media for cell culture	Preparing Media
Neural Induction Medium	50 ml STEMdiff™ Neural Induction Medium
	100 µl STEMdiff™ SMADi Neural Induction Supplement
Neural Progenitor Medium	49 ml STEMdiff™ Neural Progenitor Basal Medium
	1 ml Supplement A (50X)
	50 µl Supplement B (1000X)

"Generation and Culture of Neural Progenitor Cells using the StemdiffTM Neural System" Monolayer Culture protocol from STEMCELL Technologies was used to differentiate iPSCs into Neural Progenitor Cells (NPCs). STEMdiff Neural Induction Medium, stored at -20 C, was thawed by keeping it at +4 C overnight. It was added to 50 ml conical tubes as 50 and 25 ml and stored at -20 C. STEMdiff was aliquoted according to the medium prepared and stored in SMADi Neural Induction Supplement and stored at -20 C. While preparing each

Neural Induction complete medium, this process was done to prevent the entire medium and SMADi supplement from constantly freezing and thawing. After it was seen under the microscope that the healthy iPS cell colonies had reached a sufficient size, two wells of the Tissue culture-treated 6-well plate were covered with matrigel (plate coating with matrigel is explained in detail in the Method iPSC Culture section). Meanwhile, STEMdiff Neural Induction Medium and STEMdiff SMADi Neural Induction Supplement were mixed in accordance with the STEMdiff Neural Induction Kit (Table 3), and ROCK Inhibitor Y-27632 was added to the medium to be used on the first day of the differentiation protocol, with a final concentration of 10 μM.

After the tissue culture-treated 6-well plate was covered with matrigel, the wells containing iPSC colonies were washed with 2 ml of sterile PBS and the PBS was aspirated. 1 ml Gentle Cell Dissociation Reagent was added to each well and iPS cells were removed by incubating for 8-10 minutes at 37 C, 5% CO2. All cells were removed by pipetting 3-5 times with the help of a pipette. It was transferred to a 15 ml conical tube and gently pipetted until the cell aggregates were completely dispersed and the cells became single. The wells from which iPSCs were taken were washed with DMEM/F-12 and transferred to the conical tube containing single cell suspension. Cells were counted with the help of Trypan. After counting, cells were centrifuged at 300 × g for 5 min. STEMdiff Neural Induction Medium + SMADi + ROCK Inhibitor Y-27632 was also resuspended to a final concentration of $1x10^6$ cells/ml and 2 ml of cell + medium solution was added to each well of the matrigel-coated 6-well plate. Cells checked under a microscope were incubated at 37 ºC and 5% CO_2. Mediums were changed every day with fresh STEMdiff Neural Induction Medium+ SMADi. When ready to be passaged, the 6-well plate was coated with matrigel. Medium was withdrawn from the cells and 1 ml of Accutase was added to each well containing the cells. It was incubated for 5 minutes at 37 ºC, 5% CO_2. Shielded cells were suspended with a 1 ml pipettor and then 5 ml DMEM/F-12 was added and transferred to a 15 ml conical tube. It was centrifuged at 300 x g for 5 minutes. They were counted with the help of Trypan Blue and a hemocytometer, and $1.5 x10^6$ cells were seeded in each well with 2 ml STEMdiff Neural Induction Medium + SMADi and incubated at 37 ºC 5% CO_2. The medium was replaced with fresh STEMdiff Neural Induction Medium+ SMADi every day. This process was repeated until the cells reached the 3rd passage. STEMdiff Neural Progenitor Basal Medium, Supplement A and Supplement B were removed from -20 ºC and allowed to thaw at +4 ºC for 1 night. STEMdiff Neural Progenitor Basal Medium was

aliquoted as 50 ml into 50 ml conical tubes, 50X Supplement A as 1 ml into 1.5 ml microcentrifuge tubes, and 1000X Supplement B as 50 µl into 200 µl PCR tubes, It was stored at -20 ºC. When NPCs reached Passage 3, the 6-well plate was covered with matrigel and Neural Progenitor Medium was prepared (Table 3). The medium on the cells was removed. 1 ml accutase was added to each well. It was incubated at 37 ºC, 5% CO_2 for 5 minutes. After the cells were suspended by pipetting with the help of a 1 ml pipettor, 5 ml DMEM/F-12 medium was added and transferred to a 15 ml conical tube and centrifuged at 300 x g for 5 minutes. The cells were counted with the help of trypan blue and a hemocytometer, and $1x10^6$ cells were planted in the wells with 2 ml Neural progenitor medium and incubated at 37 ºC 5% CO_2. The medium was changed with fresh medium every day.

3.5.3. Characterization of iPSC and iPSC-derived NPC

Sterile glass coverslips were placed into the 24-well plate and covered with matrigel.

During the preparation of cells;

The mTesR complete medium on the iPSC colonies was withdrawn and 1 ml of dispase in DMEM/F-12 was added and incubated for 5 minutes at 37 ºC and 5% CO_2. After removing the dispase in DMEM/F-12, cells were washed 3 times with DMEM/F-12 medium. By adding 1 ml of mTesR complete medium, iPSC colonies were scraped from the well with the help of a 2 ml serological pipette and transferred to a 15 ml conical tube. After centrifugation at 100 g for 2 minutes, the supernatant was discarded and 6 ml DMEM/F-12 medium was added onto the cells and centrifuged again at 100 g for 2 minutes. The supernatant was discarded again and gently pipetted with the help of a serological pipette in mTesR complete medium and transferred to a 24 well plate containing matrigel-coated glass coverslips. It was incubated at 37 ºC and 5% CO_2. Mediums were changed every day until iPS cell colonies grew.

Neural Progenitor Medium was removed from the NPCs and 1 ml accutase was added and incubated at 37 ºC and 5% CO_2 for 5 minutes. After the cells are removed, they were gently pipetted using a 1 ml pipette until the cells were completely removed. Collecting into tube with 5ml DMEM/F-12 medium and centrifuged at 300 g for 5 minutes. The supernatant was discarded and the cells were added to Neural Progenitor Medium, gently pipetted using a pipette, and transferred to the wells of a 24-well plate with matrigel-coated glass coverslips. It

was placed in an incubator at 37 ºC and 5% CO_2. Mediums were changed every day until NPCs reached 50-70% confluency.

At the fixation step;

The medium on iPSCs and NPCs was removed and the cells were washed once with ice cold 1X PBS. 4% paraformaldehyde (PFA) was added onto the cells and incubated for 15 minutes at RT with slow shaking in the shaker. After removing the fixative from the cells, the cells were washed 3 times with PBS to remove the fixative. In each wash, ice cold 1X PBS was added to the cells and shaken slowly in a shaker for 5 minutes at room temperature.

In the permeabilization step;

After the final wash with PBS, ice cold 0.1% Triton-X in PBS was slowly added onto the cells and shaken slowly in a shaker at RT. The cells were washed 3 times with ice cold 1X PBS to completely remove the permeabilization solution.

In the blocking step;

PBS was withdrawn from the cells after the last washing step was completed. Blocking buffer (1% BSA in PBST (PBS with 0.1% Tween-20) was added and the cells were shaken slowly in a shaker for 1 hour at RT.

In the Primary antibody Staining step;

Antibodies were added to the Blocking buffer.

For iPS cells; Blocking solution and Mouse OCT4 (1:200) antibody were added into 1 1.5 ml microcentrifuge tube. Three separate 1.5 ml microcentrifuge tubes were prepared for NPCs. SOX1 (1:400) and OCT4 (1:200) in tube 1 with blocking buffer; SOX2 (1:400) and OCT4 (1:200) into Tube 2; PAX6 (1:200) and NESTIN (1:1500) were added to the 3rd tube. After adding the antibodies prepared with blocking buffer, the cells were incubated for 2 hours at RT in a dark environment by shaking slowly in a shaker. After the primary antibody step, the cells were washed 3 times with ice cold 1X PBS for 5 minutes each at room temperature by shaking slowly in a shaker to remove antibodies.

For the secondary antibody staining step, blocking buffers and secondary antibodies were added first. For iPSCs, Goat anti-mouse conjugated to Alexa 488 (1:500) was used. Goat anti-rabbit conjugated to Alexa 555 (1:500) and Goat anti-mouse conjugated to Alexa 488 (1:500) antibodies were added to the blocking buffer for NPCs. Cells were incubated in secondary antibody solutions for 1 hour at RT and in the dark, gently shaking in a shaker. After incubation, to remove secondary antibody from the cells, they were washed 3 times with ice cold 1X PBS

for 5 minutes each, gently shaking in a shaker. Hoechst (1:1000) was added to ice cold 1X PBS for the counterstaining step. After the washing step, Hoechst solution was added to the cells and shaken slowly in the shaker for 3 minutes in the dark and at room temperature. Hoechst solution was removed and the cells were washed once with ice cold 1X PBS.

For each coverslip, 5 µl of Mounting medium was dropped onto the slides. The coverslips were removed with the help of tweezers, and the tip of the coverslip was lightly touched to the napkin to remove the liquid on it, and the coverslip was left on the mounting medium so that the cells were on the mounting medium. She applied nail polish around the coverslips to prevent them from slipping. It was stored in the dark at +4 C until images were taken.

3.5.4. Production of Immortalize Human Astrocyte (IHA)-Conditioned Medium

The Immortalized Human Astrocyte (IHA) we use is Dr. With the help of Şevin Turcan, Prof. It is a gift from Timothy Chan. E6/E7 and hTERT independent retroviral infections were established by Sonoda and colleagues to create immortalized Human Astrocytes (Sonoda et al., 2001). Later, Prof Chan and colleagues modified these cells to express IDH1-WT and IDH1-R132H by induction with doxycycline. To ensure the expression of IDH1-WT and IDH1-R132H, IHAs were first infected with pLVX-Tet-On retrovirus, selected with 800 µg/ml G418. Then, these cells were individually infected with the retroviruses: empty pRetroX-hygro for the control group, pRetroX-hygro containing the IDH1-WT coding sequence for wild-type IDH1 expression, and pRetroX-hygro containing the IDH1-R132H coding sequence for mutant IDH1 expression. Selected with 500ug/ml hygromycin (Turcan et al., 2018) IHA-Empty cells contain the empty pRETROx-hygro vector.

First, frozen IHA-IDH1-WT and IDH-IDH1-R132H cells were opened to produce IHA-IDH1-WT and IHA-IDH1-R132H conditioned media. IHA-Empty cells were used for the control group. 10 ml of DMEM High Glucose medium supplemented with 10% FBS and 1% Pen/Strep was added to three separate 15 ml conical tubes and kept in a 37 ºC water bath to warm up. IHA-Empty, IHA-IDH1-WT and IDH-IDH1-R132H cells were removed from liquid nitrogen and quickly thawed in a 37 °C water bath and added separately to conical tubes containing 15 ml medium with a 1 ml pipette. After centrifugation for 3 minutes at 1800 rpm, the supernatant was discarded. 8 ml of High Glucose medium was added to the cell pellets, gently pipetted until the cells were homogeneously distributed in the medium and transferred

to 10 mm plates, incubated at 37 ºC, 5% CO_2. was done. IHA-Empty, IHA-IDH1-WT and IDH-IDH1-R132H cells were opened before being induced with doxycycline and then grown in doxycycline-free medium for 1 passage to ensure healthy growth. After the cells reached 80-90% density, the medium on the cells was removed, then trypsin was added and incubated for 5 minutes. After it was seen through the microscope that all the cells were removed, 4 ml of medium was added to inactivate the trypsin and they were pipetted and transferred to a 15 ml conical tube. Centrifugation was performed for 3 minutes at 1800 rpm. The supernatants were discarded and doxycycline medium was added to the cell pellet with a final concentration of 1µg/ml. They were pipetted and transferred to 10 mm plates and incubated at 37 ºC and 5% CO_2. Cells were passaged when they reached 80-90% density. Before IHA-IDH1-WT and IDH-IDH1-R132H conditioned media were taken, the cells were grown in doxycycline medium for at least two passages and their media were not stored. Before taking the IHA-IDH1-WT and IDH-IDH1-R132H conditioned media, it was checked by Western blot whether wild-type IDH1 and mutant IDH1 were produced in IHA-IDH1-WT and IDH-IDH1-R132H cells, respectively. Proteins isolated from doxycycline-induced IHA-Empty cells were used as controls. After the control, the medium on the doxycycline-induced cells was removed at each passage and transferred to a 50 ml conical tube through a 0.45 µm filter and stored at -20 ºC until use (Figure 7).

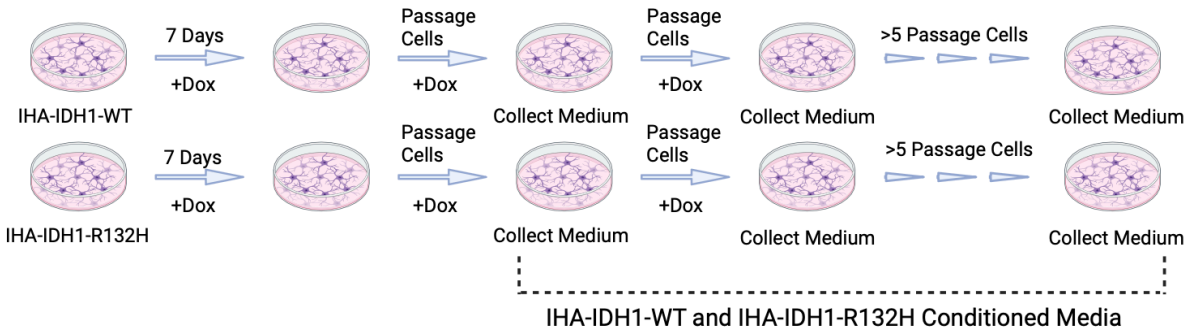

Figure 7. Schematic representation of IHA-IDH1-WT and IHA-IDH1-R132H conditioned media production

3.5.5. NPC-Alginate Bead Preparation

Before starting to create 3D culture with alginate, 2% alginate solution was prepared with ddH_2O and autoclaved. After autoclaving, it was allowed to cool at RT and stored at +4 ºC.

When the density of NPCs grown on a 10 mm plate reached 85-90%, 2 ml accutase was added and incubated for 4-5 minutes at 37 ºC and 5% CO_2. After checking with a light microscope that the cells had lifted off the plate, 8 ml DMEM/F12 medium was added to the plate. By carefully pipetting, the cells were transferred to a 50 ml conical tube. For easy counting of cells with a hemocytometer, cell density was reduced by adding DMEM/F-12 medium to the tube. It was carefully pipetted until becoming homogeneous. Tryphan Blue was used when counting with a hemocytometer. After the cells were counted, the calculation was made. A 50 ml syringe with a 21G-1-1/2 needle was used to create NPC-alginate beads. A drop of 10 µl of solution falls from the needle every second. Each NPC-alginate bead was calculated to contain approximately 2500 cells. That is, 1 ml of cell-1% alginate solution contains 250,000 cells. For this purpose, after the counting process, the amount of alginate-Neural Progenitor medium solution to be used was decided according to the total amount of cells. The 2% alginate solution was reduced to 1% with Neural Progenitor Medium. On the other hand, 15 ml of 100mM $CaCl_2$ was added to 10 cm clean plates. The cells were centrifuged for 5 minutes at 300g at room temperature, the supernatant was discarded and carefully pipetted in 1% alginate-medium solution until a homogeneous mixture was obtained. It was then transferred to a 50 ml syringe. By gravity, 1% alginate solution from the needle was allowed to drip onto the plate containing $CaCl_2$. The syringe was gently rotated on the plate to prevent the drops from overlapping. After the 1% alginate solution in the syringe was finished, the cells were incubated in the hood at RT for 15 minutes to polymerize. Afterwards, the $CaCl_2$ solution was slowly removed with a 1000 µl pipette without damaging the formed beads. To completely remove $CaCl_2$ from the environment, DMEM/F-12 was added to the cell culture containers containing the beads and incubated at RT for 5 minutes, and DMEM/F-12 was slowly withdrawn again with the help of a 1000µl pipette. This washing process was applied twice to completely remove $CaCl_2$. Then, Neural Progenitor Medium was added to the ready-made NPC-alginate beads and incubated at 37 ºC and 5% CO_2 (Figure 8).

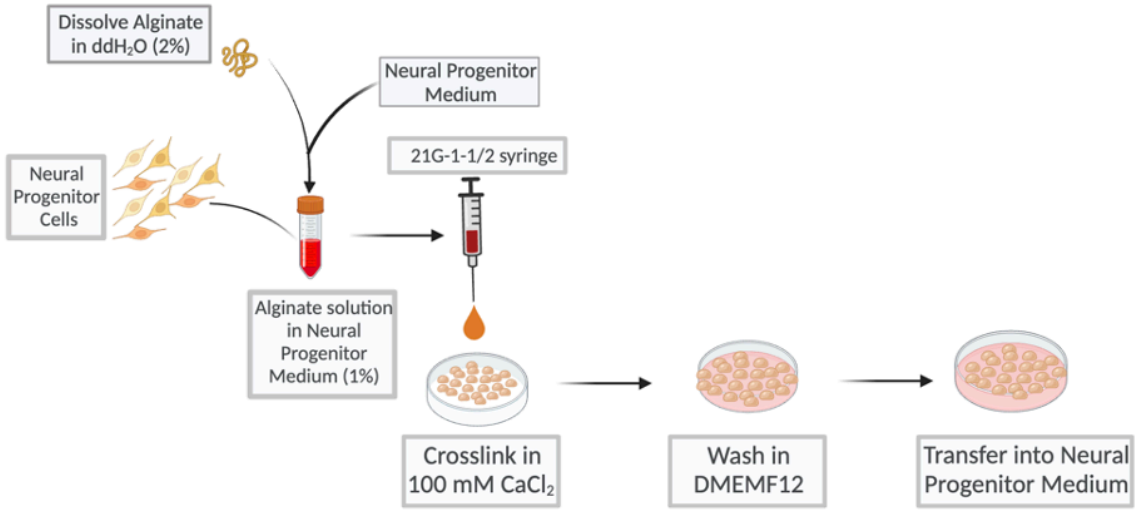

Figure 8. Schematic illustration of NPC-Alginate beads preparation

NPC-Alginate beads were incubated for 24 hours. Since there were 5 different conditions, 5 separate cell plates filled with alginate beads were prepared for each repetition. 5 different experimental conditions prepared are shown in the Table 4.

Table 4. Prepared 5 experimental conditions: NPC-Control-Day 0, NPC-IDH1_WT-Day 14, NPC-IDH1_R132H-Day 14, NPC-IDH1_WT-Day 17 and NPC-IDH1_R132H-Day 17.

Conditions	Preparation
NPC-Control-Day0	After the cell alginate beads were prepared, they were incubated for 24 hours in neural progenitor medium at 37 °C and 5% CO_2.
NPC-IDH1_WT-Day14	On day 0, Neural Progenitor medium was carefully removed from the NPC-alginate beads without damaging the beads, and IHA-IDH1-WT conditioned medium was added instead. 5 ml of fresh IHA-IDH1-WT conditioned medium was added every 2 days for 14 days.
NPC-IDH1_R132H-Day14	On Day 0, Neural Progenitor medium was carefully removed from the NPC-Alginate beads with a pipette and replaced with IHA-IDH1-R132H conditioned medium. 5 ml of fresh IHA-IDH1-R132H conditioned medium was added every 2 days for 14 days.
NPC-IDH1_WT-Day17	IHA-IDH1-WT medium was removed from the NPC-Alginate beads that were exposed to IHA-IDH1-WT medium for the 14th day, and Neural Progenitor Medium was added instead. NPC-Alginate beads were incubated with Neural Progenitor medium for 3 days.
NPC-IDH1_R132H-Day17	IHA-IDH1-R132H medium was carefully removed from the NPC-Alginate beads, which were incubated in IHA-IDH1-R132H medium for the 14th day, and Neural Progenitor Medium was replaced. Cells were maintained with Neural Progenitor medium for 3 days.

3.5.6. Calcein and PI staining- cell health Assay

Calcein/PI solution was prepared by mixing Calcein at 0.25 µl 4mM concentration and Propodium Iodide (PI) stains at 10 µl 150 µM concentration with 250 µl of 1X PBS for each condition. Beads taken from 5 different experimental conditions on Day 0, Day 14 and Day 17 were carefully transferred to glass-bottom plates. After Calcein/PI solution was put on the beads, it was kept in the dark at 37 °C for 30 minutes and images were taken with a Confocal microscope. Settings established during analysis; Extitation/emission: 490/520 for live cells, Extitation/emission setting of 535/620 for dead cells

3.5.7. Immunofluorescence Staining of NPCs isolated from alginate beads

Immunofluorescence staining was performed for our 5 different experimental conditions. First, a small amount of NPC-alginate beads from all conditions were taken and removed from the alginate cells with 0.5 M EDTA. Then, these cells were seeded individually on matrigel-coated glass-bottom plates. They were incubated in their own media (Neural Progenitor medium (day 0 and day 17) or IHA-IDH1-WT (day 14) or IHA-IDH1-R132H (day 14) conditioned media) at 37 °C, 5% CO_2 for one day. then stained as detailed in the immunofluorescence staining section.

3.5.8. RNA isolation

In 5 different experimental conditions, firstly, 4 ml of 0.5 M ethylenediaminetetraacetic acid (EDTA) was added to the culture medium containing NPC-alginate beads and the alginate polymer was broken down by Ca^{+2} chelation. After the alginate was observed to be completely dissolved, the solution in the plates was transferred to a 50 ml conical tube. To reduce the effect of EDTA, 10 ml DMEM/F-12 medium was added to the cells and the cells were sedimented by centrifugation at 300g for 5 minutes. To completely get rid of the remaining alginate, the cells were washed by adding 10 ml DMEM/F-12 medium and sedimented again by centrifugation at 300g for 5 minutes. The supernatant was completely removed from the cells, and the cells were quickly dissolved in 350 µl of TRI reagent and stored at -80 ^{0}C until RNA isolation. Samples removed from -80 ^{0}C were kept on ice until thawed. Direct-zol RNA MiniPrep Plus Kit was

used to isolate RNAs from each experimental condition. The quantity and quality of RNA samples of the conditions were measured with the Nanodrop device.

3.5.8.1.Quantitative Real Time PCR

cDNA was synthesized from the RNAs using the ProtoScriptR First Strand cDNA Synthesis Kit. RT-qPCR was performed using GoTaqR qPCR Master Mix (Promega, Cat No: A6001) and Real-Time PCR Detection System. The cycling program is given in Table 5. Primers used are listed in Table 5. The housekeeping gene GAPDH (glyceraldehyde-3-phosphate dehydrogenase) was used to normalize changes in specific gene expression. In the studies performed, melting curves were also checked to check the specificity of PCR amplifications. Relative quantification of mRNA expression levels was calculated by the ΔΔCt method (Livak & Schmittgen, 2001).

Table 5. RT-qPCR primers designed for gene expression analysis

Primer Name	Forward Primer Sequence	Reverse Primer Sequence
L1CAM	ACGAGGGATGGTGTCCACTTCAAA	TTATTGCTGGCAAAGCAGCGGTAG
MEOX2	GTCAGAAGTCAACAGCAAACCCAG	CACATTCACCAGTTCCTTTTCCCGAGCC
JMJD2A	CCTTTGCTTGGCACACTGAAGACA	TTCCATGCTCAGGTGGAACAGAGT
TERT	GTATGGCTGCTGGGTGAACT	GAGACTGGCTCTGATGGAGG
ID1	GCTCCGCACTCTCATTCCAC	CTGGCTGAAACAGAATGGGC

3.5.8.2.RNA-Seq

3.5.8.2.1. Transcriptome analysis with RNA-seq

Library preparation and sequencing

Qubit 3 fluorometer and 2100 Bioanalyzer were used during quality control procedures for total RNA samples isolated from 5 different experimental conditions studied in 2 replicates. Illumina Stranded mRNA Prep kit1 was used to prepare library for each RNA sample. Illumina NovaSeq 6000 new generation sequencing platform was used in the sequencing study. In this step, approximately 30 million paired-end reads with a length of 150 bp were planned for each sample (Table 6).

Bioinformatics analyzes

After sequencing, the FASTQC tool was used to quality control the resulting read data.

During the sequencing process, low-quality base reads and possible contaminations of adapter-index in the raw read data were removed from the reads with aid of the Trimmomatic (v0.39) tool (Bolger et al., 2014) to prevent them from causing bias in later analyses.

The sequences were then aligned to the selected genome (Homo Sapiens GRCh38.p13) using the HISAT2 (v2.1.0) tool (Kim et al., 2019). After alignment, read counts were calculated for each transcript and then normalized to the total read count. After the alignment, gene, exon and transcript information was obtained using the GENCODE 40 data set. Transcriptome read numbers were determined using the Subread tool (Liao et al., 2019). The edgeR R package (Robinson et al., 2009) was used to filter and normalize read counts for each gene as well as to find genes whose expression changed between the generated groups (Differentially expressed genes). Then, TopGO package (Alexa & Maintainer, 2021)and Kolmogorov-Smirnov (KS) statistical test to perform gene ontology analysis; clusterProfiler package (Yu et al., 2012) for path analysis; R scripts were used in data visualization applications to perform statistical comparison studies within and between groups.

Table 6. Read counts and genome alignment statistics of RNA-seq data.

Sample	Group	Total Reads	Mapped Reads	Unmapped Reads
NPC-Control-dAY0-1	NPC-Control-dAY0	93768348	92714488	1053860
NPC-Control-dAY0-2	NPC-Control-dAY0	70879144	70631240	247904
NPC-IDH1_WT-Day14-1	NPC-IDH1_WT-Day14	74794350	74590353	204097
NPC-IDH1_WT-Day14-2	NPC-IDH1_WT-Day14	73679944	73449807	230137
NPC-IDH1_R132H-Day14-1	NPC-IDH1_R132H-Day14	78806562	78549106	257456
NPC-IDH1_R132H-Day14-2	NPC-IDH1_R132H-Day14	74497228	74193941	303287
NPC-IDH1_WT-Day17-1	NPC-IDH1_WT-Day17	87516332	87218420	297912
NPC-IDH1_WT-Day17-2	NPC-IDH1_WT-Day17	63490256	63239081	251175
NPC-IDH1_R132H-Day17-1	NPC-IDH1_R132H-Day17	84588478	84191406	397072
NPC-IDH1_R132H-Day17-2	NPC-IDH1_R132H-Day17	65610956	65410126	200830

3.5.9. Chromatin Innumoprecipitation (ChIP) protocol

NPC-alginate 3D culture has been described previously. NPC-alginate 3D cultures prepared for 5 different experimental conditions at 3 different time points were prepared for the CHIP protocol on their own time. The same protocol was applied for all conditions.

EDTA (0.5 M, 4 ml) was placed on the NPC-alginate beads in the 10 cm plate and left at RT for 3-4 minutes to ensure the hydrogel structure of the alginate was broken down. To ensure that the alginate hydrogel was completely separated from the cells, gentle pipetting was performed with the help of a 10 ml serological pipette, the entire solution was collected in a 50 ml conical tube, and the cells were precipitated at 300 g for 5 minutes. The supernatant was

vacuumed and 5 ml of 1% formaldehyde parofix solution was quickly added onto the cells. It was incubated with shaking at RT for 10 minutes.

After incubation, 250 µl of 2.5M glycine (final concentration will be 0.125M) was added to stop the fixation and incubated at RT for 5 minutes on a stirrer. Then, it was centrifuged for 5 minutes at 1500 rpm, +4 ºC. 5 ml of cold 1X PBS-protease inhibitor cocktail (PBS-PIC) mixture was added to the pellet for the washing step, pipetted until the pellet dispersed, and then centrifuged at 1500 rpm at +4 ºC for 5 minutes. The washing step was repeated. The supernatant was withdrawn and cold lysis buffer solution containing 1 ml of protease inhibitor cocktail was added to the pellet, pipetted until homogeneous, and incubated on ice for 5 minutes. Since the cells were taken from cell culture dishes on separate days, at this stage the cells were stored in lysis buffer solution at -80 ºC.

After our 5 experimental conditions were completed, all samples were removed from -80 ºC and allowed to thaw on ice. After they were completely melted, pipetting was performed and first, 50 µl of each sample that was not sonicated was taken and placed in separate 1.5 ml microcentrifuge tubes and these samples were kept on ice. The remaining samples were transferred separately to glass tubes suitable for sonication (Covaris, milliTUBE 1 ml AFAFiber, #520130). Covaris S220 device was used for sonication (Table 7).

Table 7. Sonication Conditions for 5 different experimental conditions

Treatment	Peak Power	140.0	12 cycles
	Duty Factor	15.0	
	Cycles/Burst	200	
	Delay		

After the sonication process, to check the sonication efficiency, 50 µl of samples were taken from each of the 5 experimental groups and placed in separate microcentrifuge tubes and centrifuged for 10 minutes at $14x10^3$ rpm set at 4 °C. Supernatants were withdrawn from the pellets and placed new tubes and kept on ice. The remaining samples were stored in sonication tubes at +4 ºC.

Reverse of crosslink for input fraction

150 ul TE buffer was added onto 50 µl separated unsonicated and sonicated samples. Then, 4 µl of 10mg/ml RNase A (final concentration 0.2mg/ml) was added and incubated at 37°C for 30 minutes. Next, SDS was added to a final concentration of 1%, NaCl to 100mM, and Proteinase K to 200 µg/ml. It was incubated at 55°C for 2.5 hours and at 65 °C for overnight. The next day, only sonicated samples were precipitated by centrifugation at the highest speed for 10 minutes at RT, and the supernatants were transferred to new tubes. DNA elution was performed from all sonicated and unsonicated samples using the Zymo DNA Clean&Concentrator kit. To control, samples were run on 1.5% agarose gel.

An unsonicated sample was loaded on the last column, and as expected, uncut chromatin of large sizes was also seen at the top of the agarose gel. The results of 5 sonicated experimental samples have a smear image (Figure 9). After seeing that there was a smear, the immunoprecipitation step was started.

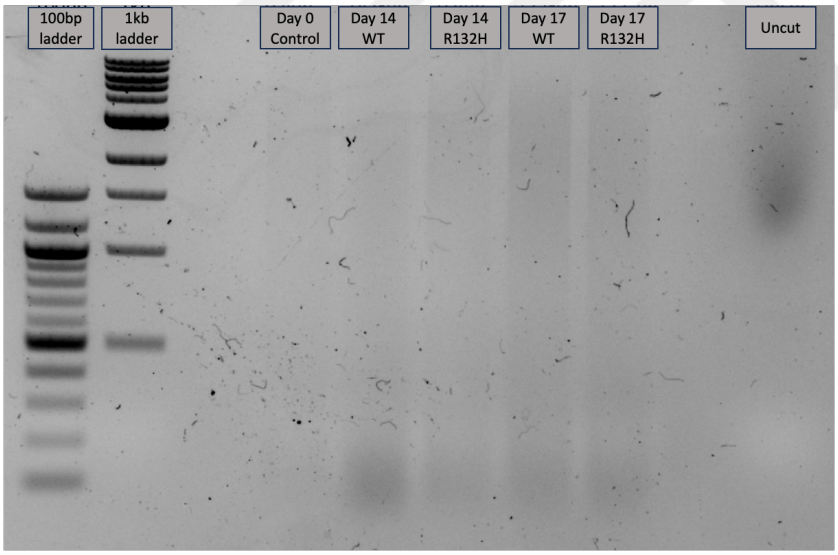

Figure 9. Agarose gel image of ChIP samples before immunoprecipitation (IP). In the last column, non-sonicated chromatin was loaded. After the chromatins of the 5 experimental conditions were sonicated, they were loaded onto the agarose gel to see whether the sonication was sufficient.

Pre-blocking of the magnetic beads

After seeing the sonicated samples in the desired sizes according to the agarose gel image, the magnetic beads were pre-blocked. 60 µl of Dynabead was used for each sample. Of this 60 µl Dynabead, 50 µl was used for immunoprecipitation and 10 µl was used for pre-clearing. First, 1 ml TE buffer solution was placed on 60 µl Dynabeadin for each sample and mixed by inverting. It was placed on a magnetic stand, left on the stand for 1 minute, and the supernatant was withdrawn and discarded without leaving the stand. This washing step was done 1 more time. At the same time, 100 µl tRNA (10 µl tRNA for each 60 µl Dynabead) was taken into a separate tube and denatured at 95 °C for 5 minutes. To each tube containing Dynabeads, 100 µl TE buffer (100 ul TE buffer for each sample), 10 µl 10 mg/ml BSA and 10 µl denatured tRNA were added and pipetted. Incubate for 2 hours at +4 °C, rotating and stirring to ensure that it did not precipitate. After incubation, dynabeads were washed 3 times with TE buffer solution using a magnetic stand. After the last wash, 60 µl of TE buffer solution for each sample was placed on the beads and the solution including dynabeads was kept at +4 ºC.

Immunoprecipitation (IP)

For each sonicated and unsonicated condition, chromatins were first precleared.

The samples in the sonication tubes were pipetted and transferred to microcentrifuge tubes. As mentioned before, 10 µl of TE buffer solution + dynabead solution was added to each sample. It was incubated with rotation at +4 ºC for 1 hour. Then, the samples were placed on the magnetic stand and the supernatants were transferred separately to 1.5 ml microcentrifuge tubes. The purpose of this process is to remove chromatin fragments that do not bind to the beads in the presence of antibody.

H3K4me3 antibody was added to each chromatin sample transferred to new tubes and incubated with rotation at +4 ºC overnight. The next day, 50 µl of pre-blocking dynabead solution was added and incubated with rotation at +4 ºC for 3 hours. After incubation, supernatants were removed from bead + chromatin + antibody with the help of a magnetic stand. And microcentrifuges were taken from the magnetic stand. 1ml lysis solution containing 40 µl Protease inhibitor cocktail was added onto bead + chromatin + antibody, incubated for 5 minutes at RT with rotation, and the supernatant was removed with the help of a magnetic stand.

This step was repeated. Then, the beads were washed with 1ml DOC buffer containing 40 µl PIC and TE buffer containing 40 µl PIC, respectively, and the supernatant was removed each time with the help of a magnetic stand. After these procedures, the beads were centrifuged at + 4 ºC, 1000 g for 3 minutes to completely remove the liquid on the beads, and the remaining liquid was completely removed with the help of a pipette.

Elution

To separate the chromatins from the beads, 100 µl of freshly prepared elution buffer was added onto the pellet and incubated for 15 minutes at 1000 rpm at RT, vortexing every two to three minutes. After incubation, it was centrifuged at 11000 rpm for 2 minutes. Supernatants were taken in to new 1.5 ml microcentrifuge tubes. Elution steps were repeated for the same beads. As a result, we had 200 µl of eluting solution for each sample.

Reversal of crosslink for IP

4 µl of 10 mg/ml RNAase A (last concentration of 0.2 mg/ml) was added to each 200 µl sample and incubated at 37 °C for 30 minutes. Then, 4 µl of 0.5 M EDTA (last concentration of 10 mM), 8 µl of 1M Tris pH 6.5 (last concentration of 40 mM), 0.5 µl of 20 mg/ml Proteinase K (last concentration of 50 µg/ml) were added. It was incubated at 55 ºC for 2.5 hours and at 65 ºC overnight. The next day, centrifugation was performed for 10 minutes at RT at the highest speed and the supernatants were transferred to new tubes and DNA elution was made from the samples using the ChIP DNA with Zymo Clean&Concentrator kit.

For ChIP-qPCR, qPCR was performed by diluting the DNA isolated from sonicated samples at a ratio of 1:4, and as a control group, the DNA isolated from unsonicated samples was diluted at a ratio of 1:20. Promega Go Tag qPCR mastermix was used when performing qPCR for the regions we determined (Table 8).

Table 8. Primer sets used in H3K4me3 ChIP-qPCR analyses.

Primer Name	Forward primer sequences	Reverse primer sequences
TERTp-1	CGTGTGCCCACGTGACGA	CCCAGAGCTGAATGCAGTAGG
CCDC26-1	TTCTCAGAGCACAAACCTCCA	TGTGCCTTTCCCATTGGCAT
CCDC26-2	ACAGATGGGAGAGTGGTCCT	CACACATCCACTGGCCTAGA
CCDC26-3	CCACGGTAGTAGCAGCAATCT	GCTGTGAGGGCTTTTGGAAT
CCDC26-4	CTCCTTAGCCCTCGTGGAAA	GAAAACCACAGTGCCAACACA
MYCP-1	TGTCCGGGGAGGAAAGAGTT	CCGGACTTCCTAAAAGGGGC
MYCTRIM28	GATGTTTCAAGCAGCGGGTG	TGTGTGTTTGGTGCACTCCT
ID1	GCTCCGCACTCTCATTCCAC	CTGGCTGAAACAGAATGGGC

3.5.9.1.H3K27ac ChIP-qPCR analysis

The ChIP protocol is the same as the method applied for H3K4me3. H3K27ac antibody was added to sonicated and unsonicated samples only during the Immunoprecipitation stage. Agarose gel image of the sonication result for H3K27ac immunoprecipitation is in Figure 10.

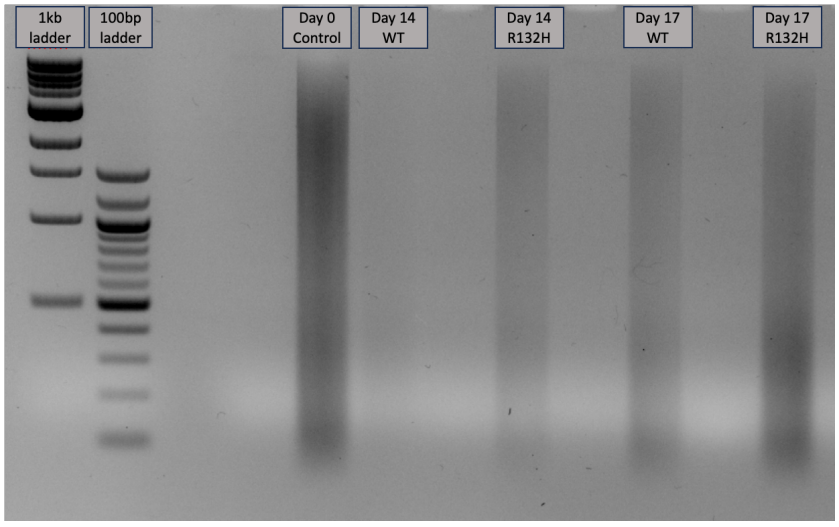

Figure 10. Agarose gel image of ChIP samples before immunoprecipitation (IP)

The results of 5 sonicated experimental samples have a smear image as expected (figüre 3.5). After seeing the smear, immunoprecipitation was performed with H3K27ac antibody.

Primers specifically designed for the regions selected in qPCR are given in Table 9. Additionally, the contents of the buffers used when applying the ChIP protocol are given in Table 10.

Table 9. Primer sets used in H3K27ac ChIP-qPCR analyzes

Primer Name	Forward primer sequences	Reverse primer sequences
GSDMCS-1	GTAAGCAGTATTGCCCCAAC	TGGCTCGCTTAGTGTTGATTCT
MYCP-1	TGTCCGGGGAGGAAAGAGTT	CCGGACTTCCTAAAAGGGGC
ID1	GCTCCGCACTCTCATTCCAC	CTGGCTGAAACAGAATGGGC
RS55705857-1	AAGGACTTGCTCAGAAGCCG	TTTGTTTGCTGGCATGGTCC
RS55705857-2	TCCAAGGACTTGCTCAGAAGC	AAAATGCCGGAAACCAGTCC
MYCTRIM28-2	GATACTGAGCCAGGACCCAAG	CCTATGGTGCTGCCTTCTCC
ID1-2	TGGCTCCGCACTCTCATTC	ATGATTCTTGGCGACTGGCT
MYCP-2	TTTGTGCATGACCGCATTTCC	ACTCTTTCCTCCCCGGACA

Tablo 10. Contents and amounts of buffer solutions used when applying the ChIP protocol

Buffer Name	Contents of Buffer
Elution Buffer	0.25 ml 20% SDS (final concantration 1%)
	0.25 ml 1M $NaHCO_3$ (final concantration 100mM)
	2 ml ddH_2O
DOC Buffer	40 µl 1M Tris pH 8.0 (final concantration 10 mM)
	1 ml 1M LiCl (final concantration 0.25 M)
	20 µl NP-40 (final concantration 0.5%)
	0.2 ml 10% DOC (final concantration 0.5%)
	8 µl 0.5 M EDTA (final concantration 1 mM)
	2732 µl ddH_2O
Lysis Buffer	25 ml 1M HEPES/KOH pH 7.5 (final concantration 50 mM
	50 ml 5M NaCl (final concantration 500 mM)
	1 ml 0.5 M EDTA (final concantration 1mM)
	5 ml Triton X-100 (final concantration 1%)
	5 ml 10% DOC (final concantration 0.1%)
	2.5 ml 20% SDS (final concantration 0.1%)
	411.5 ml ddH_2O
	Note: protease inhibitör coctail were added freshly
Protease inhibitor coctail	25X protease Inhibitors Coctail tablet
	2000 µl ddH_2O

3.5.10. **Methylated DNA immunoprecipitation (MeDIP) and MeDIP-qPCR**

4 ml 0.5 M EDTA was added to the NPC-alginate 3D cultures prepared for our 5 different experimental conditions on their respective days and incubated for 5 minutes at RT and in a hood. It was gently pipetted and transferred to 50 ml tubes. 10 ml DMEM/F-12 was added and centrifuged for 5 minutes at 300 g. 15 ml of DMEM/F-12 medium was added to the pellet to

wash it again and was carefully pipetted until the pellet dispersed. The cells were incubated in a 50 ml conical tube at RT for 20 minutes to completely disperse the alginate hydrogel on the cells. It was then centrifuged again for 5 minutes at 300 g. The supernatant on the pellet was removed and DNA was isolated with the Qiagen DNA isolation kit.

For MeDIP protocol;

After DNA isolation, three 100 µl samples were prepared for each condition, with a DNA concentration of 2000 ng in each tube.

Since 3 different antibodies will be used for each experimental condition, 3 of each condition were prepared. Then, the DNAs were transferred to Bioruptor special tubes for sonication. Additionally, at least 50 µl of each sample was reserved for the unsonice sample. The protocol used in Bioruptor is given in Table 11.

Table 11. Sonication conditions used in the bioruptor used when applying the MeDIP protocol

Bioruptor Protocol		
Time on	30 sec	8 cycles
Time off	90 sec	

The lid of the device was opened, the samples were spun and placed back into the device.

Time on	30 sec	4 cycles
Time off	90 sec	

After sonication was completed, sonicated and unsonicated 10 µl samples were taken separately for each sample and run in 1% agarose gel at 90V until the 100 bp ladder was opened (approximately 40 minutes).

After the agarose gel was visualized and it was seen that the sonication process was successful, the samples were incubated at 95 ^{o}C for 10 minutes.

910 µl of 1X IP buffer was added to each 90 µl sample.

Since three different antibodies will be used, there are three 1000 µl sample + IP buffer solutions, as stated at the beginning of the protocol.

Three different antibodies were used: IgG Mouse (Immunoglobulin G) (Control), 5-hmC (5-Hydroxymethylcytosine) and 5-mC (5-methylcytosine). Approximately 2 µg of DNA was

assumed in each tube. Antibody amounts used for each experimental condition; For IgG Mouse; 0.4 µl for hmC; 0.8 µl for mC; It is 0.4 µl.

After adding antibodies (3 separate reactions for each condition), they were incubated overnight (16-18 hours) at 4 °C with a rotator speed of 12-18. The next day, first of all, Bead preparation was made. 0.5 ml of bead (GE healthcare, protein A sepharose bead cl-4B) was added to the 15 ml conical tube and RNase/DNase free water was added until the volume reached to 14 ml. Inverted until the beads and water were mixed. It was centrifuged at 300 g for 1 minute. The supernatant was discarded, 14 ml of nuclease free water was added, inverted and mixed again, and then centrifuged. This washing process was repeated 5 times. After the final wash, ChIP dilution buffer was added and mixed. As stated in the table, buffer containing PIC, ssDNA, protein A and BSA was added to the Beads in the same amount as the ChIP solution and stored at +4 ºC.

Samples that were incubated overnight were taken and after the tip of the 200-gauge pipette was cut (the pipette tip was cut because the bead solution was too dense), 40 µl of the prepared bead solution was added. After the beads were added, they were incubated at 4 C for 2 hours with a rotator speed of 12-18 rpm. After incubation, it was centrifuged at 2000 rpm for 1 minute. The supernatant was discarded and 1 ml of 1X IP buffer was added to the pellet. It was incubated at +4 ºC for 5 minutes with a rotator speed of 12-18 rpm. After the beads were mixed, they were centrifuged at 2000 rpm for 1 minute. The washing process was repeated 3 times with 1X IP buffer. 4^{th} Washing was done with TE buffer. It was incubated at rotator speed 12-18 rpm, 5 minutes and +4 ºC, and then centrifuged at 2000 rpm for 1 minute and the supernatants on the beads were discarded. For each sample, 100µl of 10X chelex was added to the remaining beads and incubated at 95 ºC for 10 minutes. 2µl proteinase K was added to the samples and treated for 30 minutes at 55 ºC. Then, proteinase K inactivation was performed by incubating at 95 ºC for 10 minutes. The samples were centrifuged at 17000 g for 2 minutes, and the samples were placed separately in new 1.5 ml microcentrifuge tubes. 100 µl of nuclease-free water was added to the pellet, washed and centrifuged. Supernatants were collected again and added to the place collected in the previous step. In total, we received 200 µl of product for each sample. The resulting samples of approximately 200 µl were passed through the RNA violet column by centrifugation at $17x10^3$g for 2 minutes. Then, the supernatant part was transferred to tubes. Some of the samples obtained were stored at -80 ºC. Mastermix was prepared for the genes to be controlled and qPCR was performed on the ABI7500Fast device.

3.5.11. Cell cycle Analysis with PI

At least two hours before starting the protocol, 100% ethanol was placed at -20 C to cool. PI staining was performed for our five different experimental groups (DAY0_Control-NPC, DAY14_IDH1-WT_NPC, DAY14_IDH1-R132H_NPC, DAY17_IDH1-WT_NPC, DAY17_IDH1-R132H_NPC). For this study, cells were grown in 3D alginate culture for the specified time and media in three different time periods. After 5 conditions were prepared, PI staining was performed and a separate unstain (non-staining) was prepared for each 5 conditions.

EDTA was added to the plate containing NPC-Alginate beads. It was incubated for 5 minutes and the alginate was waited to dissolve. It was carefully pipetted to dissolve the remaining alginate beads without damaging the cells. After the cells were separated from the alginate, they were transferred to a 15 ml conical tube and centrifuged for 5 minutes at 300 g. To completely remove alginate, the cells were washed once with DMEM/F-12 and centrifuged for 5 minutes at 500 g. The supernatant was removed and each condition was dissolved in cold 1X PBS until a homogeneous mixture was obtained, and 4 ml of 100% cold ethanol was added and mixed by pipetting very gently. Fixed cells were stored in falcons at -20 ^{o}C for at least 1 night. When 1 set (five different experimental groups) was completed, the fixed cells stored at -20 ^{o}C were precipitated by centrifugation at 500g, 4 ^{o}C for 5 minutes, and the supernatants were aspirated. All pellets were resuspended individually by pipetting in 70 µl of PI solution (final concentrations of 50 µg/ml PI, 0.05% TritonX-100 in 1X PBS and 0.1 mg/ml RNase A). They were incubated for 40 minutes at 37 ^{o}C by vortexing every 10 minutes. PI solution was not added to the unstained condition. Only 1X PBS was added and incubated. Then, centrifugation was performed at 500 g, 4 ^{o}C for 5 minutes. Each sample was dissolved in 100 µl FACS Sheat and then passed through the mesh and transferred to a polystyrene tube. Analyzes were performed on a flow cytometer and cell cycle analyzes were performed using FlowJo software. Three independent experiments were set up for each condition.

3.5.12. Repression of MYC and ID1 genes with the dCas9-KRAB CRISPR tool

3.5.12.1. Cloning of gRNA sequences designed according to MYC and ID1 separately into the plasmid pLV hU6-sgRNA hUbC-dCas9-KRAB-T2a-GFP

The sequences of gRNAs, sense and anti-sense oligos designed for MYC and ID1 promoters using the Benchling program are given in Table 12. 7 different gRNAs were designed for the MYC promoter. Two different gRNAs were designed for the ID1 promoter.

Table 12. Sequences of gRNA sense and antisense oligos designed for MYC and ID1 promoters.

Primer Name	Sense Oligo	Antisense Oligo
MYC-gRNA1	CACCGCCAGCGTCTAAGCAGCTGCA	AAACTGCAGCTGCTTAGACGCTGGC
MYC-gRNA2	CACCGCCTTGCAGCTGCTTAGACGC	AAACGCGTCTAAGCAGCTGCAAGGC
MYC-gRNA3	CACCGAGCGGGTCCTGGCAGCGGCG	AAACCGCCGCTGCCAGGACCCGCTC
MYC-gRNA4	CACCGGGAGCAAACAAATCATGTG	AAACCACATGATTTGTTTGCTCCC
MYC-gRNA5	CACCGATTTGTCTCTTCTGAAACC	AAACGGTTTCAGAAGAGACAAATC
MYC-gRNA6	CACCGAGTTCCCAATTTCTCAGCC	AAACGGCTGAGAAATTGGGAACTC
MYC-gRNA7	CACCGAGAAATTGGGAACTCCGTGT	AAACACACGGAGTTCCCAATTTCTC
ID1-gRNA1	CACCGGCGACTGGCTGAAACAGAA	AAACTTCTGTTTCAGCCAGTCGCC
ID1-gRNA2	CACCGAGAATCATGAAAGTCGCCAG	AAACCTGGCGACTTTCATGATTCTC

Hybridization and Phosphorylation of gRNA sense and anti-sense Oligos

Sense and antisense oligos for gRNA were hybridized and phosphorylated. Reaction content and conditions are given in Table 13. pLV hU6-sgRNA cut with BsmBI cutting enzyme was diluted 1:200 using ddH2O for use in cloning into the hUbC-dCas9-KRAB-T2a-GFP plasmid. Separate annealing protocols were applied for all gRNA sense and anti-sense oligos given in Table 12.

Table 13. Hybridization and phosphorylation reaction conditions and contents of sense and antisense oligos

Compotents	Volume	Reaction condition
100 µM sense gRNA oligo	1 µl	37 °C, 30 min.; 95 °C, 5 min; Then, it was reduced to 25 °C at a rate of 5 °C per minute.
100 µM anti-sense gRNA oligo	1 µl	
T4 ligase buffer	1 µl	
T4 Polynucleotide Kinase (PNK)	0.5 µl	
ddH_2O	6.5 µl	

3.5.12.2. Restriction and Dephosphorylation of pLV hU6-sgRNA hUbC-dCas9 KRAB-T2a-GFP plasmid with BsmBI Restriction Enzyme

To cut and dephosphorylate this -dCas9-KRAB plasmid, the reaction context and conditions specified in Table 14 were established.

Table 14. Program and reaction content used to cut and dephosphorylate the pLV hU6-sgRNA hUbC-dCas9-KRAB-T2a-GFP plasmid

Competent	Volume	Reaction condition
pLV hU6-sgRNA hUbC-dCas9-KRAB-T2a-GFP plasmid	1 µg	Incubated at 37 ºC for 2 hours It was incubated at 80 ºC for 20 minutes for enzyme inactivation.
BsmBI-v2 Restriction Enzyme	1 µl	
NEB r3.1	5 µl	
ddH_2O	to 50 µl	
Calf Intestinal Alkaline Phosphatase (Quick CIP)	1 µl	20 minutes incubation at 37 C + 2 minutes incubation at 80 ºC

Then, this -dCas9-KRAB plasmid, cut with BbsI and dephosphorylated with CIP, was run on 1% agarose gel and isolated from the gel for use in subsequent steps (Figure 11). Monarch DNA Gel Extraction kit (NEB, # T1020S) was used for isolation from agarose gel. (Figure 3.6). After measuring its concentration with a nanodrop, it was stored at -20 C.

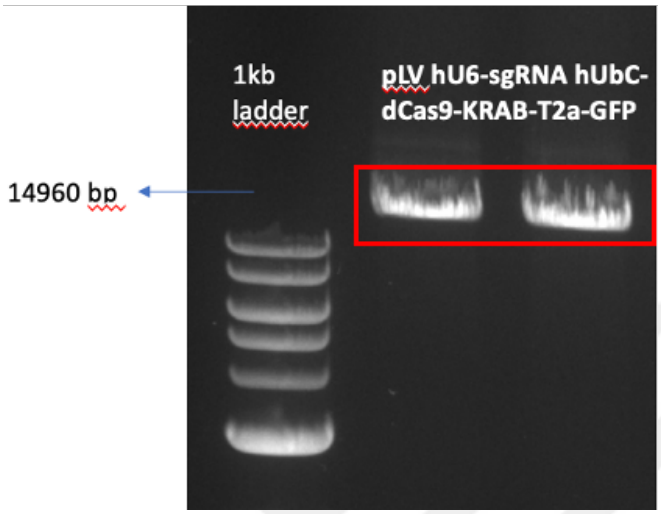

Figure 11. Cutting the pLV hU6- sgRNA hUbC-dCas9-KRAB-T2a-GFP plasmid with BsmBI restriction enzyme and running on agarose gel after treatment with Calf Intestinal Alkaline Phosphatase.

3.5.12.3. Ligation and Transformation of Hybridized Oligos with pLV hU6-sgRNA hUbC-dCas9-KRAB-T2a-GFP plasmid

The ligation reaction given below was set up with each hybridized gRNA separately (Table 15). In addition, control ligation was performed. When setting up the control ligation reaction, 1 µl of water is present instead of hybridized oligos.

Table 15. Reaction conditions for ligation of cut pLV hU6-sgRNA hUbC-dCas9-KRAB-T2a-GFP and each gRNA

Components	Volume	Reaction condition
100ng/µl cut pLV hU6-sgRNA hUbC-dCas9-KRAB-T2a-GFP	100 ng	It was incubated for 2 hours at room temperature and then at 65 °C for 10 minutes for T4 ligase inactivation.
hybridized and phosphorylated oligos (gRNA) (1:200)	1 µl	
T4 Ligation Buffer	2 µl	
T4 DNA Ligase	1 µl	
ddH_2O	To 20 µl	

Nine reaction mixtures and negative control grup were incubated at 25°C for 2 hours, and the ligation products were transformed *into E.coli* DH5α separately.

Transformation

E.Coli DH5-alpha competent bacteria stored at -80 C were placed on ice to thaw slowly. The prepared ligation products were also placed on ice. For each ligation product, 100 µl of bacteria and 10 µl of ligation product were added to microcentrifuge tube and pipetted. After incubation on ice for 20 minutes, it was kept at 42 ºC for 1 minute for heatshock and then kept on ice for 2 minutes. After the heatshock process, 900 µl of antibiotic-free LB-Broth was added and incubated with shaking for 30 minutes at 37 °C. They were then centrifuged at $1x10^4$ rpm for 1 minute at RT. The remaining supernatant was removed with the help of a pipette, leaving 80-100 µl of liquid on the pellet. They were pipetted using a 200 µl pipette and planted on a pre-warmed LB-Agar plate with ampicillin. Then, they were incubated at 37 °C for 16 hours.

The next day, the number of colonies on the plates containing the gRNA cloning plasmids was compared with the number of colonies in the control group. Since more colonies were seen on other plates compared to the control group, the insertion of gRNAs into the plasmid was checked.

Control of Insertion of gRNAs into the Plasmid

Colony PCR was performed to check the insertion of gRNAs into the plasmid. First, the PCR reaction was prepared on ice as stated in Table 16.

Table 16. PCR Reaction condition to control insertion of gRNA

Components	**Volume**	**Reaction Condition**
5X Q5 Reaction Buffer	5 µl	After dropping it into the bacteria with the help of a 10 µl pipette tip;
10mM dNTPs	0.5 µl	
anti-sense oligo	0.5 µl	Initial Denaturation 98°C, 30 sec.
hU6 forward primer	0.5 µl	Synthesis cycles (35) 98°C, 10 sec. / 60°C, 20 sec. / 72°C, 20 sec.
5X Q5 high GC enhancer	5 µl	
Q5 High-Fidelity DNA Polymerase	0.25 µl	Final extention 72°C, 2 min.
Nuclease-Free Water	13.75 µl	+4°C, ∞

After bacterial transfer from the colonies selected for PCR was completed, the PCR reaction was set up in the Thermocycler using the reaction conditions shown in Table 16.

After the PCR was finished, it was run on a 1% agarose gel at 80 V and checked with the BIO-RAD Gel Doc XR device.

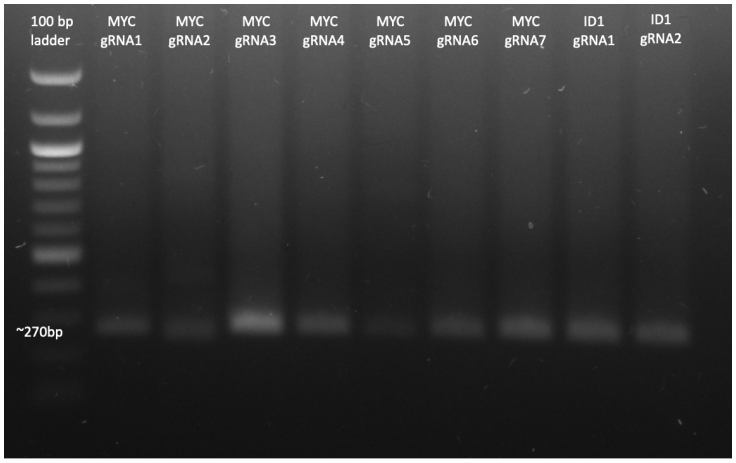

Figüre 12. Control PCR of insertion of sequences of MYC and ID1 promoter specific gRNAs into the plasmid.

After the agarose gel results showed that the gRNAs were cloned (Figure 12), a single colony that was observed to be positive for each gRNA was selected and confirmed by Sanger sequencing.

3.5.12.4. Control of Designed gRNAs in HEK293T Cells

After the gRNAs designed for MYC and ID1 were cloned separately into the -dCas9-KRAB plasmid, HEK 293T cells were first transfected to see the efficiency of the gRNAs. 100,000 HEK293T cells were seeded in each well of the 12-well plate with High Glucose medium, ensuring homogeneous distribution. Cells were incubated for 1 day. The next day, after checking under the microscope whether it spread homogeneously or not, the plasmids were transfected into the cells. Transfection conditions are given in Table 17. Each plasmid with individual gRNAs was transfected under the same conditions.

Table 17. Transfection condition for all gRNA cloned cut pLV hU6-sgRNA hUbC-dCas9-KRAB-T2a-GFP plasmids

Transfection solution	1 µg plasmid
	1.5 µl Transfection reagent (Fugene)
	To 50 µl with serum free DMEM High Glucose

The transfection solution was incubated in the tube at room temperature for 30 minutes.

Then, 50 µl of transfection solution containing the plasmid with different gRNA was added dropwise to each well and incubated for 24 hours. Transfection solution prepared with gRNA non-cloned (Empty) plasmid was added to one well as a control group. After 24 hours, the medium on the cells was changed. 72 hours after transfection, the media on the cells were withdrawn and cells were removed with trypsin. Medium was added, trypsin was inactivated. After the cells were centrifuged at 1400 rpm for 2 minutes, the RNA isolation step from the cells was started. MN Nucleospin RNA kit was used for RNA isolation. Then, cDNA was produced from RNAs using the Firs strand cDNA kit. Promega GoTaq SYBER kit was used for RT-qPCR. Samples were prepared using the own protocols of all kits used. Primers designed

for MYC and ID1 were used when preparing samples for RT-qPCR. The most effective gRNAs designed to reduce MYC and ID1 expression were determined according to RT-qPCR results. NPCs were transfected with plasmids containing these selected gRNAs.

3.5.12.5. Nucleofection

When the NPCs in the 10 cm plate, whose medium was changed every day, reached 80-90% density, 6 wells of the 24-well plate were covered with matrigel. Cells were removed with accutase. 6 ml of DMEM/F-12 medium was added onto the shielded cells and gently pipetted. Then the cells were placed in a conical tube. Before centrifugation, cells were counted with the help of a hemocytometer using tryphan blue. Three separate nucleofection reactions were established. The solutions used for each reaction, the amount of cells and the program used in the nucleofector are given in Table 18. P3 primary cell 4D- Nucleofector X Kit was used for nucleofection.

Table 18. Reaction content and program used for nucleofection of pLV hU6-sgRNA hUbC-dCas9-KRAB-T2a-GFP plasmids to silence MYC and/or ID1 genes in NPCs

	1st Nucleofection	**2nd Nucleofection**	**3rd Nucleofection**
Cells	7 x 10^5	7 x 10^5	7 x 10^5
Plasmid DNA	1µg pLV hU6-MYC-sgRNA hUbC-dCas9-KRAB-T2a-GFP	1µg pLV hU6-ID1-sgRNA hUbC-dCas9-KRAB-T2a-GFP	1µg pLV hU6-MYC-sgRNA hUbC-dCas9-KRAB-T2a-GFP + 1µg pLV hU6-ID1-sgRNA hUbC-dCas9-KRAB-T2a-GFP
P3 Primary Cell 4D-Nucleofector X Solution	100µl	100µl	100µl
Program	CB-150	CB-150	CB-150

Nucleofected cells in each condition were pipetted with 1 ml of Neural Progenitor Basal medium containing ROCK inhibitor at 37 °C and planted in two wells of 24-well as 500 µl and incubated at 37 °C, 5% CO_2. 24 hours after nucleofection, the medium was replaced with fresh Neural Progenitor basal medium. 72 hours after nucleofection, cells were removed with the help of accutase.

3.5.12.6. Neurosphere Formation

At 72 hours after nucleofection, 3 different nucleofection cells and untreated NPCs were removed with accutase. Each condition was seeded with an equal number of cells into 3 wells of a 6-well low attachment plate. 3 different media were prepared. Its contents and the way it is applied to the media and cells are shown in Figure 13.

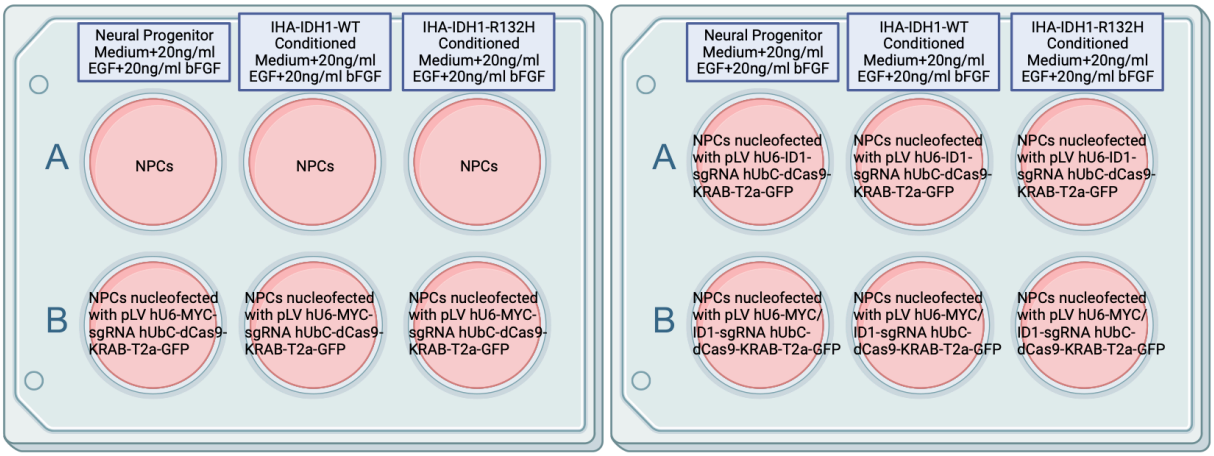

Figure 13. Visualization of experimental setups set up when creating neurospheres. Creating neurospheres with non-nucleofected NPCs, ID1 repressed NPCs, MYC repressed NPCs, and MYC and ID1 co-repressed NPCs with different media.

EGF and bFGF were added to Neural Progenitor Medium, IHA-IDH1-WT and IHA-IDH1-R132H conditioned media with a last concentration of 20 ng/ml. The given media and seeded cells are shown in Figure 13. 500 µl of fresh medium was added every day. After 8 days, neurospheres were taken from 12 different conditions and IF staining was performed.

3.5.12.7. Immunoflurescence Staining for NPC neurospheres

Immunofluorescence stainings were performed separately for 12 different neurosphere cultures. Neurospheres were transferred to separate wells of a 12-well plate using a pasteur pipette. The plate was left unmoved for 3 minutes to allow the neurospheres to settle by gravity. The immunofluorescence staining method is described in detail above. It is briefly explained in this section. Then, the plates were tilted slightly and the culture medium was cautiously removed using a 200 µl pipette. Washing with 1X PBS and gravity settling for 3 min was repeated three times. Although PBS was carefully withdrawn with the help of a pipette, the PBS taken with the pipette was placed in a clean well to prevent possible neurosphere loss, and the neurospheres taken by mistake were transferred back to their own wells. The first washings were done by looking at them under a microscope. After washing with 1X PBS, it was fixed by incubating with 4% PFA (paraformaldehyde) in a dark environment. The fixative was removed from the neurospheres again with the help of a pipette and washed 3 times with 1X PBS by gently mixing for 5 minutes and allowing the neurospheres to settle by gravity for 3 minutes. After the washing process, the permeabilization step was started. After incubation with PBS containing 0.1% triton-X for 10 minutes at RT, it was washed 3 times with 1X PBS. In the blocking step, T-PBS (PBS containinga0.1% Tween-20) containing 1% BSA was added onto the neurospheres and incubated with shaking at RT for 1 hour. After the blocking solution was removed from the medium, fresh blocking solution containing primary antibodies (Pax6, Cell Signalling, Cat#60433 at a concentration of 1:150; Nestin, Cell Signalling, Cat#33475 at a concentration of 1:2000) was added to the neurospheres and incubated with shaking at RT for 2 hours. Then, neurospheres were washed 3 times with 1X PBS and fresh blocking solution containing secondary antibodies (Goat Anti Rabbit IgG H&L Alexa Flour 555 at a concentration of 1:1000 and Goat Anti Mouse IgG H&L Alexa Flour 488 at a concentration of 1:1000) was applied to the neurospheres. was added and incubated for 1 hour in the dark at RT with shaking. After incubation, neurospheres were washed 2 times with 1X PBS. In last wash, Hoechst dye was added at a ratio of 1:1000 into 1X PBS solution and incubated for 5 minutes in the dark with slow shaking. Then, the neurospheres were carefully removed with the help of a pasteur pipette and transferred to glass-bottomed 35 mm cell culture dishes, and when covered with a coverslip, mounting media was added so that there was no gap left and covered with a coverslip. It was stored in the dark at +4 ºC until imaging with confocal microscopy.

4. RESULTS

4.1. Generation and Characterization of hiPSC-derived hNPCs

Human induced pluripotent stem cells (hiPSCs) were differentiated into Neural Progenitor Cells (NPCs) by using "Generation and Culture of Neural Progenitor Cells using the Stemdiff™ Neural System" Monolayer Culture protocol (Figure 4.1). STEMdiff Neural Induction Medium + SMADi was used to generate NPCs from hiPSCs. Dual SMAD inhibition plays an effective role in the transformation of hiPSCs into CNS-type NPCs by preventing undesirable differentiation such as non-CNS-type cells. After differentiation using Neural Induction medium in the presence of SMADi, optimized Neural Progenitor medium was used to propagate the generated NPCs (Figure 14).

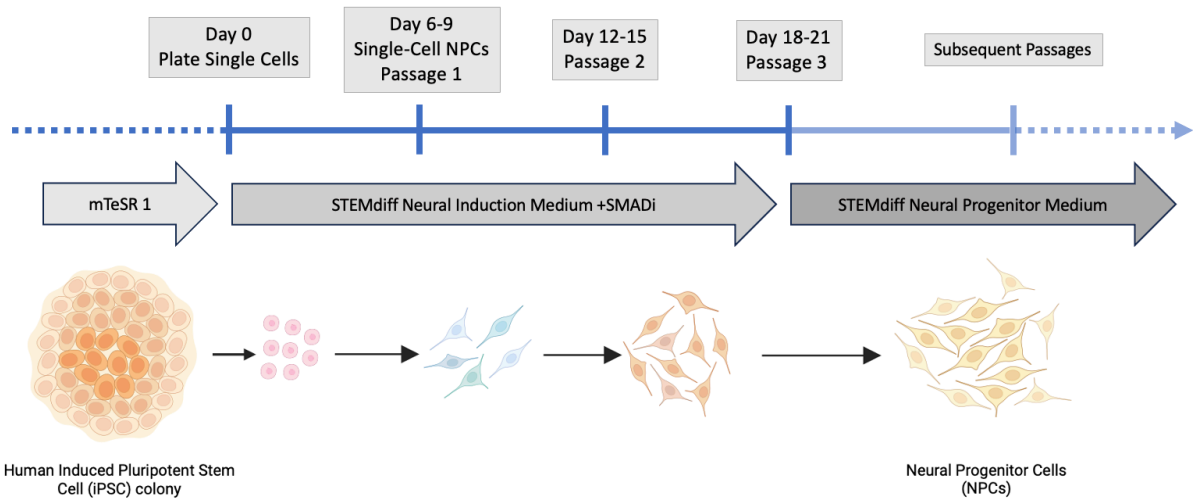

Figure 14. Schematic illustration for Monolayer Culture Protocol to differentiate from hiPSC to NPCs

To observe morphological changes during the differentiation, images were taken with the help of light microscope at regular intervals. These images show clearly distinct morphological differences between HiPSCs and hiPSC-derived NPCs (Figure 15).

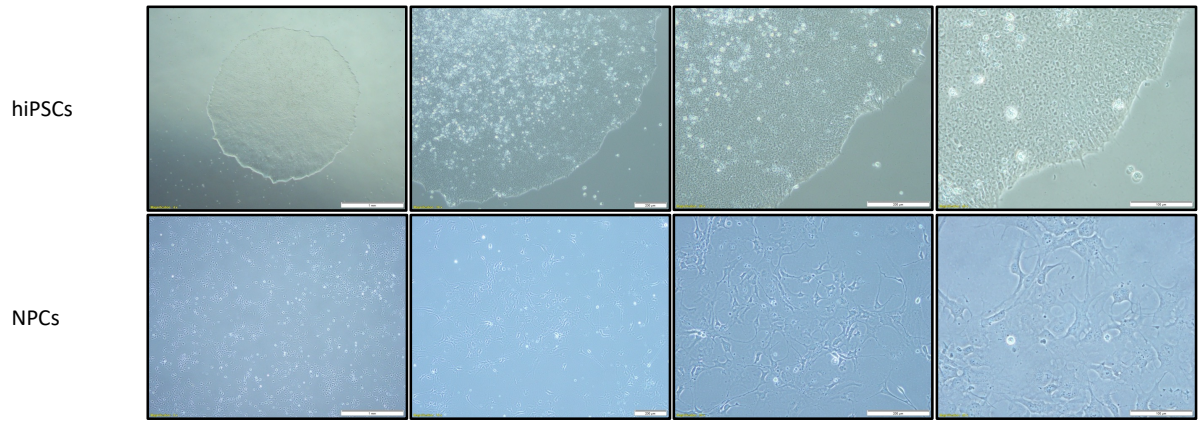

Figure 15. Images of hiPSC Colony and NPCs. Images were taken at 4X, 10X, 20X and 40X magnifications for both the iPSC colony and NPCs, respectively

Immunofluorescent staining was performed to characterize the hiPSC used for differentiation and the hiPSC-derived NPCs. The markers used when performing IF are OCT4, SOX1, SOX2, PAX6 and NESTIN. Octamer binding transcription factor 4 (OCT4), also called as OCT3 or OCT3/4, is a member of the POU- domain transcription factor family and is encoded by the Pou5f1 gene. OCT4 has critical roles in the induction of pluripotency in both mouse and human somatic cells, maintenance of pluripotency state, as well as self-renewal of ESCs and CSCs (Mohiuddin et al., 2020; S. Zhang, 2014). Nestin, the neuroepithelial stem cell protein, is a Class VI intermediate filament protein and a marker of embryonic and adult CNS stem/progenitor cells (Lendahl et al., 1990; Morshead et al., 1071; *Reynolds1992-2*, n.d.). NESTIN is expressed in various tissues such as developing myotomes, hair follicle, testis, heart, as well as stem and progenitor cells (Amoh et al., 2005; Jiang et al., 2014; Kachinsky et al., 1995; Zimmerman et al., 1994). In addition, it is known to be expressed in various types of malignant cancers such as glioma, neuroblastoma, osteosarcoma, melanoma, prostate and pancreatic cancers and to have roles in pathogenesis (Krupkova et al., 2010). Nestin, which is also used as an invasive phenotype marker, has been shown to be associated with angiogenesis in malignancies, infiltration in glioblastoma, and dissemination of epithelial and non-epithelial tumors (Chung et al., 2013; Ishiwata et al., 2011; Matsuda et al., 2013). SOX1 (sex determining region box 1) and SOX2 (transcription factor), known to have important roles in cancers and embryogenesis, are members of SOXB1, a subgroup of the Sex determining region Y (SRY) superfamily group (Archer et al., 2011; Grimm et al., 2020; Miyagi et al., 2009). SOX1, one of

the genes involved in protecting the cell line from differentiation, is defined as a stem cell marker. It also has an essential role in the renewal and survival of neurons and NSCs (Kanwore et al., 2021; M. Li et al., 2016). Transcription factor SOX2 has a critical role in maintaining the pluripotency of stem cells. In addition, it is a critical transcription factor in initiation of neural induction by preserving neural progenitor stem cell properties (S. Zhang, 2014) . Additionally, SOX1 and SOX2 have been showen to have roles in glioma stem cell invasion, migration and proliferation (Garcia et al., 2017; Grimm et al., 2020; Weina & Utikal, 2014). Paired box 6 (PAX6) have critic roles in the development of the eye, nervous system and pancreas (Ian Simpson & Price, 2002). Furthermore, PAX6 is important for regulating multipotency, proliferation and neurogenesis of NSCs (Sansom et al., 2009).

While the reason for the characterization for hIPSCs was to check whether they were still pluripotent, the reason for the characterization for NPCs was to see whether the cells differentiated from hiPSCs corresponded to NPC. To see the pluripotency of hiPCSCs, the immunofluorescence staining was performed with the pluripotency marker OCT4 and a strong OCT4 signal was seen in all cells. After checking the pluripotency of the hIPSCs we used, the differentiation process was initiated and the differentiated cells were stained with neuroectodermal stem cell markers PAX6, NESTIN, SOX1 and SOX2, as well as OCT4. The reason for staining with OCT4 is to see whether there are any cells remaining undifferentiated. It was observed that most of the cells differentiated from iPSCs were stained positively with neuroectodermal stem cell markers and not with OCT4 as expected. The stainings showed that the majority of hiPSCs successfully differentiated into NPCs (Figure 16).

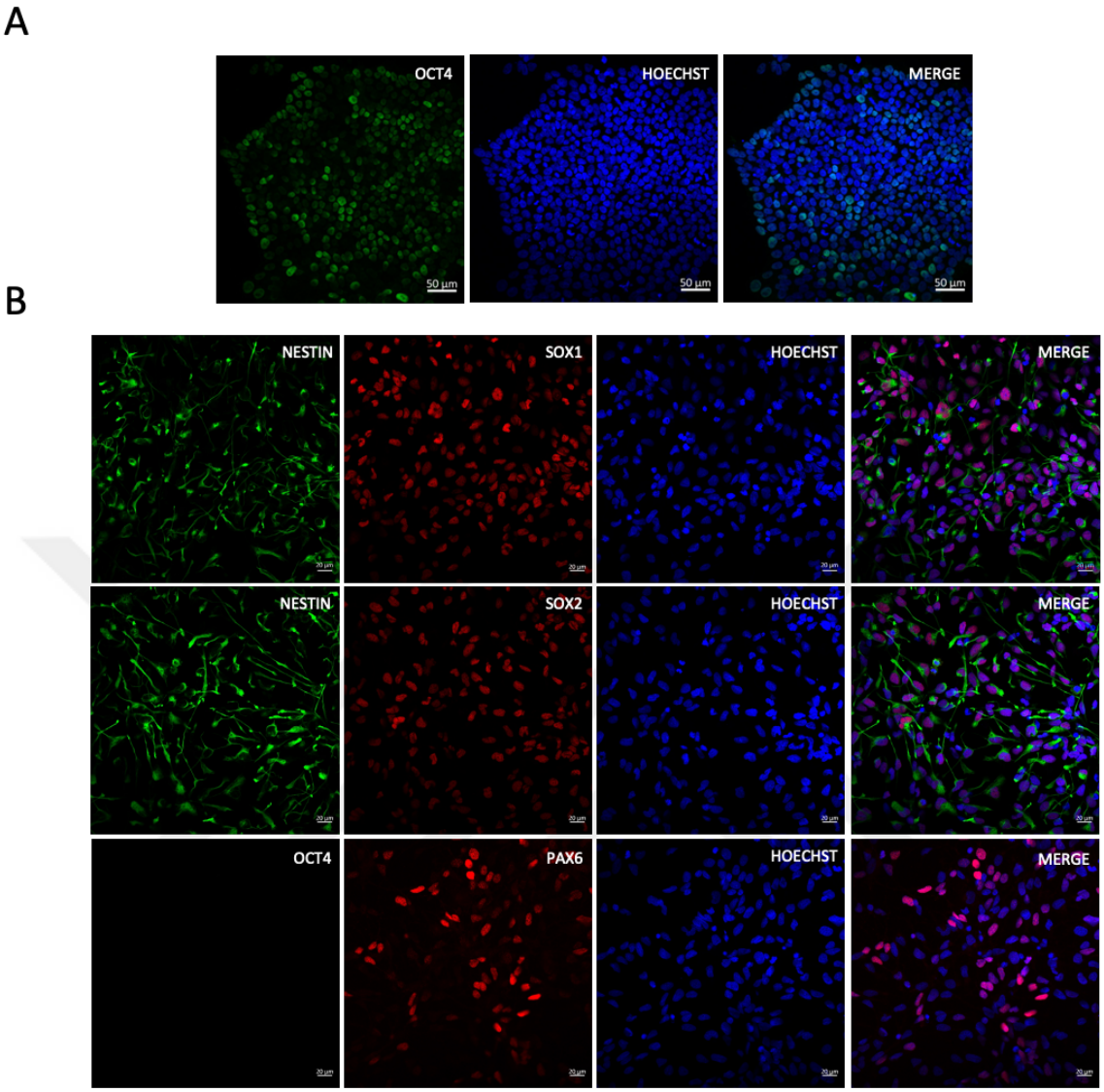

Figure 16. Immunofluorescence staining performed for characterization of hiPSCs and hiPSC-derived NPCs. A. Staining of OCT4, a pluripotency marker, was performed in hiPSCs. Scale bar: 50 µm. Immunofluorescence staining for SOX2, SOX1, PAX6, Nestin, and OCT4 was performed in B. hiPSC-derived NPCs. Three different co-stains were performed for NPCs. one; Nestin (Green), SOX1 (Red) and Hoechst (Blue). 2; Nestin (Green), SOX2 (Red) and Hoechst (Blue). 3; OCT4 (Green), PAX6 (Red) and Hoechst (Blue). Hoechst 33258 was used for nucleus staining. Scale bar: 20 µm.

4.2. The effects of 3D alginate culture of expansion and maintenance of NPCs

NPCs removed from the plate with Accutase were distributed homogeneously in 1% alginate-Neural progenitor medium and encapsulated into alginate hydrogel sphere-like beads with $CaCl_2$. Alginate, which has an easily gelling and easily soluble structure, is widely used in the creation of 3D cell culture models due to its advantageous properties such as its suitability for waste and nutrient diffusion and also allowing easy observation of cells with a microscope (Andersen et al., 2015; N. Wang et al., 2009). It is important that a 3-dimensional culture medium created with alginate provides mechanical stability, flexibility and allows nutrient diffusion (Saha et al., 2008; N. Wang et al., 2009). The low Alginate concentration in the created three-dimensional environment ensures that the pore sizes of the alginate beads are large. As a result, alginate beads with a weak structure were formed and were observed to be unable to maintain their integrity during long-term culture. At the same time, it has been reported that embryonic stem cell (ESC) proliferation is inhibited in 2% 3D alginate culture, while 1% alginate medium is the most suitable beads for ESC growth (N. Wang et al., 2009). Therefore, a three-dimensional alginate culture was created at 1% concentration to preserve the viability and proliferation of Neural Progenitor cells. 3 different time points and 5 different experimental conditions were chosen to see the effect of IDH1-R132H and whether its effect disappeared.

Alginate beads formed with NPCs on day 0 were incubated in Neural Progenitor medium at 37 ^{o}C, 5% CO_2 for 24 hours (Figure 3A). On day 14, two different experimental conditions were established; the first was cultured with IHA-IDH1-WT medium for 14 days. This medium was collected from immortalized human astrocytes (IHAs) and is a medium that inducibly expresses IDH1-WT. The second one was cultured with IHA-IDH1-R132H medium for 14 days. This medium was collected from immortalized human astrocytes (IHAs) producing mutant IDH1 and is a medium that inducibly expresses mutant IDH1. On day 17, we had two experimental groups: First, IHA-IDH1-WT medium was removed from NPC-Alginate beads on day 14 and Neural Progenitor medium was added and incubated with Neural Progenitor medium for three days (until day 17), second, IHA-IDH1-R132H conditioned medium was removed from NPC-Alginate beads on day 14 and Neural Progenitor medium was added and NPC-alginate beads were cultured with Neural Progenitor medium for 3 days (until day 17).

On day 0, alginate beads were visualized by confocal microscopy and light microscopy. NPC-alginate beads were transparent and shiny (Figure 17A and 17B). No degradation of NPC-

alginate beads was observed on day 0. However, it was observed that the structure of NPC-alginate beads treated with IHA-IDH1-WT and IHA-IDH1-R132H media was disrupted on the 14th day. In addition, surprisingly, it was observed that the NPCs inside the alginate beads managed to continue to proliferate and form an aggregate. When the 17th day groups were examined, a transparent and bright 3D environment was not seen and more deterioration was observed in the alginate beads. Again, surprisingly, the number of cells increased day by day and cell clusters were observed. These cells clusters are the most important reason for the blurriness in the light microscope image. On the other hand, in a striking detail, it was observed in the 14^{th} and 17^{th} day groups that the structure of the alginate beads was deteriorating day by day and therefore the cells escaped from the beads (Figure 17B).

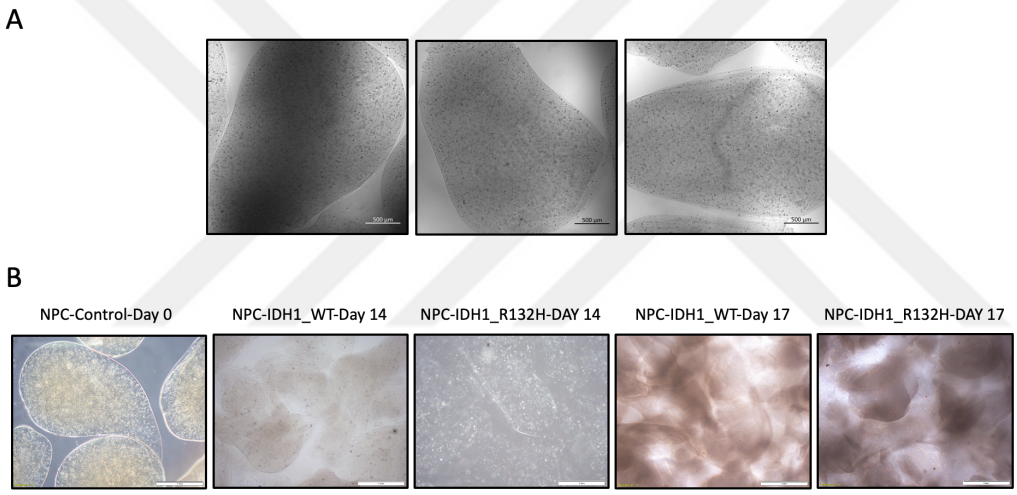

Figure 17. 3D culture of alginate beads prepared with hNPCs. A. Confocal microscope images after incubation of alginate-based 3D NPC culture in Neural progenitor medium for 1 day. Scale Bars: 500 µm. B. light microscope images of Alginate-based 3D NPC cultures on day 0 (incubated in NPC medium for one day), day 14 (incubated in IHA-IDH1-WT or IHA-IDH1-R132H conditioned medium for 14 days) and day 17 (they were first incubated in IHA-IDH1-WT and IHA-IDH1-R132H conditioned medium for 14 days, then in Neural Progenitor medium for three days). Scale Bar: 1 mm.

4.2.1. Effect of 3D culture prepared with alginate on cell viability, cell cycle and differentiation of NPCs.

Cell viability measurement with Calcein AM/PI staining

Calcein-AM/PI staining was applied to examine the short- and long-term viability and mortality rates of NPCs kept in 3D culture prepared with alginate and given IHA -IDH1-WT and IHA-IDH1-R132H conditioned medium by changing the medium at different times. Calcein AM (green) marks live cells, while PI (red) dye marks dead cells. Live and dying/dead cells were visualized by Calcein AM/PI staining (Figure 18).

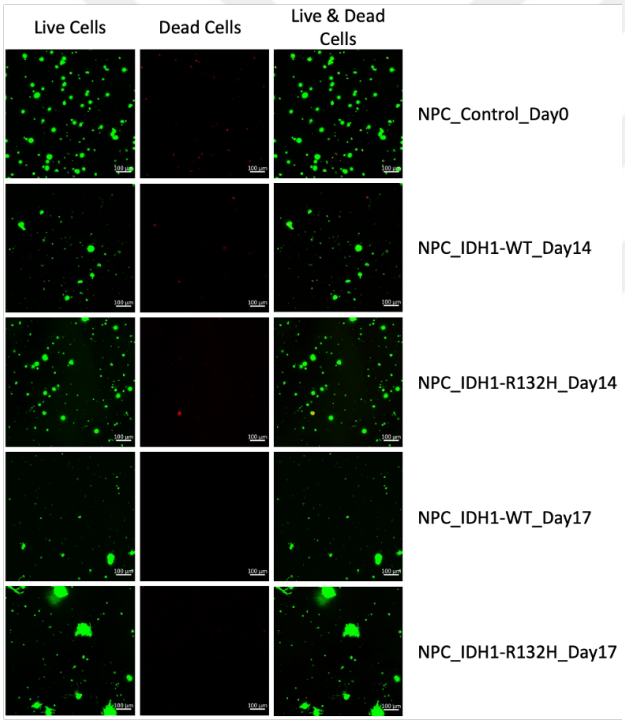

Figure 18. LIVE/DEAD imaging of Neural Progenitor cells stained with Calcein-AM/PI in three-dimensional alginate beads was performed with a confocal microscope. In the images, live cells were signed Calcein-AM (green) and dead cells were signed with PI (red). Scale bar:100µm

When we look at the live/dead staining of our 5 different experimental conditions, it is seen that on NPC_Control_Day 0 the cells appear as single cells, do not form aggregates yet,

and the number of dead cells is very low. When looking at the day 14 experimental conditions, interestingly, it was observed that there were more living cells in the NPC_IDH1-R132H_Day 14 condition than in the WT. Again, the dead cell rate is quite low under the 14th day conditions. When comparing the day 17 conditions, more cells are seen in the NPC_IDH1-R132H_Day 17 condition, which was exposed to the IHA-IDH1-R132H conditioned medium for 14 days. At the same time, on day 17, residual cells formed aggregates within the alginate beads (Figure 18).

Immunoflurescence Staining results of NPCs isolated from alginate beads

Immunoflurescence staining was performed for our 5 different experimental conditions. No images could be obtained for the 17th day conditions. 1 day after seeding on Matrigel-coated glass-bottomed plates, the cells could not bind to the plate. This may be an indication that the cells have changed morphologically. Our results supporting this conclusion are interesting. When we look at the SOX1, NESTIN and PAX6 staining of NPC cells isolated from NPC-alginate Beads in the NPC_Control_Day 0 condition, it is observed that the cells express these markers. But when we look at the cells isolated from NPC-alginate beads of both conditions on the 14th day, it is seen that the expression of SOX1 and PAX6 is greatly reduced. It was observed that PAX6 expression was almost absent, especially in the NPC_IDH1-WT_Day 14 condition, and SOX1 expression was almost absent in the NPC_IDH1-R132H_Day 14 condition (Figure 19).

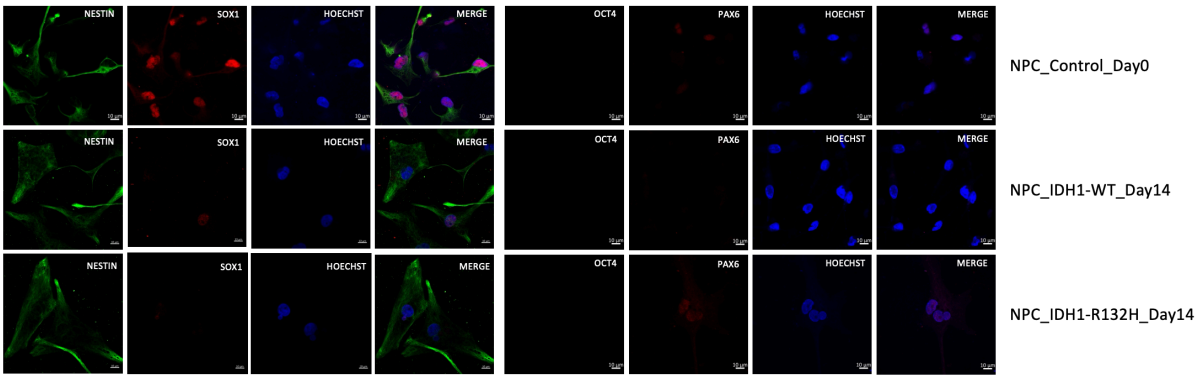

Figure 19. Immunoflurescence staining of NPCs isolated from 3D alginate cultures. Scale bar: 10µm

Cell Cycle Analysis with PI Staining

Seeing the distribution of different stages of the cell cycle and assessing the change in cell quantity is critical step to examine variations in cell growth, aging and apoptosis due to various factors (Malumbres & Barbacid, 2009). Many flow cytometry methods such as Propidium Iodide (PI) staining are available to measure the percentage of different stages of the cell cycle. PI, an intercalator dye, binds to DNA by entering between the bases in the DNA raft and allows measuring DNA content at different phases in the cell cycle. With PI staining, cells are divided into G0/G1 (2n), S (2n 4n) and G2/M (4n) phases, thus determining the current state of the cell cycle (Khurana et al., 2019).

Cell cycle analysis showed that cell cycle slowing occurred in the G2/M phase in cells maintained in 3D alginate culture and treated with different media. In particular, it was observed that the division of cells in NPC-alginate beads exposed to IHA-IDH1-R132H conditioned medium was extremely slow. Although there is a decrease in the proliferation of cells maintained in IHA-IDH1-WT medium on the 14th day compared to the control group, it is observed that the division rate is quite high compared to other conditions. It is thought that IHA-IDH1-R132H medium significantly reduces the cell cycle rate due to 2-HG. The reasons for these decreases in the division rate include the deterioration of the alginate bead structure over time and the slight damage to the NPC-alginate beads when the medium is changed at time points (Figure 20).

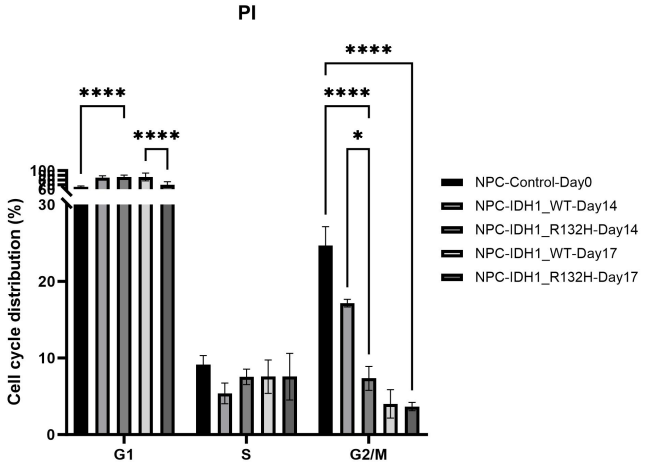

Figure 20. Cell cycle analysis by propidium iodide (PI) staining. In flow cytometry, 10000 cells were counted for each condition and 3 sets were prepared for each condition at different times.

4.3. Gene expression profiles of NPCs in different conditioned media in 3D alginate culture

4.3.1. RT-qPCR Results

Studies with the Mesenchme Homeobox 2 (MEOX2) have been shown to be effective in the malignancy and clinical prediction of hepatocarcinomas and lung cancer. Furthermore, it is known that the highest MEOX2 expression is observed in IDH1 aggressive type gliomas. Previous studies (Turcan et al., 2018), have shown that MEOX2 expression was permanently suppressed due to IDH1-R132H expression. As expected, MEOX2 expression was observed to be suppressed more strongly compared to the wild type as a result of treatment with IHA-IDH1-R132H medium in NPCs cultured in 3D medium prepared with alginate. In addition, MEOX2 expression level continued to decrease even 3 days after IHA-IDH1-R132 conditioned medium was replaced with Neural progenitor medium. The possible reason for the suppression in cells treated with IHA-IDH1-WT medium for 14 days can be interpreted as being related to the transition from Neural progenitor medium to astrocyte medium (Figure 21A).

JMJD2A (Jumonji domain containing 2A) belongs to a family of conserved Jmjc domain-containing proteins, which in turn are part of the Jmjc domain histone demethylase superfamily.

JmJC domain-containing histone lysine demethylases (KDMs:JMJD2A/2C etc.) and 5-methylcytosine hydroxylase (TET) are several enzymes that use α-KG as co-substrate and play a essential role in establishing and preservation epigenetic landscapes. In IDH mutant cells, it is targeted by D-2HG (Madala et al. 2018) and histone demethylases are inhibited by D-2HG (Matthew et al. 2015). In addition to reported genes, when we examined the expression of the JMJD2A gene, which is from the Jumonji domain family and encodes a protein that is inhibited by 2-HG, we observed an increase in both NPC_IDH1-WT and NPC_IDH1-R132H conditions on day 14. However, the disappearance of this effect on the 3rd day (day 17) of replacing the conditioned media with Neural progenitor medium indicates that JMJD2A was temporarily induced, and after removal of the IDH1-R132H IHA medium, its expression levels decreased to the same level as the wild-type IHA medium (Figure 21B).

It has been shown that the expression of L1CAM (L1 cell adhesion molecule) continues to increase after permanent removal of doxycycline by IDH1-R132H, independently of IDH1-R132H (Turcan et al., 2018). L1CAM, which plays a role in normal brain development, is a

neural cell adhesion molecule. It is overexpressed in gliomas and especially in glioma stem cells. However, we found that L1CAM was suppressed by IDH1-R132H IHA medium in alginate-embedded NPCs exposed to IHA-IDH1-R132H and IHA-IDH1-WT conditioned medium, in contrast to previously reported observations, and that this suppression was persistent (Figure 21C).

While TERT expression decreased excessively in NPCs exposed to IHA-WT medium on day 14, it was observed to increase compared to the WT and control groups as a result of exposure to IHA-R132H medium. Moreover, after replacing the IHA-IDH1-WT and IHA-IDH1-R132H conditioned media with Neural progenitor medium on day 14 and maintaining the cells with Neural progenitor medium for 3 days, TERT expression returned in NPCs exposed to IHA-IDH1-WT medium, TERT expression continued to increase in NPCs exposed to IHA-IDH1-R132H medium (Figure 21D). These results, when examined in the light of the literature, provide important clues regarding the induction of TERT expression by the IDH1-R132H mutation. Ohba et al. They reported that when they achieved stable IDH1-R132H expression in p53/pRb-KO E6E7-expressing normal human astrocytes, these cells were able to escape replicative senescence, whereas isogenic cells expressing IDH-WT could not (Ohba et al. 2016). Interestingly, researchers reported that IDH1-R132H induced TERT expression up to 40-fold, but this induction was observed only in NHAs that could recover from senescence-induced crisis and not in pre-crisis cells (Ohba et al., 2016). The fact that we were able to see this induction, albeit much weaker, in completely healthy (genetically wild-type) NPCs may be explained in two different ways: 1) NPCs more realistically mimic the onset of glioma 2) NPCs are genetically distinct from p53/pRb-KO E6E7 NHAs. It can also be explained by the fact that they are small and exist in a 3-dimensional culture environment.

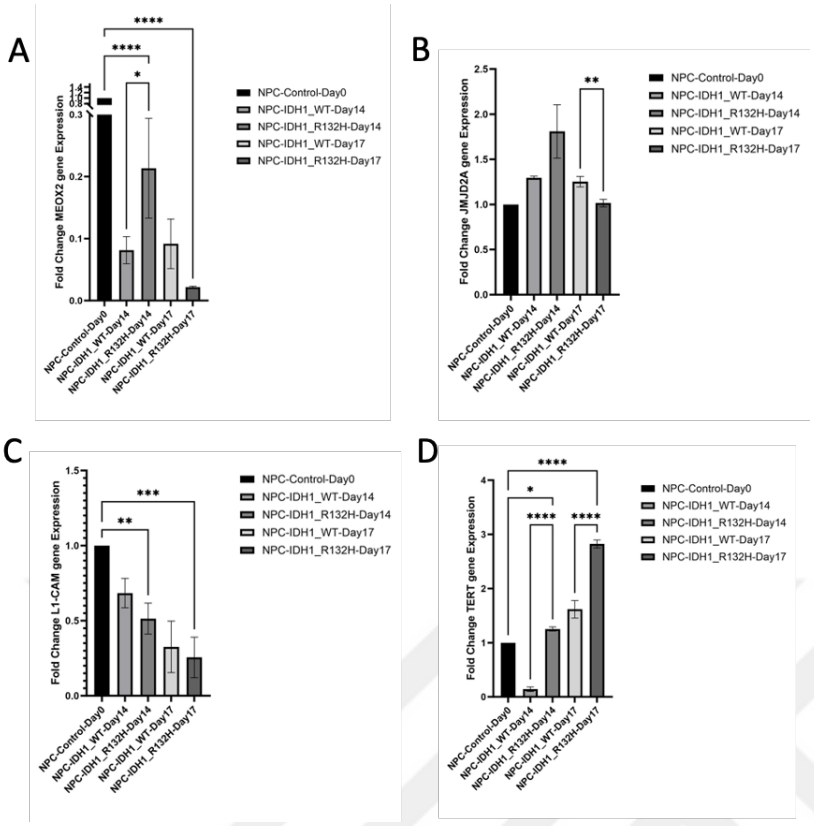

Figure 21. Graphs of the expression levels of L1-CAM, JMJD2A, TERT, TET1 and MEOX2 genes in 5 different experimental conditions. A) MEOX2 B) JMJD2A, C) L1-CAM, and D) TERT mRNA levels were measured by RT-qPCR in NPCs cultured in alginate beads for 3 different experimental conditions. ** $p < 0.01$; *** $p < 0.001$; **** $p < 0.0001$.

4.3.2. RNA-Seq Results

Normalization was performed because all samples had to have similar expression and range distributions in order for the analyzes to be performed correctly. Figure 22 shows TPM (Transcripts Per Million) distributions in raw data and normalized data. Each line shows the expression distributions of genes in a sample. Subsequent analyzes were performed on normalized data.

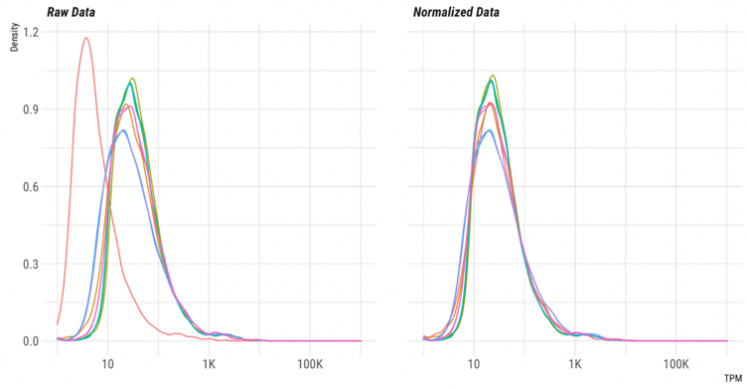

Figure 22. TPM (Transcripts per million) distributions in raw and normalized data

Transcriptome analysis with RNA-seq in NPCs in 3D alginate model

RNA was isolated from NPCs in 5 different experimental conditions and transcriptome analysis was performed. In the first stage of analysis of RNA-seq data, primary component analysis (PCA) was performed (Figure 23).

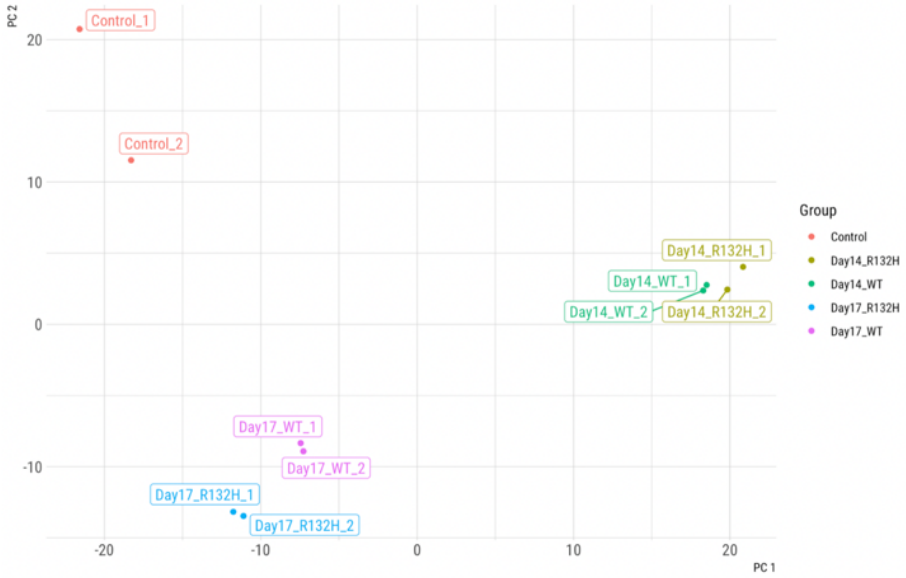

Figure 23. PCA analysis plot of RNA-seq data.

As can be seen from Figure 5, the most effective factor in the effects of IHA-IDH1-WT and IHA-IDH1-R132H conditioned media on NPCs maintained in 3D culture prepared with alginate is day/astrocyte medium exposure. It is seen that mutant and wild-type conditioned

media differentiate from each other and cluster among themselves. Another noteworthy point is that after removal of conditioned media on Day 14, the NPC transcriptome approached NPC-Control-Day0 in some respects, but a complete reversal did not occur for either group, although this was consistent between cells exposed to mutant and WT media. The differences appear to be preserved. As a result, it was concluded that, as expected, the transcriptome partially reverted in a short time, but this reversal differed depending on the mutation status. It is an extremely important outcome that the characterization of this situation, which is one of the objectives of the project, can be observed in a 3-dimensional environment and independently of other confounding mutations. In the next stage, differential gene expression (DEG) analysis was performed to obtain gene-based differences. Comparisons were made in 4 different ways (Table 19).

Table 19. Groups used to compare RNA-seq data.

Comparison 1	NPC-Control-Day0	NPC-IDH1_R132H-Day14
Comparison 2	NPC-Control-Day0	NPC-IDH1_R132H-Day17
Comparison 3	NPC-IDH1_WT-Day14	NPC-IDH1_R132H-Day14
Comparison 4	NPC-IDH1_WT-Day17	NPC-IDH1_R132H-Day17

Comparison 1: NPC-Control-Day0 vs. NPC-IDH1_R132H-Day14

According to the analysis performed in Comparison 1, there was an increase in expression in 915 genes; decrease expression of 1402 genes was detected. In Table 20 and Table 21, it has the highest fold-change (-Fold-change) (Table 20) and fold-change (Table 21) values among the first 100 genes with the lowest FDR value. The top 20 genes are listed.

Table 20. Top 20 genes with decreased expression on day 14 compared to comparison 1 (Fold-change).

Gene	↑ logFC	PValue	FDR
LGALS1	-6.6174	1.24600919014175e-12	9.44010766585e-9
TXNIP	-5.7628	9.30540707278199e-11	1.18250782590297e-7
ACTG2	-5.0345	1.99021344437536e-10	1.2787915332219e-7
CAVIN1	-4.8654	3.13759245748566e-10	1.42569558246121e-7
PMP22	-4.2211	1.98588027533477e-11	4.02984729648524e-8
S100A6	-4.1864	7.77223698401483e-10	2.37990216754095e-7
PLP2	-4.1624	1.0515995314695e-10	1.18250782590297e-7
S100A10	-4.0493	2.09524085359006e-12	9.44010766585e-9
TPM2	-3.9184	7.60886369763515e-10	2.37990216754095e-7
CAPG	-3.776	3.80000729202751e-9	6.34108624230739e-7
MYL9	-3.761	1.54224601051618e-10	1.18250782590297e-7
SFTA1P	-3.6524	8.28659582719257e-9	0.00000106672164284046
TFPI2	-3.5676	1.69408036329343e-9	3.70769578147935e-7
GJA1	-3.5231	1.52483664879392e-9	3.61586922165316e-7
TAGLN2	-3.1222	2.65293237093413e-10	1.40621021144044e-7
LMCD1	-3.1208	7.92332316349223e-10	2.37990216754095e-7
S100A11	-3.1005	2.50433141797032e-10	1.40621021144044e-7
THY1	-3.0884	1.32351894787914e-10	1.18250782590297e-7
PLAT	-2.9793	3.67238582805911e-10	1.5041758498473e-7
COTL1	-2.8295	2.2360710778411e-11	4.02984729648524e-8

Table 21. Top 20 genes with increased expression on day 14 compared to comparison 1 (Fold-change).

Gene	↓ logFC	PValue	FDR
SGCG	6.4396	5.28067393692903e-10	1.9033661138267e-7
HSPA6	5.8591	2.13643061167693e-11	4.02984729648524e-8
LAMP3	4.6133	1.09634671405818e-8	0.00000125052914435168
SLC7A3	4.3548	1.59759600394546e-8	0.00000161752107770254
GABRQ	4.2179	2.20704920367299e-8	0.00000211571493343588
HES5	3.8815	1.05996351612278e-9	2.76832628850859e-7
KCNG1	3.79	1.14230946029479e-9	2.85926404075454e-7
FXYD7	3.6579	2.41486548677797e-8	0.00000219107667506061
IGLON5	3.3975	6.3818953243521e-9	8.58317295040848e-7
PGGHG	3.37	6.66319621630163e-9	8.82971486839618e-7
ID1	3.1981	1.75624080957069e-9	3.70769578147935e-7
RIMS3	2.9009	9.97643514082399e-9	0.00000118997408527733
CCPG1	2.8884	2.88758563008792e-9	5.3102110434127e-7
PMAIP1	2.8663	4.99823229713983e-9	7.14905892532174e-7
CHAC1	2.8047	3.98510475138018e-9	6.41018443437973e-7
EBF4	2.6608	2.52182520016355e-9	4.83492912312208e-7
DDIT3	2.6216	7.22357220966865e-10	2.37990216754095e-7
BEX2	2.5299	5.74063305594966e-9	7.95582976293211e-7
ASNS	2.4803	1.9077820768311e-8	0.00000188912354882692
GTPBP2	2.4635	1.05145280098945e-9	2.76832628850859e-7

Comparison 2: NPC-Control-Day0 vs. NPC-IDH1_R132H-Day17

According to the analysis performed in Comparison 2, there was increase expression in 1183 genes; A decrease in expression was detected in 1006 genes. In Table 22 and Table 23, among the first 100 genes with the lowest FDR value, the highest fold-decrease (-Fold-change) (Table 22) and fold-increase (-Fold-change) (Table 23) values are shown. The top 20 genes that have it are listed.

Table 22. Top 20 genes with decreased expression on day 17 compared to comparison 2 (-Fold-change).

Gene	↑ logFC	PValue	FDR
IGFBP5	-4.3725	9.50146594803098e-8	0.0000129312380809108
SMOC1	-3.6891	1.05335189380118e-7	0.0000137561650942644
VGLL3	-3.5283	5.62683849071785e-9	0.00000281685786888103
TENM3	-3.4855	8.93340391650282e-9	0.00000321995610766428
THBS1	-3.0993	2.36781578453305e-10	6.39298052185666e-7
TRIL	-3.0675	2.22960170239744e-7	0.0000223232677114481
PI15	-2.9771	1.1164398408938e-8	0.00000346904807113587
PMP22	-2.6652	3.5473202318592e-10	6.39298052185666e-7
SRCAP	-2.6547	2.22335786523184e-7	0.0000223232677114481
GJA1	-2.6491	1.03917373484029e-8	0.00000334428375880209
NID1	-2.645	1.98109204592246e-7	0.0000215079764166353
PALM2AKAP2	-2.5938	2.45499728225479e-9	0.00000168145737330906
LGALS1	-2.5351	2.96341363599205e-10	6.39298052185666e-7
VCAN	-2.5291	4.06431631127514e-8	0.00000767146341732783
COL3A1	-2.4964	2.86256468068401e-7	0.0000268859786750844
CAVIN1	-2.4726	9.89694860209213e-9	0.00000330301495753527
ADAM12	-2.4442	4.8994163162829e-8	0.00000839336476899374
PLP2	-2.441	2.19087103953061e-9	0.00000164516157810086
FILIP1L	-2.4394	1.29764993605075e-7	0.000015590831431671
SESN3	-2.3262	2.05287734535715e-8	0.00000528527935971807

Table 23. Top 20 genes with increased expression on day 17 compared to comparison 2 (Fold-change).

Gene	↓ logFC	PValue	FDR
SOX14	6.0086	4.15106813807789e-8	0.00000767146341732783
NRN1	4.5135	2.66199701952179e-7	0.0000255183565350116
FXYD7	4.3244	3.11287502274544e-9	0.00000187000778866394
COL13A1	4.1941	6.7307765045395e-8	0.0000106405310670887
ID1	3.9874	8.68376389108994e-11	5.03422725668277e-7
ID3	3.9275	9.05260768968529e-10	9.58264342387132e-7
IGLON5	3.4039	7.97232535621391e-9	0.00000299327599103515
LRRC10B	3.3199	2.89417371155608e-7	0.0000268859786750844
FXYD5	3.2988	5.52111056018538e-9	0.00000281685786888103
HS3ST4	3.243	1.70208083830437e-8	0.00000464771225271537
NSG2	3.1125	2.91227806982759e-8	0.00000610291574121311
PLPPR1	3.0962	2.61240741608333e-9	0.00000168145737330906
LY6H	2.9857	6.14663726202575e-9	0.00000285195607300473
MIR9-1HG	2.7893	1.71079901070305e-9	0.00000154160098854451
C2orf80	2.6879	9.57094560146952e-10	9.58264342387132e-7
PCSK1N	2.6532	6.69155935100756e-9	0.00000285195607300473
B3GAT1	2.1498	6.96293792099701e-9	0.00000285195607300473
C1QTNF6	2.0806	1.37126996523349e-7	0.000016258570600946
ID2	1.9881	1.18497395407043e-8	0.00000355926676670955
HES4	1.9727	4.93672547726854e-8	0.00000839336476899374

Comparison 3: NPC-IDH1_WT-Day14 vs. NPC-IDH1_R132H-Day14

According to the analysis performed in Comparison 3, increase expression was seen in 17 genes; A decrease in expression was detected in 3 genes. In Table 24 and Table 25, it has the highest fold-change (-Fold-change) (Table 24) and fold-change (Table 25) values among the first 100 genes with the lowest FDR value. The top 20 genes are listed.

Table 24. Top 20 genes with decreased expression on day 14 compared to comparison 3 (-Fold-change).

Gene	↑ logFC	PValue	FDR
MT1F	-1.3138	0.00193180760677501	0.226071666813631
TTR	-1.1474	0.00137126579315387	0.186054374270528
SPP1	-1.0623	0.000203908323319151	0.0706699192857257
KCNIP4	-0.9315	0.000373022552549397	0.0988619476771357
MT1X	-0.917	0.000306380994307228	0.0963761485053122
RHOU	-0.8289	0.00158160116172419	0.20072969110277
VXN	-0.8019	0.00000596034574404585	0.0121048337614969
S100A10	-0.7945	0.000821294503607519	0.139635561735988
NNAT	-0.7696	0.000331656579808586	0.0963761485053122
SCG2	-0.7161	0.00137115085358592	0.186054374270528
NUDCD3	-0.701	0.000693186701545144	0.124926107352466
NPTX2	-0.6915	0.000213787003563698	0.0192643468911248
ELAVL4	-0.644	0.00238993412664328	0.25946622186967
CPLX2	-0.6347	0.000120591445719553	0.050546709688251
MT2A	-0.6291	0.00309683030548612	0.293742504028794
GAP43	-0.6086	0.00293010275617573	0.286990825390212
STMN2	-0.5275	0.0034883283696869	0.314333269392487
PCSK1N	-0.475	0.000467623393430407	0.102774497517107
DCX	-0.4486	0.00113511533016743	0.170475404002311
INSM1	-0.4445	0.000829977026382758	0.0415495721374168

Table 25. Top 20 genes with increased expression on day 14 compared to comparison 3 (Fold-change).

Gene	↓ logFC	PValue	FDR
7SK	8.5148	0.00221985072970725	0.250038436567401
ID1	1.5008	1.89189983503268e-8	0.000170479094134795
PIF1	1.4732	0.00124912757899774	0.18154659055401
EMP1	1.3064	0.00111505267985917	0.170475404002311
GOLGA8B	1.3004	0.000100039228025029	0.0450726741866769
ID3	1.2677	0.00000322008499175292	0.00967206195356184
TARBP1	1.1315	0.00175844718460969	0.218000926528058
AHSA2P	1.0896	0.000464714804392621	0.102774497517107
CHTF18	1.0895	0.000166196441881882	0.0599038455119054
GOLGA8A	1.0291	0.00124670067030431	0.18154659055401
NPIPA9	1.0025	0.00104880549208976	0.168764040878944
MSH5	0.9793	0.00176607120592034	0.218000926528058
SMG1P7	0.9677	0.000330165321800544	0.0963761485053122
AASS	0.952	0.000617349353914856	0.120933370176669
NPIPB3	0.9421	0.000342531839315837	0.0963761485053122
ID2	0.9322	3.92688465133553e-7	0.00176925787965922
WDR90	0.9289	0.00302138232997756	0.289634852930083
PABPC1L	0.918	0.000820366666607915	0.139635561735988
ROBO3	0.9002	0.000092305683961 4013	0.0437771851671677
CCDC14	0.8946	0.000201368865475445	0.0192643468911248

Comparison 4: NPC-IDH1_WT-Day17 vs NPC-IDH1_R132H-Day17

According to the analysis performed in Comparison 4, expression increase in 1143 genes; A decrease in expression was detected in 636 genes. In Table 26 and Table 27, it has the highest fold-change (-Fold-change) (Table 26) and fold-change (Table 27) values among the first 100 genes with the lowest FDR value. The top 20 genes are listed.

Table 26. Top 20 genes with decreased expression on day 17 compared to comparison 4 (-Fold-change).

Gene	↑ logFC	PValue	FDR
SRCAP	-2.3061	4.04376709319763e-7	0.000295588464505966
IL6ST	-2.169	0.0000028044598056467	0.000533458372735266
TMX2-CTNND1	-1.7639	2.4065608277272e-7	0.000295588464505966
AFF4	-1.6077	0.00000910349544143142	0.000743772608568373
ADAM10	-1.551	0.0000017172511114719	0.000442118564727809
MT-ND4L	-1.5182	5.24531814030076e-7	0.000295588464505966
DAAM1	-1.4543	7.79256808529184e-7	0.000295588464505966
TRIM44	-1.4539	0.0000014580230149886 3	0.000442118564727809
PALM2AKAP2	-1.4259	8.70703035166354e-7	0.000301765578841693
GAS2L3	-1.3029	6.32950537888703e-7	0.000295588464505966
DCX	-1.2852	0.0000069923702282672 7	0.000679702861628414
MT-ND5	-1.256	0.0000056458840944463 2	0.000635938269688197
GAS7	-1.244	0.0000075015139957997 9	0.000713239938283399
PDP1	-1.2189	0.0000052371234442756 9	0.000635668741902919
QKI	-1.204	0.0000019596090541470 8	0.00046178637564903
EPB41L3	-1.1897	3.46063720526638e-8	0.000155919009283277
TACC1	-1.185	0.0000015015438546177 9	0.000442118564727809
TNPO1	-1.1406	0.0000054918263305162 1	0.000635938269688197
DOCK7	-1.1355	0.0000021077919029992	0.000470777887147052
NAMPT	-1.1338	0.0000032799018199811 1	0.000533458372735266

Table 27. Top 20 genes with increased expression on day 17 (Fold-change) compared to Comparison 4.

ID1	2.857	4.30762254064597e-11	3.88159867137609e-7
ID3	1.2507	0.0000024334618087982	0.00049836191725183
ID2	1.23	8.21028688470753e-8	0.00024609650393665
MYL9	1.1839	2.12926360048365e-7	0.00029558846450596 6
WNT7B	1.1793	0.00000236523698331251	0.00049565466178207
CCDC85B	1.0669	0.00000314186944949111	0.00053345837273526 6
EVA1B	0.9978	0.00000377601394947737	0.00056709436164567 7
ATOX1	0.9741	0.00000514107789766451	0.00063566874190291 9
SCAND1	0.9485	2.86404851100281e-7	0.00029558846450596 6
MRPL23	0.9467	0.00000798502002423544	0.00072679813574126 8
PAM16	0.9384	0.00000304661152642249	
C1orf122	0.9306	3.46113720518722e-7	
RP11-425L10	0.9202	6.90612338056484e-7	
RPL26P19	0.9151	0.00000199863152261815	
DPM3	0.9088	0.00000643082338284996	
PET100	0.9079	6.1288302630108e-7	
TMEM160	0.9007	5.9223570149792e-7	
NAA38	0.8863	0.00000560955079268807	
MZT2A	0.8801	0.00000161351339047133	
DOK5	0.878	7.8727368196018e-7	

Among the genes expressed differently in the 3rd and 4th comparisons, ID1, ID2 and ID3 genes respectively stand out. Among these three genes, the ID1 (DNA binding inhibitor 1) gene stands out. Then, the expression of ID1 was tested by the RT-qPCR method and, just like the RNA-seq results, it was observed that ID1 expression was strongly induced in alginate-embedded NPCs exposed to IDH1-R132H IHA medium (Figure 23).

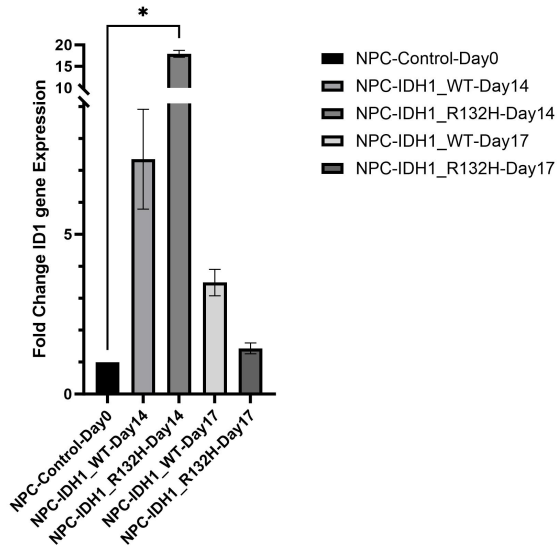

Figüre 23. RT-qPCR result for ID1 expression

Following the emergence of the ID1 gene as a target of IDH1-R132H as a result of RT-qPCR and RNA-seq analyses, genes showing differential expression in RNA-seq analysis were compared with TCGA-LGG (Cancer Genome Atlas – Low Grade Glioma) data.

For this, the genes showing an increase/decrease in expression on the 17th day were compared with the first 25 genes showing the highest correlation with ID1 expression according to TCGA-LGG RNA-seq data. It is striking that 15 of the 25 genes were expressed differently on day 17 and all of them were correlated in the same direction (positive-positive, negative-negative), and that the transcriptome changes we see in NPCs are quite similar to low-grade gliomas from an ID1-centered perspective (Table 28).

Table 28. Coincidence of the genes most highly correlated with ID1 in the TCGA-LGG cohort with expression changes in NPCs on day 17.

Gene name	logFC	PValue	FDR	ID1 correlation order - TCGA-LGG
ID3	1,2507	2,43E-06	0,000498	9
RPS21	0,8347	2,96E-05	0,001172	24
C1QL1	0,7461	0,004443	0,027612	2
RPS3	0,7266	0,000211	0,003132	16
FAU	0,7166	1,03E-05	0,00077	6
RPL18A	0,7005	0,00046	0,005227	14
MPST	0,6823	8,76E-06	0,000744	18
POLR1H	0,6606	0,009543	0,048719	20
WDR74	0,6553	0,000553	0,005965	15
RPL23	0,6256	7,75E-05	0,001742	22
ZFAS1	0,6064	0,000579	0,006113	25
ATP2B1	-0,5921	0,134541	0,305454	12
PKN1	0,5753	0,001453	0,012158	7
BCAP29	-0,2988	0,42599	0,624365	9
PLCB3	0,0903	0,789141	0,885617	23
PRR14	0,1633	0,469432	0,661773	5
EEF1G	0,536	0,00389	0,025111	21
ACSL3	-0,7337	0,000958	0,00894	1
CHL1	-2,3863	4,43E-05	0,001321	3

Since all these results highlight the ID1 gene as an important candidate for the transformative and carcinogenic effects of the IDH1-R132H mutation on NPCs, the promoter region of this gene was also included in the subsequent ChIP-qPCR and MeDIP-qPCR analyses.

Since TERT expression, one of the two genes targeted in the project, could not be detected as a result of RNA-seq analysis (due to low expression level), the change in TERT expression was examined with RT-qPCR, which is a more sensitive method (Figure 21D).

The fact that TERT is induced by the IHA-R132H conditioned medium is also interesting as it is the target gene of MYC, another target gene of the project. As a matter of fact, Ohba et al. They showed that MYC binding together with the H3K4me3 increase of TERT plays a role in the induction of TERT by IDH1-R132H. However, when the RNA-seq analysis results were examined, we observed that MYC expression was not induced by IDH1-R132H IHA medium: -0.04-fold, p=0.86 (comparison 3), 0.06-fold, p=0.81 (comparison 4). On the other hand, MYC is an immediate early gene and the stability of its mRNA is extremely low; Since mitogens in the environment are rapidly degraded at both mRNA and protein levels (half-time 25 min) as soon as they are removed (Dani et al. 1984, PMID: 6594679), examining MYC target genes is a more reliable approach for the analysis of MYC activity. For this reason, the frequently used Enrichr bioinformatics analysis tool was used to determine gene-set enrichment for the 102 genes whose expression increased the most on day 17 (Kuleshov et al. 2016, PMID: 27141961). As a result of this analysis, it is seen that MYC target genes are enriched up to 4 times among these 102 genes (Figure 24).

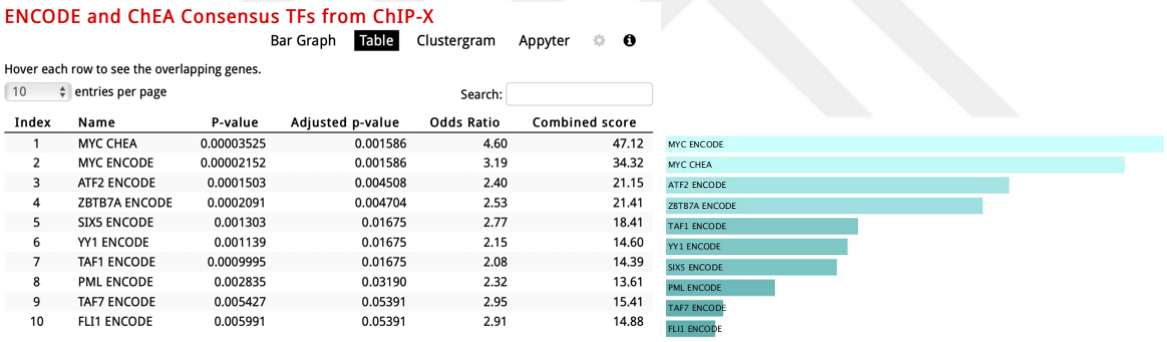

Figure 24. MYC target genes were significantly enriched among genes showing increased expression on day 17

The KEGG database was used for pathway analyzes and the data from Comparison 3 and Comparison 4 detailed above were used. At day 14, increased pathway signatures included pluripotency of stem cells, mRNA TGF-beta signaling pathway, and Hippo signaling pathway, while decreased pathways included mineral absorption and nervous system diseases such as Alzheimer's and Parkinson's (Figure 25). On the 17th day, the Ribosome pathway stands out as the most significantly increased pathway, probably due to increased MYC activity, while cancer-related pathways (e.g. Pathways in cancer, Prostate cancer, Wnt signaling pathway) and

melanogenesis stand out among the decreased pathways. Interestingly, the signaling pathway that controls pluripotency was among the pathways that both increased and decreased the most on Day 17; The possible reason for this may be that some of the different components of these critical pathways are permanently induced by 2-HG, while others are temporarily induced, that is, a rapid return to their previous levels upon withdrawal of 2-HG. As a matter of fact, the fact that cancer-related pathways are among the pathways that decrease most significantly immediately after the withdrawal of 2-HG indicates that at least some of the effects of 2-HG on cancer are temporary, indicating that 2-HG and therefore IDH1-R132H and the associated IDH1/ It can be interpreted as being dependent on the presence of 2 mutations (Figure 26).

UP

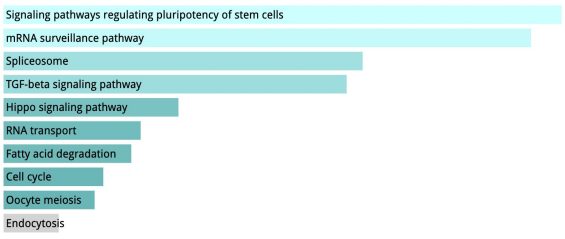

Index	Name	P-value	Adjusted p-value	Odds Ratio	Combined score
1	Signaling pathways regulating pluripotency of stem cells	0.0001872	0.01144	7.86	67.48
2	mRNA surveillance pathway	0.0002660	0.01144	9.59	78.91
3	Spliceosome	0.001826	0.04715	6.13	38.67
4	TGF-beta signaling pathway	0.002193	0.04715	7.85	48.09
5	Hippo signaling pathway	0.01504	0.2587	4.43	18.59
6	RNA transport	0.02318	0.3170	3.87	14.55
7	Fatty acid degradation	0.02580	0.3170	8.49	31.05
8	Cell cycle	0.03555	0.3750	4.34	14.47
9	Oocyte meiosis	0.03925	0.3750	4.16	13.48
10	Endocytosis	0.05920	0.5091	2.83	7.99

DOWN

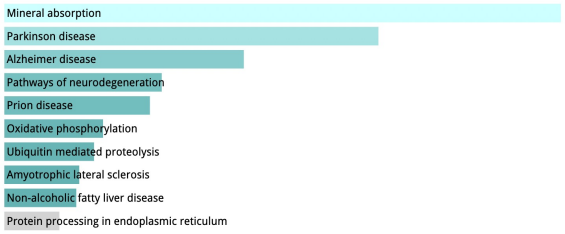

Index	Name	P-value	Adjusted p-value	Odds Ratio	Combined score
1	Mineral absorption	0.0002711	0.008405	26.86	220.58
2	Parkinson disease	0.001811	0.02806	8.47	53.48
3	Alzheimer disease	0.007344	0.07589	5.65	27.77
4	Prion disease	0.01952	0.1210	5.61	22.08
5	Pathways of neurodegeneration	0.01726	0.1210	4.36	17.68
6	Oxidative phosphorylation	0.03178	0.1446	7.57	26.10
7	Ubiquitin mediated proteolysis	0.03490	0.1446	7.18	24.09
8	Non-alcoholic fatty liver disease	0.04198	0.1446	6.47	20.52
9	Amyotrophic lateral sclerosis	0.04072	0.1446	4.18	13.37
10	Protein processing in endoplasmic reticulum	0.05007	0.1552	5.85	17.53

Figure 25. KEGG pathway analysis of genes showing increased and decreased expression on day 14

UP

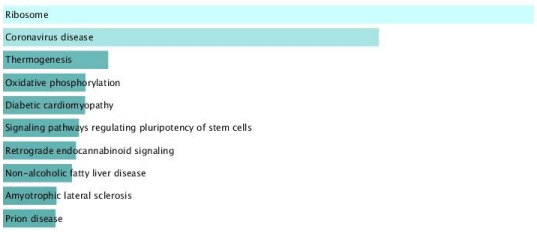

Index	Name	P-value	Adjusted p-value	Odds Ratio	Combined score
1	Ribosome	6.717e-14	7.590e-12	21.82	661.96
2	Coronavirus disease	1.848e-10	1.044e-8	13.13	294.16
3	Thermogenesis	0.0001873	0.007053	6.44	55.30
4	Oxidative phosphorylation	0.0005995	0.01377	7.96	59.07
5	Diabetic cardiomyopathy	0.0006092	0.01377	6.25	46.27
6	Signaling pathways regulating pluripotency of stem cells	0.0008321	0.01567	7.38	52.34
7	Retrograde endocannabinoid signaling	0.0009709	0.01567	7.12	49.40
8	Non-alcoholic fatty liver disease	0.001193	0.01685	6.79	45.68
9	Prion disease	0.002762	0.02912	4.60	27.07
10	Amyotrophic lateral sclerosis	0.002628	0.02912	4.03	23.96

DOWN

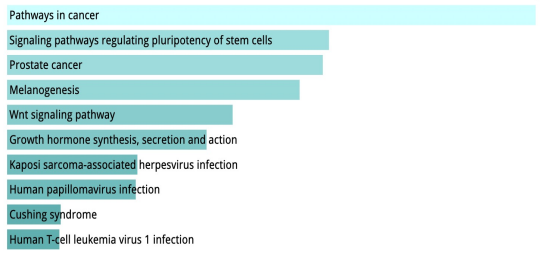

Index	Name	P-value	Adjusted p-value	Odds Ratio	Combined score
1	Pathways in cancer	0.000002738	0.0004928	5.09	65.21
2	Signaling pathways regulating pluripotency of stem cells	0.00002123	0.001278	9.24	99.42
3	Prostate cancer	0.00002257	0.001278	11.76	125.78
4	Melanogenesis	0.00002840	0.001278	11.26	117.87
5	Wnt signaling pathway	0.00005514	0.001985	7.89	77.41
6	Growth hormone synthesis, secretion and action	0.00007140	0.002142	9.46	90.29
7	Kaposi sarcoma-associated herpesvirus infection	0.0001417	0.003242	6.74	59.72
8	Human papillomavirus infection	0.0001441	0.003242	5.06	44.78
9	Cushing syndrome	0.0003031	0.005527	7.16	58.00
10	Human T-cell leukemia virus 1 infection	0.0003070	0.005527	5.90	47.76

Figure 26. KEGG pathway analysis of genes increased and decreased expression on day 17

In the next stage, we used the RNA-seq data we obtained from NPCs cultured in a 3-dimensional environment prepared with alginate and the data previously reported by Turcan et al. with Lee et al. We compared the RNA-seq data obtained from IHAs cultured in a 2-dimensional environment by (Turcan et al. 2017, Lee et al. 2022) (Table 29).

Table 29. Genes expressed differently in NPCs due to IDH mutation and common genes previously reported to be expressed differently in IHAs due to IDH mutation. Only genes that show differential expression in at least two cases are shown. Up: Its expression has increased, down: its expression has decreased, NC: its expression has not changed significantly. NPC day14: NPC-IDH1_R132H-Day14, NPC day17: NPC-IDH1_R132H-Day17

Gene Name	Turcan et al. 2018	Lee et al. 2022	NPC day14	NPC day17
ACKR3	up	down	NC	NC
ACTG2	down	down	NC	NC
ADAMTS1	down	down	NC	NC
AEBP1	down	down	NC	NC
ANXA3	up	down	NC	NC
ASS1	up	down	NC	NC
BGN	down	down	NC	NC
CACNA1C	down	up	NC	NC
CNN1	down	down	NC	NC
CNR1	NC	up	NC	down
COL3A1	down	down	NC	NC
COL6A1	down	down	NC	NC
COL6A2	down	down	NC	NC
COL9A3	up	up	NC	NC
COLEC12	up	down	NC	NC
CPLX2	NC	up	down	NC
CYB5R2	down	down	NC	NC
CYTL1	down	down	NC	NC
DCX	up	NC	down	down
DDO	up	up	NC	NC
DOK5	NC	down	up	up
DIO2	up	down	NC	NC

Gene Name	Turcan et al. 2018	Lee et al. 2022	NPC day14	NPC day17
EFEMP1	up	down	NC	NC
EFS	down	down	NC	NC
FAM49A	up	down	NC	NC
FN1	down	down	NC	NC
FOXE1	up	down	NC	NC
HAUS7	NC	down	up	NC
HES4	NC	NC	up	up
HEY2	down	up	NC	NC
HNRNPH1	down	NC	up	NC
HS3ST3A1	up	NC	NC	down
ID1	NC	NC	up	up
ID2	down	NC	up	up
ID3	NC	NC	up	up
ID4	down	NC	up	NC
IGSF9B	up	down	NC	NC
IL27RA	up	down	NC	NC
ITGA2	up	down	NC	NC
KCNIP4	NC	NC	down	down
KCNK1	up	down	NC	NC
KCNK15	up	up	NC	NC
KIT	down	up	NC	NC
L1CAM	up	up	NC	NC
LAD1	up	up	NC	NC
LBH	up	down	NC	NC
LIMCH1	up	down	NC	NC
LMOD1	down	up	NC	NC
LRP4	up	NC	up	NC
LY96	up	up	NC	NC
MAF	down	down	NC	NC
MAN1A1	down	up	NC	NC

Gene Name	Turcan et al. 2018	Lee et al. 2022	NPC day14	NPC day17
MAN1C1	up	up	NC	NC
MMP2	up	down	NC	NC
MN1	up	down	NC	NC
NDRG1	up	down	NC	NC
NMU	down	NC	NC	up
NPTX2	NC	down	down	NC
NREP	NC	down	down	NC
OPN	down	down	NC	NC
PDGFRA	up	down	NC	NC
PDLIM3	down	up	NC	NC
PNISR	up	NC	up	NC
PPP2R2B	up	up	NC	NC
RAB33A	down	down	NC	NC
RCAN3	up	up	NC	NC
RHOU	NC	NC	down	down
SCG2	up	NC	down	NC
SIX3	up	down	NC	NC
SLC4A4	down	down	NC	NC
SNCA	down	up	NC	NC
SOX3	up	NC	NC	up
SOX11	up	down	NC	NC
SPOCK1	up	down	NC	down
SRRM2	NC	NC	up	up
STOX2	NC	up	NC	down
TAGLN	NC	down	NC	up
TGM2	down	down	NC	NC
TNFRSF9	up	down	NC	NC
TSPAN2	down	down	NC	NC
VCAN	down	NC	NC	down
WNT7B	up	NC	up	up
ZNF804A	down	up	NC	NC

While some genes appear to change in the same direction, many others show changes in expression in the opposite direction. It is seen that 55 of the 83 common genes show changes specific to IHAs, and 25 of them are in the same direction. 21 genes were differentially expressed in both NPCs and IHAs, 7 of them in the same direction (LRP4, NPTX2, NREP, PNISR, SOX3, VCAN, WNT7B), 13 in the opposite direction and 1 (SPOCK1). Lee et al. In the same direction as Turcan et al. It is seen that there is a change in the opposite direction. It is seen that 6 genes are expressed differently only in NPCs (HES4, ID1, ID3, KCNIP4, RHOU, SRRM2) and all of these 6 genes show the same change in expression on both the 14th day and the 17th day. It is noteworthy that the WNT7B gene showed increased expression in 3 out of 4 conditions. In order to see the protein-protein interactions of the genes in Table 29, 83 genes were examined through the STRING database (Figure 27). Transcription factor (TF) analysis of genes showing expression changes due to IDH1 mutation in 4 different conditions was performed (Figure 28).

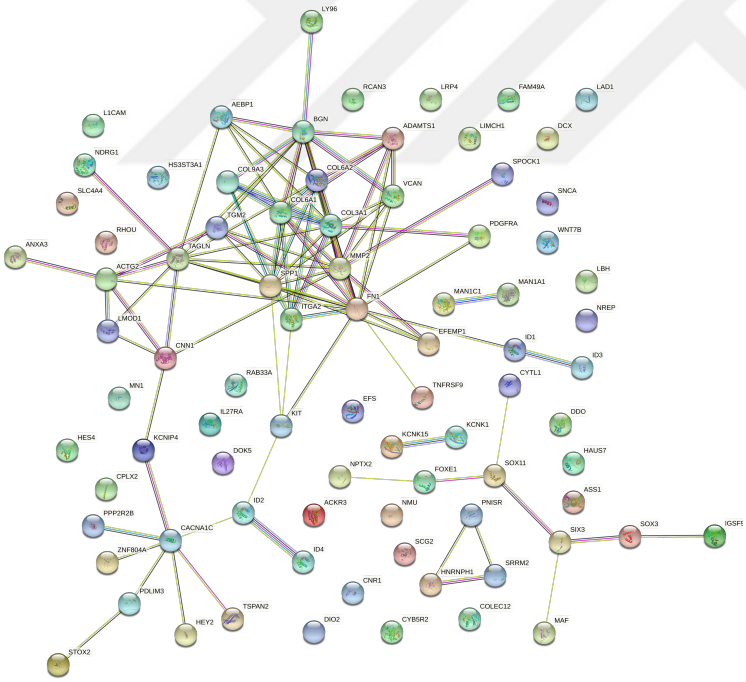

Figure 27. PPI analysis of proteins encoded by genes showing expression changes due to IDH1 mutation in 4 different conditions

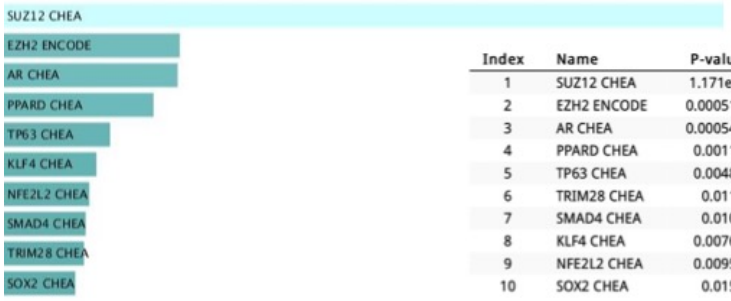

Index	Name	P-value	Adjusted p-value	Odds Ratio	Combined score
1	SUZ12 CHEA	1.171e-11	8.902e-10	5.93	149.16
2	EZH2 ENCODE	0.0005115	0.01392	5.45	41.30
3	AR CHEA	0.0005496	0.01392	3.23	24.27
4	PPARD CHEA	0.001197	0.02274	5.48	36.90
5	TP63 CHEA	0.004868	0.07400	2.48	13.22
6	TRIM28 CHEA	0.01138	0.09614	4.84	21.68
7	SMAD4 CHEA	0.01071	0.09614	3.09	14.00
8	KLF4 CHEA	0.007603	0.09614	2.66	12.96
9	NFE2L2 CHEA	0.009596	0.09614	2.56	11.89
10	SOX2 CHEA	0.01502	0.1142	2.66	11.18

Figure 28. TF analysis of genes showing expression changes due to IDH1 mutation in 4 different conditions

4.4. Effect of 2-HG on epigenetic regulation in NPCs maintained in 3D alginate culture.

Genome-wide analysis of DNA sequence and molecular components is important to understand genome activity and systems biology. Epigenetics is defined as mitotic and meiotic changes that occur in genome activity without any change in DNA sequence (Retis-Resendiz et al., 2021). Epigenetic regulation plays a fundamental role in important cellular mechanisms such as growth, gene expression, differentiation of cell, and genome stability (Meissner, 2010; Putiri & Robertson, 2011).

4.4.1. ChIP-qPCR Results

Important techniques in epigenomic research are chromatin immunoprecipitation (ChIP) and sequencing. ChIP is an important technique for genome-wide mapping of epigenetic marks and the interaction between chromatin and a specific biomolecular target and providing information about how transcriptional regulation occurs (Park, 2009). At the same time, it is critical for finding gene regulatory networks that it provides precise information about the regions where transcription factors, core transcription machinery and other DNA binding proteins bind. The dynamic modification combinations of DNA and Histones and the positioning of Nucleosomes have a very important place in gene regulation (Park, 2009).

The most prevalent post-translational modifications (PTMs) of histones are methylation and acetylation. Besides these, histone modifications such as phosphorylation, glycosylation, ubiquitination, SUMOylation and ADP ribosyl are less frequent (Albini et al., 2019).

Histone acetylation, one of the best-characterized modifications, indicates transcriptional activation. H3 Lysine 27 acetylation (H3K27ac) is often found in and around transcription start sites (TSS) and is associated with active enhancers (T. Wang et al., 2008).

H3 Lysine 4 trimethylation (H3K4me3) is associated with active promoter regions and plays a role in transcription initiation, elongation, and RNA splicing (Beacon et al., 2021).

Multiple “omics” analyzes were performed on immortalized human astrocytes (IHAs) by Dr. Şevin Turcan and her team to characterize the dynamics of epigenetic and transcriptional changes that occur as a result of the IDH-R132H mutation and to show whether the resulting changes are reversible.

In this study, a tetracycline-inducible expression system was established and IHAs were passaged in the presence of doxycycline for 30 passages. This thirtieth passage was accepted as the baseline and after the 30th passage doxycycline was withdrawn. These cells were profiled by gene expression and methylation arrays at passages of 10, 20, and 40 following doxycycline withdrawal (Turcan et al., 2018).

Capicua (CIC) mutations in oligodendroglioma (ODG) occur with IDH1/2 mutations. Considering that CIC and IDH mutations could cooperate on the transcriptome and epigenome, transcriptomic and epigenomic analyzes were performed in CIC WT and knockout cells with WT IDH1 expression and mutant IDH1 expression. CIC-KO cell line was created using the CRISPR-Cas9 technique in E6/E7/hTERT+IDH1-WT and E6/E7/hTERT+IDH1-R132H human astrocyte cells. (Lee et al., 2022-Integrative multi-omic analysis)

ChIP-Seq analysis data from doxycycline-induced CIC-WT_IDH1-WT and CIC-WT_IDH1-R132H cells of this study were used by us when designing the primer.

We aimed to find possible similarities and differences by applying conditioned mediums (IDH1-WT and IDH1-R132H) obtained from the same IHA cells (Turcan et al., 2017) to NPCs that we cultured in 3D prepared with alginate. We compared the epigenetic changes that occur by giving the media from IHA (IDH1-WT and IHA-R132H) treated with doxycycline to neural progenitor cells as detailed in the Materials and Methods section.

In this study, since the cells' own medium, neural progenitor Medium, was replaced with conditioned media IHA-IDH1-WT and IHA-IDH1-R132H, our comparisons were constructed

with NPC-IDH1_WT-Day14 vs. NPC-IDH1_R132-Day14 and NPC-IDH1_WT-Day17 vs. NPC-IDH1_ Day17, also with NPC-Control-Day0, all conditions were compared and the changes were monitored. Thus, it was aimed to determine the changes depending on the expression of IDH1-R132H, different from the effects that may arise from wild-type IDH1 expression and astrocyte medium.

Before the ChIP protocol and ChIP-qPCR experiments were set up in 5 different experimental conditions and the analyzes were performed, recent data on IHA cells were utilized (Lee et. al., 2022, Turcan et. al., 2017). Based on H3K4me3 ChIP-seq data generated in these two studies and shared in GEO (GSE189857, GSE85940), 12 candidate genomic loci, which can be grouped into 5 groups, were analyzed by ChIP-qPCR on NPCs. Based on H3K27ac ChIP-seq data shared in GEO (GSE189857), 7 different genomic loci, which can be grouped into 4 groups, were analyzed by ChIP-qPCR on NPCs.

4.4.1.1.ChIP-qPCR results for H3K4me3 antibody

After applying the ChIP protocol to NPCs maintained in 3D culture prepared with alginate using H3K4me3 antibody, ChIP-qPCR was applied to known H3K4me3 targets and our target regions in IHA-IDH1-R132H cells.

CCDC26 Locus

H3K4me3 signals distributed in the CCDC26 gene, which contains the highest risk SNPs in the 8q24-related glioma risk locus, which our group has previously shown to occur through MYC regulation, were compared. In addition to the rs55705857 locus we are interested in, 2 more loci that change with IDH1-R132H expression were selected and primers were designed for these regions.

GEO: When looking at the GSE85940 data, no signal was seen in the primary designed CCDC loci. In the GEO:189857 data, approximately twice as much signal was seen in the samples where mutant IDH1 was induced in the regions where the CCDC26-1, CCDC26-4 and CCDC26-5 primers sit (Figure 29). Although no signal was seen at the rs55705857 locus in the two experiments in which we used GEO data, primers were designed for this locus.

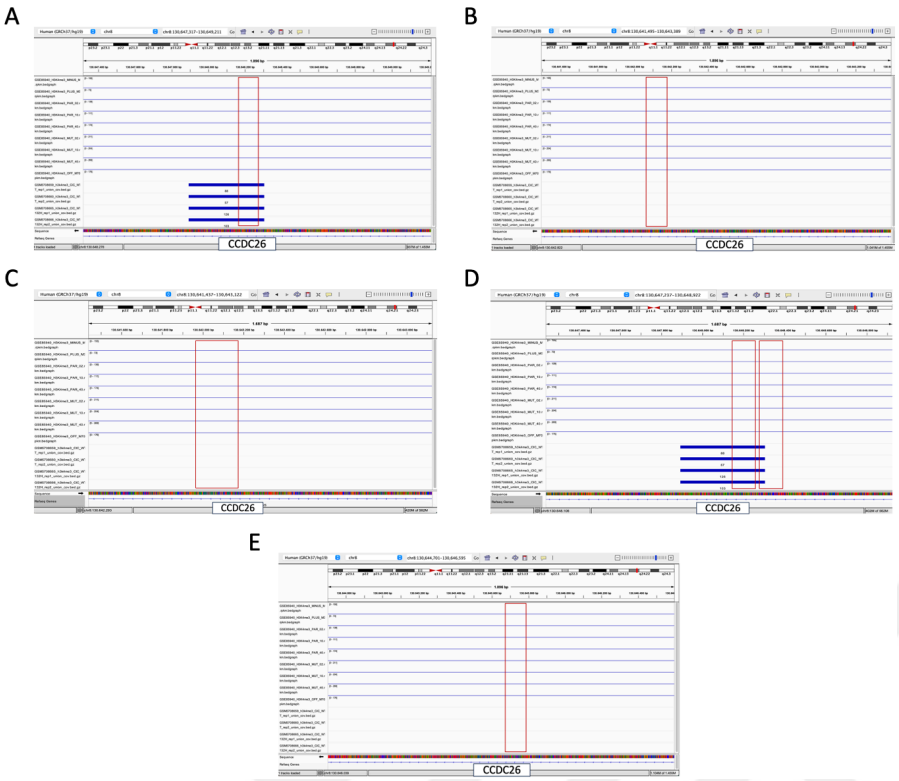

Figure 29. IHA-H3K4me3 signals in the data with GEO Codes GSE189857 and GSE85940 belonging to the CCDC26 gene. A. H3K4me3 signal (GEO: GSE189857) targeted with primers CCDC26F-1 and CCDC26R-1 and located at 130648173-130648272 (GRCh37) in chromosome 8 (Lee et al. 2022). B. H3K4me3 signal targeted with primers CCDC26F-2 and CCDC26R-2 and located at chr8:130642073-130642272182 (GRCh37). C. H3K4me3 signals targeted with primers CCDC26F-3-4 and CCDC26R-3-4 and located at chr8:130641972-130642068 and chr8:130642073-130642182 (GRCh37). D. H3K4me3 signals targeted with primers CCDC26F-5-6 and CCDC26R-5-6 and located at chr8:130648285-130648390 and chr8:130648120-130648269 (GRCh37). E. H3K4me3 signals targeted with primers rs55705857F-1 and rs55705857R1 and located at chr8:130645684-130645794 (GRCh37). The coordinate of rs55705857 is chr8:130645692 (GRCh37).

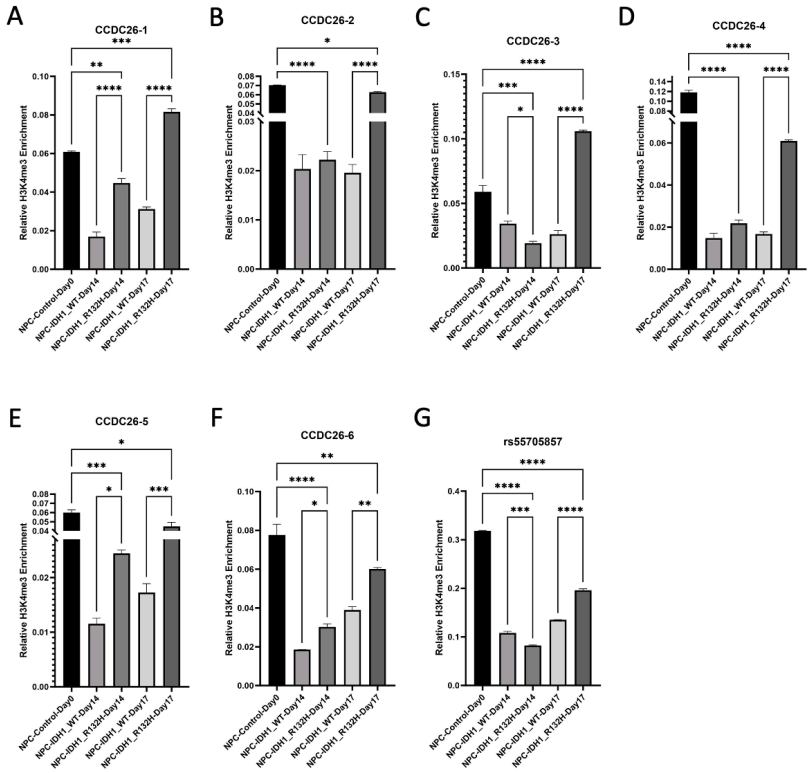

Figure 30. ChIP-qPCR results for the CCDC26 gene using H3K4me3 antibody. qPCR results performed with primers designed for A. CCDC26-1, B. CCDC26-2, C. CCDC26-3, D. CCDC26-4, E. CCDC26-5, F. CCDC26-6, G. Rs55705857 regions.

In general, in ChIP-qPCRs for the CCDC26 region, a decrease in H3K4me3 signals was observed when IHA-IDH1-WT and IHA-IDH1-R132H conditioned media were administered.

In ChIP-qPCR for the CCDC26-1 locus, when NPC-IDH1_WT-Day14 and NPC-IDH1_R132H-Day14 were compared with each other, it was detected that H3K4me3 enrichment in cells exposed to mutant IDH1 conditioned medium was more than twice as much as in cells exposed to wild-type IDH1 conditioned medium. When comparing NPC-IDH1_R132H-Day14 with the control group, a decrease in the H3K4me3 signal level is thought to be due to the medium change, as it was observed in all ChIP-qPCRs. In ChIP-qPCR for the CCDC26-1 locus, when NPC-IDH1_WT-Day17 and NPC-IDH1_R132H-Day17 were compared with each other, there was almost 3-fold more H3K4me3 enrichment in cells exposed to the mutant IDH1 conditioned medium. However, when the cells were exposed to IHA-IDH1-WT and IHA-IDH1-R132H conditioned media for 14 days and then maintained in Neural Progenitor Medium for 3 days, H3K4me3 enrichment was observed in both conditions. But

when NPC-IDH1_R132H-Day17 is compared with the control group, it is seen that the H3K4me3 signal level is significantly increased in cells exposed to mutant IDH1 conditioned medium (Figure 30A).

When the ChIP-qPCR results for the CCDC26-2 locus were examined, no significant difference could be seen between NPC-IDH1_WT-Day14 and NPC-IDH1_R132H-Day14. On the other hand, when NPC-IDH1_R132H-Day14 is compared with the control group, the decrease in H3K4me3 signal level is significant. In ChIP-qPCR for the CCDC26-2 locus, when NPC-IDH1_WT-Day17 and NPC-IDH1_R132H-Day17 were compared with each other, there was a 3-fold higher H3K4me3 enrichment in cells exposed to the mutant IDH1 conditioned medium. When NPC-IDH1_R132H-Day17 was analogized with the control group, the H3K4me3 signal level in cells exposed to the mutant IDH1 conditioned medium reached almost the same level as the control group (Figure 30B).

In the CCDC26-3 locus qPCR results, the H3K4me3 signal level in NPC-IDH1_R132H-Day14 cells is significantly lower than the control group and NPC-IDH1_WT-Day14 group. In NPC-IDH1_R132H-Day17 cells, the H3K4me3 signal level is almost 2 times higher than the control group and 4 times more signal is seen compared to NPC-IDH1_WT-Day17. H3K4me3 enrichment at the CCDC26-3 locus followed a different pattern compared to the CCDC26-1 and CCDC26-2 loci. The H3K4me3 signal level in cells under the NPC-IDH1_R132H-Day14 condition is always low compared to previous comparisons. At the same time, the H3K4me3 signal level of cells incubated in Neural Progenitor medium for 3 days after exposure to IHA-IDH1-WT conditioned medium for 14 days is lower than NPC-IDH1_WT-Day14 cells at this locus (Figure 30C).

When looking at the CCDC26-4 locus, the H3K4me3 signal level is very low compared to the control in Day 14 conditions. When NPC-IDH1_WT-Day14 and NPC-IDH1_R132H-Day14 were compared, it was observed that although the H3K4me3 signal level appeared high in NPC-IDH1_R132H-Day14 cells, there was no substantial difference. In the comparison of NPC-IDH1_WT-Day17 and NPC-IDH1_R132H-Day17, there was more than 3-fold H3K4me3 enrichment in cells exposed to the mutant IDH1 conditioned medium. Additionally, when the control group and NPC-IDH1_R132H-Day17 were compared with each other, H3K4me3 enrichment decreased significantly compared to the control (Figure 30D).

When the CCDC26-5 locus was examined for H3K4me3 enrichment, there was a 3-fold higher significant H3K4me3 enrichment in NPC-IDH1_R132H-Day14 cells when NPC-

IDH1_WT-Day14 and NPC-IDH1_R132H-Day14 were compared to each other. In addition, both NPC-IDH1_R132H-Day14 and NPC-IDH1_R132H-Day17 showed that the H3K4me3 signal level was significantly reduced compared to the control. Moreover, when comparing NPC-IDH1_WT-Day17 and NPC-IDH1_R132H-Day17, the H3K4me3 signal level is significantly higher in cells exposed to IDH1 mutant medium (Figure 30E).

At the CCDC26-6 locus, the H3K4me3 signal level of NPC-IDH1_R132H-Day14 and NPC-IDH1_R132H-Day17 conditions is lower than the control group. But there is a significant decrease. Comparing NPC-IDH1_WT-Day14 and NPC-IDH1_R132H-Day14 and comparing NPC-IDH1_WT-Day17 and NPC-IDH1_R132H-Day17 shows that H3K4me3 enrichment is significantly higher in conditions exposed to mutant IDH1 medium (Figure 30F).

When looking at the H3K4me3 enrichment at the locus where the Rs55705857 SNP region is located. The H3K4me3 signal level decreased in cells exposed to IHA-IDH1-R132H medium for 14 days, but the H3K4me3 signal level increased after the IHA-IDH1-R132H medium was withdrawn and the cells were incubated in Neural progenitor medium for 3 days (Figure 30G).

Myc promoter and MYC enhancer controlled by TRIM28

The promoter of MYC, the most important target gene of the project, was selected. The enhancer that interacts with the rs55705857 locus, the strongest 8q24-related risk SNP, and controls MYC expression by binding to the TRIM28 transcription factor, was selected. H3K4me3 signals are seen in the upstream region of the MYC gene in GEO: GSE85940 and GEO: GSE189857 data. In the GSE85940 data, it is seen that H3K4me3 enrichment is much higher in parental samples than in mutants. There is also very little H3K4me3 signal in OFF_M70 samples. GEO: GSE85940 data, as mentioned before, was obtained from Turcan et al. Taken from 2017. Samples PAR_02, PAR_10, and PAR_40 are IHA cells with passage number 30+2, 30+10, and 30+40 that were not induced by doxycycline, respectively. Samples MUT_02, MUT_10 and MUT_40 are IHA-R132H cells with passage number 30+2, 30+10 and 30+40, respectively, continuously induced by doxycycline. OFF_M70 examples are; They are IHA-R132H cells that were induced with doxycycline for up to 30 passages and then were not given doxycycline for 40 passages.

GEO:189857 data (Lee et al., 2022) are the 4 examples at the bottom of the IGV data figures. The first two are CIC-WT _IDH1-WT and last two are CIC-WT_IDH1-R132H data. These examples show that there is no variation in H3K4me3 enrichment between WT IDH1 and mutant IDH1 (Figure 31A). Although no signal was seen in the MYC enhancer locus controlled by TRIM28 in the two experiments in which we used GEO data, ChIP-qPCR was performed for this locus since it is the region of interest (Figure 31B).

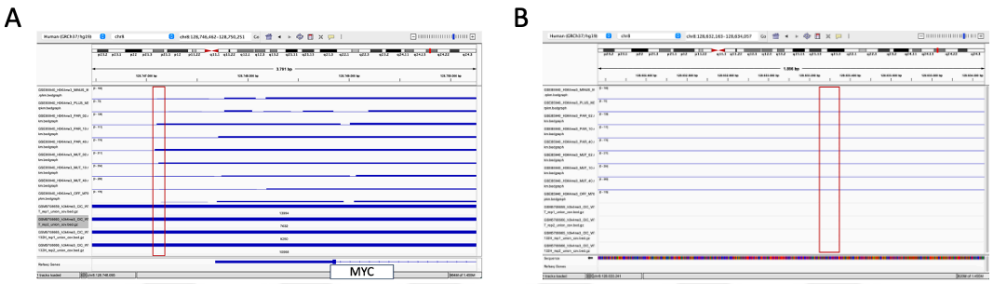

Figure 31. H3K4me3 signaling at MYC enhancer regions controlled by TRIM28 and the MYC promoter. A. H3K4me3 signal targeted by primers MYCPF1 and MYCPR1 and located at chr8:128747140-128747222 (GRCh37) (GEO: GSE189857 and GSE85940). B. H3K4me3 signal targeted with primers TRIM28MYCEF1 and TRIM28MYCER1 and located at chr8:128633241-128633354 and chr8:128632920-128633037 (GRCh37) (GEO: GSE189857 and GSE85940).

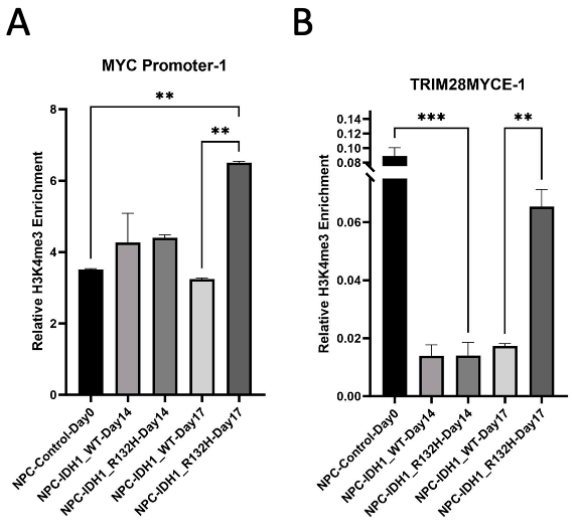

Figure 32. qPCR results performed with primers designed for the regions where A) MYC Promoter and B) TRIM28 transcription factor bind

Looking at the ChIP-qPCR results for the MYC Promoter locus, the H3K4me3 signal level increased in NPC-IDH1_WT-Day14, NPC-IDH1_R132H-Day14 and NPC-IDH1_R132H-Day17 compared to the control group. A significant increase is observed especially in NPC-IDH1_R132H-Day17. It was observed that the H3K4me3 signal level decreased in wild-type IDH1 samples in NPCs that were withdrawn from conditioned IHA media and maintained in Neural Progenitor medium for three days, and was almost the same as in the control group. But it was observed that mutant IDH1 continued its effect and there was a continuous increase in the H3K4me3 signal level. When NPC-IDH1_WT-Day17 and NPC-IDH1_R132H-Day17 are compared, H3K4me3 enrichment is 2 times higher in NPC-IDH1_R132H-Day17. When our data were compared with the results of Dr. Turcan and her team's studies, when the effect of mutant IDH1 was examined, it was seen that H3K4me3 enrichment in the MYC gene increased according to our results, while it decreased in the other study. (Figure 32A). These results indicate increased signal on day 17 in NPCs exposed to this IHA medium, whereas no significant change in H3K4me3 signal at the MYC promoter was observed in IHAs in previous studies. It is noteworthy that these changes parallel the H3K4me3 changes at the rs55705857 locus. When looking at the qPCR results for the MYC enhancer locus controlled by TRIM28, there was a decrease in H3K4me3 signal in four experimental conditions compared to NPC-Control-Day0. When NPC-IDH1_WT-Day17 and NPC-IDH1_R132H-Day17 were compared, it was observed that H3K4me3 enrichment was more than 3 times higher in NPC-IDH1_R132H-Day17. There was a sharp decrease in the H3K4me3 signal level in NPCs exposed to mutant IDH1 medium for 14 days, and after the 14th day, when the medium was replaced with Neural progenitor medium and incubated for 3 days, the H3K4me3 signal level showed a dramatic increase (Figure 32B).

H3K4me3 ChIP-qPCR result for GSDMC gene

A region was selected, approximately 100 kb on the telomeric side of the SNP numbered rs55705857 and located downstream of the GSDMC gene, very close to the locus that shows changes in the H3K4me3 signal after IDH1-R132H expression, according to GEO: GSE189857 data.

GEO: When looking at GSE85940 data, no signal was seen in the primary designed loci. In the GEO:189857 data, H3K4me3 signal was seen very close to the primer designed region. Since it was not possible to design a primer suitable for the part where the signal was seen, a primer was designed for a nearby area (Figure 33).

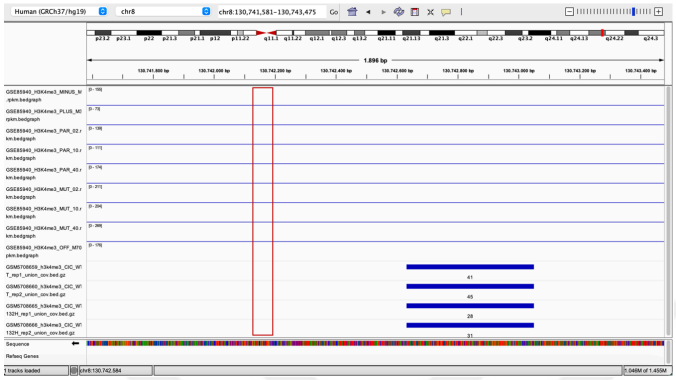

Figure 33. IHA-H3K27ac signals in the GEO: GSE85940 and GEO: GSE189857 data belonging to the GSDMC upstream region. H3K27ac signal in the downstream region of the region located chr8:130742112-130742191, targeted with GSDMCUF and GSDMCUR primers, was observed at almost the same level in both IDH1-WT and IDH1-R132H samples only in the GEO:GSE189857 data.

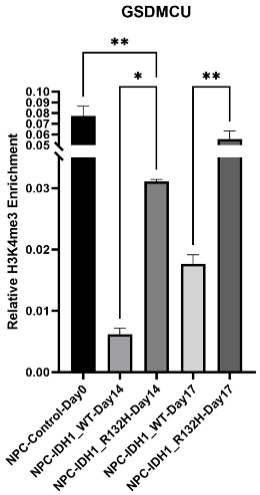

Figure 34. qPCR results for the locus located upstream of GSDMC after ChIP with H3K4me3 antibody.

According to the qPCR results for the locus upstream of the GSDMC gene, the H3K4me3 signal level in NPC-IDH1_R132H-Day14 cells was importantly reduced compared to the control. Moreover, comparing NPC-IDH1_WT-Day14 and NPC-IDH1_R132H-Day14, the H3K4me3 signal level is 6 times higher in the NPC-IDH1_R132H-Day14 condition. When NPC-IDH1_WT-Day17 and NPC-IDH1_R132H-Day17 are compared, H3K4me3 enrichment is significantly higher in cells incubated in IDH1 mutant medium for 14 days. H3K4me3 signal level increased in cells that were withdrawn from IHA-WT and IHA-R132H conditioned media and treated with Neural Progenitor medium for 3 days (Figure 34).

Although it is unclear whether this signal received from an intergenic region may act through long-distance MYC regulation or through the much closer GSDMC or another gene, it is an interesting finding that the effect seen in IHAs is also repeated in NPCs.

H3K4me3 ChIP-qPCR result for the TERT gene

The TERT gene, one of the two target genes of the project, was selected. H3K4me3 signals are seen in the TERT gene in GEO: GSE85940 and GEO: GSE189857 data. In the GSE85940 data, it is seen that H3K4me3 enrichment is very high in the parental samples, and the signal level decreases as the passage progresses in the mutants. In OFF_M70 samples, the H3K4me3 signal is very low, as in the later passages of the mutant samples. On the other hand, when looking at the IGV image of GEO:189857 data (Lee et al., 2022) in the same region (4 samples below), a slight H3K4me3 enrichment was detected in the CIC-WT_IDH1-R132H data compared to the CIC-WT_IDH1-WT data (Figure 35).

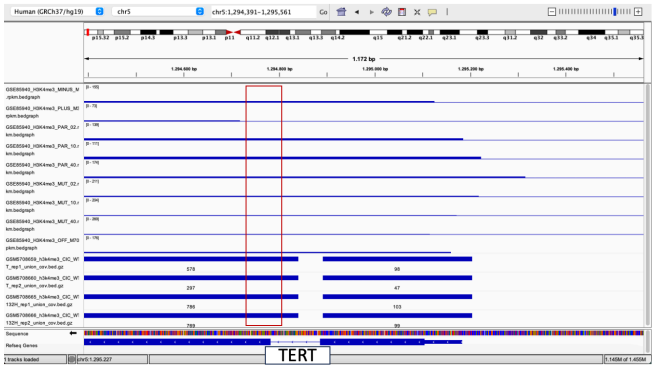

Figure 35. IHA-H3K4me3 signals of the TERT locus. IGV view of the TERT locus under different conditions according to H3K4me3 ChIP-seq data after the expression of IDH1-R132H in IHAs. A) Data from Turcan et al. Taken from 2017. Rows 1-2-3: IHAs expressing IDH1-R132H passage 30+2, 30+10, 30+40; Row 4: IHAs expressing IDH1-R132H from passage 30+2. B) Data from Lee et al. Taken from 2022. Rows 1-2: IDH1-R132H mutant, Rows 3-4: IHAs expressing IDH1-WT.

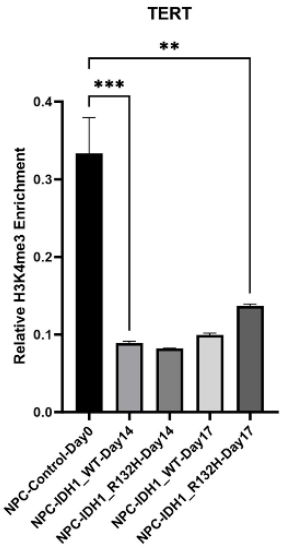

Figure 36. qPCR results for the hTERT region after ChIP with H3K4me3 antibody.

H3K4me3 signal in the hTERT region appears to decrease at the same rate on day 14 in NPCs exposed to astrocyte medium expressing both WT and mutant IDH1. On the third day (day17) after returning to NPC medium, it is observed that it shows a partial reversal and increases only in NPCs exposed to mutant IDH1 medium (Figure 36). When evaluated together with the qPCR results in Figure 21D, the TERT is relatively activated in the presence of mutant IDH1 and this activation is "permanent". Compared to the literature, this finding is interesting

because it has been reported that when p53/pRb-KO E6E7-expressing normal human astrocytes provide stable IDH1-R132H expression, these cells can escape replicative senescence, whereas isogenic cells expressing IDH-wt cannot escape (Ohba et al., 2016).

H3K4me3 ChIP-qPCR result for ID1 Promoter region

As a result of our RNA-seq analysis, the promoter of the ID1 (inhibitor of differentiation 1) gene, which we showed for the first time to be induced by IDH1-R132H expression and play a role in the advanced stages of gliomas, was selected. H3K4me3 signals are seen in the TERT gene in GEO: GSE85940 and GEO: GSE189857 data. In GSE85940 data, it is seen that H3K4me3 enrichment is higher in parental samples than in mutants. In OFF_M70 samples, it is seen that the H3K4me3 signal increases again and returns to enrichment with the parents. On the other hand, when looking at the IGV image of GEO:189857 data (Lee et al., 2022) in the same region (4 samples at the bottom), almost the same H3K4me3 enrichment was seen in CIC-WT_IDH1-R132H and CIC-WT_IDH1-WT data (figure 37).

Figure 37. IHA-H3K4me3 signals of the ID1 promoter. IGV view of this locus under different conditions according to H3K4me3 ChIP-seq data after the expression of IDH1-R132H in IHAs. B) Data from Lee et al. Taken from 2022. Rows 1-2: IDH1-WT, Rows 3-4: IHAs expressing IDH1-R132H mutant.

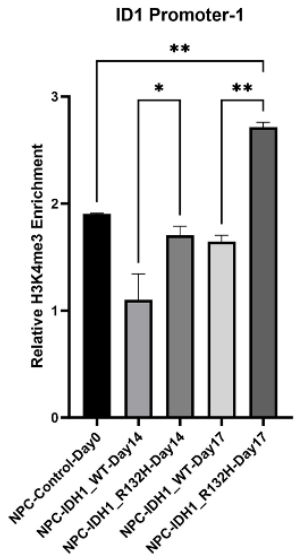

Figure 38. qPCR results for ID1 promoter after ChIP with H3K4me3 antibody.

The results obtained, unlike the results previously obtained in IHAs (Turcan et al., 2017 and Lee et al., 2022), compared to NPC-IDH1_WT-Day14 and NPC-IDH1_R132H-Day14 samples, IDH1-R132H for 14 days. indicating relatively increased H3K4me3 signaling at the ID1 promoter in NPCs exposed to the mutant medium. Moreover, this signal increase is found both in the presence of the mutant medium (day 14) and 3 days after removing this medium (day 17). Both NPC-IDH1_R132H-Day14 and NPC-IDH1_R132H-Day14 exposed to mutant IDH1 medium had significantly higher H3K4me3 signal levels compared to NPC-IDH1_WT-Day14 and NPC-IDH1_WT-Day17 exposed to wild-type IDH1 medium on their respective days. and also H3K4me3 enrichment in NPC-IDH1_R132H-Day17 cells is very high compared to the control (figure 38).

4.4.1.2.ChIP-qPCR results for H3K27ac antibody

Since ChIP analysis was not performed for the H3K27ac antibody in the study with GEO: GSE85940 data (Turcan et al., 2017), only the study with GEO: GSE189857 data (lee et al., 2022) was used, and IGV figures are presented only from the results of this study.

H3K27ac ChIP-qPCR result for CCDC26 locus and rs55705857 SNP region

GEO: Although no signal was seen in the rs55705857 locus in the two experiments in which we used GSE189857 data, ChIP-qPCR was performed for this locus since it is the region of interest (Figure 39).

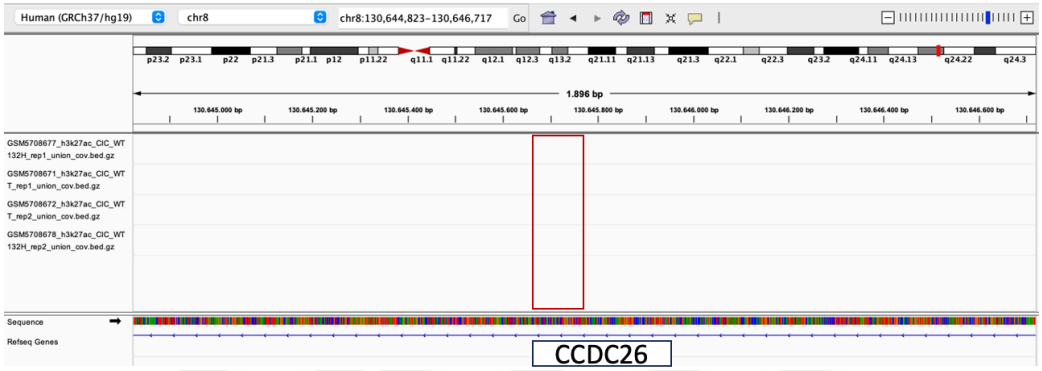

Figure 39. H3K27ac signals from the rs55705857 locus, the strongest 8q24-associated risk SNP. Since the region targeted by the two different primer sets is almost the same, it is shown in a single frame. H3K targeted with primers rs55705857F-1 and rs55705857R1 and located chr8:130645684-130645794 (GRCh37) and located chr8:130645682-130645760 targeted with primers rs55705857F-2 and rs55705857R-2. 4me3 signals. The coordinate of rs55705857 is chr8:130645692 (GRCh37).

The qPCR results for the region we targeted with two separate primer sets for the rs55705857 locus, which is the strongest 8q24-related risk SNP after ChIP with H3K27ac antibody, are given below. The qPCR results established for the two primer sets support each other (Figure 40).

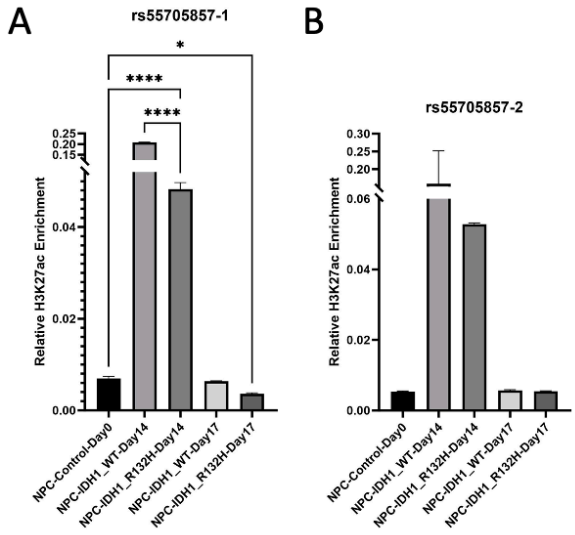

Figure 40. qPCR result using rs55705857F-1/rs55705857R-1 and rs55705857F-2/rs55705857R-2 primers after ChIP with H3K27ac antibody

Looking at the qPCR results using rs55705857 -1 and rs55705857-2 primers, it was seen that the H3K27ac signal increased approximately 5-fold in NPCs exposed to IHA medium expressing IDH1-R132H for 14 days, and in NPCs exposed to IHA medium expressing IDH1-WT for 14 days. It was observed that it increased more than 10 times. It is observed that the H3K27ac signal decreases again in NPCs exposed to NPC medium for 3 days after 14 days of exposure to IHA medium expressing IDH1-WT, and in NPCs exposed to NPC medium for 3 days after 14 days of exposure to IHA medium expressing IDH1-R132H. These results show that the H3K27ac level at the rs55705857 locus increased during the treatment with IDH1-R132H conditioned medium and returned to the control group level after the conditioned medium was withdrawn (Figure 40).

H3K27ac ChIP-qPCR result for Myc promoter and MYC enhancer controlled by TRIM28

GEO: H3K27ac signals in the MYC Promotor region are seen in GSE189857 data (Lee et al., 2022) (Figure 41). When CIC-WT_IDH1-R132H samples were compared with CIC-WT_IDH1-WT, H3K27ac was observed to be enriched in IDH1-R132H samples.

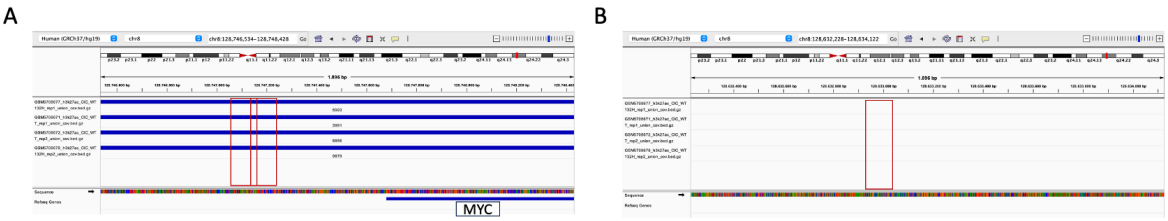

Figure 41. qPCR result using MYCPR1, MYCP2 and TRIM28MYCER primers after ChIP with H3K27ac antibody. A. H3K27ac signal (GEO:GSE189857) targeted with primers MYCPF-1 and MYCPR-1 and located at chr8:128747140-128747222 and with primers MYCPF-2 and MYCPR-2 and located at chr8:128747071-128747158 (GRCh37). B. H3K27ac signal (GEO: GSE189857) targeted with primers TRIM28MYCEF-2 and TRIM28MYCER-2 and located at chr8:128632920-128633037 (GRCh37).

The qPCR results for the region where we targeted the MYC Promoter with two separate primer sets after ChIP with the H3K27ac antibody are given (figure 42A,B). Although MYC1 and MYC2 primary regions are very close to each other, H3K27ac signal results were different from each other in cells exposed to NPC medium for 3 days after exposure to IHA medium expressing IDH1-R132H on the 14th day. MYCF1 and MYCR2 sequences are almost reverse complements of each other.

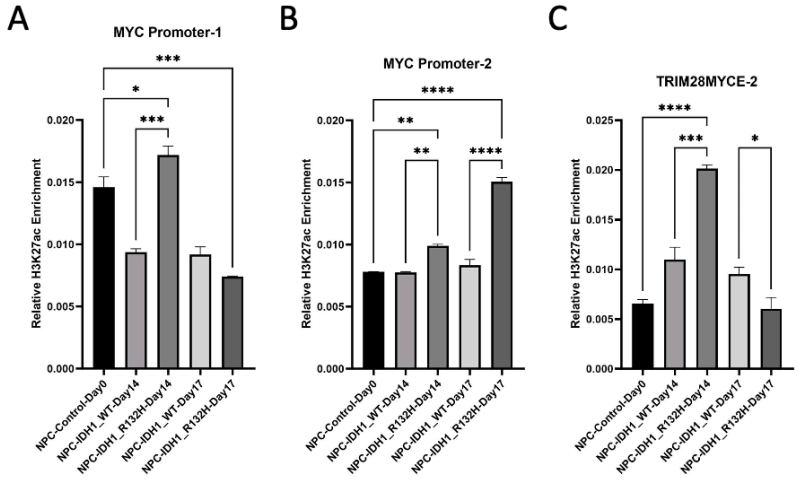

Figure 42. qPCR results performed with primers designed for the regions where A) MYC Promotor-1 B) MYC Promotor-2 and C) TRIM28 transcription factor bind

Looking at the qPCR results using MYCP-1 and MYCP-2 primers, it is seen that the H3K27ac signal in the MYC Promoter of NPCs expressing IDH1-R132H exposed to IHA conditioned medium for 14 days increased analogized to the control group and also the NPC-IDH1_WT-Day14 group. A decrease was observed in the MYC Promoter-1 locus in NPC-IDH1_WT-Day14 samples compared to NPC-Control-day0 samples. Although the MYC Promoter-2 locus is very close to the MYC Promoter-1 locus, H3K27ac signal levels differ from each other for each experimental condition. In addition, when MYC Promoter-1 and MYC Promoter-2 samples are compared, H3K27 enrichment is seen in both NPC-IDH1_R132H-Day14 samples, while a dramatic decrease in the H3K27ac signal level is seen in the MYC Promoter-1 locus in NPC-IDH1_R132H-Day17 samples, while H3K27ac is seen in the MYC Promoter-2 locus. Its enrichment continues. (figure 42A,B)

According to the qPCR results performed using MYCTRIM28-F2 and MYCTRIM28-R2 primers on the MYC enhancer region controlled by TRIM28, H3K27ac enrichment increased approximately 4-fold when compared to the control group in the NPC-IDH1_R132H-D14 condition, and when compared to the NPC-IDH1_WT-Day14 condition. It was observed that it increased approximately 2 times. In the NPC-IDH1_R132H-Day17 condition, which was incubated in Neural Progenitor medium for 3 days after treatment with IHA-IDH1-R132H condition medium for 14 days, the H3K27ac signal level decreased approximately 5-fold compared to NPC-IDH1_R132H-D14. Especially when looking at the NPC-IDH1_WT-Day14 and NPC-IDH1_WT-Day17 conditions exposed to IHA-IDH1-WT medium, the H3K27ac signal level was almost unchanged (Figure 42C). Looking at the results, the H3K27ac signal level in NPC-IDH1_R132H-Day17 cells is even less than that in the NPC-IDH1_WT-Day17 condition. These results indicate a similar profile with the MYC promoter-1 region and provide important clues about the epigenomic changes involved in the activation of the MYC gene as a result of the IDH1-R132H mutation.

H3K27ac ChIP-qPCR result for GSDMC downstream locus

As mentioned above, a region was selected about 100 kb on the telomeric side of the SNP numbered rs55705857 and located downstream of the GSDMC gene and very close to the locus showing H3K27ac signal after IDH1-R132H expression according to GEO: GSE189857 data (Figure 43).

Figure 43. IHA-H3K27ac signals in the data with GEO Codes GSE189857 belonging to the GSDMC upstream region. A. H3K27ac signal (GEO:GSE189857) targeted with primers GSDMCUF and GSDMCUR and located at chr8:130742112-130742191.

The H3K27ac signal in this locus was measured after ChIP with the help of primers specifically designed for the region located upstream of GSDMC. GSDMCDSF and GSDMCDSR primers target the sequences 130742100-130742200 in chromosome 8, according to the GRCh37 sequence.

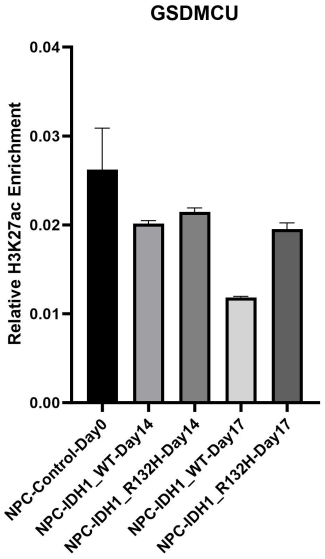

Figure 44. qPCR results for GSDMC downstream region after ChIP with H3K27ac antibody

The H3K27ac signal in the GSDMC downstream region, which we previously showed to interact with the rs55705857 locus, appears to decrease on day 14 in NPCs exposed to astrocyte medium expressing IDH1-WT and IDH1-R132H separately. On the third day (day17) after returning to Neural Progenitor medium, it is observed that the H3K27ac signal in NPCs exposed

to astrocyte medium expressing R132H mutant IDH1 for 14 days remains almost unchanged. However, compared to WT medium, there is a relative increase in H3K27ac signal on both days 14 and 17 in NPCs exposed to the medium obtained from IDH1-mutant IHAs (Figure 44). This result shows that epigenome changes in the 8q24 locus as a result of the IDH1-R132H mutation occur not only in the vicinity of MYC, but also in the loci on the other side of the risk SNP (telomeric).

H3K27ac ChIP-qPCR result for ID1 promoter

As a result of our RNA-seq analysis, the promoter of the ID1 (inhibitor of differentiation 1) gene, which we showed for the first time to be induced by IDH1-R132H expression and play a role in the advanced stages of gliomas, was selected. GEO: H3K27ac signals are seen in the ID1 Promotor region in GSE189857 data. When CIC-WT_IDH1-R132H samples were compared with CIC-WT_IDH1-WT samples, it was observed that there was almost 2-fold H3K27ac enrichment (Figure 45).

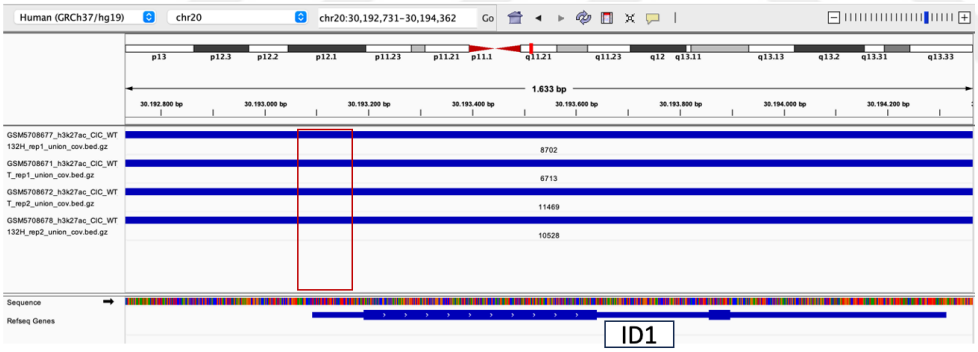

Figure 45. IHA-H3K27ac signals in the data with GEO Codes GSE189857 belonging to the ID1 promoter region. H3K27ac signals (GEO:GSE189857) targeted with primers ID1 PromoterF-1 and ID1 PromoterR-1 and located at chr20:30193079-30193179 and ID1 PromoterF-2 and ID1 PromoterR-2 and located at chr20:30193077-30193122 are in the same box because they overlap each other. shown in.

The qPCR results for the region where we targeted the ID1 Promoter with two separate primer sets after ChIP with the H3K27ac antibody are given below. ID1 Promotor-1 and ID1 Promotor-2 qPCR results support each other.

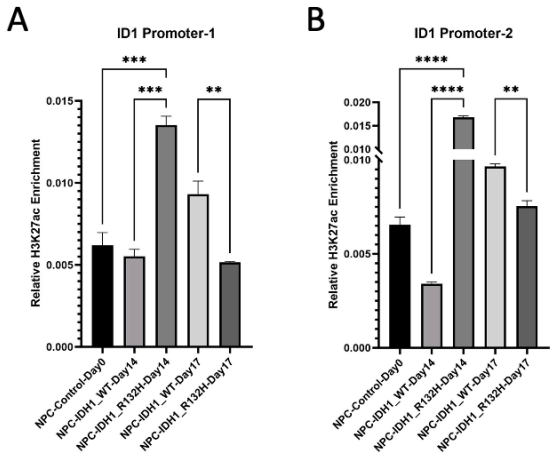

Figure 46. qPCR results for the ID1 Promoter region after ChIP with H3K27ac antibody. A) ID1PF-1 and IDP1R-1 primers B) qPCR result using ID1PF-2 and IDP1R-2 primers

qPCR results using ID1 Promotor-1 and ID1 Promotor -2 primers show that H3K27ac signal increased in NPCs exposed to IHA medium expressing IDH1-R132H for 14 days, and decreased in NPCs exposed to IHA medium expressing IDH1-WT for 14 days. There is significant H3K27ac enrichment in cells exposed to IDH1 mutant medium when NPC-IDH1_WT-Day14 and NPC-IDH1_R132H-Day14 are compared. In addition, when the NPC-IDH1_R132H-Day17 condition is compared with the control group, it is seen that the H3K27ac signal level decreased and approached the level in the control group. When NPC-IDH1_WT-Day17 and NPC-IDH1_R132H-Day17 are compared, the H3K27ac signal level in NPC-IDH1_R132H-Day17 is lower than that in NPC-IDH1_WT-Day17 (Figure 46).

As a result, it is seen that the IDH1-R132H mutation strongly increases the H3K27ac level in the ID1 promoter and that this increase is temporary - the effect disappears after the removal of the mutant medium. Considering that the H3K4me3 signal continues on day 17 (see 4.2.6), it can be concluded that the positive effects of IDH1-R132H on the ID1 promoter may be partly permanent and partly temporary.

4.4.2. MeDIP-qPCR results

DNA methylation, a stable and heritable epigenetic modification, continues to be studied extensively. DNA methylation is the methylation of cytosine residues in CpG dinucleotides by

DNA methyltransferases (DNMTs) (Meissner, 2010). Profiling DNA methylation changes that occur during the development process and disease phenotype is critical in diagnosis. Methylated DNA immunoprecipitation (MeDIP) is a method based on the method of analyzing methylated DNA by enriching it. In short, DNA fragments containing methylated cytosine are separated and analyzed by precipitation with 5-methylcytosine (5mC) antibody (Down et al., 2008). MeDIP is preferred in methylation studies because it is more affordable, reproducible and a useful method than other methylation methods. In addition, if single base resolution is not sought in experiments, MeDIP answers many questions about DNA methylation.

DNA methylation, an important epigenetic mark, was analyzed by MEDIP-qPCR at identified loci. Thanks to this method, the amounts of both 5-hydroxymethylcytosine (5-hmC) and 5-methylcytosine (5-mC) were determined in the same sample.

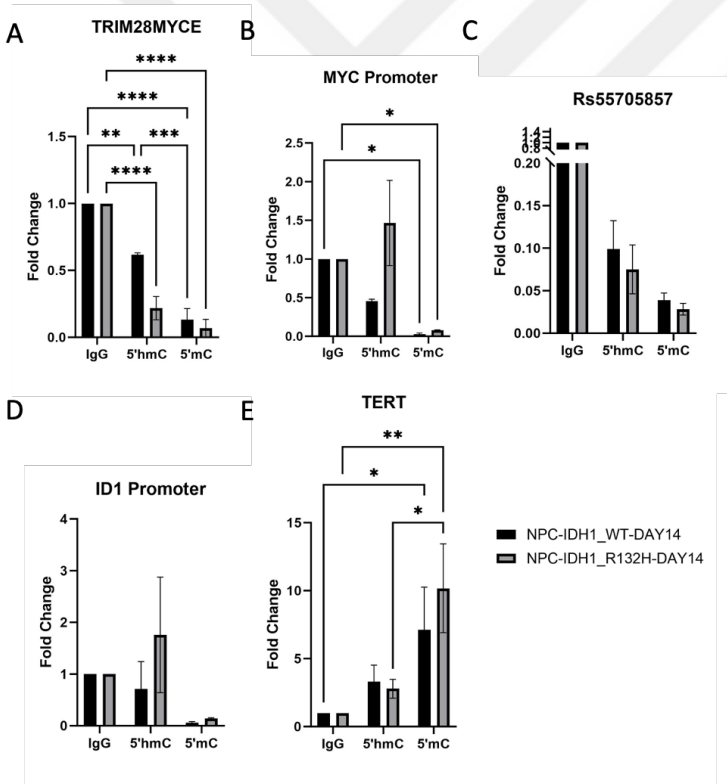

Figüre 47. MeDIP-qPCR results. (A-E) Changes of methylation levels in the loci analyzed by qPCR

Methylation analysis results performed with the MeDIP-qPCR method confirm increased genome-wide DNA methylation through the inhibition of various DNA demethylase enzymes as an oncometabolite of 2-HG, which accumulates as a result of IDH1 and IDH2 mutations

(Turcan et al., 2012). On the other hand, it is noteworthy that the methylation of the enhancer region (both 5-hmC and 5-mC), which we showed in our previous studies to interact with the rs55705857 risk SNP and regulate MYC expression through the TRIM28 repressor protein, was significantly reduced (Figure 47A). Since there is a close relationship between TRIM28-mediated suppression and DNA methylation (Turelli et al. 2014), this decrease in methylation levels can be expected to have an increasing effect on MYC expression. Although the effect of 5-hmC on transcriptional control is not fully known, the increase in 5-hmC in MYC and ID1 promoters (Figure 47D) may indicate increased TET-mediated active demethylation. The frequent occurrence of 5-hmC near active enhancers and expressed genes (Li et al. 2019) may indicate the possible positive effects of this signal increase on ID1 and MYC expression.

4.5. Functional analyzes on neurospheres

4.5.1. Effects of IDH1-R132H mutant IHA medium and suppression of ID1 and MYC with dCas9-KRAB on NPC neurospheres

MYC and ID1 genes were suppressed in neurospheres using the dCas9-KRAB approach. While the most efficient suppression for the MYC gene was obtained with gRNA5, the most efficient suppression for ID1 was obtained with gRNA1 (Figure 48).

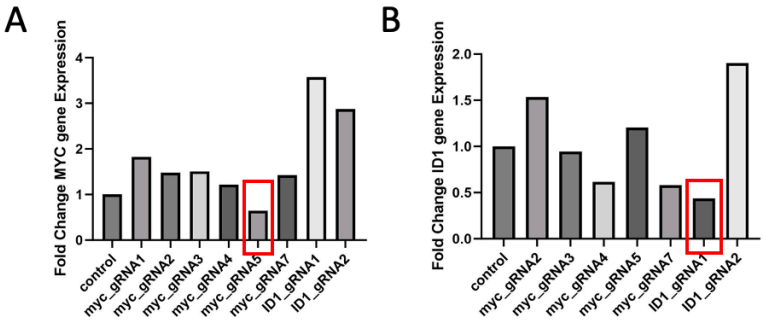

Figure 48. dCas9-KRAB-mediated MYC and ID1 gene suppression in HEK293T cells. Targeting the MYC promoter and ID1 promoter, 7 gRNAs were designed for the MYC promoter region and 2 gRNAs were designed for the ID1 promoter region. pLV hU6-sgRNA hUbC-dCas9-KRAB-T2a-GFP plasmids, in which these gRNAs were cloned, were introduced into HEK293T cells by transfection.

After determining the most suitable conditions, the effect of Neural Progenitor medium, IHA-IDH1-WT and IHA-IDH1-R132H medium on NPC-prepared neurospheres was examined alone or simultaneously with MYC and/or ID1 gene silencing.

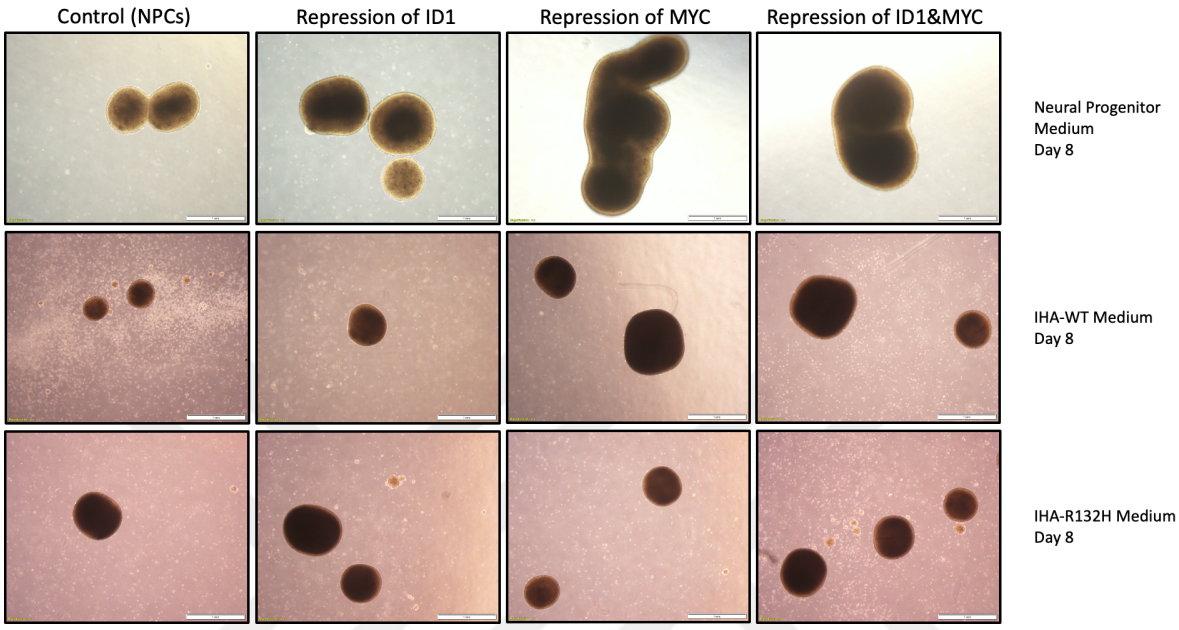

Figure 49. Microscope images of neurospheres on day 8. Control group NPCs are non-nucleofected cells. Constructed pLV hU6-sgRNA-ID1 hUbC-dCas9-KRAB-T2a-GFP plasmid targeting the ID1 promoter to repress ID1, constructed pLV hU6-sgRNA-MYC hUbC targeting the ID1 promoter to repress MYC Plasmid -dCas9-KRAB-T2a-GFP, plasmids pLV hU6-sgRNA-ID1 hUbC-dCas9-KRAB-T2a-GFP and pLV hU6-sgRNA-MYC hUbC-dCas9-KRAB-T2a-GFP were used in nucleofection to repress both simultaneously.

It is observed that control NPCs and nucleofectioned NPCs treated with Neural progenitor medium, IHA-IDH1-WT and IHA-IDH1-R132H media containing bFGF and EGF for 8 days form neurospheres. It is observed that NPC cells form Neurospheres under all conditions. Interestingly, the cell density of the neurospheres formed in Neural Progenitor medium containing bFGF and EGF is lower and the neurospheres formed come closer to each other and merge at the same time. When the control group was compared with other groups, the neurosphere size was smaller in IHA-IDH1-WT medium and it formed fewer neurospheres in IHA-IDH1-R132H conditioned medium compared to the others. When looking at the group in which ID1 is repressed, neurospheres exposed to the IHA-IDH1-R132H conditioned medium

are larger and denser. In the MYC repressed group, neurospheres treated with IHA-IDH1-WT conditioned medium are seen to be larger and have higher cell density. In the group in which MYC and ID1 are repressed, it is observed that the cells tend to form neurospheres, especially in the IHA-IDH1-R132H conditioned medium. On day 8, we observed an abundance of newly formed neurospheres (Figure 49).

4.5.2. Immunofluorescence staining of neurospheres

NESTIN and PAX6 are explained in detail in the characterization of NPCs section. In addition, NESTIN, known as a marker of glioma stem cells, is mainly expressed in precursor neurons (Wu B et al. 2015). Dysregulation of PAX6 results in developmental disorders and tumorigenesis (Lang D et al. 2007). In glioma cells, PAX6 functions as a tumor suppressor, and inhibition of PAX6 results in increased proliferation and cell migration and increased cell expansion under stressful conditions (ZhouY-H et al 2003; Chang JY et al 2007).

Control group NPCs and dCas9-KRAB-mediated ID1 and/or MYC silencing were performed by nucleofection, and immunofluorescence staining was performed separately for the groups in which neurospheres were formed with different media. At the end of staining, the neurospheres were placed in a glass-bottomed 35 mm cell culture dish and Z stack images were taken with the help of a confocal microscope. Then, the Z-stack images were combined with the ZEN program to create maximum intensity images for each group (Figure 50, 51, 52 and 53).

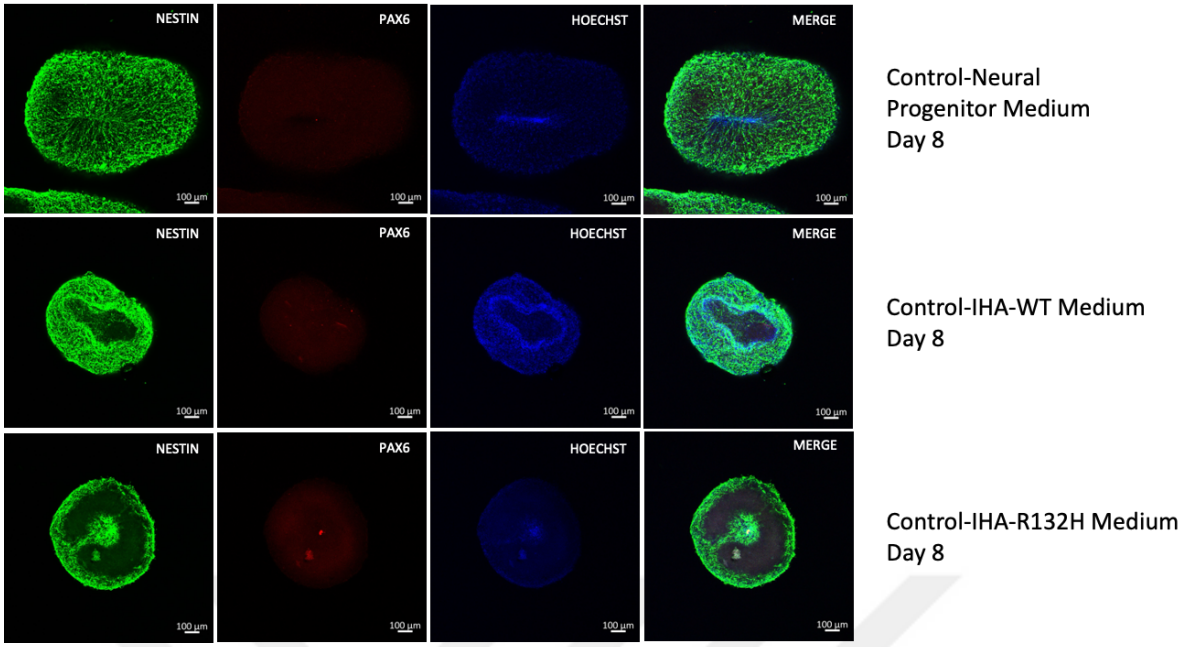

Figure 50. Merged images of confocal microscope Z Stack images of the control group. Immunofluorescence staining of neurospheres formed by treatment with Neural Progenitor medium, IHA-IDH1-WT and IHA-IDH1-R132H medium containing bFGF and EGF for 8 days.

In the neurospheres of control group, on the 8th day, Nestin expression was observed to be strong in all media used, but PAX6 expression was not strong. In fact, it was observed that there was more PAX6 expression in IHA-IDH1-R132H medium containing bFGF and EGF compared to other conditions (Figure 50).

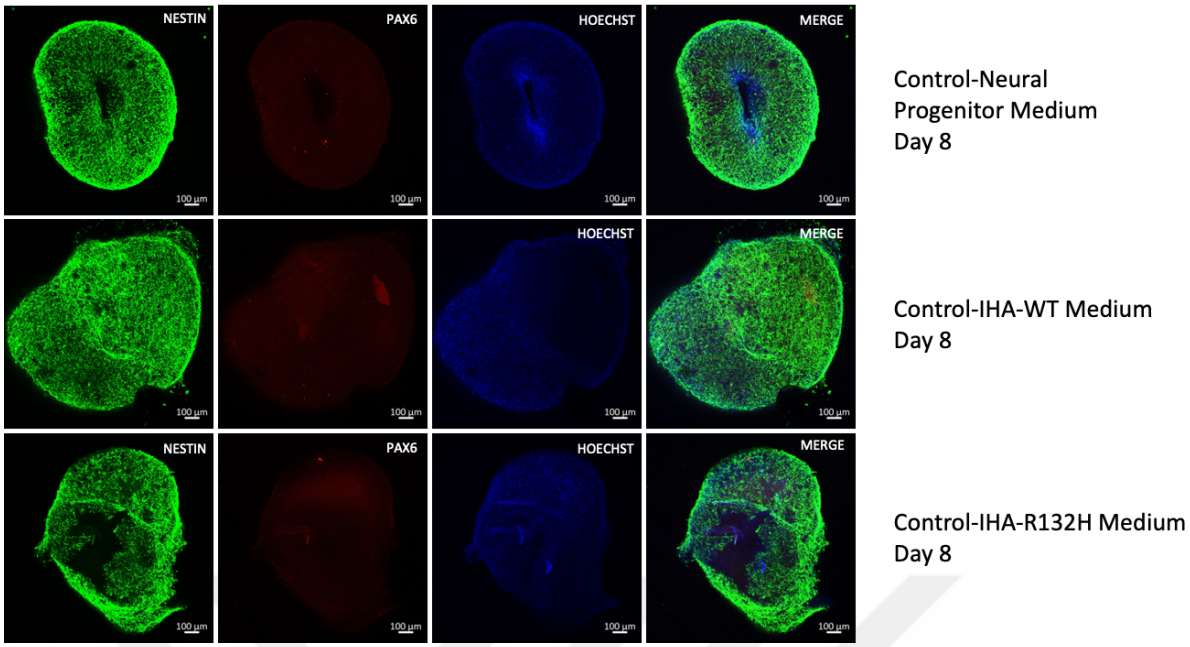

Figure 51. Immunofluorescence staining of neurospheres generated by treating NPC cells nucleofected with pLV hU6-ID1 hUbC-dCas9-KRAB-T2a-GFP plasmids with Neural Progenitor medium, IHA-IDH1-WT and IHA-IDH1-R132H medium containing bFGF and EGF for 8 days. (Image taken at 10X magnification).

In conditions where ID1 was repressed, it was observed that NESTIN expression was strong, but different media had no effect on PAX6 expression, and PAX6 expression was at a low level for all conditions (Figure 51).

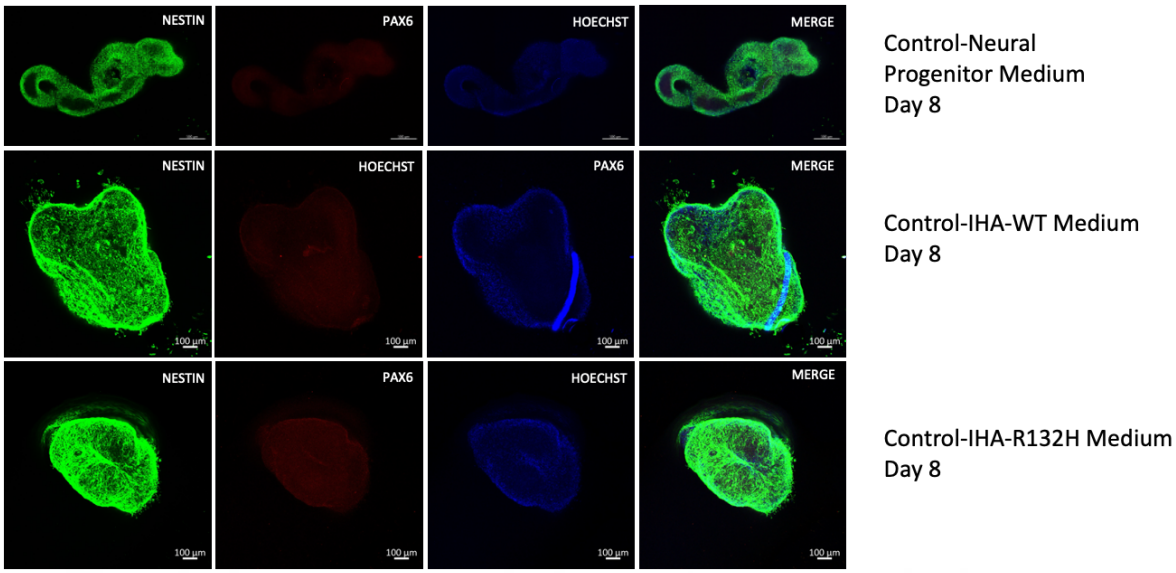

Figure 52. Immunofluorescence staining of neurospheres generated by treating NPC cells nucleofected with pLV hU6-MYC hUbC-dCas9-KRAB-T2a-GFP plasmids with Neural Progenitor medium, IHA-IDH1-WT and IHA-IDH1-R132H medium containing bFGF and EGF for 8 days. (Image taken at 10X magnification).

It was observed that NESTIN expression was strong under conditions where MYC was repressed. It is thought that different media have an effect on PAX6 expression, as shown in the figure. PAX6 expression is very low in neurospheres incubated for 8 days in neural progenitor medium containing bFGF and EGF. (Figure 52).

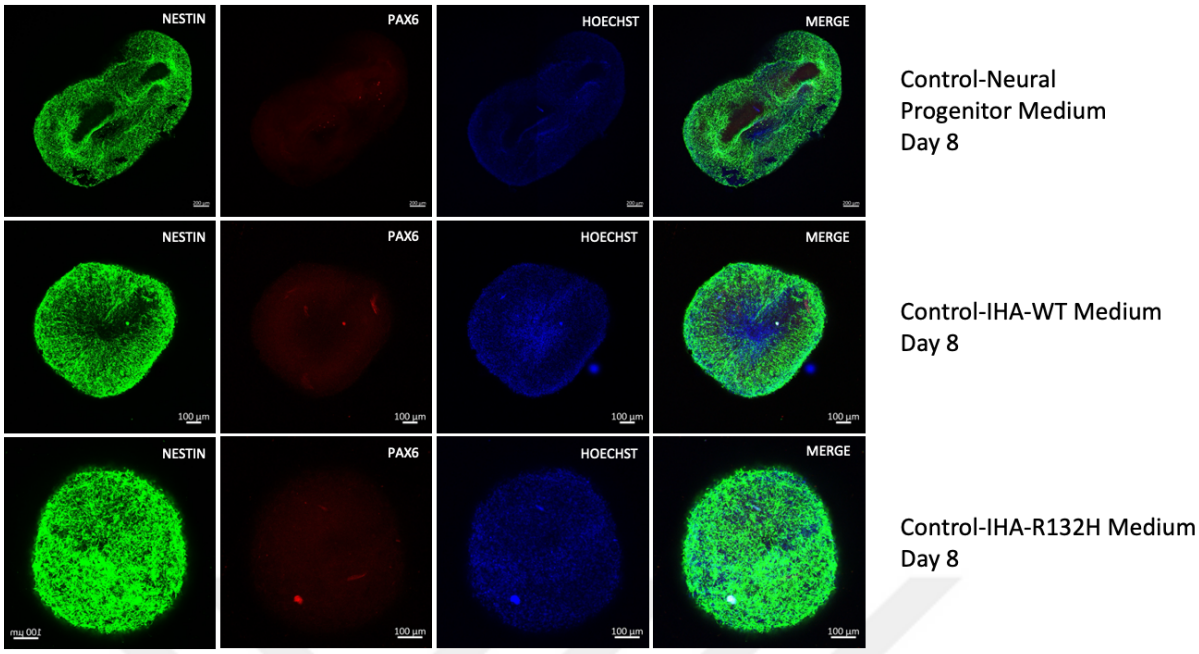

Figure 53. To suppress ID1 and MYC, NPC cells were nucleofected with pLV hU6-MYC hUbC-dCas9-KRAB-T2a-GFP and pLV hU6-ID1 hUbC-dCas9-KRAB-T2a-GFP plasmids with Neural Progenitor containing bFGF and EGF for 8 days. Immunofluorescence staining of neurospheres formed by treatment with medium, IHA-IDH1-WT and IHA-IDH1-R132H medium (image taken at 10X magnification).

NESTIN expression is strong under conditions where MYC and ID1 are repressed together. It is thought that different media have an effect on PAX6 expression. Interestingly, PAX6 expression was higher in neurospheres incubated in IHA-IDH1-WT medium containing bFGF and EGF for 8 days compared to others. (Figure 53).

5. DISCUSSION

It is known that the G-CIMP phenotype is observed in different cell types that express mutant IDH1/2 or are exposed to D-2-HG, and the cells show less differentiation (Turcan et al., 2012). *In vitro* studies on gliomas generally perform tumor cells cultured in 2D environments, and cells cultured in these environments may not fully represent the 3D *in vivo* tumor microenvironment. To date, analysis of major histone modifications, DNA methylation, transcriptome, etc. Most analyzes performed, such as the characterization of early epigenomic changes resulting from IDH1/2 mutations in non-tumor cells, including tumor cells, have been performed in cells cultured mostly in 2D environments. It is known that cells cultured in 2D environment do not fully reflect the glioma biology occurring in 3D tissue. Even if heterogeneous tumor samples are studied under this 2D cell culture condition, the 2D environment may not fully reflect the 3D culture because the micro environment cannot be fully reflected.

The cell culture method enables the understanding of cell structure, the development of tissue morphology and engineering, drug effect and disease mechanisms in pre-clinical, cancer and gene function-related research (Kapałczyńska et al., 2018). In the 2D environment, cells attached to an artificial flat and hard surface are cultured in a single layer and maintenance is low-cost, but in 2D, the metabolism and functionality of the cells change greatly because they cannot mimic the natural structures of cultured tissues or tumors. At the same time, cell-cell and cell-extracellular environment interactions cannot simulate the expected behavior *in vivo*, and 2D culturing causes various phenotype losses in cells (Kapałczyńska et al., 2018). Studying biological processes in 3D culturing has proven to be closer to the natural system *in vivo* (Ravi et al., 2015). The first three-dimensional culture was made by Hamburg and Solomon in the 1970s using solution prepared with agar (Hamburger & Salmon, 1977). In studies conducted since then, the similarity of the morphological structures and behaviors of the cells in the tumor mass and the cells cultured in 3D environment has attracted attention. At the same time, intercellular interaction; interaction of cells with the ECM; Differences in ECM components and their impact on development and morphogenesis; Our increased understanding of issues such as biochemical signaling processes to regulate stem cell differentiation has been accelerated by 3D culture (Kang et al., 2021). Nowadays, 3D environments are needed to show the growth, organization and differentiation of cells more realistically, as in tissues and organs,

to provide a controllable culture environment and to make cellular mechanisms comparable to *in vivo* conditions (Caliari & Burdick, 2016; Yamada & Cukierman, 2007). Extracellular matrix (ECM), which provides the structural scaffolding in almost all tissues of multicellular organisms, regulates the dynamic behavior of cells and intercellular communication. It also has critical roles in the proliferation, morphology, differentiation, and functions of cells and tissues. As it is known, ECM is a complex structure, and since the needs of each tissue or different types of cells are different, ECM components are different for each tissue (Kang et al., 2021). Various natural and synthetic biomaterials are available for creating 3D environments. Biomaterials make it possible to study the entire complex structure of tissues and organs in cell culture systems. Among biomaterials, hydrogels, which are hydrophilic polymers capable of retaining water, are highly preferred in cell culture studies because they can physiologically mimic the elements of natural ECM and are mechanically similar to soft tissue (Caliari & Burdick, 2016).

Hydrogels are divided into two: natural and synthetic. Synthetic ones include polyethylene glycol (PEG), polyvinyl alcohol (PVA) and polycaprolactone (PCL); Alginate, chitosan, hyaluronan and collagen can be given as examples of natural polymers (Andersen et al., 2015)

Alginate, a polysaccharide obtained from a wide variety of brown algae, pseudomanas and azotobacter bacteria, is one of the most widely used hydrogels for microencapsulation in terms of permeability and biocompatibility. It offers ease of use as it has advantages such as being easily available, maintaining its stability in the long term, having the ability to retain water, being non-toxic, having a porous structure and being biodegradable (Kang et al., 2021; Reig-Vano et al., 2021). It consists of B-(1-4)-linked β-D-mannuronic acid repeats (M-blocks) and B-(1-4)-linked α-L-guluronic acid repeats (g-blocks). These blocks are connected to each other by glycosidic bonds and can form copolymers as homopolymeric blocks (MMM- or GGG- blocks) or heteropolymeric blocks (MGMGMG-blocks) (Morris et al., 1980; Sperger et al., 2011). The configurations of M- and G- blocks are different from each other. While M-blocks have a linear and flexible structure, G-blocks provide alginate with a rigid structural feature as they create steric barriers around carboxyl functional groups. Therefore, the M- and G-block ratio of the alginate used is essential for the mechanical features of the formed hydrogels. For example, if the G-block ratio is high, a strong and hard hydrogel is produced, whereas if the M-block ratio is high, a soft and flexible hydrogel is formed (Costa et al., 2018). It forms a gel-like matrix by being activated by divalent cations such as calcium, zinc and

copper. Due to this gelling feature, it creates 3-dimensional structures and forms suitable structures for cells (Machida-Sano et al., 2014). The pore size of the alginate gel network can be adjusted between 5-200 nm. Pore size is important for cells to receive nutrients and remove waste products (Smidsr & Skj, 1990). Ionically gelled alginate can be dissolved using substances such as ethylenediaminetetraacetic acid (EDTA) hexametaphosphate.

Previous studies have shown that alginate successfully mimics the 3D environment of the CNS, and that the differentiation of stem cells into neural lineages is successfully achieved in 3D alginate culture ((Bozza et al., 2014; L. Li et al., 2011). Additionally, a model that mimics treatment conditions in drug response studies was created with a 3D culture prepared with U87 glioblastoma cells and alginate hydrogel. Cells in 3D alginate culture treated with temozolomide (TMZ) demonstrated an anti-proliferative effect, as did cells maintained in 2D cell culture medium. Moreover, it was determined that the expression of genes associated with drug resistance increased more in cells maintained in 3D alginate culture. As a result, the 3D culture model prepared with alginate has been shown to be a fast, reliable and practical model for drug testing and treatment development (Dragoj et al., 2021).

Therefore, we used alginate in modeling to shed light on the earliest stages of gliomagenesis. In this study, an alginate bead formation protocol was applied to perform alginate-based 3D culture (Davoudi et al., 2021). The diameter of the alginate-formed beads was approximately 2 mm, and there are approximately 2500 cells in each NPC alginate bead. For the first time in the literature, we showed that alginate-encapsulated NPCs survived and grew throughout the culture period (18 days) without passaging or re-encapsulation with alginate. We observed that the number of cells increased and formed dense clusters from the first day of culture, even when the medium was changed at time points.

Not knowing exactly what the cell of origin of gliomas is has been an ongoing problem for many years. It is the most critical factor to take into account when creating glioma models. This issue was mentioned in the introduction part. Neural stem cells (NSCs), which have self-renewing properties, are considered to be ideal candidates as the cell of origin of gliomas, considering their development potential and plasticity properties.

It is also known to be produced by NSCs to produce new generations of neuronal and glial lineages in neural progenitor cells (Cahill & Turcan, 2018). It is accepted that gliomas arise from differentiation by accumulation of mutations in neural stem/progenitor cells, oligodendrocyte progenitor cells or astrocytes. However, cells from high-grade tumor tissues

are mostly used in glioma cell culture models. Because cells derived from tumor tissue reflect the cellular conditions in fully developed tumors, they are not suitable for modeling the early stages of gliomas (Cahill & Turcan, 2018).

Neural progenitor cells, which are among the cell types considered as possible cells of origin, allow the development of more effective treatments, as they more realistically reflect the cellular states in the initial stages of gliomagenesis and gliomagenesis-related signals can be better captured in these cells. For this reason, NPCs created by differentiating from hiPSC without oncogenic mutations were used. iPSC generated from non-pluripotent cells are capable of differentiating into many different cell types, including neurons. Generation of iPSCs has enabled the development of disease models and novel therapies to study disease pathogenesis (Csete, 2010; Raya et al., 2009).

Basic helix-loop-helix (bHLH) proteins serve as key regulators of lineage- and organ-specific gene expression in both vertebrates and invertebrates (Coppé et al., 2003). The DNA binding inhibitor (ID) protein family dimerizes with bHLH proteins. Thus, as negative regulators of bHLH, they regulates processes important in stem cell homeostasis, such as cell cycle regulation, differentiation, stem cell niche maintenance, and cell migration (Sachdeva et al., 2019a; Soroceanu et al., 2013). The ID protein family has four subtypes: ID1, ID2, ID3, and ID4. Gene expression levels of the ID1, ID2 and ID3 subtypes, which are functionally similar in undifferentiated cells, extremely proliferative cells, embryonic cells and cancer cells, are high.

ID1 protein is the most studied subtype of all ID proteins and is involved in tumorigenesis, cell senescence, proliferation and survival (Z. Zhao et al., 2020). It is overexpressed in more than 20 types of cancer, such as prostate cancer, blood cancer, breast cancer and glioblastoma. ID1, which is considered as a tumor promoter, promotes proliferation and differentiation, metastasis, angiogenesis and Ephitelial Mesenchymal Transition (EMT) (Sachdeva et al., 2019; Z. Zhao et al., 2020). ID1 has been shown to be a critical regulator of Glioblastoma initiation and GBM chemoresistance. In the same study, it was shown that the effect of the chemotherapy drug temozolomide given after inhibition of ID1 increased on the cells, delayed tumor recurrence and prolonged life (Sachdeva et al., 2019).

It was observed that cyclinaD1, B-catenin and c-Myc, expressions decreased and expression of E-cadherin increased in ID1-silenced U87 cells with the help of small hairpin RNA (shRNA). This result shows that the Epithelial-Mesenchymal transition (EMT) is

controlled and thus the metastatic potential of GBM is regulated by ID1 (Guo et al., 2013). It was also found that ID1 increased EGF secretion in glioblastoma, thus providing EGFR activation and leading to resistance against temozolomide-mediated cell death (Sachdeva et al., 2019).

In point of fact, the increase in the H3K4me3 and H3K27ac signals of the ID1 promoter after the application of IHA-IDH1-R132H conditioned medium for 14 days explains the increased ID1 expression. Interestingly, the increase in H3K27ac histone modification was reversed after removal of IDH1-mutant medium after 14 days. This finding suggests that the activating effect at the ID1 promoter is 2-HG dependent and may be transient. However, it should not be forgotten that the IDH1 mutation is the earliest change and is found in all subclones that occur in gliomagenesis, so the induction in ID1 may not be reversible at all, or it may occur by a different mechanism. Although the level of 5mC at the ID1 promoter appears to be partially increased, the increase in the level of 5hmC can be interpreted as increased TET-mediated oxidation of 5mC and may indicate that the ID1 promoter is protected from possible 2-HG-mediated methylation.

The results of comparing the genes showing different expression in RNA-seq analysis with TCGA-LGG data also support that ID1 may have a key role in the gliomagenesis-triggering effects created by IDH1-R132H. When the genes showing an increase/decrease in expression on the 17th day as a result of RNA-seq analysis were compared with the first 25 genes showing the highest correlation with ID1 expression according to TCGA-LGG RNA-seq data, 15 of the 25 genes had different expression on the 17th day and all of them were the same. It is striking that a correlation in the direction (positive-positive, negative-negative) was observed, and that the transcriptome changes we see in NPCs are quite similar to low-grade gliomas from an ID1-centered perspective.

TERT expression was strongly induced in NPCs exposed to IHA-IDH1-R132H conditioned medium compared to NPCs exposed to IHA-IDH1-WT conditioned medium. Moreover, this induction continued despite returning to normal NPC medium for 3 days after day 14. In MeDIP-qPCR analysis, there was a substantial increase in the 5mC level of TERT in cells maintained in IHA-IDH1-R132H conditioned medium, and a partial decrease in the 5hmC level was observed compared to the wild type. In H3K4me3 ChIP-qPCR analysis, day 17 indicates a delayed activation. These results, when examined in the light of the literature, provide important clues regarding the induction of TERT expression by the IDH1-R132H

mutation. It is reported that when they achieved stable IDH1-R132H expression in p53/pRb-KO E6E7-expressing normal human astrocytes, these cells were able to escape replicative senescence, whereas isogenic cells expressing IDH-WT could not (Ohba et al., 2016). Interestingly, researchers reported that IDH1-R132H induced TERT expression up to 40-fold, but this induction was observed only in normal human astrocytes (NHA) that could recover from senescence-induced crisis, and not in pre-crisis cells (Ohba et al., 2016). The fact that we were able to see this induction, albeit much weaker, in completely healthy (genetically wild-type) NPCs may be due to the fact that NPCs are genetically different from p53/pRb-KO E6E7 NHAs, cells that more realistically mimic glioma onset. It can also be explained by the fact that they are small and exist in a 3-dimensional culture environment.

The fact that TERT was induced is also interesting as it is the target gene of MYC, another target gene of the project. As a matter of fact, they showed that MYC binding together with the increase in H3K4me3 in the TERT promoter plays a role in the induction of TERT by IDH1-R132H (Ohba et al., 2016). However, when the RNA-seq analysis results were examined, we observed that MYC expression was not induced by IDH1-R132H IHA medium: -0.04-fold, p=0.86 (comparison 3), 0.06-fold, p=0.81 (comparison 4). On the other hand, MYC is an immediate early gene and the stability of its mRNA is extremely low; Since mitogens in the environment are rapidly degraded at both mRNA and protein levels (half-time 25 min) as soon as they are removed (Dani et al. 1984), examining MYC target genes is a more reliable approach for the analysis of MYC activity. Therefore, for the 102 genes whose expression increased the most on the 17th day, MYC appeared in the top two ranks in the gene-set enrichment analysis results of the transcription factors controlling these genes (according to CHEA and ENCODE databases), indicating that MYC activity increased as a result of IDH1-R132H. A supporting finding for this finding comes from the increased level of H3K27ac in the MYC promoter; However, while the increase in one region of the promoter was permanent, the increase in the other region was reversed on the 17th day. This observation may be indicative of the known complex regulatory mechanisms of the MYC promoter (Levens 2008).

Another striking MYC-related finding is that the methylation levels of the MYC enhancer (TRIM28-related), which we identified in our previous studies and interacts with the rs55705857 glioma risk SNP, showed a significant decrease in both 5-mC and 5-hmC. In addition, H3K27ac signal at this enhancer also increases on day 14 and is reversed after removal of the mutant medium. On the other hand, it is also interesting that the H3K27ac signal in the

regions near rs55705857 was significantly suppressed after exposure to the mutant medium compared to the IDH1-WT medium. On the other hand, although no H3K4me3 signal was observed at the rs55705857 SNP locus in previous studies with IHAs (Turcan et al., 2018), in our study, an increased H3K4me3 signal due to the IDH1-R132H mutation was observed in NPCs exposed to the medium obtained from these IHAs. The reason for this result may be the analysis of changes in NPCs instead of IHA, or the qPCR method used may be more sensitive than the ChIP-seq method. In both cases, our results show that the IDH1-R132H mutation causes H3K4me3 enrichment partially at the rs55705857 locus and more strongly at a locus approximately 2.5 kb away from the SNP.

Another interesting result revealed by RNA-seq data was that the signaling pathways controlling pluripotency were among the pathways that both increased the most and decreased the most on day 17; The possible reason for this may be that some of the different components of these critical pathways are permanently induced by 2-HG, while others are temporarily induced, that is, a rapid return to their previous levels upon withdrawal of 2-HG. As a matter of fact, the fact that cancer-related pathways are among the pathways that decrease most significantly immediately after the withdrawal of 2-HG indicates that at least some of the effects of 2-HG on cancer are temporary, indicating that 2-HG and therefore IDH1-R132H and the associated IDH1/ It can be interpreted as being dependent on the presence of 2 mutations.

Although suppression of ID1 and MYC with the dCas9-KRAB method has been achieved, additional analyzes are needed in this direction. After optimization of this approach, we will be able to test more accurately to what extent suppressing these two genes can prevent the changes caused by mutant IDH1 towards glioma formation. On the other hand, neurosphere size and density in control cells exposed to IHA-IDH1-R132H medium are higher than in cells exposed to IHA-IDH1-WT medium. At the same time, it is a striking detail that when IHA-IDH1-R132H medium was given to cells in which only ID1 was suppressed and ID1 and MYC were suppressed together, their ability to form neurospheres was greater. When the conditions of suppression of MYC in cells are compared, the neurospheres formed by cells cultured in IHA-IDH1-WT medium and neural progenitor medium are larger.

These results indicate that the mutant medium can eliminate the negative effects of dCas9-KRAB-mediated gene repression of ID1 and MYC.

6. CONCLUSIONS AND FUTURE DIRECTIONS

In this study, we first showed that NPCs can be cultured for a long time in 3D culture prepared with alginate and that 3D culture prepared with alginate is suitable. At the same time, the effects of IDH mutations alone on the earliest stages of gliomas, without the confounding effect of other mutations, were demonstrated in NPCs maintained in 3D culture with IHA-IDH1-R132H conditioned medium. While the results obtained supported the hypotheses first put forward by our group regarding the role of MYC in this early stage, they also revealed ID1 as another critical factor. Previous studies have shown that ID1, which is considered a tumor promoter, is an important regulator in glioblastoma initiation and chemoresistance. The ID1-MYC-IDH1 relationship will be examined more closely in studies following functional analyzes initiated by repressing ID1 and/or MYC. The molecules and networks in which ID1 and MYC act together in the glioma-initiating effects of IDH1 can be determined, and possible targeting strategies can be developed.

7. REFERENCES

Abd-Ellah, M. K., Awad, A. I., Khalaf, A. A. M., & Hamed, H. F. A. (2019). A review on brain tumor diagnosis from MRI images: Practical implications, key achievements, and lessons learned. In *Magnetic Resonance Imaging* (Vol. 61, pp. 300–318). Elsevier Inc. https://doi.org/10.1016/j.mri.2019.05.028

Albini, S., Zakharova, V., & Ait-Si-Ali, S. (2019). Histone Modifications. In *Epigenetics and Regeneration* (pp. 47–72). Elsevier. https://doi.org/10.1016/B978-0-12-814879-2.00003-0

Alcantara Llaguno, S., Chen, J., Kwon, C. H., Jackson, E. L., Li, Y., Burns, D. K., Alvarez-Buylla, A., & Parada, L. F. (2009). Malignant Astrocytomas Originate from Neural Stem/Progenitor Cells in a Somatic Tumor Suppressor Mouse Model. *Cancer Cell*, *15*(1), 45–56. https://doi.org/10.1016/j.ccr.2008.12.006

Alcantara Llaguno, S. R., Wang, Z., Sun, D., Chen, J., Xu, J., Kim, E., Hatanpaa, K. J., Raisanen, J. M., Burns, D. K., Johnson, J. E., & Parada, L. F. (2015). Adult Lineage-Restricted CNS Progenitors Specify Distinct Glioblastoma Subtypes. *Cancer Cell*, *28*(4), 429–440. https://doi.org/10.1016/j.ccell.2015.09.007

Alexa, A., & Maintainer, J. R. (2021). *Package "topGO" Type Package Title Enrichment Analysis for Gene Ontology*. https://git.bioconductor.org/packages/topGO

Alzial, G., Renoult, O., Paris, F., Gratas, C., Clavreul, A., & Pecqueur, C. (2022). Wild-type isocitrate dehydrogenase under the spotlight in glioblastoma. In *Oncogene* (Vol. 41, Issue 5, pp. 613–621). Springer Nature. https://doi.org/10.1038/s41388-021-02056-1

Amoh, Y., Li, L., Katsuoka, K., Penman, S., & Hoffman, R. M. (2005). *Multipotent nestin-positive, keratin-negative hair-follicle bulge stem cells can form neurons*. www.pnas.orgcgidoi10.1073pnas.0501263102

Andersen, T., Auk-Emblem, P., & Dornish, M. (2015). 3D Cell Culture in Alginate Hydrogels. *Microarrays*, *4*(2), 133–161. https://doi.org/10.3390/microarrays4020133

Archer, T. C., Jin, J., & Casey, E. S. (2011). Interaction of Sox1, Sox2, Sox3 and Oct4 during primary neurogenesis. *Developmental Biology*, *350*(2), 429–440. https://doi.org/10.1016/j.ydbio.2010.12.013

Bachoo, R. M., Maher, E. A., Ligon, K. L., Sharpless, N. E., Chan, S. S., You, M. J., Tang, Y., Defrances, J., Stover, E., Weissleder, R., Rowitch, D. H., Louis, D. N., & Depinho, R. A.

(n.d.). *Epidermal growth factor receptor and Ink4a/Arf: Convergent mechanisms governing terminal differentiation and transformation along the neural stem cell to astrocyte axis*.

Badur, M. G., Muthusamy, T., Parker, S. J., Ma, S., McBrayer, S. K., Cordes, T., Magana, J. H., Guan, K. L., & Metallo, C. M. (2018). Erratum: Oncogenic R132 IDH1 Mutations Limit NADPH for De Novo Lipogenesis through (D)2-Hydroxyglutarate Production in Fibrosarcoma Cells (Cell Reports (2018) 25(4) (1018–1026.e4), (S2211124718315341) (10.1016/j.celrep.2018.09.074)). In *Cell Reports* (Vol. 25, Issue 6, p. 1680). Elsevier B.V. https://doi.org/10.1016/j.celrep.2018.10.099

Bardella, C., Al-Dalahmah, O., Krell, D., Brazauskas, P., Al-Qahtani, K., Tomkova, M., Adam, J., Serres, S., Lockstone, H., Freeman-Mills, L., Pfeffer, I., Sibson, N., Goldin, R., Schuster-Böeckler, B., Pollard, P. J., Soga, T., McCullagh, J. S., Schofield, C. J., Mulholland, P., … Tomlinson, I. (2016). Expression of Idh1R132H in the Murine Subventricular Zone Stem Cell Niche Recapitulates Features of Early Gliomagenesis. *Cancer Cell*, *30*(4), 578–594. https://doi.org/10.1016/j.ccell.2016.08.017

Beacon, T. H., Delcuve, G. P., López, C., Nardocci, G., Kovalchuk, I., van Wijnen, A. J., & Davie, J. R. (2021). The dynamic broad epigenetic (H3K4me3, H3K27ac) domain as a mark of essential genes. In *Clinical Epigenetics* (Vol. 13, Issue 1). BioMed Central Ltd. https://doi.org/10.1186/s13148-021-01126-1

Behrend, L., Henderson, G., & Zwacka, R. M. (2003). Reactive oxygen species in oncogenic transformation. In *Meeting of the Biochemical Society*. https://doi.org/https://doi.org/10.1042/bst0311441

Bleeker, F. E., Molenaar, R. J., & Leenstra, S. (2012). Recent advances in the molecular understanding of glioblastoma. In *Journal of Neuro-Oncology* (Vol. 108, Issue 1, pp. 11–27). https://doi.org/10.1007/s11060-011-0793-0

Bohman, L. E., Swanson, K. R., Moore, J. L., Rockne, R., Mandigo, C., Hankinson, T., Assanah, M., Canoll, P., & Bruce, J. N. (2010). Magnetic resonance imaging characteristics of glioblastoma multiforme: Implications for understanding glioma ontogeny. *Neurosurgery*, *67*(5), 1319–1327. https://doi.org/10.1227/NEU.0b013e3181f556ab

Bolger, A. M., Lohse, M., & Usadel, B. (2014). Trimmomatic: A flexible trimmer for Illumina sequence data. *Bioinformatics*, *30*(15), 2114–2120. https://doi.org/10.1093/bioinformatics/btu170

Bozza, A., Coates, E. E., Incitti, T., Ferlin, K. M., Messina, A., Menna, E., Bozzi, Y., Fisher, J. P., & Casarosa, S. (2014). Neural differentiation of pluripotent cells in 3D alginate-based cultures. *Biomaterials*, *35*(16), 4636–4645. https://doi.org/10.1016/j.biomaterials.2014.02.039

Brat, D. J., Verhaak, R. G. W., Aldape, K. D., Yung, A., & Morozova, O. (2015). Comprehensive, Integrative Genomic Analysis of Diffuse Lower-Grade Gliomas. *New England Journal of Medicine*, *372*(26), 2481–2498. https://doi.org/10.1056/NEJMoa1402121

Cahill, D., & Turcan, S. (2018). Origin of Gliomas. *Seminars in Neurology*, *38*(1), 5–10. https://doi.org/10.1055/s-0037-1620238

Caliari, S. R., & Burdick, J. A. (2016). A practical guide to hydrogels for cell culture. In *Nature Methods* (Vol. 13, Issue 5, pp. 405–414). Nature Publishing Group. https://doi.org/10.1038/nmeth.3839

Campian, J., & Gutmann, D. H. (2017). JOURNAL OF CLINICAL ONCOLOGY CNS Tumors in Neurofibromatosis. *J Clin Oncol*, *35*, 2378–2385. https://doi.org/10.1200/JCO.2016

Ceccarelli, M., Barthel, F. P., Malta, T. M., Sabedot, T. S., Salama, S. R., Murray, B. A., Morozova, O., Newton, Y., Radenbaugh, A., Pagnotta, S. M., Anjum, S., Wang, J., Manyam, G., Zoppoli, P., Ling, S., Rao, A. A., Grifford, M., Cherniack, A. D., Zhang, H., … Verhaak, R. G. W. (2016). Molecular Profiling Reveals Biologically Discrete Subsets and Pathways of Progression in Diffuse Glioma. *Cell*, *164*(3), 550–563. https://doi.org/10.1016/j.cell.2015.12.028

Chaumeil, M. M., Radoul, M., Najac, C., Eriksson, P., Viswanath, P., Blough, M. D., Chesnelong, C., Luchman, H. A., Cairncross, J. G., & Ronen, S. M. (2016). Hyperpolarized 13C MR imaging detects no lactate production in mutant IDH1 gliomas: Implications for diagnosis and response monitoring. *NeuroImage: Clinical*, *12*, 180–189. https://doi.org/10.1016/j.nicl.2016.06.018

Chesnelong, C., Chaumeil, M. M., Blough, M. D., Al-Najjar, M., Stechishin, O. D., Chan, J. A., Pieper, R. O., Ronen, S. M., Weiss, S., Luchman, H. A., & Cairncross, J. G. (2014). Lactate dehydrogenase A silencing in IDH mutant gliomas. *Neuro-Oncology*, *16*(5), 686–695. https://doi.org/10.1093/neuonc/not243

Chowdhury, R., Yeoh, K. K., Tian, Y. M., Hillringhaus, L., Bagg, E. A., Rose, N. R., Leung, I. K. H., Li, X. S., Woon, E. C. Y., Yang, M., McDonough, M. A., King, O. N., Clifton, I. J.,

Klose, R. J., Claridge, T. D. W., Ratcliffe, P. J., Schofield, C. J., & Kawamura, A. (2011a). The oncometabolite 2-hydroxyglutarate inhibits histone lysine demethylases. *EMBO Reports*, *12*(5), 463–469. https://doi.org/10.1038/embor.2011.43

Chowdhury, R., Yeoh, K. K., Tian, Y. M., Hillringhaus, L., Bagg, E. A., Rose, N. R., Leung, I. K. H., Li, X. S., Woon, E. C. Y., Yang, M., McDonough, M. A., King, O. N., Clifton, I. J., Klose, R. J., Claridge, T. D. W., Ratcliffe, P. J., Schofield, C. J., & Kawamura, A. (2011b). The oncometabolite 2-hydroxyglutarate inhibits histone lysine demethylases. *EMBO Reports*, *12*(5), 463–469. https://doi.org/10.1038/embor.2011.43

Christensen, B. C., Smith, A. A., Zheng, S., Koestler, D. C., Houseman, E. A., Marsit, C. J., Wiemels, J. L., Nelson, H. H., Karagas, M. R., Wrensch, M. R., Kelsey, K. T., & Wiencke, J. K. (2011). DNA methylation, isocitrate dehydrogenase mutation, and survival in glioma. *Journal of the National Cancer Institute*, *103*(2), 143–153. https://doi.org/10.1093/jnci/djq497

Chung, B. M., Rotty, J. D., & Coulombe, P. A. (2013). Networking galore: Intermediate filaments and cell migration. In *Current Opinion in Cell Biology* (Vol. 25, Issue 5, pp. 600–612). https://doi.org/10.1016/j.ceb.2013.06.008

Cohen, A. L., Holmen, S. L., & Colman, H. (2013). IDH1 and IDH2 mutations in gliomas. *Current Neurology and Neuroscience Reports*, *13*(5). https://doi.org/10.1007/s11910-013-0345-4

Coppé, J. P., Smith, A. P., & Desprez, P. Y. (2003). Id proteins in epithelial cells. *Experimental Cell Research*, *285*(1), 131–145. https://doi.org/10.1016/S0014-4827(03)00014-4

Costa, M. J., Marques, A. M., Pastrana, L. M., Teixeira, J. A., Sillankorva, S. M., & Cerqueira, M. A. (2018). Physicochemical properties of alginate-based films: Effect of ionic crosslinking and mannuronic and guluronic acid ratio. *Food Hydrocolloids*, *81*, 442–448. https://doi.org/10.1016/j.foodhyd.2018.03.014

Csete, M. (2010). Translational prospects for human induced pluripotent stem cells. In *Regenerative Medicine* (Vol. 5, Issue 4, pp. 509–519). https://doi.org/10.2217/rme.10.39

Dai, C., Celestino, J. C., Okada, Y., Louis, D. N., Fuller, G. N., & Holland, E. C. (2001). PDGF autocrine stimulation dedifferentiates cultured astrocytes and induces oligodendrogliomas from and oligoastrocytomas neural progenitors and astrocytes in vivo. *Genes and Development*, *15*(15), 1913–1925. https://doi.org/10.1101/gad.903001

Dang, L., White, D. W., Gross, S., Bennett, B. D., Bittinger, M. A., Driggers, E. M., Fantin, V. R., Jang, H. G., Jin, S., Keenan, M. C., Marks, K. M., Prins, R. M., Ward, P. S., Yen, K. E., Liau, L. M., Rabinowitz, J. D., Cantley, L. C., Thompson, C. B., Vander Heiden, M. G., & Su, S. M. (2009). Cancer-associated IDH1 mutations produce 2-hydroxyglutarate. *Nature*, *462*(7274), 739–744. https://doi.org/10.1038/nature08617

Davoudi, F., Ghorbanpoor, S., Yoda, S., Pan, X., Crowther, G. S., Yin, X., Murchie, E., Hata, A. N., Willers, H., & Benes, C. H. (2021). Alginate-based 3D cancer cell culture for therapeutic response modeling. *STAR Protocols*, *2*(2). https://doi.org/10.1016/j.xpro.2021.100391

Doetsch, F., Caillé, I., Lim, D. A., Manuel García-Verdugo, J., & Alvarez-Buylla, A. (1999). Subventricular Zone Astrocytes Are Neural Stem Cells in the Adult Mammalian Brain. In *Cell* (Vol. 97).

Doherty, J. R., & Cleveland, J. L. (2013). Targeting lactate metabolism for cancer therapeutics. In *Journal of Clinical Investigation* (Vol. 123, Issue 9, pp. 3685–3692). https://doi.org/10.1172/JCI69741

Dragoj, M., Stojkovska, J., Stanković, T., Dinić, J., Podolski-Renić, A., Obradović, B., & Pešić, M. (2021). Development and validation of a long-term 3d glioblastoma cell culture in alginate microfibers as a novel bio-mimicking model system for preclinical drug testing. *Brain Sciences*, *11*(8). https://doi.org/10.3390/brainsci11081025

Duffau, H., & Taillandier, L. (2015). New concepts in the management of diffuse low-grade glioma: Proposal of a multistage and individualized therapeutic approach. *Neuro-Oncology*, *17*(3), 332–342. https://doi.org/10.1093/neuonc/nou153

Duncan, C. G., Barwick, B. G., Jin, G., Rago, C., Kapoor-Vazirani, P., Powell, D. R., Chi, J. T., Bigner, D. D., Vertino, P. M., & Yan, H. (2012). A heterozygous IDH1R132H/WT mutation induces genome-wide alterations in DNA methylation. *Genome Research*, *22*(12), 2339–2355. https://doi.org/10.1101/gr.132738.111

Eckel-Passow, J. E., Lachance, D. H., Molinaro, A. M., Walsh, K. M., Decker, P. A., Sicotte, H., Pekmezci, M., Rice, T., Kosel, M. L., Smirnov, I. V., Sarkar, G., Caron, A. A., Kollmeyer, T. M., Praska, C. E., Chada, A. R., Halder, C., Hansen, H. M., McCoy, L. S., Bracci, P. M., … Jenkins, R. B. (2015). Glioma Groups Based on 1p/19q, IDH , and TERT Promoter Mutations in Tumors . *New England Journal of Medicine*, *372*(26), 2499–2508. https://doi.org/10.1056/nejmoa1407279

Gabriel, J. L., Zervos, P. R., & Plaut, G. W. E. (n.d.). *Activity of Purified NAD-Specific Isocitrate Dehydrogenase at Modulator and Substrate Concentrations Approximating Conditions in Mitocbondria*.

Garcia, I., Aldaregia, J., Vicentic, J. M., Aldaz, P., Moreno-Cugnon, L., Torres-Bayona, S., Carrasco-Garcia, E., Garros-Regulez, L., Egaña, L., Rubio, A., Pollard, S., Stevanovic, M., Sampron, N., & Matheu, A. (2017). Oncogenic activity of SOX1 in glioblastoma. *Scientific Reports*, *7*. https://doi.org/10.1038/srep46575

González-Castro, T. B., Juárez-Rojop, I. E., López-Narváez, M. L., Tovilla-Zárate, C. A., Genis-Mendoza, A. D., Pérez-Hernández, N., Martínez-Magaña, J. J., & Rodríguez-Pérez, J. M. (2019). Genetic Polymorphisms of CCDC26 rs891835, rs6470745, and rs55705857 in Glioma Risk: A Systematic Review and Meta-analysis. *Biochemical Genetics*, *57*(4), 583–605. https://doi.org/10.1007/s10528-019-09911-7

Grimm, D., Bauer, J., Wise, P., Krüger, M., Simonsen, U., Wehland, M., Infanger, M., & Corydon, T. J. (2020). The role of SOX family members in solid tumours and metastasis. In *Seminars in Cancer Biology* (Vol. 67, pp. 122–153). Academic Press. https://doi.org/10.1016/j.semcancer.2019.03.004

Guo, P., Lan, J., Ge, J., Mao, Q., & Qiu, Y. (2013). ID1 regulates U87 human cell proliferation and invasion. *Oncology Letters*, *6*(4), 921–926. https://doi.org/10.3892/ol.2013.1507

Haddock, S., Alban, T. J., Turcan, Ş., Husic, H., Rosiek, E., Ma, X., Wang, Y., Bale, T., Desrichard, A., Makarov, V., Monette, S., Wu, W., Gardner, R., Manova, K., Boire, A., & Chan, T. A. (2022). Phenotypic and molecular states of IDH1 mutation-induced CD24-positive glioma stem-like cells. *Neoplasia (United States)*, *28*. https://doi.org/10.1016/j.neo.2022.100790

Hamburger, A. W., & Salmon, S. E. (1977). Primary Bioassay of Human Tumor Stem Cells. In *Bull. Environ. Contam. Toxicol* (Vol. 9). Cambridge Univ. Press. https://doi.org/10.1126/science.560061

Han, S., Liu, Y., Cai, S. J., Qian, M., Ding, J., Larion, M., Gilbert, M. R., & Yang, C. (2020a). IDH mutation in glioma: molecular mechanisms and potential therapeutic targets. In *British Journal of Cancer* (Vol. 122, Issue 11, pp. 1580–1589). Springer Nature. https://doi.org/10.1038/s41416-020-0814-x

Han, S., Liu, Y., Cai, S. J., Qian, M., Ding, J., Larion, M., Gilbert, M. R., & Yang, C. (2020b). IDH mutation in glioma: molecular mechanisms and potential therapeutic targets. In

British Journal of Cancer (Vol. 122, Issue 11, pp. 1580–1589). Springer Nature. https://doi.org/10.1038/s41416-020-0814-x

He, F., Wu, H., Zhou, L., Lin, Q., Cheng, Y., & Sun, Y. E. (2020). Tet2-mediated epigenetic drive for astrocyte differentiation from embryonic neural stem cells. *Cell Death Discovery*, *6*(1). https://doi.org/10.1038/s41420-020-0264-5

Holland, E. C., Celestino, J., Dai, C., Schaefer, L., Sawaya, R. E., & Fuller, G. N. (2000). *Combined activation of Ras and Akt in neural progenitors induces glioblastoma formation in mice*. http://genetics.nature.com

Hvinden, I. C., Cadoux-Hudson, T., Schofield, C. J., & McCullagh, J. S. O. (2021). Metabolic adaptations in cancers expressing isocitrate dehydrogenase mutations. In *Cell Reports Medicine* (Vol. 2, Issue 12). Cell Press. https://doi.org/10.1016/j.xcrm.2021.100469

Ichimura, K. (2012). Molecular pathogenesis of IDH mutations in gliomas. *Brain Tumor Pathology*, *29*(3), 131–139. https://doi.org/10.1007/s10014-012-0090-4

Ishiwata, T., Teduka, K., Yamamoto, T., Kawahara, K., Matsuda, Y., & Naito, Z. (2011). Neuroepithelial stem cell marker nestin regulates the migration, invasion and growth of human gliomas. *Oncology Reports*, *26*(1), 91–99. https://doi.org/10.3892/or.2011.1267

Itsumi, M., Inoue, S., Elia, A. J., Murakami, K., Sasaki, M., Lind, E. F., Brenner, D., Harris, I. S., Chio, I. I. C., Afzal, S., Cairns, R. A., Cescon, D. W., Elford, A. R., Ye, J., Lang, P. A., Li, W. Y., Wakeham, A., Duncan, G. S., Haight, J., … Mak, T. W. (2015). Idh1 protects murine hepatocytes from endotoxin-induced oxidative stress by regulating the intracellular NADP +/NADPH ratio. *Cell Death and Differentiation*, *22*(11), 1837–1848. https://doi.org/10.1038/cdd.2015.38

Jacques, T. S., Swales, A., Brzozowski, M. J., Henriquez, N. V., Linehan, J. M., Mirzadeh, Z., O'Malley, C., Naumann, H., Alvarez-Buylla, A., & Brandner, S. (2010). Combinations of genetic mutations in the adult neural stem cell compartment determine brain tumour phenotypes. *EMBO Journal*, *29*(1), 222–235. https://doi.org/10.1038/emboj.2009.327

Jiang, M. H., Cai, B., Tuo, Y., Wang, J., Zang, Z. J., Tu, X., Gao, Y., Su, Z., Li, W., Li, G., Zhang, M., Jiao, J., Wan, Z., Deng, C., Lahn, B. T., & Xiang, A. P. (2014). Characterization of Nestin-positive stem Leydig cells as a potential source for the treatment of testicular Leydig cell dysfunction. *Cell Research*, *24*(12), 1466–1485. https://doi.org/10.1038/cr.2014.149

Johannessen, T.-C. A., Mukherjee, J., Viswanath, P., Ohba, S., Ronen, S. M., Bjerkvig, R., Pieper, R. O., Kristian, T., Brain, G. J., & Ucsf, H. (2016). *Rapid Conversion of Mutant IDH1 from Driver to Passenger in a Model of Human*. https://doi.org/10.1158/1541-7786.MCR-16-0141

Kachinsky, A. M., Dominov, J. A., & Boom Miller', J. (1995). *The J o d of Histochcmisuy and CytochemiSUy Brief Report Intermediate Filaments in Cardiac Myogenesis: Nestin in the Developing Mouse Heart'* (Vol. 43, Issue 8).

Kang, S. M., Lee, J. H., Huh, Y. S., & Takayama, S. (2021). Alginate Microencapsulation for Three-Dimensional in Vitro Cell Culture. In *ACS Biomaterials Science and Engineering* (Vol. 7, Issue 7, pp. 2864–2879). American Chemical Society. https://doi.org/10.1021/acsbiomaterials.0c00457

Kanwore, K., Guo, X. xiao, Abdulrahman, A. A., Kambey, P. A., Nadeem, I., & Gao, D. (2021). SOX1 Is a Backup Gene for Brain Neurons and Glioma Stem Cell Protection and Proliferation. In *Molecular Neurobiology* (Vol. 58, Issue 6, pp. 2634–2642). Springer. https://doi.org/10.1007/s12035-020-02240-6

Kapałczyńska, M., Kolenda, T., Przybyła, W., Zajączkowska, M., Teresiak, A., Filas, V., Ibbs, M., Bliźniak, R., Łuczewski, Ł., & Lamperska, K. (2018). 2D and 3D cell cultures – a comparison of different types of cancer cell cultures. *Archives of Medical Science*, *14*(4), 910–919. https://doi.org/10.5114/aoms.2016.63743

Khurana, L., ElGindi, M., Tilstam, P. V., & Pantouris, G. (2019). Elucidating the role of an immunomodulatory protein in cancer: From protein expression to functional characterization. In *Methods in Enzymology* (Vol. 629, pp. 307–360). Academic Press Inc. https://doi.org/10.1016/bs.mie.2019.05.053

Khurshed, M. (2017). *In silico gene expression analysis reveals glycolysis and acetate anaplerosis in IDH1 wild-type glioma and lactate and glutamate anaplerosis in IDH1-mutated glioma*. https://doi.org/https://doi.org/10.18632/oncotarget.17106

Kim, D., Paggi, J. M., Park, C., Bennett, C., & Salzberg, S. L. (2019). Graph-based genome alignment and genotyping with HISAT2 and HISAT-genotype. *Nature Biotechnology*, *37*(8), 907–915. https://doi.org/10.1038/s41587-019-0201-4

Kloosterhof, N. K., French, P. J., Van Den Bent, M. J., Van Den Bent, M. J., Kloosterhof, N. K., Bralten, L. B. C., Dubbink, H. J., & French, P. J. (2011). Isocitrate dehydrogenase-1

mutations: a fundamentally new understanding of diff use glioma? *Lancet Oncology*, *12*, 83–91. https://doi.org/10.1016/S1470

Kohli, R. M., & Zhang, Y. (2013). TET enzymes, TDG and the dynamics of DNA demethylation. In *Nature* (Vol. 502, Issue 7472, pp. 472–479). https://doi.org/10.1038/nature12750

Krell, D., Mulholland, P., Frampton, A. E., Krell, J., Stebbing, J., & Bardella, C. (2013). IDH mutations in tumorigenesis and their potential role as novel therapeutic targets. In *Future oncology (London, England)* (Vol. 9, Issue 12, pp. 1923–1935). https://doi.org/10.2217/fon.13.143

Krupkova, O., Loja, T., Zambo, I., & Veselska, R. (2010). Nestin expression in human tumors and tumor cell lines. In *Neoplasma* (Vol. 57, Issue 4, pp. 291–298). SAP - Slovak Academic Press, spol. s.r.o. https://doi.org/10.4149/neo_2010_04_291

Lah, T. T., Novak, M., & Breznik, B. (2020). Brain malignancies: Glioblastoma and brain metastases. In *Seminars in Cancer Biology* (Vol. 60, pp. 262–273). Academic Press. https://doi.org/10.1016/j.semcancer.2019.10.010

Lai, A., Kharbanda, S., Pope, W. B., Tran, A., Solis, O. E., Peale, F., Forrest, W. F., Pujara, K., Carrillo, J. A., Pandita, A., Ellingson, B. M., Bowers, C. W., Soriano, R. H., Schmidt, N. O., Mohan, S., Yong, W. H., Seshagiri, S., Modrusan, Z., Jiang, Z., … Phillips, H. S. (2011). Evidence for sequenced molecular evolution of IDH1 mutant glioblastoma from a distinct cell of origin. *Journal of Clinical Oncology*, *29*(34), 4482–4490. https://doi.org/10.1200/JCO.2010.33.8715

Lauko, A., Lo, A., Ahluwalia, M. S., & Lathia, J. D. (2022). Cancer cell heterogeneity & plasticity in glioblastoma and brain tumors. In *Seminars in Cancer Biology* (Vol. 82, pp. 162–175). Academic Press. https://doi.org/10.1016/j.semcancer.2021.02.014

Le, A., Cooper, C. R., Gouw, A. M., Dinavahi, R., Maitra, A., Deck, L. M., Royer, R. E., Vander Jagt, D. L., Semenza, G. L., & Dang, C. V. (2010). Inhibition of lactate dehydrogenase A induces oxidative stress and inhibits tumor progression. *Proceedings of the National Academy of Sciences of the United States of America*, *107*(5), 2037–2042. https://doi.org/10.1073/pnas.0914433107

Lendahl, U., Zimmerman, L. B., & Mckay', R. D. G. (1990). *CNS Stem Cells Express a New Class of Intermediate Filament Protein* (Vol. 60).

Li, L., Davidovich, A. E., Schloss, J. M., Chippada, U., Schloss, R. R., Langrana, N. A., & Yarmush, M. L. (2011). Neural lineage differentiation of embryonic stem cells within alginate microbeads. *Biomaterials*, *32*(20), 4489–4497. https://doi.org/10.1016/j.biomaterials.2011.03.019

Li, M., Zou, Y., Lu, Q., Tang, N., Heng, A., Islam, I., Tong, H. J., Dawe, G. S., & Cao, T. (2016). Efficient derivation of dopaminergic neurons from SOX1- floor plate cells under defined culture conditions. *Journal of Biomedical Science*, *23*(1). https://doi.org/10.1186/s12929-016-0251-6

Liao, Y., Smyth, G. K., & Shi, W. (2019). The R package Rsubread is easier, faster, cheaper and better for alignment and quantification of RNA sequencing reads. *Nucleic Acids Research*, *47*(8). https://doi.org/10.1093/nar/gkz114

Lim, D. A., Cha, S., Mayo, M. C., Chen, M. H., Keles, E., Vandenberg, S., & Berger, M. S. (2007). Relationship of glioblastoma multiforme to neural stem cell regions predicts invasive and multifocal tumor phenotype. *Neuro-Oncology*, *9*(4), 424–429. https://doi.org/10.1215/15228517-2007-023

Liu, Y., Lu, Y., Celiku, O., Li, A., Wu, Q., Zhou, Y., & Yang, C. (2019). Targeting IDH1-mutated malignancies with NRF2 blockade. *Journal of the National Cancer Institute*, *111*(10), 1033–1041. https://doi.org/10.1093/jnci/djy230

Livak, K. J., & Schmittgen, T. D. (2001). Analysis of relative gene expression data using real-time quantitative PCR and the 2-ΔΔCT method. *Methods*, *25*(4), 402–408. https://doi.org/10.1006/meth.2001.1262

Louis, D. N., Ohgaki, H., Wiestler, O. D., Cavenee, W. K., Burger, P. C., Jouvet, A., Scheithauer, B. W., & Kleihues, P. (2007). The 2007 WHO classification of tumours of the central nervous system. *Acta Neuropathologica*, *114*(2), 97–109. https://doi.org/10.1007/s00401-007-0243-4

Louis, D. N., Perry, A., Reifenberger, G., von Deimling, A., Figarella-Branger, D., Cavenee, W. K., Ohgaki, H., Wiestler, O. D., Kleihues, P., & Ellison, D. W. (2016). The 2016 World Health Organization Classification of Tumors of the Central Nervous System: a summary. In *Acta Neuropathologica* (Vol. 131, Issue 6, pp. 803–820). Springer Verlag. https://doi.org/10.1007/s00401-016-1545-1

Louis, D. N., Perry, A., Wesseling, P., Brat, D. J., Cree, I. A., Figarella-Branger, D., Hawkins, C., Ng, H. K., Pfister, S. M., Reifenberger, G., Soffietti, R., Von Deimling, A., & Ellison,

D. W. (2021). The 2021 WHO classification of tumors of the central nervous system: A summary. *Neuro-Oncology*, *23*(8), 1231–1251. https://doi.org/10.1093/neuonc/noab106

Lu, C., Ward, P. S., Kapoor, G. S., Rohle, D., Turcan, S., Abdel-Wahab, O., Edwards, C. R., Khanin, R., Figueroa, M. E., Melnick, A., Wellen, K. E., Oĝrourke, D. M., Berger, S. L., Chan, T. A., Levine, R. L., Mellinghoff, I. K., & Thompson, C. B. (2012). IDH mutation impairs histone demethylation and results in a block to cell differentiation. *Nature*, *483*(7390), 474–478. https://doi.org/10.1038/nature10860

Machida-Sano, I., Hirakawa, M., Matsumoto, H., Kamada, M., Ogawa, S., Satoh, N., & Namiki, H. (2014). Surface characteristics determining the cell compatibility of ionically cross-linked alginate gels. *Biomedical Materials (Bristol)*, *9*(2). https://doi.org/10.1088/1748-6041/9/2/025007

Madala, H. R., Punganuru, S. R., Arutla, V., Misra, S., Thomas, T. J., & Srivenugopal, K. S. (2018). Beyond brooding on oncometabolic havoc in IDH-mutant gliomas and AML: Current and future therapeutic strategies. In *Cancers* (Vol. 10, Issue 2). MDPI AG. https://doi.org/10.3390/cancers10020049

Malumbres, M., & Barbacid, M. (2009). Cell cycle, CDKs and cancer: A changing paradigm. In *Nature Reviews Cancer* (Vol. 9, Issue 3, pp. 153–166). https://doi.org/10.1038/nrc2602

Matsuda, Y., Hagio, M., & Ishiwata, T. (2013). Nestin: A novel angiogenesis marker and possible target for tumor angiogenesis. In *World Journal of Gastroenterology* (Vol. 19, Issue 1, pp. 42–48). Baishideng Publishing Group Co. https://doi.org/10.3748/wjg.v19.i1.42

Maus, A., & Peters, G. J. (2017). Glutamate and α-ketoglutarate: key players in glioma metabolism. In *Amino Acids* (Vol. 49, Issue 1, pp. 21–32). Springer-Verlag Wien. https://doi.org/10.1007/s00726-016-2342-9

McNamara, C., Mankad, K., Thust, S., Dixon, L., Limback-Stanic, C., D'Arco, F., Jacques, T. S., & Löbel, U. (2022). 2021 WHO classification of tumours of the central nervous system: a review for the neuroradiologist. In *Neuroradiology* (Vol. 64, Issue 10, pp. 1919–1950). Springer Science and Business Media Deutschland GmbH. https://doi.org/10.1007/s00234-022-03008-6

Meissner, A. (2010). Epigenetic modifications in pluripotent and differentiated cells. *Nature Biotechnology*, *28*, 1079–1088.

Metellus, P., Colin, C., Taieb, D., Guedj, E., Nanni-Metellus, I., De Paula, A. M., Colavolpe, C., Fuentes, S., Dufour, H., Barrie, M., Chinot, O., Ouafik, L., & Figarella-Branger, D. (2011). IDH mutation status impact on in vivo hypoxia biomarkers expression: New insights from a clinical, nuclear imaging and immunohistochemical study in 33 glioma patients. *Journal of Neuro-Oncology*, *105*(3), 591–600. https://doi.org/10.1007/s11060-011-0625-2

Mich, J. K., Signer, R. A. J., Nakada, D., Pineda, A., Burgess, R. J., Vue, T. Y., Johnson, J. E., & Morrison, S. J. (2014). Prospective identification of functionally distinct stem cells and neurosphere-initiating cells in adult mouse forebrain. *ELife*, *2014*(3). https://doi.org/10.7554/eLife.02669

Miller, J. J., Gonzalez Castro, L. N., McBrayer, S., Weller, M., Cloughesy, T., Portnow, J., Andronesi, O., Barnholtz-Sloan, J. S., Baumert, B. G., Berger, M. S., Bi, W. L., Bindra, R., Cahill, D. P., Chang, S. M., Costello, J. F., Horbinski, C., Huang, R. Y., Jenkins, R. B., Ligon, K. L., … Wen, P. Y. (2023). Isocitrate dehydrogenase (IDH) mutant gliomas: A Society for Neuro-Oncology (SNO) consensus review on diagnosis, management, and future directions. *Neuro-Oncology*, *25*(1), 4–25. https://doi.org/10.1093/neuonc/noac207

Miyagi, S., Kato, H., & Okuda, A. (2009). Role of SoxB1 transcription factors in development. In *Cellular and Molecular Life Sciences* (Vol. 66, Issue 23, pp. 3675–3684). https://doi.org/10.1007/s00018-009-0097-0

Mohiuddin, I. S., Wei, S. J., & Kang, M. H. (2020). Role of OCT4 in cancer stem-like cells and chemotherapy resistance. In *Biochimica et Biophysica Acta - Molecular Basis of Disease* (Vol. 1866, Issue 4). Elsevier B.V. https://doi.org/10.1016/j.bbadis.2019.03.005

Morris, E. R., Rees, D. A., & Thom, D. (1980). CHARACTERISATION OF ALGINATE COMPOSITION AND BLOCK-STRUCTURE BY CIRCULAR DICHROISM. In *Curb&&ate Researrh* (Vol. 81).

Morshead, C. M., Reynolds, B. A., Craig, C. C., Mcburney, M. W., Staines, W. A., Morassutti, D., Weiss, S., & Van Der Kooy, D. (1071). Neural Stem Cells in the Adult Mammalian Forebrain: A Relatively Quiescent Subpopulation of Subependymal Cells. In *Neuron* (Vol. 13).

Nayak, D. R., Padhy, N., Mallick, P. K., Bagal, D. K., & Kumar, S. (2022). Brain Tumour Classification Using Noble Deep Learning Approach with Parametric Optimization

through Metaheuristics Approaches. *Computers*, *11*(1). https://doi.org/10.3390/computers11010010

Nayak, D. R., Padhy, N., Mallick, P. K., Zymbler, M., & Kumar, S. (2022). Brain Tumor Classification Using Dense Efficient-Net. *Axioms*, *11*(1). https://doi.org/10.3390/axioms11010034

Noushmehr, H., Weisenberger, D. J., Diefes, K., Phillips, H. S., Pujara, K., Berman, B. P., Pan, F., Pelloski, C. E., Sulman, E. P., Bhat, K. P., Verhaak, R. G. W., Hoadley, K. A., Hayes, D. N., Perou, C. M., Schmidt, H. K., Ding, L., Wilson, R. K., Van Den Berg, D., Shen, H., … Aldape, K. (2010). Identification of a CpG Island Methylator Phenotype that Defines a Distinct Subgroup of Glioma. *Cancer Cell*, *17*(5), 510–522. https://doi.org/10.1016/j.ccr.2010.03.017

Ohba, S., Yokoyama, J., Kojima, M., Fujimaki, M., Anzai, T., Komatsu, H., & Ikeda, K. (2016). Significant preservation of swallowing function in chemoradiotherapy for advanced head and neck cancer by prophylactic swallowing exercise. *Head and Neck*, *38*(4), 517–521. https://doi.org/10.1002/hed.23913

Ostrom, Q. T., Cioffi, G., Gittleman, H., Patil, N., Waite, K., Kruchko, C., & Barnholtz-Sloan, J. S. (2019). CBTRUS Statistical Report: Primary Brain and Other Central Nervous System Tumors Diagnosed in the United States in 2012-2016. In *Neuro-Oncology* (Vol. 21, pp. V1–V100). Oxford University Press. https://doi.org/10.1093/neuonc/noz150

Ostrom, Q. T., Gittleman, H., Truitt, G., Boscia, A., Kruchko, C., & Barnholtz-Sloan, J. S. (2018). CBTRUS statistical report: Primary brain and other central nervous system tumors diagnosed in the United States in 2011-2015. In *Neuro-Oncology* (Vol. 20, pp. iv1–iv86). Oxford University Press. https://doi.org/10.1093/neuonc/noy131

Park, P. J. (2009). ChIP-seq: Advantages and challenges of a maturing technology. In *Nature Reviews Genetics* (Vol. 10, Issue 10, pp. 669–680). https://doi.org/10.1038/nrg2641

Parsons, D. W., Jones, S., Zhang, X., Lin, J. C. H., Leary, R. J., Angenendt, P., Mankoo, P., Carter, H., Siu, I. M., Gallia, G. L., Olivi, A., McLendon, R., Rasheed, B. A., Keir, S., Nikolskaya, T., Nikolsky, Y., Busam, D. A., Tekleab, H., Diaz, L. A., … Kinzler, K. W. (2008). An integrated genomic analysis of human glioblastoma multiforme. *Science*, *321*(5897), 1807–1812. https://doi.org/10.1126/science.1164382

Picard-Riera, N., Nait-Oumesmar, B., & Baron-Van Evercooren, A. (2004). Endogenous Adult Neural Stem Cells: Limits and Potential to Repair the Injured Central Nervous System. *Journal of Neuroscience Research*, *76*(2), 223–231. https://doi.org/10.1002/jnr.20040

Polívka, J., Pešta, M., Pitule, P., Hes, O., Holubec, L., Kubíková, T., & Tonar, Z. (n.d.). *IDH1 mutation is associated with lower expression of VEGF but not microvessel formation in glioblastoma multiforme*. www.oncotarget.com

Putiri, E. L., & Robertson, K. D. (2011). Epigenetic mechanisms and genome stability. In *Clinical Epigenetics* (Vol. 2, Issue 2, pp. 299–314). https://doi.org/10.1007/s13148-010-0017-z

Ravi, M., Paramesh, V., Kaviya, S. R., Anuradha, E., & Paul Solomon, F. D. (2015). 3D cell culture systems: Advantages and applications. *Journal of Cellular Physiology*, *230*(1), 16–26. https://doi.org/10.1002/jcp.24683

Raya, Á., Rodríguez-Piz, I., Guenechea, G., Vassena, R., Navarro, S., Barrero, M. J., Consiglio, A., Castell, M., Río, P., Sleep, E., González, F., Tiscornia, G., Garreta, E., Aasen, T., Veiga, A., Verma, I. M., Surrallés, J., Bueren, J., & Belmonte, J. C. I. (2009). Disease-corrected haematopoietic progenitors from Fanconi anaemia induced pluripotent stem cells. In *Nature* (Vol. 460, Issue 7251, pp. 53–59). https://doi.org/10.1038/nature08129

Reddy, A. V. N., Krishna, C. P., Mallick, P. K., Satapathy, S. K., Tiwari, P., Zymbler, M., & Kumar, S. (2020). Analyzing MRI scans to detect glioblastoma tumor using hybrid deep belief networks. *Journal of Big Data*, *7*(1). https://doi.org/10.1186/s40537-020-00311-y

Reifenberger, G., Wirsching, H. G., Knobbe-Thomsen, C. B., & Weller, M. (2017). Advances in the molecular genetics of gliomas-implications for classification and therapy. In *Nature Reviews Clinical Oncology* (Vol. 14, Issue 7, pp. 434–452). Nature Publishing Group. https://doi.org/10.1038/nrclinonc.2016.204

Reig-Vano, B., Tylkowski, B., Montané, X., & Giamberini, M. (2021). Alginate-based hydrogels for cancer therapy and research. In *International Journal of Biological Macromolecules* (Vol. 170, pp. 424–436). Elsevier B.V. https://doi.org/10.1016/j.ijbiomac.2020.12.161

Reitman, Z. J., Jin, G., Karoly, E. D., Spasojevic, I., Yang, J., Kinzler, K. W., He, Y., Bigner, D. D., Vogelstein, B., & Yan, H. (2011). Profiling the effects of isocitrate dehydrogenase 1 and 2 mutations on the cellular metabolome. *Proceedings of the National Academy of*

Sciences of the United States of America, *108*(8), 3270–3275. https://doi.org/10.1073/pnas.1019393108

Reitman, Z. J., & Yan, H. (2010). Isocitrate dehydrogenase 1 and 2 mutations in cancer: Alterations at a crossroads of cellular metabolism. In *Journal of the National Cancer Institute* (Vol. 102, Issue 13, pp. 932–941). https://doi.org/10.1093/jnci/djq187

Retis-Resendiz, A. M., González-García, I. N., León-Juárez, M., Camacho-Arroyo, I., Cerbón, M., & Vázquez-Martínez, E. R. (2021). The role of epigenetic mechanisms in the regulation of gene expression in the cyclical endometrium. In *Clinical Epigenetics* (Vol. 13, Issue 1). BioMed Central Ltd. https://doi.org/10.1186/s13148-021-01103-8

Reuss, D. E. (2023). Updates on the WHO diagnosis of IDH-mutant glioma. In *Journal of Neuro-Oncology* (Vol. 162, Issue 3, pp. 461–469). Springer. https://doi.org/10.1007/s11060-023-04250-5

Reuss, D. E., Sahm, F., Schrimpf, D., Wiestler, B., Capper, D., Koelsche, C., Schweizer, L., Korshunov, A., Jones, D. T. W., Hovestadt, V., Mittelbronn, M., Schittenhelm, J., Herold-Mende, C., Unterberg, A., Platten, M., Weller, M., Wick, W., Pfister, S. M., & von Deimling, A. (2015). ATRX and IDH1-R132H immunohistochemistry with subsequent copy number analysis and IDH sequencing as a basis for an "integrated" diagnostic approach for adult astrocytoma, oligodendroglioma and glioblastoma. *Acta Neuropathologica*, *129*(1), 133–146. https://doi.org/10.1007/s00401-014-1370-3

reynolds1992-2. (n.d.).

Robinson, M. D., McCarthy, D. J., & Smyth, G. K. (2009). edgeR: A Bioconductor package for differential expression analysis of digital gene expression data. *Bioinformatics*, *26*(1), 139–140. https://doi.org/10.1093/bioinformatics/btp616

Rousseau, A., Mokhtari, K., & Duyckaerts, C. (2008). The 2007 WHO classification of tumors of the central nervous system - What has changed? In *Current Opinion in Neurology* (Vol. 21, Issue 6, pp. 720–727). https://doi.org/10.1097/WCO.0b013e328312c3a7

Sachdeva, R., Wu, M., Smiljanic, S., Kaskun, O., Ghannad-Zadeh, K., Celebre, A., Isaev, K., Morrissy, A. S., Guan, J., Tong, J., Chan, J., Wilson, T. M., Al-Omaishi, S., Munoz, D. G., Dirks, P. B., Moran, M. F., Taylor, M. D., Reimand, J., & Das, S. (2019a). ID1 is critical for tumorigenesis and regulates chemoresistance in glioblastoma. *Cancer Research*, *79*(16), 4057–4071. https://doi.org/10.1158/0008-5472.CAN-18-1357

Sachdeva, R., Wu, M., Smiljanic, S., Kaskun, O., Ghannad-Zadeh, K., Celebre, A., Isaev, K., Morrissy, A. S., Guan, J., Tong, J., Chan, J., Wilson, T. M., Al-Omaishi, S., Munoz, D. G., Dirks, P. B., Moran, M. F., Taylor, M. D., Reimand, J., & Das, S. (2019b). ID1 is critical for tumorigenesis and regulates chemoresistance in glioblastoma. *Cancer Research*, *79*(16), 4057–4071. https://doi.org/10.1158/0008-5472.CAN-18-1357

Saha, K., Keung, A. J., Irwin, E. F., Li, Y., Little, L., Schaffer, D. V., & Healy, K. E. (2008). Substrate modulus directs neural stem cell behavior. *Biophysical Journal*, *95*(9), 4426–4438. https://doi.org/10.1529/biophysj.108.132217

Sansom, S. N., Griffiths, D. S., Faedo, A., Kleinjan, D. J., Ruan, Y., Smith, J., Van Heyningen, V., Rubenstein, J. L., & Livesey, F. J. (2009). The level of the transcription factor Pax6 is essential for controlling the balance between neural stem cell self-renewal and neurogenesis. *PLoS Genetics*, *5*(6). https://doi.org/10.1371/journal.pgen.1000511

Sasaki, M., Knobbe, C. B., Itsumi, M., Elia, A. J., Harris, I. S., Chio, I. I. C., Cairns, R. A., Mccracken, S., Wakeham, A., Haight, J., Ten, A. Y., Snow, B., Ueda, T., Inoue, S., Yamamoto, K., Ko, M., Rao, A., Yen, K. E., Su, S. M., & Mak, T. W. (2012). D-2-hydroxyglutarate produced by mutant Idh1 perturbs collagen maturation and basement membrane function. *Genes and Development*, *26*(18), 2038–2049. https://doi.org/10.1101/gad.198200.112

Seetha, J., & Raja, S. S. (2018). Brain tumor classification using Convolutional Neural Networks. *Biomedical and Pharmacology Journal*, *11*(3), 1457–1461. https://doi.org/10.13005/bpj/1511

Seltzer, M. J., Bennett, B. D., Joshi, A. D., Gao, P., Thomas, A. G., Ferraris, D. V., Tsukamoto, T., Rojas, C. J., Slusher, B. S., Rabinowitz, J. D., Dang, C. V., & Riggins, G. J. (2010). Inhibition of glutaminase preferentially slows growth of glioma cells with mutant IDH1. *Cancer Research*, *70*(22), 8981–8987. https://doi.org/10.1158/0008-5472.CAN-10-1666

Smidsr, O., & Skj, G. (1990). Alginate as immobilization matrix for cells. In *Ind. Eng. Chem. Process Des. Dev* (Vol. 8).

Solomou, G., Finch, A., Asghar, A., & Bardella, C. (2023). Mutant IDH in Gliomas: Role in Cancer and Treatment Options. *Cancers*, *15*(11). https://doi.org/10.3390/cancers15112883

Sonoda, Y., Ozawa, T., Hirose, Y., Aldape, K. D., Mcmahon, M., Berger, M. S., & Pieper, R. O. (2001). Formation of Intracranial Tumors by Genetically Modified Human Astrocytes Defines Four Pathways Critical in the Development of Human Anaplastic Astrocytoma 1.

In *CANCER RESEARCH* (Vol. 61). http://aacrjournals.org/cancerres/article-pdf/61/13/4956/2485597/4956.pdf

Soroceanu, L., Murase, R., Limbad, C., Singer, E., Allison, J., Adrados, I., Kawamura, R., Pakdel, A., Fukuyo, Y., Nguyen, D., Khan, S., Arauz, R., Yount, G. L., Moore, D. H., Desprez, P. Y., & McAllister, S. D. (2013). Id-1 is a key transcriptional regulator of glioblastoma aggressiveness and a novel therapeutic target. *Cancer Research*, *73*(5), 1559–1569. https://doi.org/10.1158/0008-5472.CAN-12-1943

Sperger, D. M., Fu, S., Block, L. H., & Munson, E. J. (2011). Analysis of composition, molecular weight, and water content variations in sodium alginate using solid-state NMR spectroscopy. *Journal of Pharmaceutical Sciences*, *100*(8), 3441–3452. https://doi.org/10.1002/jps.22559

Steed, T. C., Treiber, J. M., Patel, K., Ramakrishnan, V., Merk, A., Smith, A. R., Carter, B. S., Dale, A. M., Chow, L. M. L., & Chen, C. C. (n.d.). Differential localization of glioblastoma subtype: implications on glioblastoma pathogenesis. In *Oncotarget* (Vol. 7, Issue 18). www.impactjournals.com/oncotarget/

Sun, X., & Turcan, S. (2021). From laboratory studies to clinical trials: Temozolomide use in idh-mutant gliomas. In *Cells* (Vol. 10, Issue 5). MDPI. https://doi.org/10.3390/cells10051225

Sun, Z.-L., Chan, A. K.-Y., Chen, L.-C., Tang, C., & Zhang, Z.-Y. (2015). TERT promoter mutated WHO grades II and III gliomas are located preferentially in the frontal lobe and avoid the midline. *International Journal of Clinical and Experimental Pathology*, 11485–11494.

Sung, H., Ferlay, J., Siegel, R. L., Laversanne, M., Soerjomataram, I., Jemal, A., & Bray, F. (2021). Global Cancer Statistics 2020: GLOBOCAN Estimates of Incidence and Mortality Worldwide for 36 Cancers in 185 Countries. *CA: A Cancer Journal for Clinicians*, *71*(3), 209–249. https://doi.org/10.3322/caac.21660

Suzuki, H., Aoki, K., Chiba, K., Sato, Y., Shiozawa, Y., Shiraishi, Y., Shimamura, T., Niida, A., Motomura, K., Ohka, F., Yamamoto, T., Tanahashi, K., Ranjit, M., Wakabayashi, T., Yoshizato, T., Kataoka, K., Yoshida, K., Nagata, Y., Sato-Otsubo, A., … Ogawa, S. (2015). Mutational landscape and clonal architecture in grade II and III gliomas. *Nature Genetics*, *47*(5), 458–468. https://doi.org/10.1038/ng.3273

Turcan, S., Makarov, V., Taranda, J., Wang, Y., Fabius, A. W. M., Wu, W., Zheng, Y., El-Amine, N., Haddock, S., Nanjangud, G., Lekaye, H. C., Brennan, C., Cross, J., Huse, J. T., Kelleher, N. L., Osten, P., Thompson, C. B., & Chan, T. A. (2018a). Mutant-IDH1-dependent chromatin state reprogramming, reversibility, and persistence. *Nature Genetics*, *50*(1), 62–72. https://doi.org/10.1038/s41588-017-0001-z

Turcan, S., Makarov, V., Taranda, J., Wang, Y., Fabius, A. W. M., Wu, W., Zheng, Y., El-Amine, N., Haddock, S., Nanjangud, G., Lekaye, H. C., Brennan, C., Cross, J., Huse, J. T., Kelleher, N. L., Osten, P., Thompson, C. B., & Chan, T. A. (2018b). Mutant-IDH1-dependent chromatin state reprogramming, reversibility, and persistence. *Nature Genetics*, *50*(1), 62–72. https://doi.org/10.1038/s41588-017-0001-z

Turcan, S., Rohle, D., Goenka, A., Walsh, L. A., Fang, F., Yilmaz, E., Campos, C., Fabius, A. W. M., Lu, C., Ward, P. S., Thompson, C. B., Kaufman, A., Guryanova, O., Levine, R., Heguy, A., Viale, A., Morris, L. G. T., Huse, J. T., Mellinghoff, I. K., & Chan, T. A. (2012). IDH1 mutation is sufficient to establish the glioma hypermethylator phenotype. *Nature*, *483*(7390), 479–483. https://doi.org/10.1038/nature10866

Uhrbom, L., Dai, C., Celestino, J. C., Rosenblum, M. K., Fuller, G. N., & Holland, E. C. (2002). Ink4a-Arf Loss Cooperates with KRas Activation in Astrocytes and Neural Progenitors to Generate Glioblastomas of Various Morphologies Depending on Activated Akt 1. In *CANCER RESEARCH* (Vol. 62). http://aacrjournals.org/cancerres/article-pdf/62/19/5551/2497185/ch1902005551.pdf

Unruh, D., Zewde, M., Buss, A., Drumm, M. R., Tran, A. N., Scholtens, D. M., & Horbinski, C. (2019). Methylation and transcription patterns are distinct in IDH mutant gliomas compared to other IDH mutant cancers. *Scientific Reports*, *9*(1). https://doi.org/10.1038/s41598-019-45346-1

Visvader, J. E. (2011). Cells of origin in cancer. In *Nature* (Vol. 469, Issue 7330, pp. 314–322). https://doi.org/10.1038/nature09781

Waitkus, M. S., Pirozzi, C. J., Moure, C. J., Diplas, B. H., Hansen, L. J., Carpenter, A. B., Yang, R., Wang, Z., Ingram, B. O., Karoly, E. D., Mohney, R. P., Spasojevic, I., McLendon, R. E., Friedman, H. S., He, Y., Bigner, D. D., & Yan, H. (2018). Adaptive evolution of the GDH2 allosteric domain promotes gliomagenesis by resolving IDH1R132H-induced metabolic liabilities. *Cancer Research*, *78*(1), 36–50. https://doi.org/10.1158/0008-5472.CAN-17-1352

Wang, N., Adams, G., Buttery, L., Falcone, F. H., & Stolnik, S. (2009). Alginate encapsulation technology supports embryonic stem cells differentiation into insulin-producing cells. *Journal of Biotechnology*, *144*(4), 304–312. https://doi.org/10.1016/j.jbiotec.2009.08.008

Wang, T., Baron, M., & Trump, D. (2008). *An overview of Notch3 function in vascular smooth muscle cells*. *96*, 499–509. https://doi.org/10.1016/j.pbiomolbio.2007.07.006

Ward, P. S., Cross, J. R., Lu, C., Weigert, O., Abel-Wahab, O., Levine, R. L., Weinstock, D. M., Sharp, K. A., & Thompson, C. B. (2012). Identification of additional IDH mutations associated with oncometabolite R(-)-2-hydroxyglutarate production. *Oncogene*, *31*(19), 2491–2498. https://doi.org/10.1038/onc.2011.416

Ward, P. S., Patel, J., Wise, D. R., Abdel-Wahab, O., Bennett, B. D., Coller, H. A., Cross, J. R., Fantin, V. R., Hedvat, C. V., Perl, A. E., Rabinowitz, J. D., Carroll, M., Su, S. M., Sharp, K. A., Levine, R. L., & Thompson, C. B. (2010). The Common Feature of Leukemia-Associated IDH1 and IDH2 Mutations Is a Neomorphic Enzyme Activity Converting α-Ketoglutarate to 2-Hydroxyglutarate. *Cancer Cell*, *17*(3), 225–234. https://doi.org/10.1016/j.ccr.2010.01.020

Weina, K., & Utikal, J. (2014). SOX2 and cancer: current research and its implications in the clinic. *Clinical and Translational Medicine*, *3*(1). https://doi.org/10.1186/2001-1326-3-19

Weller, M., & Le Rhun, E. (2020). How did lomustine become standard of care in recurrent glioblastoma? In *Cancer Treatment Reviews* (Vol. 87). W.B. Saunders Ltd. https://doi.org/10.1016/j.ctrv.2020.102029

Whitfield, B. T., & Huse, J. T. (2022). Classification of adult-type diffuse gliomas: Impact of the World Health Organization 2021 update. In *Brain Pathology* (Vol. 32, Issue 4). John Wiley and Sons Inc. https://doi.org/10.1111/bpa.13062

Williams, S. C., Karajannis, M. A., Chiriboga, L., Golfinos, J. G., Von Deimling, A., & Zagzag, D. (2011). R132H-mutation of isocitrate dehydrogenase-1 is not sufficient for HIF-1α upregulation in adult glioma. *Acta Neuropathologica*, *121*(2), 279–281. https://doi.org/10.1007/s00401-010-0790-y

Xu, S., Tang, L., Li, X., Fan, F., & Liu, Z. (2020). Immunotherapy for glioma: Current management and future application. In *Cancer Letters* (Vol. 476, pp. 1–12). Elsevier Ireland Ltd. https://doi.org/10.1016/j.canlet.2020.02.002

Xu, W., Yang, H., Liu, Y., Yang, Y., Wang, P., Kim, S. H., Ito, S., Yang, C., Wang, P., Xiao, M. T., Liu, L. X., Jiang, W. Q., Liu, J., Zhang, J. Y., Wang, B., Frye, S., Zhang, Y., Xu, Y. H.,

Lei, Q. Y., … Xiong, Y. (2011a). Oncometabolite 2-hydroxyglutarate is a competitive inhibitor of α-ketoglutarate-dependent dioxygenases. *Cancer Cell*, *19*(1), 17–30. https://doi.org/10.1016/j.ccr.2010.12.014

Xu, W., Yang, H., Liu, Y., Yang, Y., Wang, P., Kim, S. H., Ito, S., Yang, C., Wang, P., Xiao, M. T., Liu, L. X., Jiang, W. Q., Liu, J., Zhang, J. Y., Wang, B., Frye, S., Zhang, Y., Xu, Y. H., Lei, Q. Y., … Xiong, Y. (2011b). Oncometabolite 2-hydroxyglutarate is a competitive inhibitor of α-ketoglutarate-dependent dioxygenases. *Cancer Cell*, *19*(1), 17–30. https://doi.org/10.1016/j.ccr.2010.12.014

Xu, W., Yang, H., Liu, Y., Yang, Y., Wang, P., Kim, S. H., Ito, S., Yang, C., Wang, P., Xiao, M. T., Liu, L. X., Jiang, W. Q., Liu, J., Zhang, J. Y., Wang, B., Frye, S., Zhang, Y., Xu, Y. H., Lei, Q. Y., … Xiong, Y. (2011c). Oncometabolite 2-hydroxyglutarate is a competitive inhibitor of α-ketoglutarate-dependent dioxygenases. *Cancer Cell*, *19*(1), 17–30. https://doi.org/10.1016/j.ccr.2010.12.014

Yamada, K. M., & Cukierman, E. (2007). Modeling Tissue Morphogenesis and Cancer in 3D. In *Cell* (Vol. 130, Issue 4, pp. 601–610). Elsevier B.V. https://doi.org/10.1016/j.cell.2007.08.006

Yan, H., Williams, D., Jin, G., Mclendon, R., Rasheed, B. A., Yuan, W., Kos, I., Batinic-Haberle, I., Jones, S., Riggins, G. J., Friedman, H., Friedman, A., Reardon, D., Herndon, J., Kinzler, K. W., Velculescu, V. E., Vogelstein, B., & Bigner, D. D. (2009). IDH1 and IDH2 Mutations in Gliomas A bs tr ac t. In *N Engl J Med* (Vol. 360).

Yang, K., Wu, Z., Zhang, H., Zhang, N., Wu, W., Wang, Z., Dai, Z., Zhang, X., Zhang, L., Peng, Y., Ye, W., Zeng, W., Liu, Z., & Cheng, Q. (2022). Glioma targeted therapy: insight into future of molecular approaches. In *Molecular Cancer* (Vol. 21, Issue 1). BioMed Central Ltd. https://doi.org/10.1186/s12943-022-01513-z

Yu, G., Wang, L. G., Han, Y., & He, Q. Y. (2012). ClusterProfiler: An R package for comparing biological themes among gene clusters. *OMICS A Journal of Integrative Biology*, *16*(5), 284–287. https://doi.org/10.1089/omi.2011.0118

Zhang, N., Zhang, L., Qiu, B., Meng, L., Wang, X., & Hou, B. L. (2012). Correlation of volume transfer coefficient Ktrans with histopathologic grades of gliomas. *Journal of Magnetic Resonance Imaging*, *36*(2), 355–363. https://doi.org/10.1002/jmri.23675

Zhang, S. (2014). Sox2, a key factor in the regulation of pluripotency and neural differentiation. *World Journal of Stem Cells*, *6*(3), 305. https://doi.org/10.4252/wjsc.v6.i3.305

Zhao, S. (2009). Glioma-derivedmutationsinIDH1 dominantly inhibit IDH1 catalytic activity and induce HIF-1alpha. *Journal of Biological Chemistry*, *324*, 261–265.

Zhao, Z., Bo, Z., Gong, W., & Guo, Y. (2020). Inhibitor of differentiation 1 (Id1) in cancer and cancer therapy. In *International Journal of Medical Sciences* (Vol. 17, Issue 8, pp. 995–1005). Ivyspring International Publisher. https://doi.org/10.7150/ijms.42805

Zimmerman, L., Lendahl, U., Cunningham, M., Mckay, R., Parr, B., Gavin, B., Mann&, J., Vassileva, C., & Mcmahonll#, A. (1994). Independent Regulatory Elements in the Nestin Gene Direct Transgene Expression to Neural Stem Cells or Muscle Precursors. In *Neuron* (Vol. 12).

8. ADDENDA

8.1.Ethics Committee Report

İZMİR BİYOTIP VE GENOM MERKEZİ
GİRİŞİMSEL OLMAYAN ARAŞTIRMALAR ETİK KURULU (İBG-GOEK)
KARARI

Toplantı Tarihi	: 27/11/2020	**Toplantı Günü**	: Cuma
Toplantı Sayısı	: 14	**Toplantı Saati**	: 10:30

Sayın Dr.Öğr.Üyesi Yavuz OKTAY,

2020-042 Protokol No'lu; sorumlusu olduğunuz "Gliom oluşumunun en erken aşamalarında IDH1 mutasyonlarının epigenomda yol açtığı değişimlerin karakterizasyonu" başlıklı araştırmanın uygulanmasında etik açıdan sakınca olmadığına oy birliği ile karar verilmiştir.

Bilgilerinizi ve gereğini rica ederiz.

Prof. Dr. H. Alper BAĞRIYANIK **Başkan** (Katılmadı)	**Prof. Dr. Hilmi ORHAN** **Başkan Yardımcısı** (Katılmadı)
Prof. Dr. Sedef AKGÜNGÖR **Üye**	**Prof. Dr. İnci ALACACIOĞLU** **Üye** (Katılmadı)
Prof. Dr. Gülgün OKTAY **Üye**	**Dr. Öğr. Üyesi Serhan DERİCİ** **Üye** (Katılmadı)
Dr. Serap ERKEK ÖZHAN **Üye**	**Avukat Şemra MARMARA** **Üye**
Doç. Dr. Canan Aslı YILDIRIM **Üye**	**Prof. Dr. İbrahim SEVİNÇ** **Üye** (Katılmadı)
Prof. Dr. Yeşim TUNÇOK **Üye**	

8.2.Curriculum Vitae

BURCU EKİNCİ GÖRGÜN

Personal Information

Contact Information

Contact Address

Telephone

Email

Web Page

Education Information

02 February 2018 - Now (5 Year 11 Month)
Doktora, Doktora, DOKUZ EYLÜL ÜNİVERSİTESİ, TÜRKİYE
İZMİR ULUSLARARASI BİYOTIP VE GENOM ENSTİTÜSÜ, MOLEKÜLER BİYOLOJİ VE GENETİK (DR) (İNGİLİZCE)
Diploma Number: -
Cumulative Grade Point Average: 3.5 / 4.0

03 September 2013 - 26 January 2016 (2 Year 5 Month)
Yüksek Lisans, Tezli Program, İZMİR YÜKSEK TEKNOLOJİ ENSTİTÜSÜ, TÜRKİYE
MÜHENDİSLİK VE FEN BİLİMLERİ ENSTİTÜSÜ, MOLEKÜLER BİYOLOJİ VE GENETİK (YL) (TEZLİ)
Diploma Number: LU1661
Cumulative Grade Point Average: 3.0 / 4.0

06 September 2007 - 18 July 2013 (5 Year 11 Month)
Lisans, Anadal/Normal Öğretim, İZMİR YÜKSEK TEKNOLOJİ ENSTİTÜSÜ, TÜRKİYE
FEN FAKÜLTESİ, MOLEKÜLER BİYOLOJİ VE GENETİK PR. (İNGİLİZCE)
Diploma Number: 2199
Cumulative Grade Point Average: 2.55 / 4.0

R&D Competency

Articles

B. T. OZTURK, F. OZEL, T. YARAS, B. EKİNCİ, Y. OKTAY, E. O. AYSEVENER, T. ALKİN & N. DİREK, The Relationship Between Cardiovascular Disease Risk and Major Depression, NOROPSIKIYATRI ARSIVI-ARCHIVES OF NEUROPSYCHIATRY, 2023, 1300-0667, 60, 2, 5.

S. H. KURUL, Y. OKTAY, A. TOPF, N. Z. SZABO, S. GUNGOR, A. YARAMİS, E. SONMEZLER, L. MATALONGA, U. YİS, K. SCHON, I. PARAMONOV, I. P. KALAFATCİLAR, F. GAO, A. RİEGER, N. ARSLAN, E. YİLMAZ, B. EKİNCİ, P. P. EDEM, M. ASLAN, B. OZGOR, A. LOCHMULLER, A. NAİR, E. O'HEİR, A. K. LOVGREN, R. MAROOFİAN, H. HOULDEN, K. POLAVARAPU, A. ROOS, J. S. MULLER, D. HATHAZİ, P. F. CHİNNERY, S. LAURİE, S. BELTRAN, H. LOCHMUELLER & R. HORVATH, High diagnostic rate of trio exome sequencing in consanguineous families with neurogenetic diseases, BRAIN, 2022, 0006-8950, 145, 4, 1507-1518.

M. TETİK, B. O. UZGAN, C. AYKAC, B. EKİNCİ, T. YARAS, A. KURUOGLU, O. AKGUL & T. ALKİN, Relation of ASC and IL-1beta with neurocog-nitive parameters in patients with Obsessive-Compulsive Disorder, KLINIK PSIKIYATRI DERGISI-TURKISH JOURNAL OF CLINICAL PSYCHIATRY, 2022, 1302-0099, 25, 1, 75-83.

K. OKAY, P. U. VARİS, S. MİRAL, B. EKİNCİ, T. YARAS, G. KARAKULAH & Y. OKTAY, Alternative splicing and gene co-expression network-based analysis of dizygotic twins with autism-spectrum disorder and their parents, GENOMICS, 2021, 0888-7543, 113, 4, 2561-2571.

S. GUNGOR, Y. OKTAY, S. HİZ, A. ARANGUREN-IBANEZ, I. KALAFATCİLAR, A. YARAMİS, E. KARACA, U. YİS, E. SONMEZLER, B. EKİNCİ, M. ASLAN, E. YİLMAZ, B. OZGOR, S. BALARAJU, N. SZABO, S. LAURİE, S. BELTRAN, D. G. MACARTHUR, D. HATHAZİ, A. TOPF, A. ROOS, H. LOCHMULLER, I. VERNOS & R. HORVATH, Autosomal recessive variants in TUBGCP2 alter the gamma-tubulin ring complex leading to neurodevelopmental disease, ISCIENCE, 2021, 2589-0042, 24, 1.

T. ZENGİN, B. EKİNCİ, C. KUCUKKOSE & O. YALCİN-OZUYSAL, IRF6 Is Involved in the Regulation of Cell Proliferation and Transformation in MCF10A Cells Downstream of Notch Signaling, PLOS ONE, 2015, 1932-6203, 10, 7.

Conference Papers

T. YARAŞ, B. EKİNCİ, E. DİLER & Y. OKTAY, Epigenomic and Transcriptomic analysis of the Intrinsic and Extrinsic Molecular Mechanism at the Earliest Stages of Gliomagenesis in Precancerous Cell Models, Poster Sunumu, European Human Genetics Conference, 11 June 2022, 14 June 2022.

B. EKİNCİ, T. YARAŞ & Y. OKTAY, Modelling the earliest stages of gliomagenesis using iNPCs in a three-dimensional alginate-based matrix, Poster Sunumu, European Human Genetics Conference, 11 June 2022, 14 June 2022.

B. EKİNCİ, T. YARAŞ, F. ÖZTOPRAK & Y. OKTAY, Gliomlara genetik yatkınlığın moleküler temellerinin hücre modellerinde genomik ve transkriptomik analizi, Sözlü Sunum, Onkolojide İz Bırakanlar Zirvesi, 14 November 2019, 17 November 2019, 26 - 27.

B. EKİNCİ, T. YARAŞ & Y. OKTAY, Functional Analysis of Glioma Associated SNP rs55705857 Located at 8q24.21, Poster Sunumu, 6th International Congress of the Molecular Biology Association of Turkey, 05 September 2018, 08 September 2018, 143 - 143.

B. EKİNCİ & Ö. YALÇIN ÖZUYSAL, Irf6 Is A Determinant In Notch Induced Cell Fate And P63 Downregulation In Normal Breast Epithelial Cells, Poster Sunumu, 3rd International Congress of the Molecular Biology Association of Turkey , 10 September 2014, 12 September 2014, 135 - 135.

TÜBİTAK Scholarships and Fundings

Project Info

20AG006, Hedefe Özgü Pan-Kanser Terapiler (PAN-TER), Burslu, Yürürlükte, KAMAG - Kamu Araştırmaları Destek Grubu, 1004 - Mükemmeliyet Merkezi Destek Programı, ARDEB, Project Participation/Leave Dates: 7/3/23 - Devam ediyor, Project Start/End Dates: 10/15/21 - 10/15/25.
120S404, Katanin-A Benzeri Protein 2 (Katanin-Like 2) KATNAL2 Geninde İlk Kez Görülen Bir Yanlış Anlam Mutasyonunun Etkilerinin Hasta Fibroblastları ve Bunlardan Türetilen Hücrelerde İşlevsel Analiz Yöntemleri ile İncelenmesi, BİDEB Burslusu, Sonuçlandı, SBAG - Sağlık Bilimleri Araştırma Destek Grubu, 1001 - Araştırma, ARDEB, Project Participation/Leave Dates: 9/12/22 - 7/3/23, Project Start/End Dates: 7/15/20 - 7/15/23.
118Z955, Tekrar Artışı ile Giden Nörogelişimsel Hastalıkların Tanı ve DNA Analizine Yönelik Crispr/Cas Aracılı Üçüncü Nesil DNA Dizileme Yöntemleri Geliştirilmesi, BİDEB Burslusu, Sonuçlandı, KBAG - Kimya Biyoloji Araştırma Destek Grubu, Uluslararası / COST, ARDEB, Project Participation/Leave Dates: 3/1/22 - 9/12/22, Project Start/End Dates: 9/15/19 - 9/15/22.
117Z981, Gliom Oluşumunda Rol Oynayan Kalıcı Epigenomik Değişimlerin IDH1-TERT-MYC Ekseninde Karakterizasyonu, Burslu, Yürürlükte, KBAG - Kimya Biyoloji Araştırma Destek Grubu, 1001 - Araştırma, ARDEB, Project Participation/Leave Dates: 7/10/18 - 2/28/22, Project Start/End Dates: 6/15/18 - 6/15/22.
113Z088, Notch Yolağının Epitelyal-Mezenkimal Geçişte ve Migrasyon/Invazyonu Tetiklemede Aracı Olarak Kullandığı Yeni Hedef Genlerinin Tanımlanması, Burslu, Sonuçlandı, KBAG - Kimya Biyoloji Araştırma Destek Grubu, 1001 - Araştırma, ARDEB, Project Participation/Leave Dates: 1/1/15 - 10/31/15, Project Start/End Dates: 6/15/14 - 6/15/17.
110T895, Irf6'Nın Notch Yolağının Hücre Bölünmesini Engelleyici Ya Da Uyarıcı Etkilerindeki Belirleyici Rolünün Araştırılması, Burslu, Sonuçlandı, KBAG - Kimya Biyoloji Araştırma Destek Grubu, 1001 - Araştırma, ARDEB, Project Participation/Leave Dates: 11/1/13 - Devam ediyor, Project Start/End Dates: 4/15/11 - 9/15/14.

BIDEB Supports

BURCU EKİNCİ GÖRGÜN, Etkinlik Destekleri ve Eğitim Bursları Müdürlüğü, 2250-Lisansüstü Bursları Performans Programı, Destek Sona Erdi, 2022 - 1.
BURCU EKİNCİ GÖRGÜN, Etkinlik Destekleri ve Eğitim Bursları Müdürlüğü, 2250-Lisansüstü Bursları Performans Programı, Destek Sona Erdi, 2023 - 1.
BURCU EKİNCİ GÖRGÜN, Etkinlik Destekleri ve Eğitim Bursları Müdürlüğü, 2250-Lisansüstü Bursları Performans Programı, Destekleniyor, 2023 - 2.
BURCU EKİNCİ GÖRGÜN, Etkinlik Destekleri ve Eğitim Bursları Müdürlüğü, 2211-A Genel Yurt İçi Doktora Burs Programı, Başvurusu Reddedildi, 2018 - 2, 6/1/18 - 5/31/22.
BURCU EKİNCİ GÖRGÜN, Etkinlik Destekleri ve Eğitim Bursları Müdürlüğü, 2211-A Genel Yurt İçi Doktora Burs Programı, Bursu Kesildi, 2019 - 2, 6/1/19 - 5/31/23.

Number of Panelist/Observer/Reporter Jobs

Refereeing/Panelist/Outer Consultant Count	ARDEB/BİDEB 0	TEYDEB 0	Total 0
Number of Observer/Consultant Jobs	ARDEB/BİDEB 0	TEYDEB 0	Total 0
Number of Reporter Jobs	ARDEB/BİDEB 0	TEYDEB 0	Total 0

8.3.Publication from the thesis

Ekinci, B., Yaraş T., Oktay Y. (2023). Modeling The Earliest Stages Of Gliomagenesis Using Human iPSC-derived NPCs In A Three-dimensional Alginate-based Matrix. *The anatolian journal of medicine*

Modeling The Earliest Stages Of Gliomagenesis Using Human iPSC-derived NPCs In A Three-dimensional Alginate-based Matrix

Üç Boyutlu Aljinat-Bazlı Bir Matriste İnsan iPSC'lerinden Türetilmiş NPC'leri Kullanarak Gliomagenezin En Erken Aşamalarının Modellenmesi

Burcu Ekinci[1], Tutku Yaraş[1,2], Yavuz Oktay[1,2,3]

[1]Dokuz Eylül University, Izmir International Biomedicine and Genome Institute, Izmir, Turkey

[2]Izmir Biomedicine and Genome Center, Izmir, Turkey

[3]Dokuz Eylül University, Faculty of Medicine, Department of Medical Biology, Izmir, Turkey

Abstract

Objective: The development of gliomas is believed to be triggered by isocitrate dehydrogenase (IDH1/2) mutations, but there is limited information on how IDH1/2 mutations trigger gliomagenesis. This is because studies over the years have often used patient humor samples or transformed cells or normal stem cells with driver mutations to explore the early stages of glioma development. Here, we constructed a model to understand the specific effects of IDH1-R132H mutation alone by preparing an alginate-based 3D culture with NPCs and hence sought to avoid the effects of other driver mutations.

Methods: Human induced Pluripotent Stem Cells (hiPSCs) were differentiated into Neural Progenitor Cells (NPCs). NPCs embedded in an alginate-based 3D matrix were incubated in Neural Progenitor Medium for 1 day (day 0). Then, Neural Progenitor Medium was removed from the NPC-alginate beads and incubated for 14 days with conditioned media from Immortalized Human Astrocytes (IHAs) that produced doxycycline-induced wild-type IDH1

and Mutant IDH1. On day 14, IHA-conditioned media were replaced with Neural Progenitor Medium and incubated for 3 days (day 17). RNA was isolated from NPCs at day 0 and 17, and key genes (Tet methylcytosine dioxygenase 1 *(TET1)* and Mesenchyme Homeobox 2 (*MEOX2)*), previously reported to be altered in IDH1-mutant gliomas, were evaluated by RT-qPCR.

Results: Optimal alginate-based 3D culture conditions were established with NPCs. Expression of key genes was examined at day 0 and day 17. In the NPC-alginate bead 3D culture model, *TET1* was upregulated and *MEOX2* tended to be downregulated after exposure to IHA-IDH1-R132H conditioned medium.

Conclusion: We have developed a novel NPC-alginate bead 3D culture model for the first time in the literature. By recapitulating the earliest stages of gliomagenesis, this model will allow studying the effects of the IDH1-R132H mutation without confounding effects of the other mutations.

Keywords: Glioma, Isocitrate Dehydrogenase, IDH1, Immortalized Human Astrocytes, Neural Progenitor Cells, NPCs.

Özet

Amaç:

Glioma gelişiminin izositrat dehidrojenaz (IDH1/2) mutasyonları tarafından tetiklendiğine inanılmaktadır, ancak IDH1/2 mutasyonlarının gliomagenezi nasıl tetiklediğine dair sınırlı bilgi bulunmaktadır. Bunun nedeni, yıllar boyunca yapılan çalışmalarda, glioma gelişiminin erken aşamalarını araştırmak için sıklıkla hasta tümör örneklerini veya dönüştürülmüş hücreleri veya sürücü mutasyonlara sahip normal kök hücreleri kullanmasıdır. Burada, NPC'lerle aljinat bazlı bir 3 boyutlu kültür hazırlayarak tek başına IDH1-R132H mutasyonunun spesifik etkilerini anlamak için bir model oluşturduk ve dolayısıyla diğer sürücü mutasyonlarının etkilerinden kaçınmaya çalıştık.

Yöntemler: İnsan İndüklenmiş Pluripotent Kök Hücreler (hiPSC'ler), Nöral Progenitör Hücrelere (NPC'ler) farklılaştırıldı. Aljinat bazlı bir 3D matrise gömülü NPC'ler, Nöral Progenitör Ortamında 1 gün (0. gün) boyunca inkübe edildi. Daha sonra, Nöral Progenitör Ortamı, NPC-aljinat boncuklarından uzaklaştırıldı ve doksisiklin kaynaklı vahşi tip IDH1 ve Mutant IDH1 üreten Ölümsüzleştirilmiş İnsan Astrositlerinden (IHA'lar) şartlandırılmış ortamla 14 gün boyunca inkübe edildi. 14. günde, IHA koşullu ortam, Nöral Progenitör Ortamı ile değiştirildi ve 3 gün boyunca (17. gün) inkübe edildi. RNA, 0. ve 17. günde NPC'lerden izole edildi ve daha önce IDH1 mutant gliomalarda değiştirildiği bildirilen anahtar genler (Tet metilsitozin dioksijenaz 1 (TET1) ve Mesenchyme Homeobox 2 (MEOX2)) RT-qPCR ile değerlendirildi.

Bulgular: NPC'lerle optimum aljinat bazlı 3 boyutlu kültür koşulları oluşturuldu. Anahtar genlerin ekspresyonu 0. günde ve 17. günde incelendi. NPC-aljinat boncuk 3D kültür modelinde, TET1 yukarı regüle edildi ve MEOX2, IHA-IDH1-R132H koşullu ortama maruz bırakıldıktan sonra aşağı regüle edilme eğilimindeydi.

Sonuç: Literatürde ilk kez yeni bir NPC-aljinat boncuk 3 boyutlu kültür modeli geliştirdik. Bu model, gliomajenezin en erken aşamalarını taklit ederek, diğer mutasyonların karıştırıcı etkileri olmadan IDH1-R132H mutasyonunun etkilerini inceleme olanağı sağlayacaktır.

Anahtar Kelimeler: Glioma, İzositrat Dehidrojenaz, IDH1, Ölümsüzleştirilmiş İnsan Astrositleri, Nöral Progenitör Hücreler, NPC'ler.

Introduction

Gliomas, a deadly brain tumor type, have poor prognosis, high morbidity and mortality, while being rare compared to other tumors (1). According to data from the Central Brain Tumor Registry of the United States, the worldwide incidence rate of primary malignant brain and other CNS tumors was 3.5 per 100,000 population (2) .

Gliomas, the most common type of cancer arising from brain tissue, are devastating cancers that are often incurable due to their heterogeneity and invasive properties (3,4) . Current treatment modalities such as surgical resection, radiation, and chemotherapy provide modest benefits for patient survival (5,6) and no significant advances has been made in treatment of gliomas in the past >20 years (6,7).

Isocitrate dehydrogenases (IDH), whose mutations are one of the most important diagnostic markers of gliomas, act as core metabolic enzymes in the citric acid cycle and convert isocitrate to α-ketoglutarate (α-KG) (8,9). Mutations in IDH1 or IDH2 enzymes in lower-grade glioma (LGG) and secondary GBMs are usually heterozygous missense mutations and frequently affect amino acids 132 of the IDH1 and 172 of the IDH2 (10).

Mutated IDH1 and IDH2 enzymes acquire a neomorphic feature, leading to the production of 2-Hydroxyglutarate (R-2-HG), an oncometabolite (8). 2-HG is structurally similar to α-KG and competitively inhibits α-KG-dependent dioxygenases, including DNA demethylases (e.g., TET family) and histone demethylases (e.g., Jumonji family) (11,12). As a result, the epigenetic landscape of histones and DNA changes, which result in numerous cellular changes (13–15). *IDH1/2* mutations are considered to be the earliest genetic alterations that trigger the development of gliomas, as it has been shown to precede mutations in genes, such as *TP53* mutations known to play roles in glioma development, or the glioma-specific 1p/19q codeletion, or *genome-wide CpG island methylator phenotype* (G-CIMP) (16).

Existing cellular models to mimic early gliomagenesis often include transformed cells or normal stem cells with driver mutations, such as those in *TP53*, ATRX, 1p/19q-codeletion, *EGFR*, *PTEN*, *NF1*, *CDKN2A/B*, etc.. Although the origins of gliomas are still unclear, studies in developmental biology, patients, and experimental glioma models suggest that glioma origins may be neural progenitor or stem cells, oligodendrocyte precursor/progenitor cells, or astrocytes (17).

Self-renewing, multipotent and GFAP-expressing neural stem cells (NSCs) transform into neural progenitor cells that generate neurons and glial cells (18,19) . Due to the developmental potential and plasticity of NSCs, they are ideal candidates for glioma cells of origin because multiple oncogenic mutations are required for gliomagenesis, and the self-renewal and proliferative properties of NSCs may result in the endogenous accumulation of somatic mutations (20,21). However, the role of postmitotic and differentiated astrocytes in glioma formation is still debated (20).

Previous studies have often used 2D cultures which force cells to adapt to an artificial, flat and hard surface. The 2D cultures can alter the metabolism and degree of functionality of cells, which may significantly differ from the behavior of cells *in vivo* (22,23).

In contrast, 3D cellular systems reflect and allow the study of biological processes such as interactions between cells, the effect of the extracellular matrix on cells, and different external physical and chemical stimuli (24–26). Alginate derived from algae is the most widely used natural polymer for microencapsulation due to its permeability, biocompatibility, long-term stability and water retention ability. Unmodified alginate is ionically crosslinked by activation with divalent cations such as Ca^{2+} (27). Alginate is used during differentiation of stem cells into neural lineages, as it successfully mimics the 3D environment of the central nervous system (28,29), and therefore we decided to use alginate to develop a novel model of the earliest stages of gliomagenesis.

Our knowledge of how the cascade initiated by *IDH1/2* mutations triggers or facilitates gliomagenesis is limited. In comprehensive multi-omic studies that have been going on for years, either patient tumor samples or glioma models created by combining many oncogenic mutations were used. However, *IDH1/2* mutations are known to be genetic changes that occur at the earliest stage of gliomagenesis, and therefore, models with additional mutations may not recapitulate the oncogenic changes leading to glioma development. In this study, we have

shown that the NPC-alginate bead 3D culture model combined with conditioned media from immortalized human astrocytes (IHAs) expressing mutant IDH1 inducibly, is a suitable model to examine the earliest stages of gliomagenesis and how the IDH1-R132H mutation affects cells with brain tumor initiation potential. Importantly, this model is the first to reveal how the IDH1-R132H mutation alone acts in the earliest stages of gliomagenesis, independent of the confounding oncogenic effects of other driver mutations that are used in the existing models generated to date.

Methods

Immortalized Human Astrocytes

Immortalized Human Astrocytes (IHA) were a gift from Prof. Timothy Chan, assisted by Dr. Sevin Turcan. IHA-IDH1-WT and IHA-IDH1-R132H cells were induced by doxycycline (Sigma, Cat No: D9891-5G) to produce wild-type IDH1 and mutant IDH1, respectively. IHA cells were maintained in DMEM High glucose (Gibco, Cat No: 41965-039) supplemented with 10% FBS (Gibco, Cat No: 10500-064) and penicillin/streptomycin (Gibco, Cat No: 15140122).

To produce IHA-IDH1-WT and IHA-IDH1-R132H conditioned media, IHA-IDH1-WT and IHA-IDH1-R132H cells were cultured in DMEM High Glucose Medium in the presence of doxycycline. When the cells reached 80-90% confluency, media in which the cells were cultured were collected, filtered with 0.45 uM filter and then stored at -20 ^{0}C. After IHA-IDH1-WT and IHA-IDH1-R132H conditioned media were removed, IHA-IDH1-WT and IHA-IDH1-R132H cells were passaged with trypsin and grown in 1μg/ml doxycycline-containing DMEM High Glucose.

hiPS Cell Culture

Mouse embryonic fibroblast (MEF) cells were cultured in MEF medium (DMEM High Glucose, 10%FBS, 2mM GlutaMAX, 1% pen/strep, 1X MEM-NEAA and 1X Sodium

Pyruvate) in a gelatin coated 6-well plate. When the confluency of MEF cells in a plate reached 85-90%, cells were treated with Mitomycin-C (Biovision, Cat No: 2713-5) at 10 ug/ml final concentration for 3 hours at 37 ^{0}C and 5% CO_2.

After incubation, medium containing mitomycin-C was aspirated and cells were washed with DMEM High Glucose. Human iPSCs were opened with HESC Medium (containing DMEM-F12 medium, 20% Knock-out SR, 1X MEM-NEAA, 2-Mercaptoethanol, 15mM HEPES and 100 ng/ml bFGF) on mitotically inactivated MEF feeder cells. Cells were incubated at 37 ^{0}C and 5% CO_2 and medium was changed every day with fresh HESC Medium. When iPSCs colonies reached sufficient size, colonies were detached with dispase in DMEM-F12 (Stemcell Technologies, Cat No: 07923). The hiPSCs colonies were cultured in mTESR™ 1 complete medium (mTESR Basal Medium and mTESR 5X Supplement) in matrigel (Corning, Cat No: 354277) coated wells of a 6-well plate. When cells reach 70-80% confluency, colonies were removed with dispase and replated in fresh mTESR™ 1 complete medium in a 6-well plate.

Generating Neural Progenitor Cells (NPCs) from human iPS Cells

To generate Neural Progenitor Cells (NPCs) from hiPSCs, "Generation and Culture of Neural Progenitor Cells using the STEMdiff™ Neural System" Monolayer Culture protocol from STEMCELL Technologies was used. Firstly, after iPSC colonies were washed with sterile PBS, cells were dissociated with Gentle Cell Dissociation Reagent (StemCell, Cat No: 07174). Cells in STEMdiff™ Neural Induction Medium + SMADi (StemCell, Cat No: 08581) were plated in a single well of a matrigel-coated 6-well plate and incubated at 37 ^{0}C and 5% CO_2. Every day, the whole medium was changed with fresh STEMdiff™ Neural Induction Medium + SMADi until cell confluency reached 90%. Cells were treated with accutase (Stemcell, Cat No: 07923) and then cells in STEMdiff™ Neural Induction Medium + SMADi were cultured in a well of matrigel coated 6-well plate. Cells were passaged one more time and plated with

STEMdiff™ Neural Induction Medium + SMADi. After two passages, the Neural Progenitor Cell (NPC) Culture protocol was used for expansion of NPCs.

Cells were treated with accutase and plated in a matrigel coated 6-well plate in STEMdiff™ Neural Progenitor Medium (Stemcell, Cat No: 05833). At 90% confluency, cells were passaged and placed in fresh STEMdiff™ Neural Progenitor Medium in a matrigel-coated 6-well plate.

Immunofluorescence Staining for characterization of hiPSCs and NPC

Cells were seeded on matrigel coated coverslips in a 24-well plate. After cells were attached to the coverslips and were 50-60 % confluent, they were fixed with 4% paraformaldehyde (PFA) (Sigma-Aldrich, Cat No: 158127-100G) for 15 min at RT. Then, cells attached to coverslips were washed with 1X PBS three times. They were permeabilized with 0.1% Triton X-100 in 1X PBS for 10 min at RT. After 10 min, cells were washed with 1X PBS three times. For blocking, 1% BSA in PBST (PBS with 0.1% Tween-20) was added on cells and incubated for 1 hour at RT. Cells were incubated with primary antibodies in blocking solution for 2 hours at RT. NPCs were detected with Mouse NESTIN (1:1500, Cell Signaling, Cat No: 33475), Rabbit SOX2 (1:400, Cell Signaling, Cat No: 3579), Rabbit SOX1(1:400, Cell Signaling, Cat No: 4194S), Mouse OCT4 (1:200, Cell Signaling, Cat No: 75463) and Rabbit PAX6 (1:200, Cell Signaling, Cat no: 60433). iPSCs were detected with Mouse OCT4 (1:200, Cell Signaling, Cat No: 75463). After primary antibody staining, cells were washed with 1X PBS three times. Secondary antibodies in blocking solution were added on cells and incubated for 1 hour at RT in dark. Goat Anti-Rabbit conjugated to Alexa 555 (1:500, Abcam, Cat No: ab150078) and Goat Anti-Mouse conjugated to Alexa 488 (1:500, Abcam, Cat No: ab150113) were applied. After being washed with 1X PBS three times, cells were counterstained with Hoechst (1:1000) in PBS to stain nuclei for 3 min at RT. Then cells were washed with 1X PBS. Coverslips were flipped onto a drop of mounting medium placed on a slide.

Alginate-Based 3D Neural Progenitor Cell Culture

Alginate solution (2%) (Sigma, Cat No: 1112) was prepared with ddH_2O and autoclaved. This solution was filtered with a 0.2 µM filter and then stored +4 ^{0}C. When alginate beads formed with NPCs were prepared, Neural Progenitor Medium and 2% alginate solution were mixed equally. The concentration of alginate solution was reduced from 2% to 1% with medium.

Before embedding NPCs in alginate beads, accutase was used to collect NPCs from 10 cm plates. Viable cells were counted using Trypan Blue and a hemocytometer. Each alginate bead consists of 10 µl of alginate solution formed with the help of a syringe with a 21G X 1-½" needle. Cells were centrifuged, supernatants were removed and the volume of 1% alginate solution to be added was adjusted so that the cell concentration in alginate was 250,000 cells/ml. Cell-alginate suspension was dropped onto 100 mM $CaCl_2$ buffer with the help of a syringe to form alginate beads containing NPCs. The $CaCl_2$ buffer was removed and then cells were washed with DMEM-F12. After the washing step, Neural Progenitor Medium was added onto NPC-alginate beads and incubated at 37 ^{0}C and 5% CO_2.

3 different time points (Day 0, Day14 and Day 17) and 5 different experimental conditions were selected to develop the model.

In the first group (control), there was no manipulation of cells. NPC-alginate beads were incubated in the Neural Progenitor Medium for 24 hours.

In the second group, The Neural Progenitor Medium on the NPC-alginate beads was replaced with IHA-IDH1-WT conditioned medium after 24 hours. 3-4 ml of medium was withdrawn from the plates and 4-5 ml of fresh IHA-IDH1-WT conditioned medium was added every three days for 14 days.

In the third group, The Neural Progenitor Medium on the NPC -alginate beads was replaced with IHA-IDH1-R132H conditioned medium after 24 hours. 3-4 ml of medium was

withdrawn from the plates and 4-5 ml of fresh IHA-IDH1-R132H conditioned medium was added every three days for 14 days.

In forth and fifth groups; after 14 days, IHA-IDH1-WT and IHA-IDH1-R132H conditioned mediums on NPC- alginate beads were replaced with Neural Progenitor Medium and for 3 days, NPCs alginate beads were incubated separately for 3 days at 37 ^{0}C and 5% CO_2.

Recovering cells from alginate beads for further experiments

0.5 M ethylenediaminetetraacetic acid (EDTA) (Invitrogen, Cat No: 15575-020) was added to the culture medium containing NPC-alginate beads to disrupt alginate polymer by Ca^{+2} chelation. After alginate was dissolved, the solution in the plate was transferred to a 50 ml canonical tube. Cells were pelleted by centrifugation at 300 x g for 5 min and washed with DMEM-F12 medium. Next, the supernatant was completely removed and discarded. TRI Reagent (Sigma, Cat No: 93289-100ML) was added to the cells to be used for RNA isolation and stored at -80 ^{0}C.

RNA isolation and Real Time Quantitative PCR (RT-qPCR)

Cells, recovered from beads at day 0 and day 17 were lysed in TRI reagent. Direct-zol RNA MiniPrep Plus Kit (Zymo Research, Cat No: R2072) was used to isolate RNA. RNA concentration was determined with a Nanodrop (Thermo Scientific, Nanodrop 2000 spectrometer) instrument.

cDNA was synthesized from extracted RNA using ProtoScript^R First Strand cDNA Synthesis Kit (New England BioLabs, Cat No: E6300S). GoTaq^R qPCR Master Mix (Promega, Cat No: A6001) and Real-Time PCR Detection System (Applied Biosystems 7500 Fast Instrument) were used according to the manufacturers' instructions. Primers are listed in Table 1. GAPDH, the housekeeping gene, was used to normalize changes in specific gene expression.

Table 1: Primer List for RT-qPCR

Primer Name	Forward Primer Sequence	Reverse Primer Sequence
TET1	CAGAACCTAAACCACCCGTG	TGCTTCGTAGCGCCATTGTAA
MEOX2	GTCAGAAGTCAACAGCAAACCCAG	CACATTCACCAGTTCCTTTTCCCGAGCC
GAPDH	TGCACCACCAACTGCTTAGC	GGCATGGACTGTGGTCATGAG

Result

Generation and Characterization of hiPSC-derived hNPCs

In order to differentiate hiPSCs to NPCs, dual SMAD inhibition of iPSCs in monolayer culture conditions was performed using the STEMdiff reagents. Upon induction of differentiation using the Neural Induction Medium in the presence of SMADi, Neural Progenitor Medium was used to expand the generated NPCs. Figure 1A illustrates the morphological changes of cells throughout the differentiation process. (Figure 1A). The morphological differences between hiPSCs and hiPSC-derived NPCs were readily visible (Figure 1B).

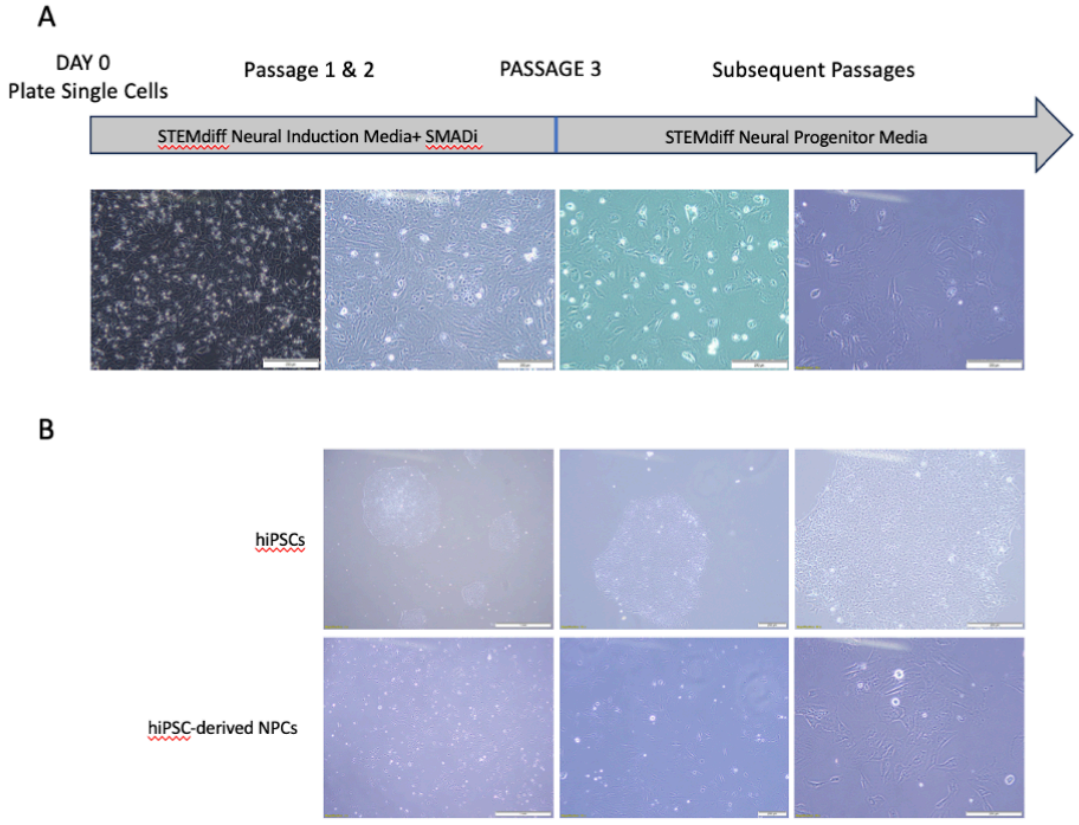

Figure 1. Generation of human NPCs from hiPSCs. A. Images were taken during various stages of hNPCs differentiation and show cell morphology during each differentiation step. Scale bar: 200 µm B. Representative images of hiPSC colonies and iPSC-derived NPCs. Scale bar: 1 mm, 200 µm and 200 µm respectively.

Immunocytochemical staining was performed to characterize whether hiPSC-differentiated cells correspond to NPCs. However, before starting differentiation, we checked whether the hiPSCs to be used for differentiation into NPCs were still pluripotent. OCT4 (encoded by *POU5F1*, also known as Oct3, Oct3/4), a member of the POU transcription factor family, is an ESC- and germline-specific transcription factor. OCT4 plays a critical role in the maintenance of pluripotency and self-renewal of ESCs (30) and it is highly expressed in pluripotent cells, whereas its expression decreases during differentiation (31). Therefore,

hiPSCs were stained with an antibody against the pluripotency marker OCT4 and as expected, all cells were stained strongly for OCT4 (Figure 2A).

Following the confirmation of hiPSCs pluripotency, differentiation was initiated and at the end of the differentiation process, cells were stained for neuroectodermal stem cell markers, namely NESTIN, SOX1, SOX2 and PAX6, and the pluripotency marker OCT4 (Figure 2B).

The type IV intermediate filament (IF) protein NESTIN is specifically expressed in NPCs and is a well-known neural stem cell marker. It is not expressed in post-mitotic neurons or glia (32). SOX1, a member of the B1 group of the SRY homology box (SOX) transcription factor family, has been shown to be an important regulator in cell fate determination of neural lineage cells and is used to identify neural progenitor cells (33). Sex determining region Y-box2 (SOX2), also a member of the SOX family of transcription factors, is a factor that has very important roles in the control of pluripotency, the neural differentiation of pluripotent stem cells, and the self-renewal of neural progenitor stem cells (34,35). The paired box 6 protein (PAX6) is a transcription factor that plays an important role in the development of the central nervous system, particularly of the eye, spinal cord and cerebral cortex (36). PAX6 regulates many vital aspects of NSCs, such as proliferation, self-renewal, differentiation, and apoptosis.

We found that most of the NPCs were stained positively with neuroectodermal stem cell markers. Also, the cells were not stained with OCT4, as expected. These results indicated that most of hiPSCs differentiated into NPCs successfully (Figure 2B).

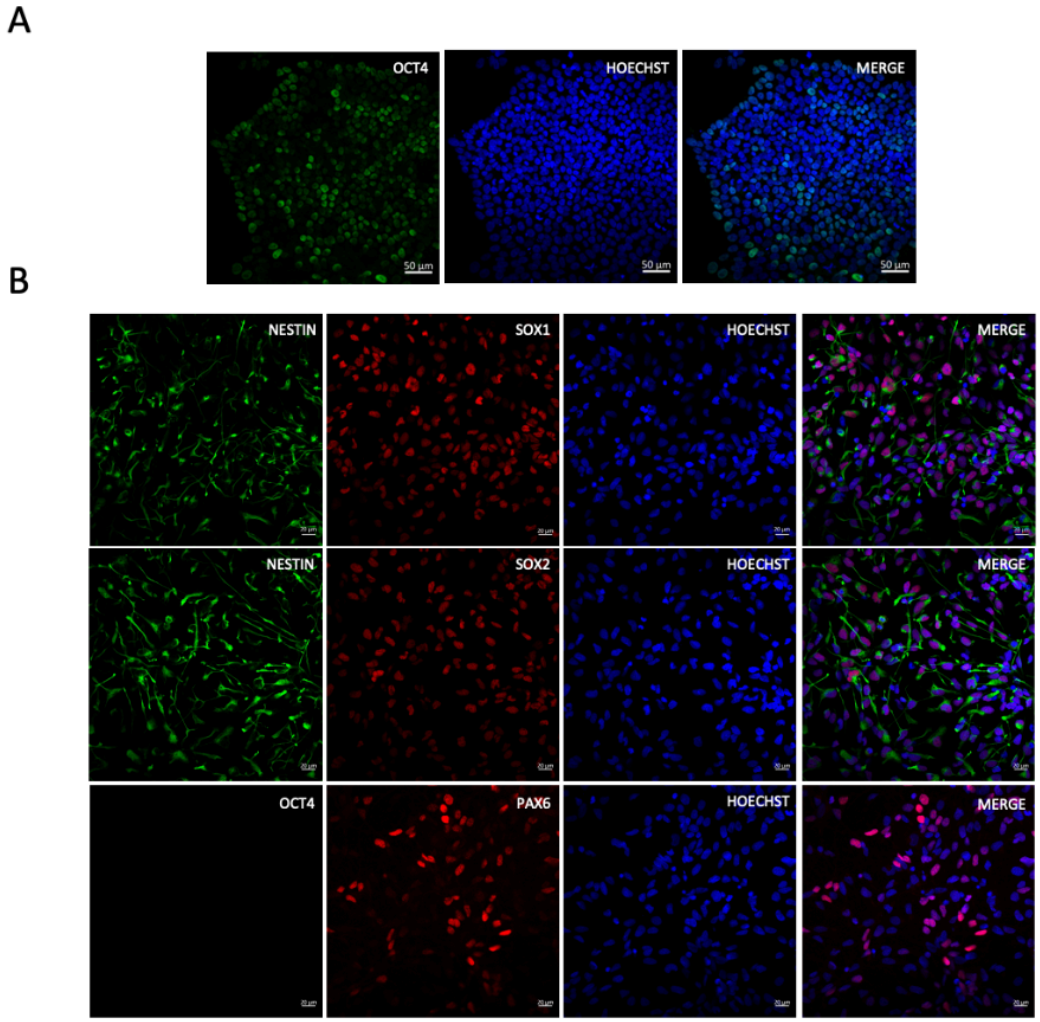

Figure 2. Characterization of hiPSCs and hiPSC-derived NPCs. Representative cells from the hiPSCs and hiPSC-derived NPCs were fixed and stained with the antibodies against lineage-specific marker proteins. A. hiPSCs express pluripotency marker OCT4. Scale bar: 50 µm. B. Immunocytochemistry staining showing hiPSC-derived NPCs expressing SOX2, SOX1, PAX6 and Nestin. For NPCs, three different co-stainings were performed. 1; Nestin (Green), SOX1 (Red) and Hoechst (Blue). 2; Nestin (Green), SOX2 (Red) and Hoechst (Blue). 3; OCT4 (Green), PAX6 (Red) and Hoechst (Blue). Nuclei were stained with Hoechst 33258. Scale bar: 20 µm.

Alginate bead-based 3D NPC culture

Human Neural Progenitor Cells (NPCs) that had been homogeneously dispersed were encapsulated inside alginate hydrogel sphere-like beads. Alginate is widely used in the creation of 3D cell culture models due to its advantageous properties, such as easy gelling under physiological conditions, easy dissolution, ease of microscopic observation, and a structure that allows efficient nutrient and waste diffusion (37,38).

The concentration of alginate is important for mechanical stability, flexibility, and nutrient diffusion when creating a 3D culture (38,39). It was observed that alginate beads prepared at low alginate concentration had large pore sizes, had a weak structure, and failed to maintain integrity during long-term culture. It was also reported that the proliferation of embryonic stem cells (ESCs) was inhibited in alginate beads prepared at the concentration of 2%, whereas the beads prepared at 1% alginate concentration are the most suitable for ESC growth (38).

For this reason, 3D culture was created with 1% concentration of alginate to maintain cell viability and proliferation of NPCs. 3 different time points and 5 different experimental conditions were selected to develop the model (Figure 3).

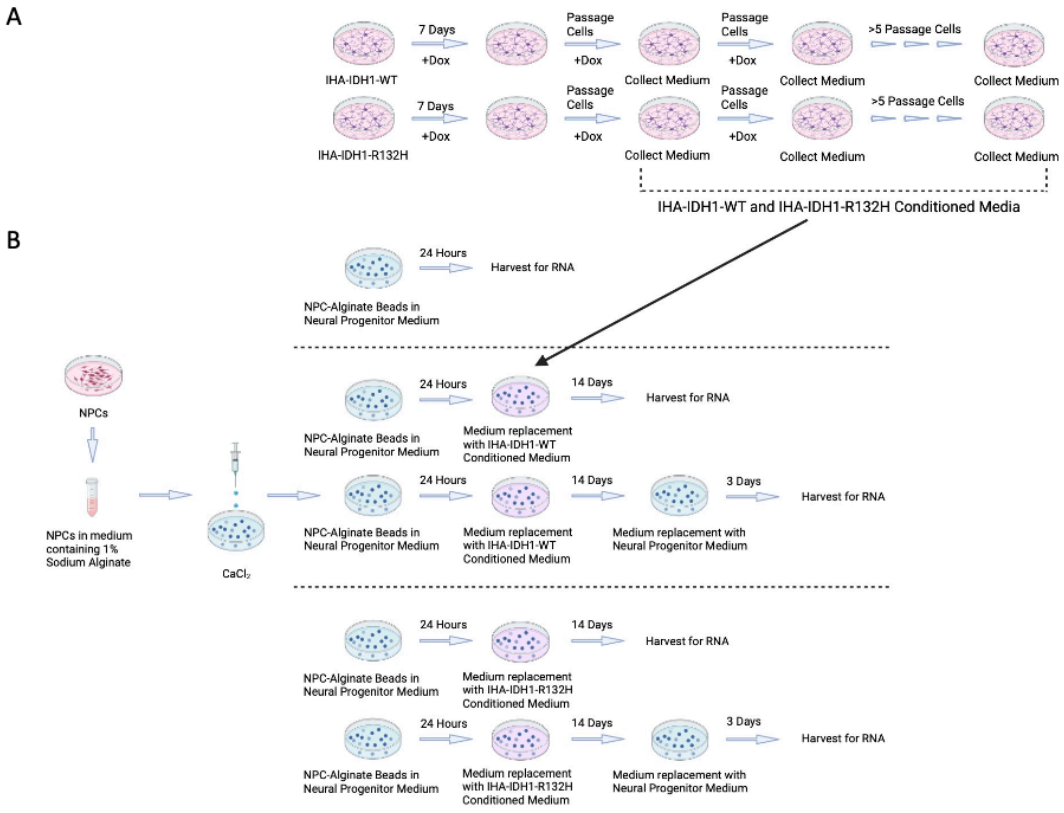

Figure 3. Schematic representation of experimental design A) IHA-IDH1-WT and IHA-IDH1-R132H conditioned media production B) Preparation of 5 experimental conditions: NPC-Control-Day 0, NPC-IDH1_WT-Day 14, NPC-IDH1_R132H-Day 14, NPC-IDH1_WT-Day 17 and NPC-IDH1_R132H-Day 17

Alginate beads formed with NPCs on day 0 were incubated in the Neural Progenitor medium for 24 hours (Figure 4A). At day 14, we had two different experimental groups: the first was cultured with a medium collected from immortalized human astrocytes (IHAs), inducibly expressing IDH1-WT for 14 days. The second was cultured with medium collected from IHAs expressing the IDH1-R132H for 14 days. At day 17, we had two experimental groups: i) conditioned medium collected from IHAs inducibly expressing IDH1-WT were removed from NPC-Alginate beads on day 14 and Neural Progenitor medium was added, and cells were cultured with Neural Progenitor medium for 3 days (until day 17), ii) conditioned

medium collected from IHAs inducibly expressing IDH1-R132H were removed from NPC-Alginate beads on day 14 and Neural Progenitor medium was added, and cells were cultured with Neural Progenitor medium for 3 days (until day 17),

At day 0 the alginate beads were transparent and shiny (Figure 4A). No degradation of the beads was observed at day 0, but at day 14, the beads that were treated with IHA-IDH1-WT and IHA-IDH1-R132H mediums began to deteriorate. However, the cells within the beads were able to keep proliferating, forming an aggregate. Deterioration of more beads was observed on the day 17 groups; more frequent clustering was observed due to the increase in the number of cells. In addition, it was observed that cells escaped from the beads due to deterioration of the alginate beads in the 14th and 17th day groups (Figure 4B).

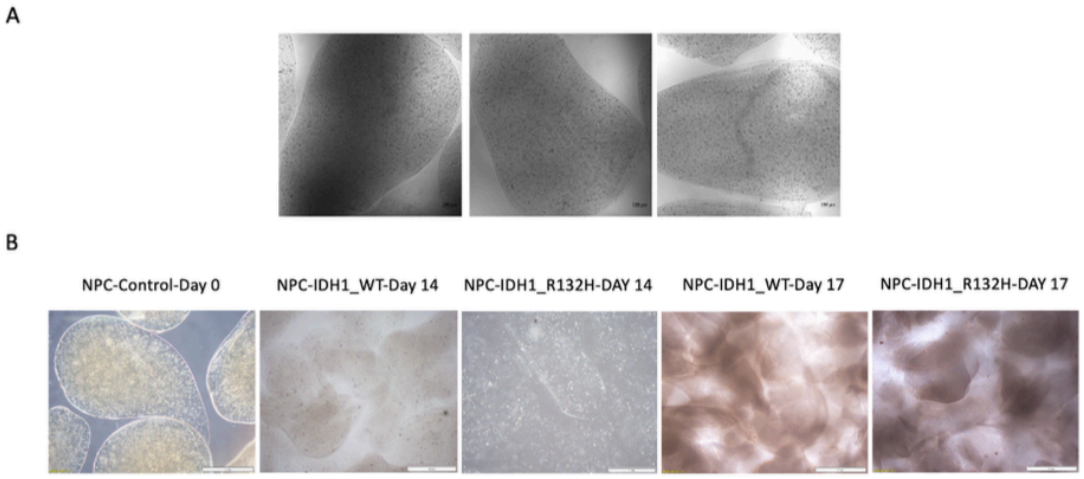

Figure 4. 3D culture of hNPCs in alginate beads. A. Confocal microscope images of alginate-based 3D NPC culture at day 1. Scale Bars: 500 µm. B. Light microscope images of alginate based 3D NPC cultures at day 0 (in NPC medium), day 14 (in IHA-IDH1-WT and IHA-IDH1-R132H conditioned-medium) and day 17. On day 14, IHA-IDH1-WT and IHA-IDH1-R132H conditioned-medium were changed with regular NPC medium and cultured for three days before imaging on day 17. Scale Bar: 1 mm.

RT-qPCR analysis confirms upregulation of IDH1-R132H induced genes

To confirm that NPCs exposed to IHA-R132H conditioned medium display alterations observed in IDH1-R132H expressing glial cells, we analyzed the expression levels of the genes known to be upregulated (*TET1*) and down-regulated (*MEOX2*) by IDH1-R132H in NPCs at two time-points (day 0 and day 17) by RT-qPCR.

Cells were recovered from the beads at indicated time-points and expression of *TET1* and *MEOX2* was examined. On the third day after returning the cells to the Neural Progenitor medium (day 17), the expression level of *TET1* in NPCs exposed to IHA-IDH1-WT conditioned medium was almost the same as in day 0 NPCs. On the other hand, it was observed that in the NPCs exposed to IHA-IDH1-R132H conditioned medium *TET1* expression increased almost 3.5 times compared to day 0. Furthermore, a significant difference in *TET1* expression was observed when NPC-IDH1_R132H-Day17 cells were compared with NPC-IDH1_WT-Day17 cells (Figure 5A). Therefore, we conclude that growing NPCs in IHA-IDH1-R132H conditioned medium induces expression of TET1, in line with the reported induction of *TET1* in IDH1/2 mutant gliomas (40).

On the other hand, it was observed that *MEOX2* expression was suppressed both in NPCs cultured in IHA-IDH1-R132H conditioned medium and in IHA-IDH1-WT conditioned medium. However, the suppression showed a tendency to be stronger in NPCs cultured in IHA-IDH1-R132H conditioned medium, compared to the IHA-IDH1-WT conditioned medium (2.2 fold, p=0.21, after multiple-test correction in ANOVA) (Figure 5B).

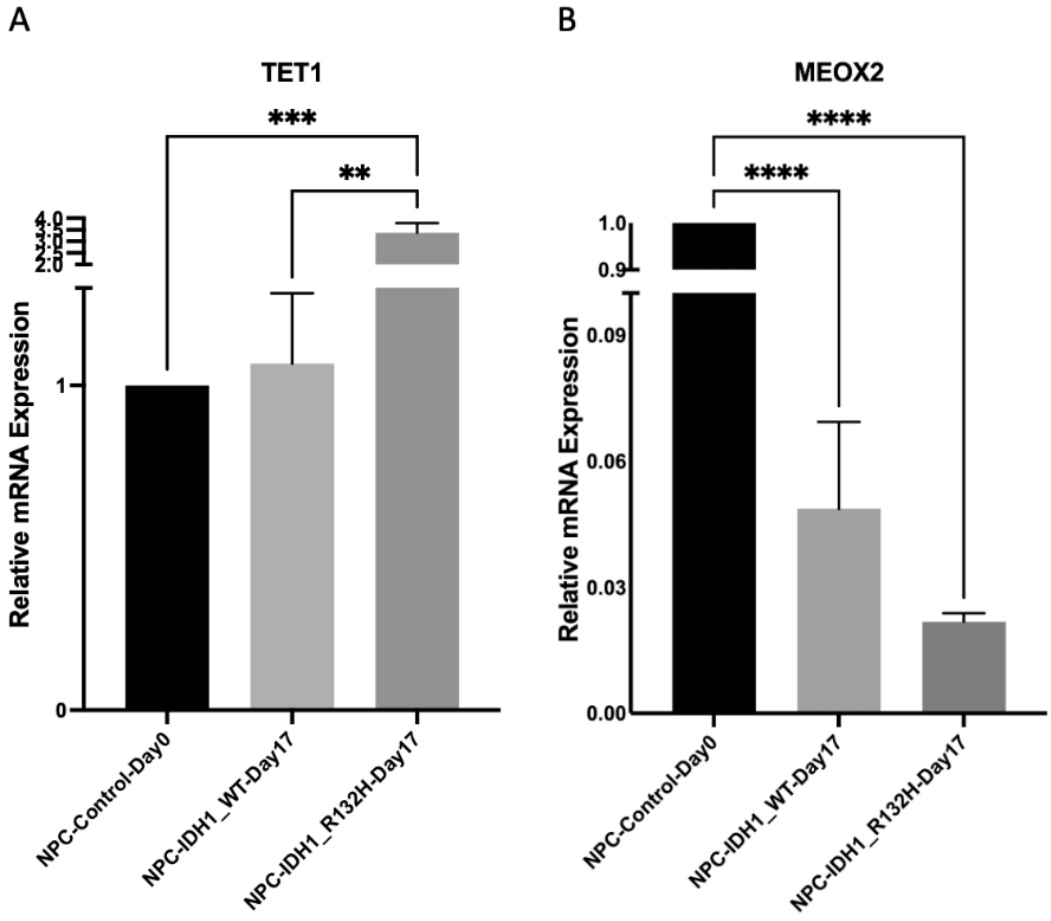

Figure 5. The expression patterns of *TET1* and *MEOX2* genes. A) *TET1* **B)** *MEOX2* mRNA levels were analyzed by RT-qPCR in NPCs cultured inside alginate beads for 3 different experimental conditions. *GAPDH* was used as the housekeeping gene. ** $p < 0.01$; *** $p < 0.001$; **** $p < 0.0001$.

Discussion

It is known that mutant IDH1/2 expression or exposure to D-2-HG leads to the G-CIMP phenotype in different cell types and drives the cells to a less differentiated point (14). However, most in vitro studies of gliomas rely on tumor cells cultured in 2D environments and may not fully recapitulate the 3D in vivo tumor microenvironment. Therefore, the characterization of early epigenomic changes resulting from IDH1/2 mutations in non-tumor cells, including

analysis of major histone modifications, DNA methylation, transcriptome etc., has largely been performed in cells cultured in 2D. In addition, some of these studies were carried out under cell culture conditions with heterogeneous tumor samples or cells (e.g., astrocyte) that could not fully reflect the glioma biology occurring in three-dimensional tissue. However, IDH1/2 mutations are genetic changes that occur at the earliest stages of gliomagenesis, when other oncogenic changes are not yet present.

Another factor to be considered when creating glioma models is the "*cell-of-origin*" problem. Neural stem cells (NSCs), which have self-renewal properties, are considered ideal candidates as the origin cells of gliomas due to their development potential and plasticity properties. Neural progenitor cells are also produced by NSCs to produce progeny along neuronal and glial lineages (20). While it is widely accepted that gliomas result from accumulation of mutations in neural stem/progenitor cells, oligodendrocyte progenitor cells, or dedifferentiation of astrocytes, most cell culture models of glioma rely on tumor cell lines generated from high-grade tumor tissues (20). Because these cells are more likely to reflect the cellular states in full-blown tumors, rather than the earliest cells-of-origin that give rise to gliomas, they are not suitable for modeling the early stages of gliomas. As the likely cells-of-origin, neural progenitor cells could better reflect the cellular states at initial stages of gliomagenesis and some features associated with gliomagenesis can be better understood in these cells, which could lead to development of more effective therapies. It is critical that the model in which the analysis will be performed is capable of reflecting the earliest stages of glioma, in which IDH mutations exert their effects, and that it can be easily intervened under controlled conditions. Therefore, human induced pluripotent stem cell (hiPSC)-derived NPCs with no oncogenic mutation were used. The ability of iPSC produced from non-pluripotent cells to differentiate into many different cell types, including neurons, has enabled the development of better disease models that could be used for studying disease etiopathogenesis and

developing novel therapies, either using cells from healthy donors or patient-derived cells (41,42).

In order to develop a model based on hiPSC-derived NPCs, we needed a source for IDH1 mutations. One way to achieve this could be introduction of the mutant IDH1 into NPCs and engineering them to express it either in a constitutive or inducible manner. However, the former would not allow us to investigate the immediate effects of IDH1, while the latter may suffer from leaky expression leading to possibly irreversible epigenomic changes. Therefore, we sought to expose NPCs to conditions that could mimic IDH1-R132H induced alterations. To this end, we used immortalized human astrocytes (IHAs) that inducibly express IDH1-R132H and as a control, we used IHAs that inducibly express wild-type (WT) IDH1. Since the immortalized human astrocyte cells we used to produce the IHA-IDH1-WT and IHA-IDH1-R132H condition mediums were generated by infection with pLVX-Tet-On retroviruses, they can be induced with doxycycline to produce IDH1-WT or IDH1-R132H (43). In addition to expressing E6/E7, these cells were also infected with hTERT (44). Although these cells were previously used to characterize early epigenomic changes in gliomas, their expression of E6/E7 and particularly hTERT, one of the defining early mutations of oligodendrogliomas and GBMs, they may not reflect the earliest cell state that precedes IDH1/2 mutations. However, they could still be used as a source of 2-HG and other IDH mutation-induced cellular alterations that are released to the culture medium. Therefore, we used these IHAs that express IDH1-R132H to generate such conditioned medium, and IHAs that express WT-IDH1 to generate control conditioned medium, in our model.

Many of the most recently cited protocols for the production of NPCs are monolayer and embryoid body (EBs) protocols. In both protocols, NPC generation from iPSCs takes 21-30 days (45). In this study, the monolayer protocol has been implemented to generate NPCs from healthy iPSCs. NPC markers such as NESTIN, PAX6, SOX1, SOX2, and DACH1 should

be expressed in iPSC-derived NPCs, while pluripotency markers such as OCT4, NANOG, DNMT3B, and DPPA4 should be down-regulated. Besides, these cells continue to maintain their morphology and multipotential identity after freezing and thawing (46). The characterization of NPCs and iPSCs used in this study was demonstrated by immunohistochemical staining. Cells differentiated into iPSCs with the STEMdiff™ monolayer culture protocol lost the pluripotency marker OCT4 and were shown to be positive for NESTIN, PAX6, SOX1 and SOX2.

2D culture systems cannot fully provide the physiological environment faced by the tumor cells *in vivo*. In order to better reflect the cell-cell and cell-ECM interactions, biomaterials are good candidates for mimicking *in vivo* conditions *in vitro*. Alginate is a polymer that is readily available, economical, has long-term stability and water retention, and has the advantages of biocompatibility, biodegradability and non-toxicity (47,48). Since alginate-based hydrogels carry several such preferable properties, they are widely used as scaffolds in processes, such as cell encapsulation and tissue engineering (49).

A 3D glioblastoma cell culture model was developed with U87 glioblastoma cells and alginate microfiber, which mimics the treatment conditions for drug response studies (50). Cells in 3D alginate culture treated with temozolomide (TMZ) showed an anti-proliferative effect as in 2D cell culture medium. On the other hand, when compared to 2D cell culture, it was determined that the expression of the genes related to drug resistance increased more in 3D alginate culture. The alginate-based 3D culture model has been proposed as a fast, reliable and practical model for drug testing and therapy development (50).

In our study to make alginate-based 3D culture, the bead generation protocol was used (51). The alginate beads were approximately 2 mm in diameter and each bead contained approximately 2500 cells. For the first time in the literature, we show that alginate allows the survival and growth of encapsulated NPCs during the culture period (18 days). From the first

day of culture, the cells increased in number and formed dense clusters. We observed that the alginate beads swelled and did not deteriorate as the number of cells increased.

One of the two genes we selected to confirm their altered expression in response to IDH1-R132H-expressing IHA conditioned medium, was Tet methylcytosine dioxygenase 1 (*TET1)*. D-2-HG, an α-KG antagonist, competitively inhibits α-KG-dependent dioxygenases, including the Ten-Eleven Translocation (TET) family. TET1 is a member of the TET family that catalyzes the conversion of 5-methylcytosine (5mC) to 5-hydroxymethylcytosine (5hmC) (52). It is known that *TET1* deficiency is associated with greater genomic instability in glioma cell lines and increases resistance to ionizing radiation therapy. Furthermore, the amount of *TET1* expression varies according to the histological type of the disease. Importantly, it is expressed at higher levels in IDH-mutant low-grade gliomas and IDH-mutant GBMs, compared to IDH wild-type LGGs and GBMs (40), which makes it an ideal gene to test in our model.

Since Mesenchyme Homeobox 2 (*MEOX2* or *GAX*), a member of the Homeobox gene family, activates p16 and p21, overexpression of *MEOX2* stops growth and causes endothelial cell senescence (53). It has been shown that *MEOX2* expression is permanently suppressed in immortalized human astrocyte cells that express IDH1-R132H (43). Therefore, we selected MEOX2 as another gene to test our model. RT-qPCR analysis of *TET1* and *MEOX2* at two time points (day0 and day17) in NPCs exposed to IHA-IDH1-R132H or IHA-IDH1-WT conditioned medium yielded results that are consistent with the literature, albeit MEOX2 expression change not reaching statistical significance ($p=0.21$), possibly due to low replicate number ($n=2$).

On this basis of our findings in this study, we conclude that the alginate-based 3D NPC culture model exposed to IHA-conditioned media, is suitable to study the effects of IDH mutations on the earliest stages of gliomas, without the confounding effects of other oncogenic mutations. Further characterization of NPCs could potentially reveal the effects of 3D culture

compared to the 2D culture and established this novel model for further epigenomic investigations of gliomas.

References

1. González-Castro TB, Juárez-Rojop IE, López-Narváez ML, Tovilla-Zárate CA, Genis-Mendoza AD, Pérez-Hernández N, et al. Genetic Polymorphisms of CCDC26 rs891835, rs6470745, and rs55705857 in Glioma Risk: A Systematic Review and Meta-analysis. Biochem Genet. 2019 Aug 1;57(4):583–605.
2. Sung H, Ferlay J, Siegel RL, Laversanne M, Soerjomataram I, Jemal A, et al. Global Cancer Statistics 2020: GLOBOCAN Estimates of Incidence and Mortality Worldwide for 36 Cancers in 185 Countries. CA Cancer J Clin. 2021 May;71(3):209–49.
3. Haddock S, Alban TJ, Turcan Ş, Husic H, Rosiek E, Ma X, et al. Phenotypic and molecular states of IDH1 mutation-induced CD24-positive glioma stem-like cells. Neoplasia (United States). 2022 Jun 1;28.
4. Xu S, Tang L, Li X, Fan F, Liu Z. Immunotherapy for glioma: Current management and future application. Vol. 476, Cancer Letters. Elsevier Ireland Ltd; 2020. p. 1–12.
5. Stupp R, Mason WP, Van Den Bent MJ, Weller M, Fisher B, Taphoorn MJB, et al. Radiotherapy plus Concomitant and Adjuvant Temozolomide for Glioblastoma [Internet]. Available from: www.nejm.org
6. Yang K, Wu Z, Zhang H, Zhang N, Wu W, Wang Z, et al. Glioma targeted therapy: insight into future of molecular approaches. Vol. 21, Molecular Cancer. BioMed Central Ltd; 2022.
7. Bush NAO, Chang SM, Berger MS. Current and future strategies for treatment of glioma. Vol. 40, Neurosurgical Review. Springer Verlag; 2017.
8. Dang L, White DW, Gross S, Bennett BD, Bittinger MA, Driggers EM, et al. Cancer-associated IDH1 mutations produce 2-hydroxyglutarate. Nature. 2009 Dec 10;462(7274):739–44.
9. Louis DN, Perry A, Wesseling P, Brat DJ, Cree IA, Figarella-Branger D, et al. The 2021 WHO classification of tumors of the central nervous system: A summary. Neuro Oncol. 2021 Aug 1;23(8):1231–51.
10. Yan H, Williams D, Jin G, Mclendon R, Rasheed BA, Yuan W, et al. IDH1 and IDH2 Mutations in Gliomas A bs tr ac t. Vol. 360, N Engl J Med. 2009.
11. Chowdhury R, Yeoh KK, Tian YM, Hillringhaus L, Bagg EA, Rose NR, et al. The oncometabolite 2-hydroxyglutarate inhibits histone lysine demethylases. EMBO Rep. 2011 May 1;12(5):463–9.
12. Xu W, Yang H, Liu Y, Yang Y, Wang P, Kim SH, et al. Oncometabolite 2-hydroxyglutarate is a competitive inhibitor of α-ketoglutarate-dependent dioxygenases. Cancer Cell. 2011 Jan 18;19(1):17–30.
13. Lu C, Ward PS, Kapoor GS, Rohle D, Turcan S, Abdel-Wahab O, et al. IDH mutation impairs histone demethylation and results in a block to cell differentiation. Nature. 2012 Mar 22;483(7390):474–8.

14. Turcan S, Rohle D, Goenka A, Walsh LA, Fang F, Yilmaz E, et al. IDH1 mutation is sufficient to establish the glioma hypermethylator phenotype. Nature. 2012 Mar 22;483(7390):479–83.
15. Oktay Y, Ülgen E, Can Ö, Akyerli CB, Yüksel Ş, Erdemgil Y, et al. IDH-mutant glioma specific association of rs55705857 located at 8q24.21 involves MYC deregulation. Sci Rep. 2016 Jun 10;6.
16. Suzuki H, Aoki K, Chiba K, Sato Y, Shiozawa Y, Shiraishi Y, et al. Mutational landscape and clonal architecture in grade II and III gliomas. Nat Genet. 2015 May 30;47(5):458–68.
17. Jiang Y, Uhrbom L. On the origin of glioma. Ups J Med Sci. 2012 May;117(2):113–21.
18. Doetsch F, Caillé I, Lim DA, Manuel García-Verdugo J, Alvarez-Buylla A. Subventricular Zone Astrocytes Are Neural Stem Cells in the Adult Mammalian Brain. Vol. 97, Cell. 1999.
19. Mich JK, Signer RAJ, Nakada D, Pineda A, Burgess RJ, Vue TY, et al. Prospective identification of functionally distinct stem cells and neurosphere-initiating cells in adult mouse forebrain. Elife. 2014 May 7;2014(3).
20. Cahill D, Turcan S. Origin of Gliomas. Semin Neurol. 2018 Feb 1;38(1):5–10.
21. Lee JH, Lee JH. The origin-of-cell harboring cancer-driving mutations in human glioblastoma. BMB Rep. 2018 Oct 1;51(10):481–3.
22. Engineering 3D Tissue Systems to Better Mimic Human Biology [Internet]. Available from: https://www.researchgate.net/publication/245161944
23. Lee J, Cuddihy MJ, Kotov NA. Three-dimensional cell culture matrices: State of the art. Vol. 14, Tissue Engineering - Part B: Reviews. 2008. p. 61–86.
24. Albrecht DR, Underhill GH, Wassermann TB, Sah RL, Bhatia SN. Probing the role of multicellular organization in three-dimensional microenvironments. Nat Methods. 2006 May;3(5):369–75.
25. Beningo KA, Dembo M, Wang YL. Sciences of the USA 18024-18029 PNAS [Internet]. Vol. 101. 2004. Available from: www.pnas.orgcgidoi10.1073pnas.0405747102
26. Discher DE, Janmey P, Wang YL. Tissue Cells Feel and Respond to the Stiffness of. Vol. 310, Source: Science, New Series. 2005.
27. Choukaife H, Doolaanea AA, Alfatama M. Alginate nanoformulation: Influence of process and selected variables. Vol. 13, Pharmaceuticals. MDPI AG; 2020. p. 1–35.
28. Bozza A, Coates EE, Incitti T, Ferlin KM, Messina A, Menna E, et al. Neural differentiation of pluripotent cells in 3D alginate-based cultures. Biomaterials. 2014;35(16):4636–45.
29. Li L, Davidovich AE, Schloss JM, Chippada U, Schloss RR, Langrana NA, et al. Neural lineage differentiation of embryonic stem cells within alginate microbeads. Biomaterials. 2011 Jul;32(20):4489–97.
30. Mehravar M, Ghaemimanesh F, Poursani EM. An Overview on the Complexity of OCT4: at the Level of DNA, RNA and Protein. Vol. 17, Stem Cell Reviews and Reports. Springer; 2021. p. 1121–36.
31. Schoorlemmer J, Jonk L, Shen S, Van Puijenbroek A, Feijen A, Kruijer W. Regulation of Oct-4 gene expression during differentiation of EC cells. Vol. 21, Molecular Biology Reports. KluwerAcademic Publishers; 1995.
32. Lendahl U, Zimmerman LB, Mckay' RDG. CNS Stem Cells Express a New Class of Intermediate Filament Protein. Vol. 60. 1990.

33. Venere M, Han YG, Bell R, Song JS, Alvarez-Buylla A, Blelloch R. Sox1 marks an activated neural stem/progenitor cell in the hippocampus. Development (Cambridge). 2012 Nov 1;139(21):3938–49.
34. Ring KL, Tong LM, Balestra ME, Javier R, Andrews-Zwilling Y, Li G, et al. Direct reprogramming of mouse and human fibroblasts into multipotent neural stem cells with a single factor. Cell Stem Cell. 2012 Jul 6;11(1):100–9.
35. Zhang S. Sox2, a key factor in the regulation of pluripotency and neural differentiation. World J Stem Cells. 2014;6(3):305.
36. Ian Simpson T, Price DJ. Pax6; a pleiotropic player in development. Vol. 24, BioEssays. 2002. p. 1041–51.
37. Andersen T, Auk-Emblem P, Dornish M. 3D Cell Culture in Alginate Hydrogels. Microarrays. 2015 Mar 24;4(2):133–61.
38. Wang N, Adams G, Buttery L, Falcone FH, Stolnik S. Alginate encapsulation technology supports embryonic stem cells differentiation into insulin-producing cells. J Biotechnol. 2009 Dec;144(4):304–12.
39. Saha K, Keung AJ, Irwin EF, Li Y, Little L, Schaffer D V., et al. Substrate modulus directs neural stem cell behavior. Biophys J. 2008 Nov 1;95(9):4426–38.
40. Luechtefeld T, Lin N, Paller C, Kuhns K, Laterra JJ, Bressler JP. Measuring Cancer Hallmark Mediation of the TET1 Glioma Survival Effect with Linked Neural-Network Based Mediation Experiments. Sci Rep. 2020 Dec 1;10(1).
41. Csete M. Translational prospects for human induced pluripotent stem cells. Vol. 5, Regenerative Medicine. 2010. p. 509–19.
42. Raya Á, Rodríguez-Piz I, Guenechea G, Vassena R, Navarro S, Barrero MJ, et al. Disease-corrected haematopoietic progenitors from Fanconi anaemia induced pluripotent stem cells. Vol. 460, Nature. 2009. p. 53–9.
43. Turcan S, Makarov V, Taranda J, Wang Y, Fabius AWM, Wu W, et al. Mutant-IDH1-dependent chromatin state reprogramming, reversibility, and persistence. Nat Genet. 2018 Jan 1;50(1):62–72.
44. Sonoda Y, Ozawa T, Hirose Y, Aldape KD, Mcmahon M, Berger MS, et al. Formation of Intracranial Tumors by Genetically Modified Human Astrocytes Defines Four Pathways Critical in the Development of Human Anaplastic Astrocytoma 1 [Internet]. Vol. 61, CANCER RESEARCH. 2001. Available from: http://aacrjournals.org/cancerres/article-pdf/61/13/4956/2485597/4956.pdf
45. Bell S, Hettige NC, Silveira H, Peng H, Wu H, Jefri M, et al. Differentiation of Human Induced Pluripotent Stem Cells (iPSCs) into an Effective Model of Forebrain Neural Progenitor Cells and Mature Neurons. Bio Protoc. 2019 Mar 5;9(5).
46. Annika Zink, Pawel Lisowski, Alessandro Prigione. Generation of Human iPSC-derived Neural Progenitor Cells (NPCs) as Drug Discovery Model for Neurological and Mitochondrial Disorders. Bio Protoc. 2021;11(5).
47. Łabowska MB, Cierluk K, Jankowska AM, Kulbacka J, Detyna J, Michalak I. A review on the adaption of alginate-gelatin hydrogels for 3D cultures and bioprinting. Vol. 14, Materials. MDPI AG; 2021. p. 1–28.
48. Reig-Vano B, Tylkowski B, Montané X, Giamberini M. Alginate-based hydrogels for cancer therapy and research. Vol. 170, International Journal of Biological Macromolecules. Elsevier B.V.; 2021. p. 424–36.
49. Liu Y, Song B, Chen X, Cai Q, Tian W. Alginate-based hydrogels encapsulated TWS119 for inducing neuronal differentiation of neural stem cells. J Biomater Tissue Eng. 2014;4(12):1087–92.
50. Dragoj M, Stojkovska J, Stanković T, Dinić J, Podolski-Renić A, Obradović B, et al. Development and validation of a long-term 3d glioblastoma cell culture in alginate

microfibers as a novel bio-mimicking model system for preclinical drug testing. Brain Sci. 2021 Aug 1;11(8).
51. Davoudi F, Ghorbanpoor S, Yoda S, Pan X, Crowther GS, Yin X, et al. Alginate-based 3D cancer cell culture for therapeutic response modeling. STAR Protoc. 2021 Jun 18;2(2).
52. Wu X, Zhang Y. TET-mediated active DNA demethylation: Mechanism, function and beyond. Vol. 18, Nature Reviews Genetics. Nature Publishing Group; 2017. p. 517–34.
53. Douville JM, Cheung DYC, Herbert KL, Moffatt T, Wigle JT. Mechanisms of MEOX1 and MEOX2 regulation of the cyclin dependent kinase inhibitors p21 CIP1/WAF1 and p16 INK4a in vascular endothelial cells. PLoS One. 2011 Nov 20;6(12).